An investigation of fungal rust hyperparasitism: the genes behind eating rust spores

Jack Wess

A thesis submitted for the degree of

Doctor of Philosophy of

The Australian National University



Australian National University

June 2026

© Copyright by Jack Wess, 2026

All rights Reserved

Disclaimer

I hereby declare that the work undertaken in this thesis has been conducted by me alone, except where indicated in the text. I conducted this work between 2022 and 2026 while I was a PhD student at the Australian National University.



Jack Wess

19 June 2026

Acknowledgements

Olga, you are one of the most selfless people I have ever met. Your endless generosity has carried me through much of this PhD and I would definitely not have survived the lead up to my exit seminar without your help. Thank you for listening to all my quotes. But not only are you kind, you are also hilarious, it was a joy to spend so much time exploring, geocaching, ranting, dancing and getting a bit more than tipsy with you the last few years. A photo of a photo of a photo! It's the same place as on an English computer! Baltazar! PASHTA DE NASHTA! Nah Nah Nah Nah Nah! The Mr Batty voice! Duxton and Tradies! The Lego Premier! It is an honour to call you my best friend.

Jesús, you are definitely one of the most hilarious people I know. I often tell people that you are the only person I've ever met who will have a story for me when I wake up, a story for me when you come see me at my desk in the morning, another at lunch, another at dinner, and another before saying goodnight. Pum! Checkkkkkkk. Living in Unit 192 has been one big endless laugh with you, so many late-night conversations, gym sessions, dinners, parties and hypothetical questions. I will always consider you my brother, and you will always be welcome wherever I live. I will miss you immensely when we move out.

Dan, my love, come on what can I say? My best friend, my pal, my home-boy, my rotten soldier, my sweet cheese, my good-time boyeh. What a time we had in this PhD. Endless banter, endless inside jokes, endless dodgy photos, endless suits and endless cake! Even if we look and dress almost entirely opposite, I'm still not sure we aren't two brothers separated at birth. You and I literally redefined the vocabulary of the gang over our PhDs, who else can say that! Come on, brilliant! CHARGE! EH! Abandon ship! Is that so! Come on Pastor! We took it by storm! You are going to do amazing things in your life and I hope I will stay a part of it to see them.

Ming, Mingandrist, Miffy, you are my bestie now and always. The one who introduced me to NFSA, to Letterboxd, to Mama Dough and the Carillion. Come on who else better to visit BallinaBattle or Wombat. I am so proud of the woman you have grown to become; you learned the number one lesson. You can't win the throne to save the kingdom, you have to save the kingdom to win the throne. Thanks for always keeping me on the right track and not taking it too seriously when I beat you in Mariokart. I am so glad Marvin brought you to meet us all those nights ago at Badgers, it has been a joy being part of your life ever since.

Marvin, my Batman, my Mario, the James (or Jesse) to my Meowth, you were a true brother to me in my PhD and beyond. Whenever I have a problem, I know that I can tell you and that I will instantly feel better. When I think of someone who will instantly get a joke, a call back, or a reference to a Bulgarian cartoon from 1987 that wasn't even shown on TV outside Sofia, I think of you. Having you at my back

during our generational run in ruling the HDR life of RSB was one of the greatest pleasures and I will always covet it in my heart.

Davin, you are one of the smartest people I know and you are going to get a Nobel for sure. Don't forget all of us in your speech. You are the smart one of the gang, we would still be stuck in that escape room without you! Thank you for your banter, your sarcasm, and for always staying behind to help clean after parties.

Mackenzie, my first friend in RSB and one of my dearest. We are like two sides of the same coin, with you as the wiser more mature version of me. Thank you for our curry nights, our HALO nights, for introducing me to Magic, for explaining Magic and for always reminding me to be gentler and kinder. I remember that night in Kioloa when we got locked out of the room and ended up talking for hours about HALO, Star Wars, Battlefront and Battlefield. You could name all of the BF3 maps! Even the DLCs! Is there a world record for that? If not get in there. I will always be thankful that you chose to come introduce yourself to me before we got on that bus, it changed the course of my future in RSB.

Hafiz. We are so different yet so identical. I know that I have a kindred spirit in you downstairs. Thank you for your brotherly spirit and for teaching me about Pakistan and Islam, I know I have found a brother for life in you. I would say a lot of other things and call you a lot of other things, but I think ANU is pretty squeamish it seems about swearing, so I'll just call you brother.

Joseph, my Ugandan brother. Every talk with you is so full of wisdom, it is like you have lived a thousand lives. I miss us bumping into each other on the corridor and ending up chatting for hours. One day I am going to come to Uganda and we drink Waragi and watch your cows until the sun comes up.

Going, Sharon and the Mercedes, I miss you, move back to Canberra already. Jokes aside, you are two of the most thoughtful girls I've ever met. Pilates, karaoke, the photos climbing Black Mountain, the knife at golden drum and the garlic brownie! What a laugh! Thank you for all your presents, your cooking, your baking and your company. We took this city by storm and now you are taking Sydney the same way. I wish you both prosperity, money and beautiful husbands who come home and just give you their pay checks.

Zhao, my big little sister. You are the hardest working person I know and an unbelievable inspiration. How you manage to work so much and still find time to be so charming, so kind, so full of life I will never know. Thank you for the reagents, for the time you gave me explaining protocols, for the cooking, for the endless thoughtful presents and your kind spirit. You will always be my sister.

Héber, the nights with you and Jesús in the early years of my PhD are some of my favourite memories. Delicious pasta and red sauce, delicious brownies, Overcooked, Age of Empires, laughing till our sides hurt. I hope you are enjoying Portugal and I can't wait till you are back here for more memories!

Jeffrey, the king! Thank you for your gentle soul and great gifts over the years, hopefully I'm gonna see you in Taiwan and we go for stinky tofu.

Noah and Dora, two of the greatest soldiers to ever walk through the doorway into Unit 192. What bants we have had!!! I know whenever you will turn up to a party it's about to get better. Thank you for always being so full of life and energy and for always keeping a bev in my hands or a pic on my linkedin.

Nixy, you are a devious man. But I love you anway, I hope you love Melbourne and come back to visit us whenever you can. Slappy Salmon! Nils, thank you for being the voice of reason at lunch times. You are such a good sport and one of the funniest people in RSB.

Woojin, Gary and Chae. Thank you for being true friends to me when I was not to you. I hope you are all doing well and are happy and healthy. Thank you for staying by my side in my honours, I definitely did not deserve your kindness. I'm sorry for how I was.

John, thanks for giving me the opportunity to do a PhD.

Xiaoxiao, thank you for being my big sister in the lab. There was a time when it was just you and I in the lab and we would talk for hours even after it was time to go home. Thank you for sitting with me when I did my first PCR because I was so nervous about it. You are going to be a fantastic lab leader and take great care of your students. I wish you and baby Michael the best, I am sure he will grow up to be as strong and smart as his Mum.

Na, my partner in crime, you need no introduction. You are like an angel came to earth and decided to do a PhD with the Rathjen lab. You made life in the lab such a dream, always helpful, always up for a laugh, always bringing me snacks or just the exact reagent I needed in that exact moment. I can't even think of how many problems we solved together in that lab, disassembling CO_2 chambers, fighting fungicides, *Pst, Pst, Pst* and wheat, wheat, wheat! I hope we will always stay in touch and that you find a highly paid job where you get to put pipettes into boxes for 8 hours a day and go home at 5pm, no! 4.30! Thank you, genuinely, for joining the lab, I could never have survived three and a half years in the trenches without you.

Rita, you are a powerhouse. I was so lucky to have a friend who is so smart and generous sitting just the office over. Thank you for your help with my bioinformatics, I would still be sat trying to make Phobius work right now if it wasn't for you. I hope I did not drive you insane with all my questions. You were a fantastic friend and ally in the lab and now the PhD is done we can for real play some Age of Empires, shotgun Vikings. You are going to achieve great things with whatever you decide to do after your PhD, I just know it.

Abigail, not only are you endlessly smart, you are endlessly funny. Our Friday coffees at the French place were such a beautiful way to decompress and lick my wounds after those meetings. Oh, and how

could I not mention the rust collecting trip! Some of the most hilarious moments of my PhD were in that gorge and we definitely defied death a bit to get those samples… I still laugh thinking about your face when you said you love to eat a whole burrata and I asked if you just picked it up and bit into it like an apple.

Eric. We started out as colleagues and became friends. When we first met, we only talked about science and our careers, I'm glad we now talk about science, our careers and debauchery. Let's go to Queensland get chill government jobs and surf the rest of the time. Thanks for your help with my thesis and for being my mentor in RSB.

Jialing, thank you for your humour and generosity in the lab and during my day in China. It truly meant so much that you came all the way out to look after me for the day in Guangzhou. I had so much fun exploring the city with you and I hope the wishes you made in the temple are coming true!

Yiheng, Sam and Alex, thanks for everything. To Yiheng, thank you for being my big brother in the beginning of my honours, I now understand just how hard a task that was and you did it with such grace. To Alex, you sat with me and helped edit my entire honours thesis, you will forever have my gratitude for the day you dedicated solely to saving me. To Sam, you started it all, *Penicillium* X was one of the most impactful gifts I've ever received. Thank you, Sam Fleming!

David, Lucy and Harrison, thank you for the opportunity to repay the favour Yiheng gave to me in being my big brother in the lab. You were great and it was a privilege to meet you and get to help each other out.

Thank you so much to the professional support staff of RSB. Especially to the plant services team, Chris, Jenny, Darren and Patrick, thank you for all of your help with my plants (and microbes) in the CEF, greenhouses and beyond. Doing the weekend watering was so rewarding and I truly appreciate you giving me that opportunity to put more money in my pocket. Thank you as well to James down in the autoclave room for sterilising probably 1000 L of media for me over the long course of this journey.

Thank you to Bioplatforms Australia for the incredibly generous funding to sequence genomes and transcriptomes for my fungi. Thank you especially to Sophie Mazard for your patience with the continual issues with DNA and RNA isolation. Thanks as well to Corina and Lache at the BRF for helping so much with my samples and for giving me such fantastic data.

Ash, you are a legend. Your intelligence and expertise literally saved my honours and my PhD several times. You are a jedi in all thing's nucleic acid, thank you so much for all your help over the last five years. Erin, your generosity and patience with my endless questions was amazing. You and Peter saved Chapter Three many times over by teaching me so much about CRISPR.

Ryan, our time hanging out in Maastricht was an absolute blast. Especially the hilarious walk around the old city after that great pizza, all the best in your future.

I would also like to show my appreciation to DavidReadsAsoiaf on youtube, I spent a lot of my PhD in the lab late at night, listening to those great books with your fantastic readings made it seem worth it.

Mum and Dad, I owe it all to you. Thank you for teaching me kindness, generosity, humour, love, selflessness and that when you truly want something, there is no surrender until you get it. Mum, you are the most determined and loving person I know, so many times late at night in the lab when I felt my eyes closing I thought of you to give me strength to not give up till the work was done. Dad, you are the guiding voice I think of before each decision on this crazy PhD journey. Thank you for your care and for always keeping me on my toes. I dedicate this thesis to you both. Laura and Andrew, I love you both kite kazillions, thank you for making coming home so much fun.

Abstract

Global food security is under threat from fungal plant pathogens. Wheat stripe rust caused by the fungus *Puccinia striiformis* f. sp. *tritici* (*Pst*) is currently the most destructive disease of wheat. Traditional control methods including development of resistant wheat cultivars and the application of chemical fungicides are rapidly losing efficiency as the fungus rapidly evolves. As natural antagonists of *Pst*, rust hyperparasites may be the only option for environmentally sustainable control of disease outbreaks. This thesis investigates the genetic basis of rust hyperparasitism and how these genes enable fungi to antagonise and consume *Pst*. The thesis begins with a review of the limited literature on wheat rust hyperparasites, highlighting how previous investigations have remained largely observational and identifying major knowledge gaps regarding hyperparasite genomes and the transcriptional responses deployed during growth on *Pst*. Prompted by a serendipitous discovery, the thesis next presents an in-depth investigation of the novel *Pst* hyperparasite *Penicillium coffeae* strain ANU01. Integrated genomic and transcriptomic analysis suggested that, during growth on *Pst*-infected wheat, *P. coffeae* ANU01 may deploy a depudecin-like secondary metabolite to suppress urediniospore germination, followed by secretion of cell wall degrading enzymes to penetrate the spore coat and mobilisation of lipases and sugar transporters to exploit *Pst*-derived nutrients. The thesis next focuses on *P. coffeae* ANU01, using CRISPR-mediated knockouts to investigate the contribution of 18 carefully selected candidate genes to growth on *Pst*. Transformation of *P. coffeae* ANU01 targeting 15 of these candidate genes ultimately resulted in the successful disruption of nine, generating individual mutant strains that were used in subsequent phenotypic assays. Despite the development of multiple phenotyping approaches, no reliable differences in parasitic fitness were detected between wild type and loss-of-function mutants. However, the ability of all mutant *P. coffeae* ANU01 strains to grow with *Pst* urediniospores as the sole source of nutrition suggests that the targeted genes are important but not individually essential for parasitic growth. This apparent resilience may reflect functional redundancy within the *P. coffeae* ANU01 genome, where numerous homologous or genes with similar functions potentially compensate for the loss of individual functions. The thesis then shifts to the host side of the interaction, examining *Pst* gene expression during parasitism by *P. coffeae* ANU01 in the first investigation of rust hyperparasitism from the perspective of the host. Although urediniospores have traditionally been considered dormant or inert until germination, transcriptomic analyses revealed a complex and coordinated defence response to parasitic attack. This response can be divided into six putative aspects; recognition of attack and downstream signalling, fortification of the urediniospore coat to protect against enzymatic and mechanical damage, maintenance of homeostasis in a rapidly changing environment, detoxification of secondary metabolites and harmful ROS induced by *P. coffeae* ANU01, repair of damage to DNA, and finally a mobilisation of metabolites, primarily lipids, to fuel the defence. However, limitations regarding experimental differences in sample age, humidity and tissue collection

methods, impact the certainty of these conclusions. Finally, the thesis expands beyond *P. coffeae* ANU01 to investigate the genomic and transcriptomic profiles of eight additional hyperparasite candidates isolated from diverse potential rust hosts. Genome assemblies and gene expression profiles during growth on *Pst* were examined for each candidate. Comparative analyses revealed several features that were consistently upregulated during parasitic growth, including the production of secondary metabolites via biosynthetic gene clusters, secretion of cell wall degrading enzymes and mobilisation of metabolic machinery and nutrient transporters. Together, these shared responses suggest that there are key gene groups that underpin rust hyperparasitism, despite substantial differences between candidates.

Contents

Chapter One	**The Enemy of My Enemy: Fungal hyperparasites that target wheat rust**	
1.1	Abstract	**12**
1.2	From Vulnerability to Opportunity	**12**
1.3	Rust fungi have enemies too	**13**
1.4	How hyperparasites disarm stripe rust	**14**
1.5	The promise and the pitfalls	**16**
1.6	Future directions: From organisms to molecules	**17**
1.7	Bibliography	**18**
Chapter Two	**Global transcriptome changes during growth of a novel *Penicillium coffeae* isolate on the wheat stripe rust fungus, *Puccinia* f. sp. *tritici***	
2.1	Supplementary Material	**21**
Chapter Three	**Which genes contribute to hyperparasitism? A CRISPR-mediated loss-of-function investigation of candidate *P. coffeae* ANU01 genes**	
3.1	Background	**29**
3.2	Materials and Methods	**30**
3.3	Results	**36**
	Selecting candidate genes for knock out	**36**
	Generating loss-of-function in candidate genes	**39**
	Measuring impact of loss-of-function on growth on *Pst on planta*	**41**
	Measuring impact of loss-of-function on growth on *Pst in vitro*	**44**
3.4	Discussion	**55**
3.5	Bibliography	**61**
3.6	Supplementary Material	**64**
Chapter Four	**A hidden defence: Investigating rust hyperparasitism from the perspective of *Pst***	
4.1	Background	**66**
4.2	Materials and Methods	**67**
4.3	Results and Discussion	**69**

	Global gene expression	**69**
	Gene Ontology enrichment analysis during parasitic attack	**70**
	COG enrichment analysis during parasitic attack	**80**
	Top most upregulated genes during parasitic attack	**81**
4.4	Bibliography	**84**
Chapter Five	**Beyond *P. coffeae* ANU01: Identifying and Investigating further rust hyperparasites**	
5.1	Background	**88**
5.2	Materials and Methods	**89**
5.3	Results and Discussion	**93**
	Isolating and identifying new hyperparasite candidates	**93**
	Generation of annotated genome assemblies	**104**
	Global transcriptome changes during growth on *Pst* urediniospores	**110**
	GO enrichment in candidates during growth on *Pst* urediniospores	**114**
	COG enrichment in candidates during growth on *Pst* urediniospores	**138**
	Top upregulated genes during growth on *Pst* urediniospores	**147**
	Candidate cornerstone genes involved in rust parasitism	**158**
5.4	Conclusions	**162**
5.5	Bibliography	**164**
5.6	Supplementary Material	**172**
Chapter Six	**General Discussion and Concluding Remarks**	
6.1	Preface	**174**
6.2	Chapter Summaries	**175**
6.3	What is a hyperparasite?	**177**
6.4	Limitations and Future Directions	**181**
6.5	Conclusions	**183**
6.6	Bibliography	**184**

Chapter One

The Enemy of My Enemy: Fungal hyperparasites that target wheat rust

Chapter One lays the foundation for this thesis by presenting a literature review on the species of filamentous fungi that parasitise wheat rusts, the molecular mechanisms they deploy in doing so, and the agricultural and environmental impacts of their research.

1.1 Abstract

Wheat rusts remain a persistent threat to global food security due to its rapid evolution and prolific spore production. While breeding and fungicides have long been the cornerstones of disease management, an overlooked opportunity lies in the natural enemies of the pathogen itself, the hyperparasites. These mycoparasitic fungi can colonize rust pustules, reduce spore viability, and interfere with pathogen reproduction through direct invasion, enzymatic degradation, and secondary metabolite production. However, their potential remains largely untapped due to ecological constraints and knowledge gaps in their biology, host specificity, and environmental compatibility. Here, I explore the diversity, modes of action, and biocontrol potential of fungal hyperparasites targeting stripe rust, and discuss future strategies to harness their activities through metabolite-based or recombinant approaches. By turning the enemy's enemy into an ally, hyperparasites may offer a novel and ecologically grounded solution for sustainable rust management.

1.2 From vulnerability to opportunity

Wheat rusts, including stem rust (*Puccinia graminis* f. sp. *tritici, Pgt*), leaf rust (*P. triticina, Pt*), and stripe rust (*P. striiformis* f. sp. *tritici, Pst*), are among the most economically devastating fungal pathogens of wheat globally (Rehman *et al.,* 2024). These obligate biotrophic fungi require living host tissue to develop and complete complex life cycles (Lorrain *et al.,* 2019). Stripe rust has received growing attention in recent years due to its aggressive spread in temperate and subtropical regions and its significant contribution to yield losses under favourable climatic conditions (Schwessinger 2017).

A defining trait of stripe rust is its capacity for prolific asexual reproduction within the plant tissue which culminates in the form of pustules on the leaf surface, each containing thousands of individual

urediniospores. These lipid- and protein-rich structures are well adapted for wind dispersal, environmental persistence, and rapid reinfection cycles. This enables *Pst* to rapidly colonise wheat fields, especially in cool, moist environments, making it a persistent threat to global food security (Chen *et al.*, 2014). Importantly, the epidermal localisation of uredinia and the external exposure of spores make them accessible not only to fungicides and environmental stress but also to microbial antagonists such as hyperparasites. Despite decades of efforts in breeding rust-resistant wheat varieties and applying fungicidal controls, stripe rust remains a formidable challenge. The genetic plasticity of *Pst* populations allows for the frequent emergence of new virulent races capable of overcoming host resistance genes (Wellings, 2011; Ali *et al.*, 2017). Furthermore, overreliance on fungicides contributes to resistance development and environmental concerns.

1.3 Rust fungi have enemies too

While much attention has focused on the co-evolutionary arms race between rust pathogens and their host plants, far less is known about the third party in this ecological triangle, the hyperparasites. These fungal mycoparasites colonize the reproductive structures of rust fungi, targeting the uredinia and telia where spores are formed and released. These interactions often lead to reduced spore viability, altered pustule morphology, and suppression of pathogen fitness (Zhan *et al.*, 2014).

Multiple fungal taxa have been reported as natural hyperparasites of rusts. Among those most frequently isolated from rust pustules are *Cladosporium cladosporioides, Alternaria alternata, Simplicillium obclavatum, Clonostachys rosea, Lecanicillium psalliotae*, and *Epicoccum nigrum* (Wang *et al.*, 2020; Wilson et. al., 2020; Zhan *et al.*, 2014; Zhang *et al.*, 2022; Zheng *et al.*, 2017). These organisms may reduce the viability of rust spores or even limit their capacity to infect new hosts, suggesting an untapped reservoir of biological control potential. However, despite repeated observations, the biology, diversity, host specificity and ecological roles of these hyperparasites remain poorly understood.

The existence of these hyperparasites, often dismissed as saprophytes or contaminants, challenges the traditional binary model of host and pathogen. In reality, *Pst* occupies a microbial battlefield, where even the pathogen is vulnerable. These hyperparasites may play a larger role in the natural regulation of rust epidemics than currently appreciated, offering an untapped reservoir of biological control agents adapted to the very structures that drive *Pst* epidemics. Unlocking their potential will require shifting our perspective, from seeing rust pustules as the endpoint of infection to recognizing them as contested microbial niches.

1.4 How hyperparasites disarm stripe rust

1. *Pst* urediniospores are rich in nutrients and sit openly on the leaf surface, forming pustules containing thousands of spores that are theoretically ideal targets for microbial antagonists. These spores are particularly abundant in lipids (~20%), carbohydrates (~22%) and protein (~25%) and sit exposed in pustules on the leaf surface (Staples and Wynn 1965, Tulloch *et al.,* 1959). Several hyperparasitic fungi have evolved to exploit these structures, attacking *Pst* through three primary mechanisms, such as direct invasion, enzymatic degradation, and antibiosis (Table 1.1).
2. Direct penetration and invasion of *Pst* urediniospores via hyperparasite hyphae has been observed using scanning electron microscopy (SEM) in multiple parasitic fungi (Wang *et al.,* 2020; Zhan *et al.,* 2014; Zhang *et al.,* 2022). Infected urediniospores frequently exhibit morphological collapse, loss of turgor, and reduced germination capacity, indicating effective parasitism and suppression of spore viability. Such damage suggests both mechanical invasion and biochemical degradation are involved. These effects are evident in species such as *Cladosporium cladosporioides*, *Simplicillium obclavatum*, and *Alternaria alternata*, all of which visibly degrade *Pst* urediniospores *in situ* (Table 1.1).
3. Enzymatic attack is another common mechanism for spore penetration that involves the secretion of cell-wall degrading enzymes (CWDE), which degrade the polysaccharide-rich spore walls, facilitating fungal penetration. In the case of *Pgt*, the hyperparasite *Aphanocladium album* penetrates urediniospores via the germ pore after enzymatic lysis of the germ tube, a process facilitated by glucanases and chitinases (Srivastava *et al.,* 1985). Little is known regarding cell wall degrading enzymes in fungi that hyperparasitise *Pst*. However, upregulation of several cell wall degrading enzymes, including a β-glucanase, was observed in the putative *Pst* hyperparasite *Penicillium coffeae* while growing on *Pst* pustules (Wess *et al.*, 2025).
4. Antibiosis, defined as the production of metabolites that inhibit other organisms (Fravel 1988), is another critical mechanism. Hyperparasites produce toxic secondary metabolites (SMs) that inhibit urediniospore germination and fungal growth (Speckbacher & Zeilinger 2018). These compounds may serve multiple functions, such as immobilizing the host to prevent nutrient loss, reducing fungal defences, or modifying the local leaf environment to support hyperparasite colonization. A reduction in *Pst* urediniospore viability and germination rate is a commonly observed effect after colonization of pustules by hyperparasites (Wang *et al.,* 2020; Zhang *et al.*, 2022; Zhan *et al.,* 2014). Hyperparasites have also been shown capable of inhibiting rust germination in *in vitro* assays. *Cladosporium tenuissimum* produces cladosporols A–C, resorcylic acid lactone-derived compounds, that have been shown to suppress rust spore germination *in vitro* (Nasini *et al.,* 2004).

Table 1.1. Summary of fungal species observed acting as wheat rust hyperparasites

Hyperparasite	**Phylum**	**Mechanism**	**Confirmed Interaction with *Pst*?**	**References**
Cladosporium cladosporioides	*Ascomycota*	Direct hyphal penetration; possible antibiosis	Yes, SEM	Zhan *et al.,* 2014; Zhang *et al.,* 2022
Penicillium coffeae	*Ascomycota*	Possible CWDE production (β-glucanase, chitinase); possible antibiosis	Yes, light microscopy and qPCR	Wess *et al.,* 2025
Alternaria alternata	*Ascomycota*	Direct hyphal penetration; reduces urediniospore viability	Yes, SEM	Zheng *et al.,* 2017
Simplicillium obclavatum	*Ascomycota*	Hyphal invasion; reduces urediniospore germination	Yes, SEM	Wang *et al.,* 2020
Penicillium simplicissimum	*Ascomycota*	Direct hyphal penetration; reduces urediniospore viability. Induce plant resistance.	Yes, SEM	Esmail *et al.,* 2022
Trichoderma asperellum	*Ascomycota*	Direct hyphal penetration; reduces urediniospore viability. Induce plant resistance.	Yes, SEM	Esmail *et al.,* 2022
Aphanocladium album	*Ascomycota*	CWDE (via germ pore); enzymatic lysis	No, but in several other cereal rusts	Srivastava *et al.,* 1985
Cladosporium tenuissimum	*Ascomycota*	Secondary metabolites (Cladosporols) inhibiting germination	No, but several other rust fungi	Nasini *et al.,* 2004

These strategies are not mutually exclusive; many hyperparasites may combine mechanical, enzymatic, and chemical modes of action. Despite their efficacy in controlled settings, the relative contribution of each mode in natural environments remains poorly characterized. Understanding how these mechanisms interact will be crucial for designing hyperparasite-based biocontrol strategies that are robust across environmental contexts.

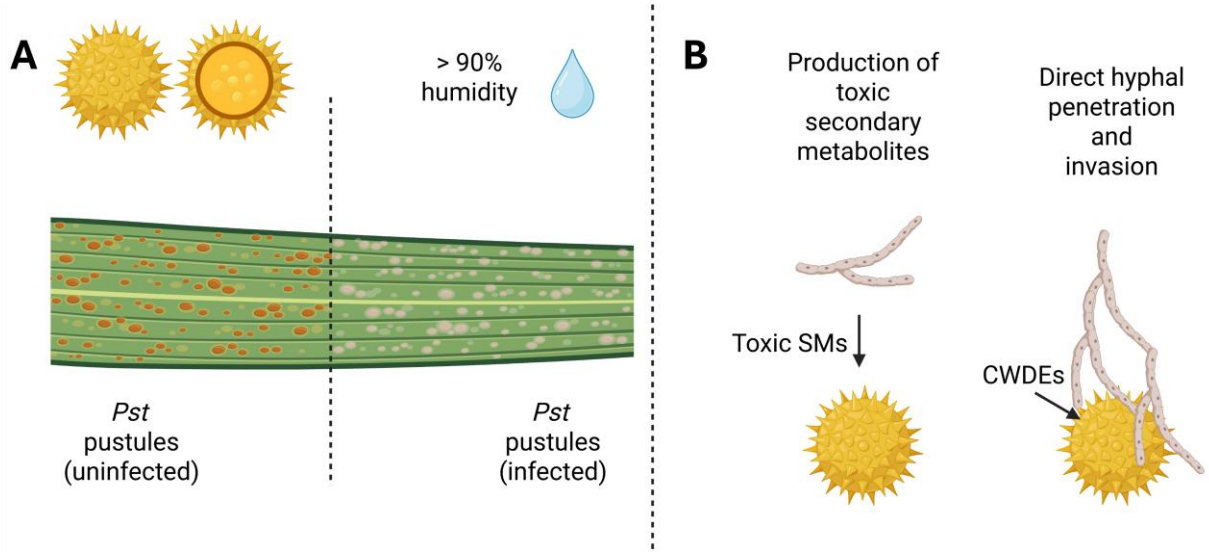

Figure 1.1. A – The pustule niche – infection site of opportunistic hyperparasites as nutrient-dense urediniospores sit exposed in pustules. **B –** Hyperparasites use chemical, enzymatic and mechanical means to suppress, degrade and invade *Pst* spores.

1.5 The promise and the pitfalls

Despite promising laboratory observations, environmental constraints remain a significant barrier to the widespread deployment of rust hyperparasites in field conditions. One of the primary limitations is their reliance on high relative humidity (>90%) for successful spore colonization and proliferation (Zhan *et al.*, 2014). In contrast, *Pst* can thrive under moderate humidity and temperature ranges (Chen *et al.*, 2014), allowing it to persist even when hyperparasites cannot be established. This climatic mismatch limits the efficacy of live hyperparasites in semi-arid or dryland wheat-growing regions, precisely where rust outbreaks can be most devastating.

Research on hyperparasite-rust host interactions often overlooks two crucial components: the plant itself, and its microbiome. Microbes can benefit plant health not only by suppressing pathogens directly, but also by inducing systemic resistance through activation of plant defence mechanisms, as seen with biocontrol-effective isolates of *Trichoderma* (Gomes *et al.*, 2017). The ability to induce plant resistance coupled while directly targeting *Pst* spores has been shown by the hyperparasites *Penicillium simplicissimum* and *Trichoderma asperellum* (Esmail *et al.*, 2022). Research has assessed the impact of *Trichoderma* isolates on the wheat microbiome, including beneficial microbes, to identify the most suitable isolates for specific biocontrol functions (Alukumbura *et al.*, 2022). Therefore, the interplay between parasite, plant and microbiome, encompassing both mutualistic and potentially harmful relationships, should be thoroughly examined before deploying any hyperparasitic fungi as biological control agents against *Pst*. Hyperparasites are not plug-and-play biocontrol tools but living components of complex ecological networks. Understanding and respecting that complexity is the first step toward successful, sustainable deployment.

1.6 Future directions: From organisms to molecules

Future efforts may benefit from identifying and isolating the key metabolites and enzymes involved in hyperparasitism that can be decoupled from the organism and used as biocontrol agents. Recombinant production of antifungal proteins or chemical synthesis of bioactive SMs could enable applications under field conditions where humidity requirements cannot be met. Additionally, genetic and metabolic characterization of effective hyperparasites will be essential to develop formulations that balance ecological compatibility with efficacy.

1.7 Bibliography

Ali, S., Rodriguez-Algaba, J., Thach, T., Sørensen, C. K., Hansen, J. G., Lassen, P., Nazari, K., Hodson, D. P., Justesen, A. F., & Hovmøller, M. S. (2017). Yellow rust epidemics worldwide were caused by pathogen races from divergent genetic lineages. Frontiers in Plant Science, 8. https://doi.org/10.3389/fpls.2017.01057

Alukumbura, A. S., Bigi, A., Sarrocco, S., Fernando, W. G. D., Vannacci, G., Mazzoncini, M., & Bakker, M. G. (2022). Minimal impacts on the wheat microbiome when *Trichoderma gamsii* T6085 is applied as a biocontrol agent to manage *Fusarium* head blight disease. Frontiers in Microbiology, 13. https://doi.org/10.3389/fmicb.2022.972016

Chen, W., Wellings, C., Chen, X., Kang, Z., & Liu, T. (2014). Wheat stripe (yellow) rust caused by *Puccinia striiformis* f. sp. *tritici*. Molecular Plant Pathology, 15(5), 433-446. https://doi.org/10.1111/mpp.12116

Esmail, S. M., Draz, I. S., Saleem, M. H., Mumtaz, S., & Elsharkawy, M. M. (2022). *Penicillium simplicissimum* and *Trichoderma asperellum* counteract the challenge of *Puccinia striiformis* f. sp. *tritici* in wheat plants. Egyptian Journal of Biological Pest Control, 32(1), 116. https://doi.org/10.1186/s41938-022-00614-7

Fravel, D. R. (1988). Role of Antibiosis in the Biocontrol of Plant Diseases*. Annual Review of Phytopathology, 26, 75-91. https://doi.org/https://doi.org/10.1146/annurev.py.26.090188.000451

Gomes, E. V., Ulhoa, C. J., Cardoza, R. E., Silva, R. N., & Gutiérrez, S. (2017). Involvement of *Trichoderma harzianum* Epl-1 Protein in the regulation of *Botrytis* virulence- and tomato defense-related genes. Frontiers in Plant Science, 8. https://doi.org/10.3389/fpls.2017.00880

Lorrain, C., Gonçalves dos Santos, K. C., Germain, H., Hecker, A., & Duplessis, S. (2019). Advances in understanding obligate biotrophy in rust fungi. New Phytologist, 222(3), 1190-1206. https://doi.org/https://doi.org/10.1111/nph.15641

Nasini, G., Arnone, A., Assante, G., Bava, A., Moricca, S., & Ragazzi, A. (2004). Secondary mould metabolites of *Cladosporium tenuissimum*, a hyperparasite of rust fungi. Phytochemistry, 65(14), 2107-2111. https://doi.org/10.1016/j.phytochem.2004.03.013

Rehman, S. U., Qiao, L., Shen, T., Hua, L., Li, H., Ahmad, Z., & Chen, S. (2024). Exploring the frontier of wheat rust resistance: latest approaches, mechanisms, and novel insights. Plants, 13(17), 2502.

Schwessinger, B. (2017). Fundamental wheat stripe rust research in the 21st century. New Phytologist, 213(4), 1625-1631. https://doi.org/10.1111/nph.14159

Speckbacher, V., & Zeilinger, S. (2018). Secondary metabolites of mycoparasitic fungi. Secondary metabolites-sources and applications, 37-55.

Srivastava, A. K., Défago, G., & Kern, H. (1985). Hyperparasitism of *Puccinia horiana* and other microcyclic rusts. Journal of Phytopathology, 114(1), 73-78. https://doi.org/10.1111/j.1439-0434.1985.tb04338.x

Staples, R. C., & Wynn, W. K. (1965). The physiology of uredospores of the rust fungi. The Botanical Review, 31(4), 537-564. https://doi.org/10.1007/BF02858608

Tulloch, A. P., Craig, B. M., & Ledingham, G. A. (1959). The oil of wheat stem rust uredospores: II. The isolation of *cis*-9,10-epoxyoctadecanoic acid, and the fatty acid composition of the oil. Canadian Journal of Microbiology, 5(5), 485-491. https://doi.org/10.1139/m59-060

Wang, N., Fan, X., Zhang, S., Liu, B., He, M., Chen, X., Tang, C., Kang, Z., & Wang, X. (2020). Identification of a hyperparasitic *Simplicillium obclavatum* strain affecting the infection dynamics of *Puccinia striiformis* f. sp. *tritici* on wheat. Frontiers in Microbiology, 11. https://doi.org/10.3389/fmicb.2020.01277

Wellings, C. R. (2011). Global status of stripe rust: a review of historical and current threats. Euphytica, 179(1), 129-141. https://doi.org/10.1007/s10681-011-0360-y

Wess, J., Hu, Y., Periyannan, S., Jones, A., & Rathjen, J. P. (2025). Global transcriptome changes during growth of a novel *Penicillium coffeae* isolate on the wheat stripe rust fungus, *Puccinia striiformis* f. sp. *tritici*. Fungal Genetics and Biology, 176, 103956. https://doi.org/https://doi.org/10.1016/j.fgb.2024.103956

Wilson, A., Cuddy, W. S., Park, R. F., Harm, G. F. S., Priest, M. J., Bailey, J., & Moffitt, M. C. (2020). Investigating hyperparasites as potential biological control agents of rust pathogens on cereal crops. Australasian Plant Pathology, 49(3), 231-238. https://doi.org/10.1007/s13313-020-00695-8

Zhan, G., Tian, Y., Wang, F., Chen, X., Guo, J., Jiao, M., Huang, L., & Kang, Z. (2014). A novel fungal hyperparasite of *Puccinia striiformis* f. sp. *tritici*, the causal agent of wheat stripe rust. PLoS One, 9(11), e111484. https://doi.org/10.1371/journal.pone.0111484

Zhang, H., He, M., Fan, X., Dai, L., Zhang, S., Hu, Z., & Wang, N. (2022). Isolation, identification and hyperparasitism of a novel *Cladosporium cladosporioides* isolate hyperparasitic to *Puccinia striiformis* f. sp. *tritici*, the wheat stripe rust pathogen. Biology, 11(6), 892.

Zheng, L., Zhao, J., Liang, X., Zhan, G., Jiang, S., & Kang, Z. (2017). Identification of a novel *Alternaria alternata* strain able to hyperparasitize *Puccinia striiformis* f. sp. *tritici*, the causal agent of wheat stripe rust. Frontiers in Microbiology, 8. https://doi.org/10.3389/fmicb.2017.00071

Chapter Two

Global transcriptome changes during growth of a novel *Penicillium coffeae* isolate on the wheat stripe rust fungus, *Puccinia striiformis* f. sp. *tritici*

"One sometimes finds what one is not looking for" – Alexander Fleming

A fungus discovered growing on *Pst* pustules entirely by chance became the starting point for my journey into rust hyperparasitism and all of the research presented in this thesis. In this chapter I introduce *Penicillium coffeae* ANU01, its genes, and how it might use them to act as a rust hyperparasite.

Wess, J., Hu, Y., Periyannan, S., Jones, A., & Rathjen, J. P. (2025). Global transcriptome changes during growth of a novel *Penicillium coffeae* isolate on the wheat stripe rust fungus, *Puccinia striiformis* f. sp. *tritici*. Fungal Genetics and Biology, 176, 103956. https://doi.org/https://doi.org/10.1016/j.fgb.2024.103956

Fungal Genetics and Biology 176 (2025) 103956

Contents lists available at ScienceDirect

Fungal Genetics and Biology

journal homepage: www.elsevier.com/locate/yfgbi

Global transcriptome changes during growth of a novel *Penicillium coffeae* isolate on the wheat stripe rust fungus, *Puccinia striiformis* f. *sp. tritici*

Jack Wess, Yiheng Hu [1], Sambasivam Periyannan [2], Ashley Jones, John P. Rathjen [*]

Research School of Biology, The Australian National University, 134 Linnaeus Way, Canberra, ACT 2601, Australia

ARTICLE INFO

Keywords:
Hyperparasitism
Penicillium
Genome
Transcriptome
Stripe rust
Metabolism

ABSTRACT

Wheat stripe rust caused by the fungus *Puccinia striiformis* f. *sp. tritici* (*Pst*) is currently the most destructive disease of wheat. The major control methods which include the deployment of resistant wheat cultivars and application of chemical fungicides are losing efficiency as the fungus evolves. Natural antagonists of *Pst* may be an avenue for alternative and environmentally sustainable control of the disease in the field. Here we describe a novel fungus found growing on *Pst* pustules. We identified the fungus as a novel isolate of the plant endophyte *Penicillium coffeae*. We present a high-quality reference genome and a comparative transcriptomic analysis used to investigate how the fungus deploys its genes during growth amongst *Pst* spores. The gene content of the *P. coffeae* ANU01 genome is suggestive of a generalist that makes use of diverse substrates. An abundance of genes related to lipid, amino acid and carbohydrate metabolism indicate that *P. coffeae* ANU01 has evolved the ability to exploit nutrient stores in *Pst* urediniospores. *P. coffeae* ANU01 deploys a number of biosynthetic gene clusters during growth on *Pst* spores, potentially to inhibit urediniospores germination and halt defence responses. A number of genes encoding carbohydrate active enzymes are also highly upregulated, suggesting targeting and degradation of *Pst* urediniospores structures. Alongside carbohydrates, *P. coffeae* ANU01 appears to target spore lipids as a nutrient source, secreting several highly upregulated lipases. Our findings broaden the understanding of growth associated with rust spores as an evolutionary strategy and provide insight into the genes potentially required for this process.

1. Introduction

Wheat is one of the most important crops worldwide supplying approximately 20 % of human calories (Hartmann et al., 2017). Diseases caused by fungal plant pathogens are some of the greatest contributors to wheat yield losses worldwide and are a major threat to global food security (Godfray et al., 2016). Rusts are amongst the most important fungal diseases on wheat causing USD $4.3–5.0 billion in losses annually (Figueroa et al., 2018). Wheat stripe rust, caused by the pathogen *Puccinia striiformis* f. *sp. tritici* (*Pst*), is currently the most destructive disease on wheat and exists on all continents where wheat is grown (Schwessinger, 2017).

Classical methods of fungal control include breeding wheat cultivars with resistance traits and the application of fungicides. Development of resistant cultivars is difficult and slow (Summers and Brown, 2013). Newly developed cultivars might maintain resistance for only a few years before they are overcome by the rapidly evolving fungus (Sobhy Draz, 2019). This has led to an increased reliance on chemical fungicides, which in turn leads to the evolution of fungicide-resistant fungi (Estep et al., 2015). Fungicides are also under increased regulatory scrutiny due to their harmfulness both to human health and the environment (European Food Safety et al., 2018). Whilst these regulations protect the health of the environment, they may come at the cost of food security.

Biocontrol agents (BCA) provide options to traditional fungal control methods with the potential for economic and environmental sustainability. A biocontrol involves the intentional release of a BCA into the environment to control a pest or disease (Barratt et al., 2018). Fungal hyperparasites are well suited to this role. A hyperparasite is a parasitic organism whose host is also itself a parasite (Parratt and Laine, 2016).

* Corresponding author.
E-mail addresses: jack.wess@anu.edu.au (J. Wess), yiheng.hu@zmbp.uni-tuebingen.de (Y. Hu), sambasivam.periyannan@unisq.edu.au (S. Periyannan), ashley.jones@anu.edu.au (A. Jones), john.rathjen@anu.edu.au (J.P. Rathjen).
[1] Current address: Microbial Interactions in Plant Ecosystems, Center for Plant Molecular Biology, University of Tübingen, 72076 Tübingen, Germany.
[2] Current address: School of Agriculture and Environmental Science, University of Southern Queensland, Toowoomba Campus, 4350 Toowoomba, Australia.

https://doi.org/10.1016/j.fgb.2024.103956
Received 23 May 2024; Received in revised form 13 December 2024; Accepted 20 December 2024
Available online 17 January 2025
1087-1845/Crown Copyright © 2025 Published by Elsevier Inc. All rights are reserved, including those for text and data mining, AI training, and similar technologies.

Several *Trichoderma spp.* are used successfully as biocontrol products, for example Trichodex™, as an alternative to chemical fungicides (Topolovec-Pintarić, 2019).

Molecular mechanisms underlying fungal hyperparasitism are generally poorly described. They include the production of toxic secondary metabolites (SMs), and direct invasion of the host *via* the action of cell-wall degrading enzymes (Howell, 2003). Production of SMs is often coordinated by biosynthetic gene clusters (BGCs), groups of adjacent genes that are associated with SM synthesis and secretion (Medema et al., 2015). One such SM is 6-n-pentyl-2H-pyran-2-one (6PAP) produced by several species of *Trichoderma*, which is necessary for hyperparasitism (Jeleń et al., 2014). Carbohydrate Active enZYmes (CAZYs), groups of carbohydrate hydrolysis enzymes with diverse functions, also contribute. Recently, Eitzen et al. (2021) used a combination of comparative transcriptomics and gene knockouts to discover a secreted glycoside hydrolyse (GH) 25 lysozyme CAZY required for fungal hyperparasitism of an oomycete pathogen of *Arabidopsis thaliana.*

Fungi that parasitise cereal rust fungi remain under-researched. Novel isolates of *Alternaria alternata, Cladosporium cladosporioides* and *Simplicillium obclavatum* have been described as *Pst* hyperparasites (Zhan et al., 2014; Zheng et al., 2017; Wang et al., 2020). These studies observed the hyphae of each species physically invading *Pst* urediniospores. More recently, Wilson et al. (2020) found that an isolate of *Penicillium brevicompactum* was capable of controlling *P. coronata* var. *avenae* germination without colonising rust pustules, suggesting the production of an antifungal secondary metabolite. One *Penicillium simplicissimum* isolate controlled *Pst via* induction of resistance genes in the plant itself, as well as physical invasion and production of SMs (Esmail et al., 2022). These reports help to understand pathogenesis mechanisms but neglect the underlying genetic and transcriptomic mechanisms.

Here we report *Penicillium coffeae* ANU01 as an associated fungus and potential hyperparasite of *Pst*. It was discovered growing on *Pst* pustules on wheat within a controlled plant growth cabinet. We describe its identification, assemble its genome and analyse its transcriptomic profiles to uncover its molecular strategies for growth on *Pst*.

2. Materials and methods

2.1. Fungal materials

The wheat stripe rust pathogen *Puccinia striiformis* f. *sp. tritici (Pst)* isolate 104 E137 A- (Schwessinger et al., 2018) was used for all parts of this research and maintained as dried urediniospores stocks at −80 °C. *Penicillium coffeae* isolate ANU01 was discovered in a plant growth cabinet within the Controlled Environment Facility at the Research School of Biology, The Australian National University (RSB, ANU), growing as white fluffy tissue on *Pst* 104 E137 A- pustules on wheat. Some white fluffy tissue was scraped from excised leaves and used to inoculate potato dextrose agar plates (PDA; 25 g/l potato dextrose broth, 15 g/l agar). Plates were incubated in a controlled temperature room at 22 °C under a 12 h day/night cycle to allow growth of mature flat circular colonies with pale blue-grey colouration. Once colonies were mature, the fungus was maintained *via* subculturing onto PDA plates and as 25 % glycerol stocks at −80 °C. Glycerol stocks were made by mixing 500 µl 50 % glycerol (*v*/v) solution with 500 µl spore suspension (made as below) in an autoclaved cryofreeze tube (SSIBIO), and stored at −80 °C.

2.2. Growth of P. coffeae ANU01 on Pst urediniospores on the surface of wheat leaves

Eight pots of wheat (cv.) Morocco containing 15 seedlings each were grown and half were infected as described below (comparative transcriptomics section). All pots were subsequently moved to a growth chamber under a 16 h/8 h day/night cycle with a light intensity of 100 µmol m^{-2} s^{-1} and allowed to grow until *Pst* pustules appeared on the infected wheat (13 dpi). At this point plants from two pots of infected wheat and two pots of uninfected wheat were each sprayed with 2 ml of *P. coffeae* ANU01 spore suspension (made as below). Wheat in the remaining pots were sprayed with 2 ml of sterile MQ water. All wheat pots were enclosed in transparent cellophane sleeves and returned to the growth chamber. Three leaf samples from each condition were collected at 0 h (immediately after spraying), 3 d and 6 d post spraying, imaged under a dissection microscope and stored at −20 °C. A leaf disc (4 mm) was taken from each leaf sample, for a total of 36 discs. DNA was isolated from the 36 samples as described by Liu et al. (2000), each sample of DNA was eluted in 70 µl of nuclease-free water. DNA was used in a qPCR reaction using the *P. coffeae* ANU01 specific primers FQ5 (5' ACCCTGAACGCTGTCTGAAG 3′) and RQ6 (5' CGCTGCGTTCTTCATCGATG 3′). Each 10 µl qPCR reaction contained 5 µl of Fast SYBR™ Green Master Mix (ThermoFisher), 1.5 µl of each primer (10 µM), 1 µl of DNA-sample and 1 µl of nuclease-free water, three technical replicates were conducted for each sample. Cycle-threshold (Ct) values for samples collected at 3 d and 6 d were subtracted from their mean Ct at 0 h to calculate ΔCt for these time points. The ΔCt for each point was then converted into fold-change difference in biomass *via* the formula: 2^ (ΔCt). Fold-change values for *P. coffeae* ANU01 biomass over the two time points were plotted in a bar graph.

2.3. Growth of P. coffeae ANU01 on Pst urediniospores in vitro

Approximately 10 mg of *Pst* urediniospores were suspended in 2 ml of NovecTM7100 (3 M), mixed thoroughly and dispensed in 50 µl aliquots onto the surface of sterile glass microscope slides. The dried *Pst* patches were then inoculated with 10 µl of *P. coffeae* ANU01 spores (5,000,000 spores/ml MQ water) or sterile MQ water (*Pst* only controls). Additionally, a *Pst*-absent control was included which consisted solely of 10 µl of the *P. coffeae* ANU01 spore suspension. Microscope slides were placed in Petri dishes, sealed with parafilm and grown in a controlled temperature room at 22 °C under a 12 h day/night cycle. Microscope images of the slides were taken at 7 days post inoculation.

2.4. Internal transcribed spacer (ITS) phylogenies

The sequences for the *ITS* regions of 417 *Penicillium* species were imported manually to the Geneious Prime® (Dotmatics) software from the National Center for Biotechnology Information (NCBI) nucleotide database. Genomic DNA was isolated from *P. coffeae* ANU01 hyphal tissue growing on PDA plates using a DNeasy plant mini kit (QIAGEN). The *ITS* region was amplified from genomic DNA using PCR with the primers ITS1F (5' CTTGGTCATTTAGAGGAAGTAA 3′) and LR6 (5' CGCCAGTTCTGCTTACC 3′). The resulting amplicon was sequenced using Sanger sequencing and the output sequence imported into Geneious Prime® (Dotmatics). An alignment was generated using all imported *ITS* sequences and the default 'Geneious alignment' algorithm. From this alignment, a phylogenetic tree was built using the Tamura-Nei Neighbor-Joining method. A tree was built from this tree using the Bootstrap resampling method and 100 replicates. After establishing *P. coffeae* ANU01 as a member of the clade shown in Fig. 2, *ITS* sequences for all isolates of species within the clade were downloaded from NCBI and constructed into a second phylogenetic tree also using the Tamura-Nei Neighbor-Joining method, with a tree built using the bootstrap resampling method and 100 replicates.

2.5. Long-read DNA sequencing

Spore and mycelial tissues were scraped from the surface of *Penicillium* colonies (~6.5 cm diameter) grown on PDA media. Genomic DNA was isolated using a method optimized for extraction of high molecular weight DNA (Jones et al., 2021). Prior to the chemical lysis step, tissue was homogenised in 2 ml microfuge tubes using two sterile ball bearings and the TissueLyserLT (Qiagen) apparatus for four rounds of thirty

seconds at 25 Hz. DNA was isolated from solution *via* the addition of Sera-Mag (Cytiva) DNA-binding beads, which were then washed three times with 70 % EtOH, before elution in 52 µl of nuclease-free water. DNA was quantified on a Qubit® 2.0 Fluorometer (Broad Range) (Invitrogen), and purity was assessed on Nanodrop™ (ThermoFisher) and Quickdrop™ Micro-Volume Spectrophotometers (SpectraMax®). About 9.2 µg of pure genomic DNA was loaded onto a 0.75 % PippinHT Gel Casette (Sage Science) for ≥15 kb size selection and clean-up following the manufacturer's protocol. From this, 1.6 µg of DNA was used in library preparation using the 1D-ligation SQK-LSK110 kit (Oxford Nanopore Technologies) following the manufacturer's instructions. A total of 400 ng prepared DNA was loaded onto a Nanopore FLO-MIN106D 9.4.1 Flowcell (Oxford Nanopore Technologies) and sequenced on a MinION™ Mk1B device (Oxford Nanopore Technologies). The Guppy (v4.2.2) (Oxford Nanopore Technologies) script was used for base calling, using the super accuracy (sup) configuration file.

2.6. Short-read sequencing

Paired-end Illumina sequence reads (150 bp) were generated from *P. coffeae* ANU01 tissue growing axenically on PDA. Spore and mycelial tissue were isolated and disrupted as above and DNA was isolated using the DNeasy Plant Mini Kit (QIAGEN) following manufacturers' protocols. Paired-end reads were trimmed of adapters using the TrimGalore (v0.6.6) software (Martin 2011) and parameters '-q 20 –nextera –paired'. The quality of Illumina reads was checked with the FASTQC software (Andrews, 2010).

2.7. Bioinformatics

Details of the software used in this methods section, as well as links to their respective Github pages are available at the Github for this project: https://github.com/Jack-WessANU/Genomics_of_a_Pst_hyperparasite

2.8. Genome assembly

Adapters were trimmed from Nanopore reads using Porechop (v0.2.4) (Wick, 2018). The quality and length of basecalled Nanopore reads were assessed with NanoPlot (v1.36.2) (De Coster et al., 2018). Reads were subset into different groups based on length and Phred score using the Nanofilt (v2.7.1) software (De Coster et al., 2018). Nanopore reads >10 kb and Phred score > 8 were assembled into a preliminary scaffold using Canu (v2.1.1) (Koren et al., 2017). The draft assembly was polished with 10 iterations of the Medaka (v1.2.1) polishing tool (Oxford Nanopore Technologies) using the original long reads as input. The assembly was further polished with Illumina data and the POLCA polishing tool (Zimin and Salzberg, 2020). In the finished assembly, telomeric repeats were identified using the FindTelomeres python script developed by Sperschneider (2020). Completeness of the assembly was assessed with a BUSCO (v4.1.4) analysis using the *Eurotiales* dataset (Simão et al., 2015).

2.9. Genome dotplot

The *P. chermesinum* IBT 19713 (GCA_028974085.1) genome sequence was downloaded from the NCBI nucleotide database and aligned with the *P. coffeae* ANU01 genome using the nucmer (v4.0.0rc1) software (Marçais et al., 2018). The resulting delta file was processed with the DotPrep.py script and visualised with the Dot software (Nattestad, 2023).

2.10. Genome annotation

Functional annotation of the *P. coffeae* ANU01 genome was completed using the funannotate (v1.5.3) pipeline with the assistance of Dr. Benjamin Schwessinger (RSB, ANU) (Palmer and Stajich, 2019). Raw Illumina RNAseq reads (see Comparative transcriptomics section below) were downloaded from the GeneWiz server and trimmed using the Trimmomatic (v0.39) software (Bolger et al., 2014). The trimmed RNAseq reads for all samples were merged and used in the funannotate pipeline to annotate the genome. The *P. coffeae* ANU01 transcriptomes generated in this annotation were used for all downstream transcriptomic analyses.

The *P. coffeae* ANU01 mitochondrial genome was annotated with the GeSeq annotation software (Tillich et al., 2017), using *P. citrinum, P. digitatum, P. polonicum, P. roqueforti* and *P. solitum* as references. To identify possible duplication, the mitogenome was aligned against itself to produce a dotplot using the software Gepard (v2.0) (Krumsiek et al., 2007). This revealed that the contig contained two identical assemblies of the mitogenome in tandem; the second copy was removed.

2.11. Comparative transcriptomics

Twelve pots each containing 15 wheat cultivar (cv.) Morocco seedlings were watered with 200 ml (over all pots) 0.5 % (*v*/v) maleic hydroxide at six days post planting. At eight days post planting, approximately 0.2 g of *Pst* 104 E137 A- spores were suspended in 2 ml of Novec™7100 (3 M) and applied evenly to seedling leaves with a paintbrush. Seedlings were moved to a plastic container and kept at 8 °C and 100 % relative humidity (RH) for 48 h to promote *Pst* germination and infection. After 48 h, seedlings were moved to a new growth chamber and kept under a 16 h/8 h day/night cycle with a light intensity of 100 µmol m^{-2} s^{-1}. Fourteen days post infection (dpi), plants were sprayed with a *P. coffeae* ANU01 spore suspension made as follows: Three PDA plates containing mature (~6.5 cm diameter) *P. coffeae* ANU01 colonies were flooded with sterile water and a sterile razor blade used to scrape spore and mycelial tissue from the agar surfaces. Fungal debris was filtered from the spore suspension using Miracloth (Merck Millipore) and the filtrate transferred to a sterile spray bottle. This suspension was sprayed evenly onto rust pustules on the infected wheat plants. The sprayed pots were covered individually with transparent cellulose sleeves to create a humid atmosphere necessary for hyperparasitism (Zhan et al., 2014). Fluffy white tissue indicative of *P. coffeae* ANU01 growth was observed on the surface of rust pustules at 8 dpi. For sampling, the pots were split into three groups of four to create three biological replicates and tissue was harvested 24 h later. *Penicillium coffeae* ANU01 tissue was scraped from the surface of leaves into 2 ml microfuge tubes and flash frozen in liquid nitrogen. Tissue was collected over three days and combined into three fresh 2 ml microcentrifuge tubes (one per replicate) each containing two clean steel ball bearings. For *in vitro* samples, spore and mycelial tissues were scraped from the surface of mature (~4.5 cm diameter) colonies cultured on PDA into 2 ml Eppendorf tubes containing two clean steel ball-bearings. Three plates each containing a single *P. coffeae* ANU01 colony, grown in a temperature-controlled room at 22 °C under a 12 h day/night cycle for 15 days, were used for the three biological replicates. Tubes were immediately snap frozen in liquid nitrogen and all samples were kept at –80 °C until ready for processing.

2.12. RNA extraction and sequencing

For RNA extraction, tissue was disrupted using the TissueLyser LT (QIAGEN) for four rounds of 30 s at 25 Hz. Extracts were processed using the RNeasy® Plant Mini Kit (QIAGEN) following the manufacturer's protocol. RNA samples were eluted in 32 µl RNAse free water supplied with the kit. Concentration and absorbance purity ratios of eluted RNA were assessed using a Quickdrop™ Micro-Volume Spectrophotometer (SpectraMax®). Intactness of the RNA was assessed by running a sample on a 1 % agarose gel as per Green and Sambrook (2019). Half of the volume of each sample was transferred to an individual RNA Stabilization Tube (GeneWiz). All six samples were then shipped to GeneWiz

(Suzhou, China) for library preparation and Illumina sequencing. The 20 million reads per sample option was chosen prior to sending samples.

Prior to quantification, contaminant reads were removed *via* alignment to the wheat genome (GCA_900519105.1) and *Pst* 104 E137 A- (GCA_002900275.1) genomes using the hisat2 software (Kim et al., 2019). Transcript expression in RNAseq samples was quantified *via* mapping filtered reads to the *P. coffeae* ANU01 transcriptome with Salmon (v1.4.0) software from Patro et al. (2017). Salmon outputs were imported into an R-studio session for comparative transcriptomic (differential gene expression) analysis using the Limma package (Ritchie et al., 2015). All code used to generate the comparative transcriptomic analysis (Volcano plot Fig. 7) and GO enrichment dotplots (Fig. 8) are presented in the GitHub page for this project https://github.com/Jack-WessANU/Genomics_of_a_Pst_antagonist.

3. Results

3.1. *Penicillium coffeae* ANU01 grows on wheat stripe rust urediniospores

This study was prompted by the chance observation that infections of wheat with *Pst* sometimes led to growth of white fluffy material on rust pustules when the infected plants were enclosed in cellophane bags within a growth cabinet (Fig. 1A, B). We sampled the fluffy material including some *Pst* spores and viewed it under a compound microscope. In addition to the large ovate rust spores, we observed the apparent presence of a filamentous fungus as evidenced by thin elongate branched hyphae and fruiting bodies associated with small spores. Transfer of this material to potato dextrose agar (PDA) plates resulted in slow growing colonies that were pale blue-grey in colour, with blue aerial mycelia. We isolated spores from the plates and used them to inoculate *Pst*-infected wheat. This reproduced the fluffy white pustules phenotype but not in non-inoculated *Pst* controls. We used the new material to inoculate PDA plates and were able to grow fungal colonies of similar colour and morphology as previously. Spores isolated from these plates sprayed onto *Pst*-infected wheat again produced the white fluffy phenotype; this process was repeated a further two times.

To determine whether *P. coffeae* ANU01 growth is increased in the presence of *Pst* on wheat, we measured *P. coffeae* ANU01 biomass on infected and uninfected wheat leaves. We sprayed the wheat leaves with either sterile water or a *P. coffeae* ANU01 spore suspension and collected leaf samples from plants at 3 and 6 d post spraying. After 6 d, *Penicillium coffeae* ANU01 displayed a 40-fold change increase in biomass on infected leaves, compared to only a 4-fold change increase after 6 d in the *Pst*-absent control (Supplementary Fig. 1) [see Additional File 1]. The presence of *Pst* therefore substantially increases growth of *P. coffeae* ANU01 on the wheat leaf. Importantly, microscope images of the leaves at these time points showed no visible growth of *P. coffeae* ANU01 on uninfected wheat, but extensive growth on infected wheat at 6 d post inoculation (Supplementary Fig. 2L, 2F) [see Additional File 1]. The appearance of light/white spots on the leaf surface in 2 L is due to light from the microscope reflecting off the tissue, and is not due to growth of the fungus. This supports the hypothesis that *P. coffeae* ANU01 represents the causative agent and is capable of growth on *Pst* spores. To confirm that the isolate can utilise rust spores for growth, we showed that it can complete its lifecycle on glass slides using *Pst* urediniospores as the sole source of nutrition (Supplementary Fig. 3) [see Additional File 1].

To identify the fungus, we prepared genomic DNA from mycelia and amplified the internal transcribed spacer (*ITS*) region. A preliminary BLAST using the sequenced amplicon suggested that it belongs to the *Penicillium* genus. We next constructed a Tamura-Nei tree based on *ITS* sequences from all *Penicillium* species available on NCBI. This analysis placed the isolate in a clade alongside *P. chermesinum, P. cuddlyae, P. indicum, P. lunae* and closest to *P. coffeae* (Fig. 2). To refine this analysis,

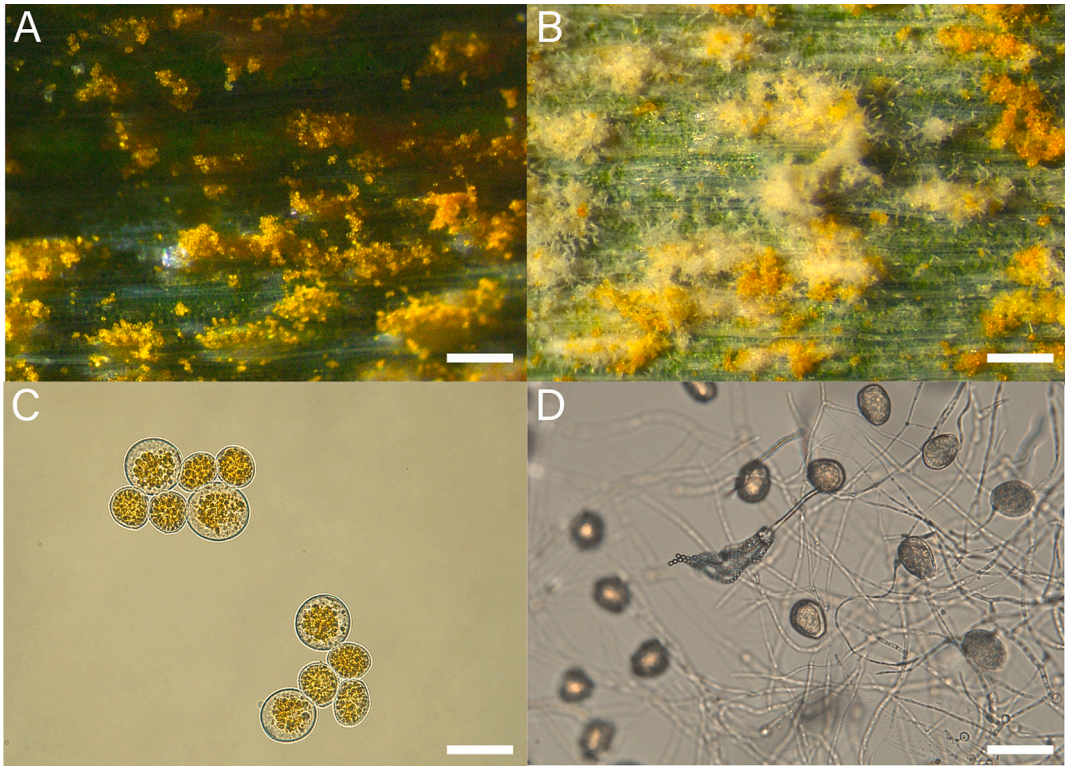

Fig. 1. A novel fungal interaction with *Pst*. A. Uninfected *Pst* pustules growing from the surface of wheat leaves. B. Infected *Pst* pustules on wheat showing white fluffy growth and sporulating tissue. C. Uninfected *Pst* urediniospores. D. Material sampled from *Pst* pustules showing white fluffy growth. The large ovate orange/yellow objects are *Pst* spores. The smaller paint brush-like sporulating structures are *Penicillium* fruiting bodies. Scale bars represent 0.5 mm in A and B and 35 μm in C and D.

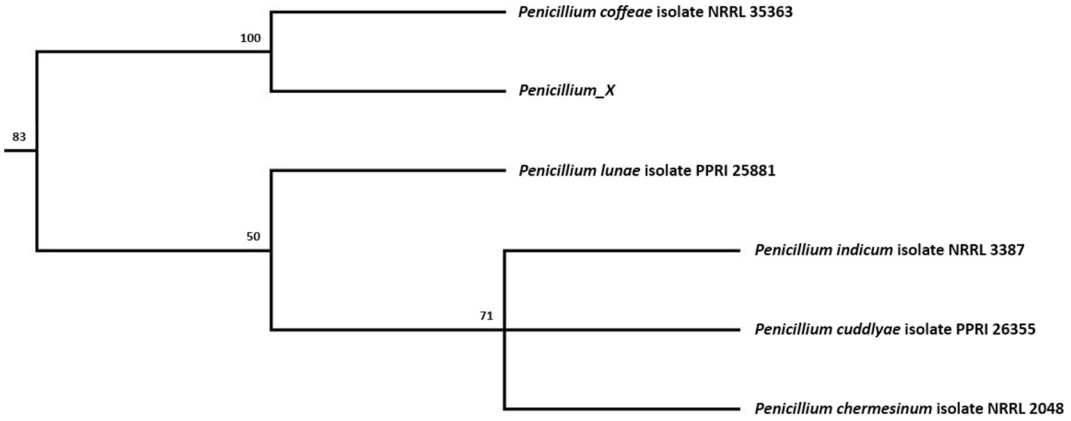

Fig. 2. A node within a larger rooted phylogenetic tree built from Geneious superalignments of *Penicillium spp.* using *ITS* sequences downloaded from NCBI and the amplicon generated here (*Penicillium_X*). The tree was constructed using the Tamura-Nei Neighbor-Joining method in Geneious. Numbers on nodes denote confidence rating output of bootstrapping statistical analysis.

we built a further phylogeny using the *ITS* sequences of the 99 available isolates for the closely related species stated above (Fig. 3). This placed our isolate within a branch that contained only *P. coffeae* isolates, separate from other species within the clade, indicating that it is a novel isolate of this species. Based on this identification and the location of its discovery, we named the fungus *Penicillium coffeae* ANU01.

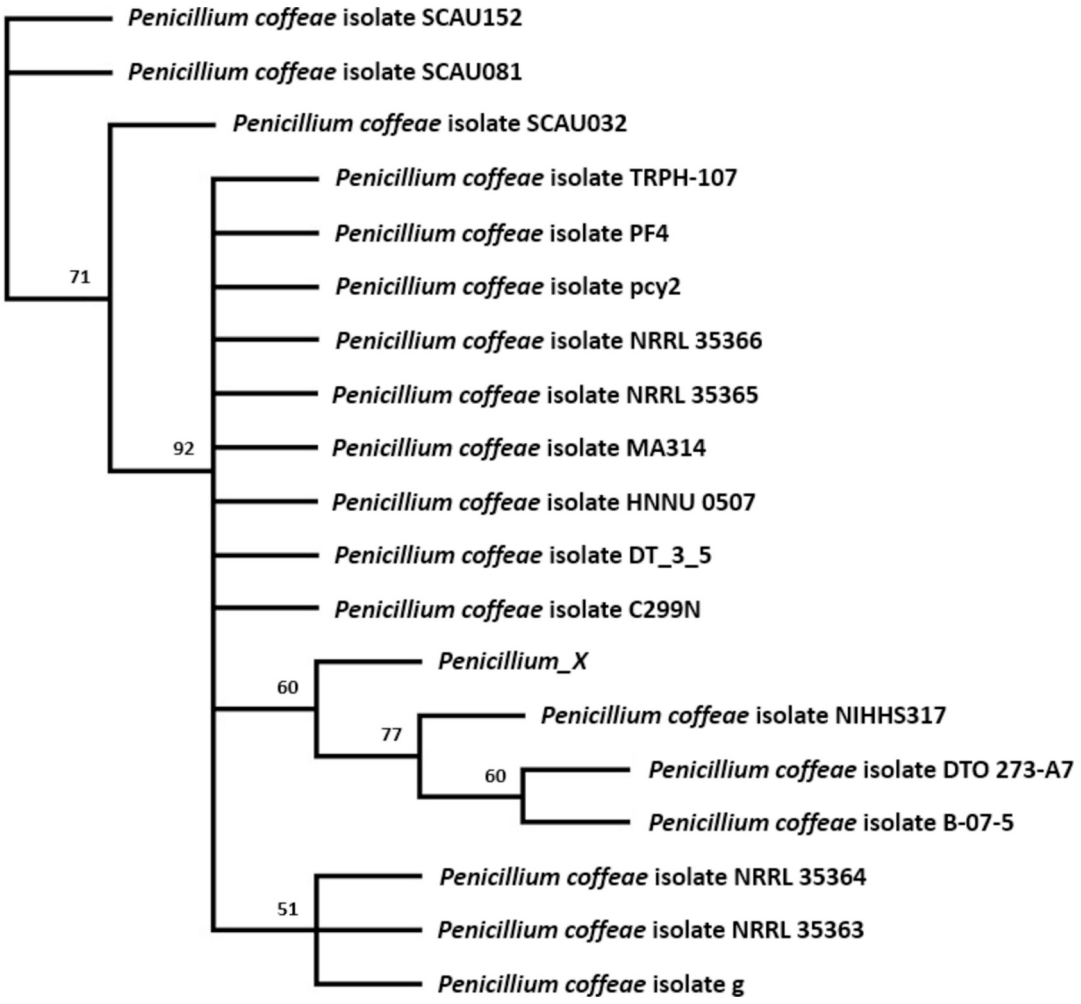

Fig. 3. A node of a larger phylogenetic tree of all available isolates of *Penicillium* within a clade including *Penicillium_X*. The tree was built from Geneious alignments of *ITS* sequences downloaded from the NCBI database, as well as the *Penicillium_X* amplicon generated here. The tree was constructed using the Tamura-Nei Neighbor-Joining method in Geneious. This tree represents a subsample of 18 isolates within a tree of 99 isolates, due to the difficulty in presenting all of the data in the complete tree. A full phylogenetic tree of all 99 isolates is presented in Supplementary Fig. 4.

3.2. Generation of a highly contiguous and complete P. coffeae ANU01 genome assembly

We assembled the *P. coffeae* ANU01 genome by using Nanopore long sequence reads to construct a high-quality scaffold before polishing with both long reads and then Illumina short reads. Briefly, 400 ng of library-prepared high molecular weight DNA was sequenced on an Oxford Nanopore MinION Mk1B device, then basecalled with the Guppy (v4.2.2) software. A total of 575,122 reads were generated with an average read length of 7 kb and an average read quality of Q11.8 Phred score (Table 1). We found that the most contiguous and complete assembly came from using reads subset to a minimum of Q8 Phred score and 10 kb in length. With this increased stringency, mean read length increased to 18,284 bp and the mean read quality to Q13.2 Phred score. Assembly of these reads using the Canu (v2.1.1) software resulted in an assembly with 79× coverage of the approximately 31 Mb genome. A summary of the statistics on the final polished assembly is presented in Table 1. We assessed completeness of the assembly using a BUSCO analysis which identified 4085 complete BUSCOs of a possible 4191, indicating that the assembly is 97.4 % complete.

The final assembly consists of seven linear and one circular contigs, with a total size of 30.9 Mb. The largest and smallest linear contigs were 7.66 Mb and 1.51 Mb respectively. Six linear contigs contained both forward and reverse telomeric regions, whilst the fifth contig contained only a forward telomere.

To compare synteny with a closely related species and help determine if we had achieved a chromosome level assembly, we made a whole genome alignment between *P. coffeae* ANU01 and *P. chermesinum* IBT 19713 (GCA_028974085.1). We chose *P. chermesinum* IBT 19713 due to its close relatedness to *P. coffeae* ANU01 (Fig. 2) and low number of contigs (nine linear, one mitochondrial). A dotplot generated from the alignment is presented in Fig. 4.

The discontinuous diagonal lines in the plot indicate regions of high synteny, with diagonal lines facing upwards representing areas of synteny that have been inverted. The short diagonal lines away from the centre represent areas of weak synteny between the isolates. The second *P. coffeae* ANU01 contig shows the highest synteny with *P. chermesinum* IBT 19713 with two large inversions towards the centre of the contig. The first and fourth *P. coffeae* ANU01 contigs also showed synteny to the *P. chermesinum* sequence. The fifth and seventh *P. coffeae* ANU01 contigs showed the weakest synteny, whilst the third contig showed stronger synteny only towards the beginning and end of the chromosome. The clear difference between the end of the fifth and start of the sixth *P. coffeae* ANU01 contigs suggests that the reverse telomere on the fifth contig is missing from the assembly and does not suggest that a larger contig has been incorrectly assembled. The presence of forwards and reverse telomeres in six of the seven linear contigs and synteny with *P. chermesinum* IBT 19713 contigs suggests that we have assembled a chromosome-level assembly for *P. coffeae* ANU01.

Table 1
Summary statistics for the final polished assembly of the *Penicillium coffeae* ANU01 genome.

Measurement	*Penicillium coffeae* ANU01 genome assembly
Sequencing technology	Nanopore MinION
Assembler	Canu (v2.1.1)
Coverage	79×
# Total contigs	8
# Circular contigs	1
Total length (bp)	30,965,311
Largest contig (bp)	7,664,923
N50	4,566,672
N75	3,598,224
GC content (%)	48.82
# Telomeres - Contiguity	7 forward 6 reverse
BUSCO - *Eurotiales*	
# Complete BUSCOs	4085 (97.4 %)
# Complete and single-copy BUSCOs	4067 (97.0 %)
# Complete and duplicated BUSCOs	18 (0.4 %)
# Fragmented BUSCOs	18 (0.4 %)
# Missing BUSCOs	88 (2.1 %)
# Total BUSCO groups searched	4191

3.3. Assembly of a complete mitochondrial genome

The eighth contig of 55,939 bp assembled by Canu (Koren et al., 2017) was identified as circular using QUAST (Mikheenko et al., 2018), suggesting that it represents the mitochondrial genome. Alignment of the contig to itself to *via* dotplot showed that the contig had been duplicated during assembly (Supplementary Fig. 5A). Removal of the second copy (Supplementary Fig. 5B) resulted in a monomeric contig of 27,970 bp. Functional annotation of the chromosome using software Geseq (Tillich et al., 2017) revealed a characteristic gene set possessing the 14 expected conserved protein coding genes *nad1–6, nad4L*, *atp6, atp8, atp9*, *cob*, and *cox1–3,* as well as the ribosomal protein S3 gene *rps3* (Aguileta et al., 2014). The mitogenome contains the open reading frames (ORFs) *orf239* and *orf285*. The contig contains 39 tRNA genes (including four duplicated and two fragmented genes) and four rRNA genes (one fragmented and one duplicated) (Supplementary Table 2). A graphic representation of the *P. coffeae* ANU01 mitogenome including all annotation and arrangement is presented in Supplementary Fig. 5.

3.4. Functional annotation of the P. coffeae ANU01 genome

We predicted 12,181 genes in the *P. coffeae* ANU01 genome using the funannotate pipeline developed by Palmer and Stajich (2019) using two RNA-seq datasets as inputs (see below). This was produced from 64,456 initial gene models which were reduced by its Evidence Modeler (EVM) module after weighting. Funannotate called 12,732 mRNA transcripts and 118 tRNA transcripts. The average gene size was 1818 bp, with 78.3 % of transcripts containing multiple exons, the average distance between genes was 377.1 bp. Exons were an average length of 516 bp, and protein coding regions an average of 470 bp.

We assessed completeness of the gene set using the Benchmarking Universal Single-Copy Orthologs (BUSCO) software and the *Dikarya* gene set (Simão et al., 2015). A total of 1276 (97.2 %) complete BUSCOs were identified out of a possible 1312. To gain perspective on functional annotation of its genome, we compared the *P. coffeae* ANU01 gene with two other *Penicillium* species not known to parasitise rusts and for which high quality genome assemblies were available. These include *P. oxalicum* I1R1 isolated from the roots of *Ixora chinensis* (Pham et al., 2023), and the post-harvest citrus mould *P. digitatum* PDW03 (Wang et al., 2021). The *Penicillium oxalicum* I1R1 assembly consists of 9 contigs and has a similar sized genome to *P. coffeae* ANU01 (30.8 Mb). The *P. digitatum* PDW03 genome is 26.3 Mb and comprises six chromosomes.

We used a cluster of orthologous genes (COG) analysis to annotate the *P. coffeae* ANU01 gene set. COG terms assign a predicted function to a protein based on its similarity to a database of proteins of known function (Fig. 5) (Galperin et al., 2019). A total of 10,154 protein coding genes (83.3 %) were assigned to a COG category. The five largest groups were “S: Function unknown” (2837 genes, 27.9 %), “G: Carbohydrate transport and metabolism” (767 genes, 7.2 %), “E: Amino acid metabolism and transport” (765 genes, 7.5 %), “Q: Secondary metabolites biosynthesis, transport and catabolism” (746 genes, 7.3 %) and “O: Post-translational modification, protein turnover, chaperone functions” (623 genes, 6.1 %). We defined a functional group as enriched if it contained >50 % more genes than the average of the comparators. For example, *P. coffeae* ANU01 possesses over twice as many genes in the most enriched category; secondary metabolite biosynthesis, transport and catabolism (130 %, 422.5 genes). Similarly, cell wall/membrane/envelope biogenesis (121 %, 90 genes), nuclear structure (115 %), defence mechanisms (100 %, 32 genes), cell motility (100 %, 4 genes), cytoskeleton (72 %, 72 genes), amino acid metabolism and transport (67 %,

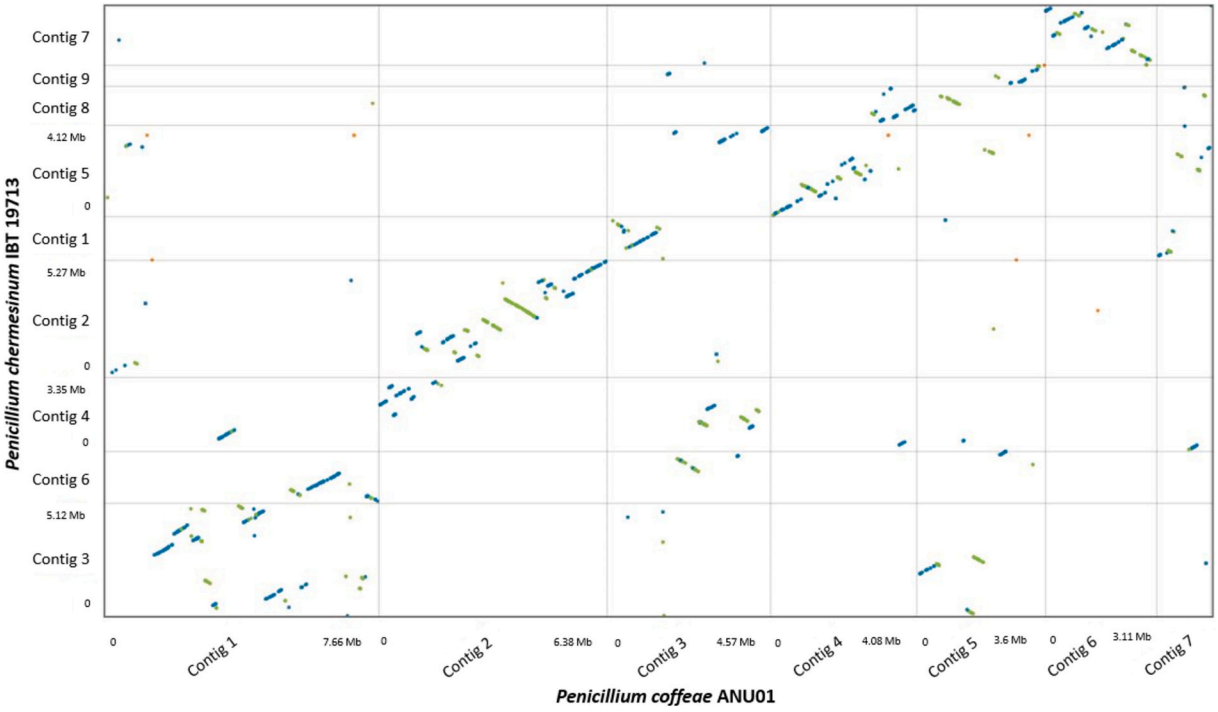

Fig. 4. Dotplot representing a whole genome comparison between isolates *P. coffeae* ANU01 (X axis) and *P. chermesinum* IBT 19713 (Y axis). Dots represent similarity at a given position between the two isolates. Blue dots represent positions with forwards sequence similarity, green dots represent positions of reverse sequence similarity. Vertical grid lines represent the beginning and end of contigs for *P. coffeae* ANU01. Horizontal grid lines represent the beginning and end of contigs for *P. chermesinum* IBT 19713. (For interpretation of the references to colour in this figure legend, the reader is referred to the web version of this article.)

309 genes), lipid transport and metabolism (62 %, 181 genes), carbohydrate transport and metabolism (57 %, 280 genes), energy production and conversion (56 %, 182 genes), transcription (56 %, 212.5 genes) and inorganic ion transport and metabolism (53 %, 127 genes) are enriched. The gene set appears to be enriched in areas related to nutrition, specifically protein, carbohydrate and lipid metabolism, and a large number of SM genes with possible roles in microbial antagonism and defence.

Carbohydrate-Active enZymes (CAZys) are involved in the degradation, assembly and modification of carbohydrates (Lombard et al., 2014). Rust urediniospores are rich in carbohydrates (~22 %), including spore coats and glycogen stores (Staples and Wynn, 1965). The *P. coffeae* ANU01 genome contains a total of 435 genes encoding CAZYs (Fig. 6). The most abundant subcategory is glycoside hydrolases (GHs) comprising of 205 genes, followed by 84 glycosyl transferases (GTs), 69 carbohydrate esterases (CEs), 67 auxiliary activities (AAs), 7 carbohydrate-binding modules (CBMs) and three polysaccharide lyases (PLs). With the exception of CE and AA content, the CAZY content of *P. coffeae* ANU01 more closely resembles the post-harvest mould *P. digitatum* PDW03 than *P. oxalicum* I1R1. This suggests an ability to target plant tissue opportunistically. Interestingly, *P. coffeae* ANU01 possesses very few PLs, genes that could be important for degrading the *Pst* spore coat (Michaud et al., 2003). *Penicillium coffeae* ANU01 possessed 25 more CEs than *P. oxalicum* and 56 more than *P. digitatum*. This expanded gene content might suggest that carbohydrate esterases play a role in the interaction between *P. coffeae* ANU01 and rust spores. The CAZY content of *P. coffeae* ANU01 is diverse, indicating that the substrates that it is adapted to make use of are also diverse. The fungus may be more adapted to life as a generalist that has acquired specific CAZYs or can use its generalist CAZYs to feed on *Pst* spores when they are present.

3.5. The biosynthetic gene cluster (BGC) content of Penicillium coffeae ANU01

Biosynthetic gene clusters (BGCs) are clustered groups of genes associated with the production of specific secondary metabolites such as toxins (Medema et al., 2015). We used antiSMASH complimented with our RNAseq data to predict 43 BGCs in *P. coffeae* ANU01. Seven different BGC types were identified including 13 Type 1 polyketide synthases (T1PKS), ten nonribosomal peptide synthases (NRPS) and eight NRPS-like BGCs, eight terpene BGCs, two indole BGCs, one betalactone BGC and one fungal ribosomally synthesised and post-translationally modified peptide (RiPP) BGC. A summary of the total BGC content of *P. coffeae* ANU01 is shown in Supplementary Table 3 [see Additional file 1]. Full clusters (100 % similarity) were identified for biosynthesis of choline and fellutamide B by comparison to characterised BGCs of *Aspergillus nidulans*. Fellutamide B is capable of potent inhibition of the *Mycobacterium tuberculosis* proteasome (Lin et al., 2010). We also identified BGCs for synthesis of ACR-toxin, which underlies virulence of *Alternaria alternata* causing rough lemon leaf spot disease (Gardner et al., 1985), and burnettiene A, an *Aspergillus burnettii* SM which is cytotoxic on mouse myeloma cells (Roux et al., 2021). Finally, we found a full cluster for clavaric acid biosynthesis first identified in *Hypholoma sublateritium* (Godio and Martín, 2009). Partial clusters were found for nidulanin A synthesis (75 % identity) from *Aspergillus nidulans* (Raffa and Keller, 2019) and the fusarochromanone BGC (70 %) of *Fusarium equisetii* (Mahdavian et al., 2014). *Penicillium coffeae* ANU01 possesses clusters similar to the depudecin BGC (66 %) of *Alternaria brassicicola* and the squalestatin BGC (60 %) of *Aspergillus sp.* Z5 (Bonsch et al., 2016; Wight et al., 2009). Loss of function depudecin mutants showed a small but significant reduction in virulence against *Brassica oleracea*. Depudecin also exhibits moderate toxic activity against the protozoan *Plasmodium* and the fungus *Neospora caninum* (Kwon et al., 2003). The composition of the cluster is variable with the efflux transporter (*DEP3*) and transcription factor (*DEP6*) genes most commonly present (Reynolds

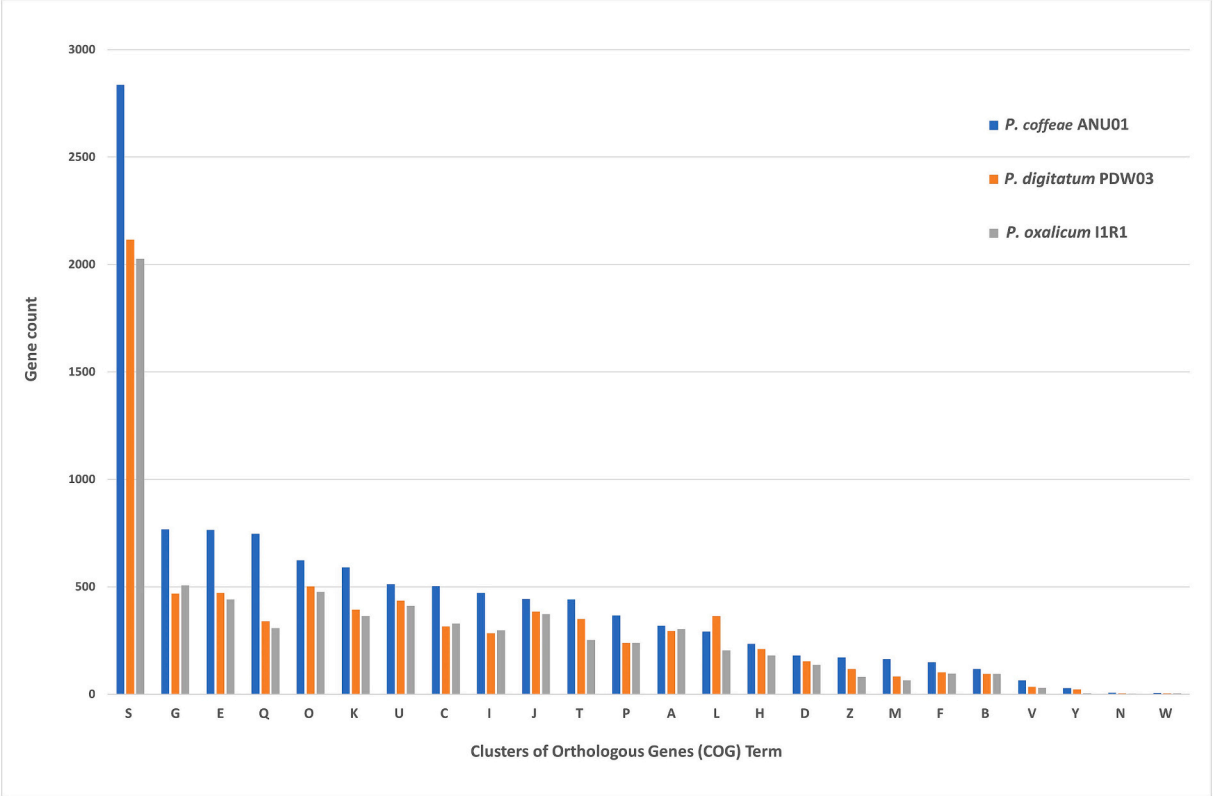

Fig. 5. Bar graph showing the number of genes assigned to each of the 24 clusters of orthologous genes (COG; Y axis) functional groups for *P. coffeae* ANU01, *P. digitatum* PDW03 and *P. oxalicum* I1R1. Each COG family is identified as follows; S, Function unknown, G, Carbohydrate transport and metabolism, E, Amino acid metabolism and transport, Q, Secondary metabolites biosynthesis, transport and catabolism, O, Post-translational modification, K, Transcription, U, Intracellular trafficking, secretion and vesicular transport, C, Energy production and conversion, I, Lipid transport and metabolism, J, Translation, ribosomal structure and biogenesis, T, Signal transduction mechanisms, P, Inorganic ion transport and metabolism, A, RNA processing and modification, L, Replication, recombination and repair, H, Coenzyme transport and metabolism, D, Cell cycle control, cell division, chromosome partitioning, Z, Cytoskeleton, M, Cell wall/membrane/envelope biogenesis, F, Nucleotide transport and metabolism, B, Chromatin structure and dynamics, V, Defence mechanisms, Y, Nuclear structure, N, Cell motility and W, Extracellular structures.

et al., 2017). *Penicillium coffeae* ANU01 possesses a *DEP3* homolog as well as homologs of the monooxygenases *DEP1* and *DEP2*.

Penicillium coffeae ANU01 shares several BGCs with the comparator species included above. All three species contain whole or partial clusters for synthesis of squalestatin and nidulanin A. The clavaric acid biosynthesis cluster is present in both *P. coffeae* ANU01 and *P. oxalicum* I1R1 but not *P. digitatum* PDW03. *Penicillium coffeae* ANU01 possesses four more BGCs than *P. digitatum* PDW03 and seven more than *P. oxalicum* I1R1 and was the only species to contain a fungal RiPP BGC. The unique RiPP showed no similarity to known BGCs, though the grouping is largely predicted to be involved in the production of toxins as well as defence against competitor fungi (Ford et al., 2022).

3.6. Global changes in the P. coffeae ANU01 transcriptome during growth associated with Pst

We conducted a comparative transcriptomic analysis to identify *P. coffeae* ANU01 genes associated with interaction with *Pst*. To do this, we isolated and sequenced mRNA from the fungus growing either axenically on PDA or on *Pst* pustules on wheat (hereafter referred to as growth *in situ*). On average, 64 % of reads aligned to the *P. coffeae* ANU01 genome whereas 27 % reads mapped to the *Pst* genome and 0.0067 % of reads mapped to the wheat genome, per treatment. Contaminating reads were removed from subsequent analyses. Alignment of the remaining reads against the *P. coffeae* ANU01 transcriptome allowed a differential gene expression analysis (DEG).

To identify *Penicillium coffeae* ANU01 genes upregulated during *in situ* growth, quantified transcript counts from Salmon (Patro et al., 2017) were loaded into Limma (Ritchie et al., 2015) to calculate relative gene expression values. The output is shown in the form of a volcano plot in Fig. 7. We defined a gene as differentially expressed if it exhibited an adjusted *P*-value of <0.05; upregulated if it also possessed a $\log_2$ fold change of >1, and downregulated if it possessed a $\log_2$ fold change of <-1. A total of 2422 genes were upregulated and 2314 genes were downregulated (alternatively stated; 2314 genes were upregulated during PDA growth) when *P. coffeae* ANU01 was grown on *Pst* pustules on wheat. Therefore, there are major changes in the *P. coffeae* ANU01 transcriptome associated with growth on *Pst* pustules. A summary of the *P. coffeae* ANU01 transcriptome expression during growth *in situ* and functional annotation of transcripts is presented in Supplementary Table 4 [see Additional file 2].

3.7. Changes in Penicillium coffeae ANU01 gene expression during in situ growth

We conducted a gene ontology (GO) enrichment analysis to identify functional pathways upregulated during growth associated with *Pst* spores (Fig. 8).

During growth *in situ*, the five most significantly upregulated GO terms contain genes associated with carbohydrate metabolism (114 genes, 40.7 % of genes in term), transmembrane transport (193 genes, 23.25 %), lipid catabolism (10 genes, 55 %), DNA replication initiation (9 genes, 60 %) and microtubule-based movement (9 genes, 60 %). This focus on substrate metabolism is illustrated by upregulated genes

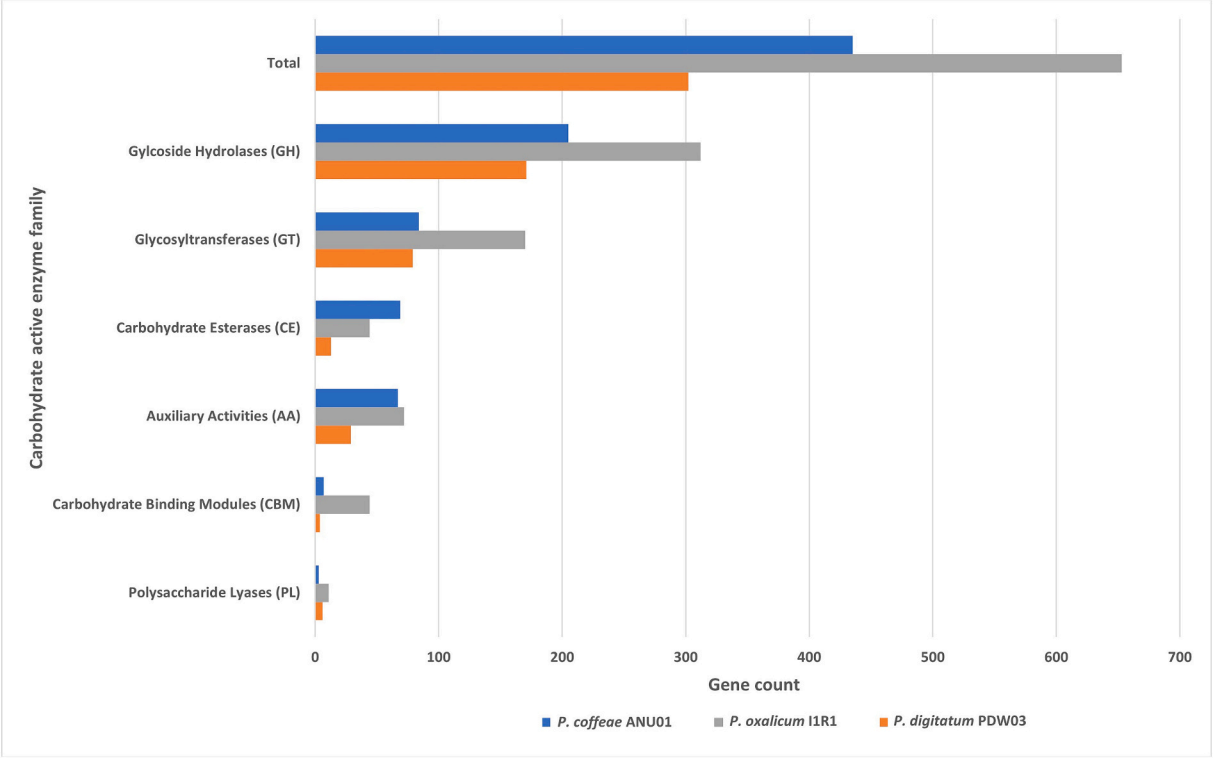

Fig. 6. Bar graph showing the number of genes assigned to each of the six carbohydrate active enzyme (CAZy) families (left axis) for *P. coffeae* ANU01, *P. oxalicum* I1R1 and *P. digitatum* PDW03.

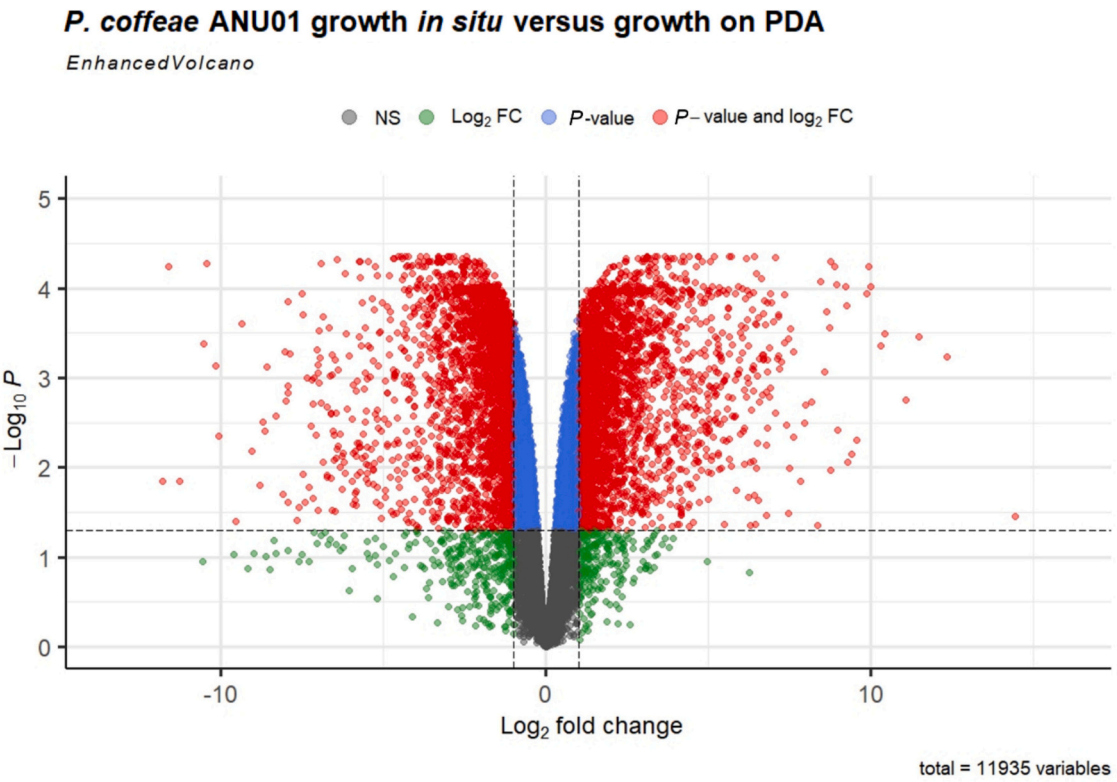

Fig. 7. Volcano plot of differentially expressed genes on *Pst* pustules *versus in vitro* on PDA. The dashed line on the y axis indicates adjusted *P* value of 0.05; the dashed lines on the x axis indicate $\log_2$ fold changes of −1 and 1 respectively. Red dots represent genes considered differentially expressed, downregulated on the left and upregulated on the right. Green dots represent genes considered differentially expressed between the two conditions but not sufficiently statistically significant. Blue dots represent genes considered statistically significantly expressed but not sufficiently differentially expressed. Grey dots represent genes that were neither sufficiently differential nor statistically significant in their expression. (For interpretation of the references to colour in this figure legend, the reader is referred to the web version of this article.)

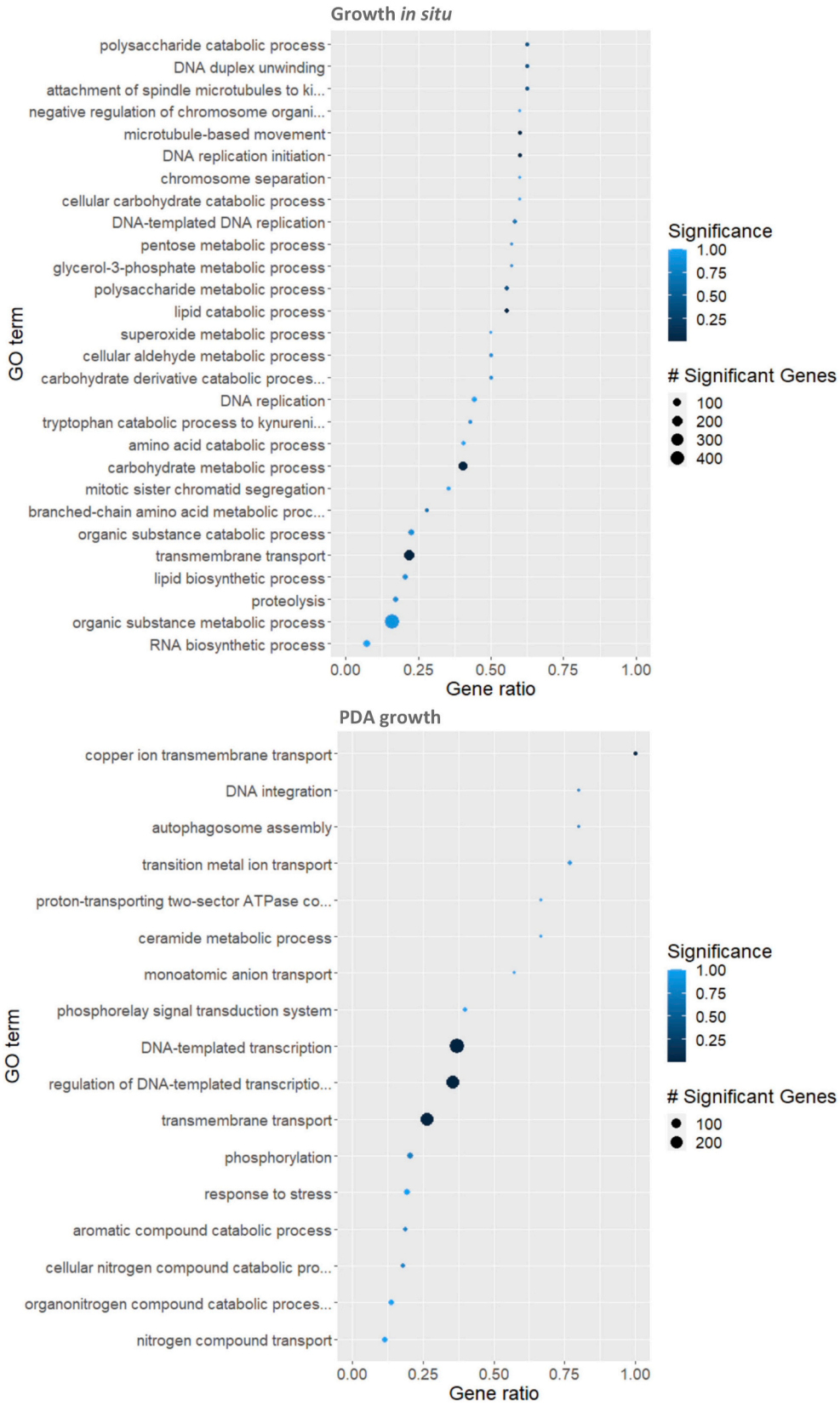

Fig. 8. Dotplots representing the results of a gene ontology (GO) enrichment analysis. Top, GO terms significantly upregulated during *in situ* growth. Bottom, GO terms significantly upregulated during growth on PDA. In both dotplots the dot size is calculated by the total number of significant genes within the associated GO term, whilst position along the "Gene ratio" X axis represents the ratio of significant to total genes in the GO term. Dot colour represents the degree of significance of the GO term according to an adjusted Fisher's exact test. The shortened GO terms on the y axis are: attachment of spindle microtubules to kinetochore, negative regulation of chromosome organisation, carbohydrate derivative catabolic process, tryptophan catabolic process to kynurenine, branched-chain amino acid

metabolic process, proton-transporting two-sector ATPase complex assembly, cellular nitrogen compound catabolic process, and organonitrogen compound catabolic process.

involved in polysaccharide metabolism (10 genes, 55 %) and amino acid metabolism (18 genes, 42.8 %). Potential defence mechanisms such as superoxide metabolism (4 genes, 50 %) were also increased. Other upregulated categories were aspects of DNA replication and expression, such as DNA replication initiation (9 genes, 60 %), DNA duplex unwinding (5 genes, 60.25 %) and chromosome separation (3 genes, 60 %).

Genes associated with copper ion transmembrane transport (5 genes, 100 %), DNA-templated transcription (308 genes, 38.5 %), regulation of DNA-templated transcription (231 genes, 37 %) and transmembrane transport (230 genes, 27 %) were upregulated during growth on PDA (Fig. 8). *Penicillium coffeae* ANU01 mobilises all of its genes related to Cu^{2+} transport and 77 % of its overall transition metal transport gene set during PDA growth. Potato dextrose agar is deficient in Cu^{2+} (Griffith et al., 2007), suggesting that *P. coffeae* ANU01 is not deficient in Cu^{2+} while growing on spores. Genes associated with nitrogen metabolism and transport were also upregulated, also perhaps suggesting a deficiency in the nutrient media. The fewer GO terms upregulated significantly during PDA growth (18) compared to *in situ* growth (29) is consistent with the idea that *Pst* spores are a more complex nutrient source than PDA, and the wheat leaf a more complex and competitive environment than the Petri dish.

Functional groups such as CAZYs and BGCs were upregulated during *in situ* growth on *Pst* urediniospores. One hundred and ninety two CAZYs (44 % of the total CAZY gene set) were upregulated (> 1 LFC) during *in situ* growth, compared to 58 (13 % of the total CAZY gene set) upregulated during growth on PDA. Of the top 100 most upregulated genes during growth *in situ*, thirteen are putative CAZYs, eight of which are GHs. Eight of the 50 genes most upregulated during growth on *Pst* urediniospores are members of BGCs. The upmost upregulated gene during *in situ* growth is a homolog of the DEP3 efflux transporter, from a cluster classified as responsible for synthesis of depudecin.

4. Discussion

This the first report of an isolate of *Penicillium coffeae* that grows in association with *Pst* urediniospores. *P. coffeae* ANU01 may exist as an endophyte that can act as a facultative antagonist or hyperparasite of *Pst,* capable of using rust spores as a source of nutrients when they are present. This view is supported by its increased growth and upregulation of genes related to SM production and nutrient acquisition in the presence of *Pst* urediniospores. An alternate possibility is that *P. coffeae* ANU01 feeds on weakened wheat tissue in the presence of *Pst* pustules. We believe this idea is less likely due to its almost complete lack of growth on uninfected plants measured using extremely sensitive qPCR detection, and the ability of the isolate to grow on *Pst* spores *in vitro* in the absence of wheat leaves. We also note that *P. coffeae* ANU01 hyphae contact *Pst* spores directly during *in vitro* growth, giving a very simple model for nutrient acquisition. Future studies should include scanning electron microscopy to help determine if the interaction is directly parasitic or simply antibiosis followed by saprophytic feeding on dead urediniospores. We discuss our data in view of the possibility that *P. coffeae* ANU01 is a hyperparasite, below.

Species level identification of this isolate was important to address the lack of data regarding rust hyperparasite biodiversity. *Penicillium coffeae* was first described as a plant endophyte of *Coffea arabica* (coffee) in Hawaii (Peterson et al., 2005). Its designation as a plant endophyte was determined by sterilising the leaf surface to remove epiphytes before cutting and culturing leaf tissue on yeast malt agar. It has also been isolated from leaves of the marine mangrove plant *Languncularia racemosa* (Cao et al., 2019) and from soil in India, where it showed bioremediation ability against arsenate contamination (Bhargavi and Savitha, 2014). It is unknown whether association with Pucciniales is a trait common to other isolates of *P. coffeae* or is unique to our isolate. *Coffea arabica* is susceptible to its own rust, *Hemileia vastatrix,* which produces urediniospores which can be antagonised by ascomycete hyperparasites (Vandermeer et al., 2009). Metabolites isolated from *P. coffeae* MA-314 inhibited the plant pathogenic fungi *Fusarium oxysporum* and *Colletotrichum gloeosporioides* (Cao et al., 2019). These isolates should also be tested for their ability to antagonise *Pst*.

The genome assembly presented here is highly complete and contiguous. The 30.9 Mb genome contains 7 linear chromosomes and one circular chromosome representing the mitochondrial genome. This is within the range of 25.4–46.5 Mb and four to eight chromosomes expected for *Penicillium spp.* (Yin et al., 2021). A BUSCO analysis suggested that our genome is 97.4 % complete, this is slightly less than the average (97.87 %) for *Penicillium* genome assemblies (Petersen et al., 2023). The 27,970 bp mitochondrial genome possesses all of the conserved genes expected (Kang et al., 2017). A high-quality genome assembly is essential for functional annotation and differential gene expression analysis. *Penicillium coffeae* ANU01 contains 12,181 protein coding genes, 205 more than average (Petersen et al., 2023), and 3684 and 3168 more than the comparators *P. oxalicum* I1R1 and *P. digitatum* PDW03 respectively. It also has a greater number of functionally unassigned genes (2836 or 23.3 %) with respect to the two comparators. These could represent functions related to rust parasitism that have not yet been characterised. This discrepancy in gene count is likely not due to poor gene calling because of the high completeness of these genomes (> 95 % BUSCOs), although the comparator genomes were not annotated with RNAseq data. The *P. coffeae* ANU01 gene set is enriched in functional groups potentially related to hyperparasitism. We defined a functional group as enriched if it contained >50 % more genes than the average of the comparators, *P. digitatum* PDW03 and *P. oxalicum* I1R1. The increases in genes related to nutrient acquisition and use are broadly compatible with what might be expected for an opportunistic hyperparasite. Possession of expanded gene sets related to carbohydrate, lipid and protein metabolism supports our previous idea of facultative exploitation of *Pst* spores when available. An expanded carbohydrate metabolism gene set is expected for *P. coffeae* ANU01 to degrade rust spores as a hyperparasite and dead plant material as a saprophyte, both of which are rich in simple and complex carbohydrates (Shaw, 1964). Polysaccharides such as chitin are particularly abundant in the coats of urediniospores (Xiao et al., 2023). This emphasis on carbohydrate metabolism is expanded in the *P. coffeae* ANU01 CAZY gene content and expression.

Other sources of nutrition include lipids and protein. Lipids make up approximately 20 % of rust spore weight and are the major source of nutrients used by *Pst* during germination (Tulloch et al., 1959; Staples and Wynn, 1965). Concordantly, *P. coffeae* ANU01 contains a relatively large number of genes related to lipid metabolism and transport. Rust spores contain approximately 25 % protein (Staples and Wynn, 1965). The high number of genes dedicated to amino acid metabolism and transport indicates their importance as a nutritive source. The broad increase in nutrient acquisition genes is consistent with a life strategy as a general scavenger, but does not exclude that *P. coffeae* ANU01 has acquired accessory genes particularly to make use of fungal spores as substrates. *Penicillium coffeae* ANU01 possesses only six genes related to the COG term cell motility, however this is two more than the average of the comparators. This small but expanded group might help *P. coffeae* ANU01 in polar growth towards *Pst* on the leaf, rather than in motility *per se* which is not a feature of *Penicillium* growth. An increase in genes related to SM production might be necessary for production of toxins against host spores but also antagonism against and defence from other microbial competitors on the leaf. The genetic emphasis on nutrient

acquisition, mobility and SM production hints at the mode of interaction of *P. coffeae* ANU01 with *Pst* urediniospores on the leaf. However, to understand how *P. coffeae* ANU01 deploys its genes during interaction with rust spores we needed to investigate their expression during growth on different substrates.

We compared transcriptomes from *P. coffeae* ANU01 growing axenically on PDA to growth on *Pst* pustules on wheat (*in situ*). Differential gene expression analysis revealed that there are major changes in the *P. coffeae* ANU01 transcriptome associated with growth on *Pst* pustules. The distribution of genes upregulated during *in situ* (2422) and PDA (2314) growth were approximately even, indicating a substantial shift when making use of *Pst* spores. It would be informative to characterise *P. coffeae* ANU01 gene expression on other complex substrates to further identify genes associated strongly with antagonistic growth.

During growth on PDA, genes related to transport of substrates across membranes and gene transcription were upregulated. There was a specific accent on nutrient acquisition. Investigating the top 50 upregulated genes within the term, the largest groups consisting of genes related to carbohydrate transport (17 genes), amino acid transport (7 genes) and ion transport (5 genes). This is broadly within expectation for a fungus growing on a sugar-rich substrate. The upregulation of certain genes associated with amino acid transport is interesting as the protein content of potatoes is low (~2 %; King and Slavin, 2013) whereas urediniospores are high in protein (Staples and Wynn, 1965). This implies that the fungus is protein limited when growing on PDA. Similarly, a small group of genes involved in copper ion transport including the copper influx transporter genes *CTR2* and *CTR3* (Knight et al., 1996) were significantly upregulated during PDA growth. Cu^{2+} is known to be limiting in PDA (Griffith et al., 2007), so this was not surprising, and underscores our point about protein levels. Inversely, the downregulation of these genes while growing on *Pst* suggests either that urediniospores are abundant in Cu^{2+} or may use Cu^{2+} as a defence mechanism, requiring *P. coffeae* ANU01 to reduce influx to avoid overaccumulation. Genes related to transcription were another large group enriched during growth on PDA. It is difficult to determine why this might be, however it could be a result of increased growth and particularly abundant sporulation on a rich and easily metabolised substrate. Overall, a simpler gene set was upregulated during growth on PDA compared to growth on urediniospores.

During *in situ* growth, 193 of the 826 genes related to transmembrane transport were upregulated significantly. These genes encode two major groups; efflux and influx transporters. Potential roles for efflux transporters include secretion of antibiotic secondary metabolites to disable or kill fungal spores and to fend off competition from other microbes. An example of an upregulated transporter gene is the glycerol transporter *STL1_1* predicted to transport glycerol released during fatty acid catabolism and glycogen breakdown (Klein et al., 2017). Glycogen is broken down during germination in *Pst* urediniospores, which results in glycerol production (Garnica et al., 2013). Fatty acids are abundant in the form of lipid droplets within rust urediniospores (Tulloch et al., 1959; Staples and Wynn, 1965). All of the upregulated genes related to lipid metabolism during growth *in situ* were secreted lipases, potentially secreted to make use of these abundant fat stores. The *in situ* growth transcriptome also showed upregulation of polysaccharide and carbohydrate metabolism genes. The majority encode glycoside hydrolase enzymes, most containing a secretion signal peptide. These secreted carbohydrate degrading enzymes could be used in breaking down urediniospore coats or accessing stored carbohydrates such as glycogen. Genes related to microtubule-based movement, specifically kinesin related genes linked to polar growth and internal transport in fungi (Konzack et al., 2005) were also upregulated during growth on spores. This may be related to polar growth towards the *Pst* spores, guided by urediniospore chemoattractant(s) or alternatively growth away from antagonistic fungi. This contrasts from growth on PDA where nutrients are readily available and *P. coffeae* ANU01 is free from microbial competition.

Penicillium coffeae ANU01 possesses a diverse set of carbohydrate active enzymes that are preferentially expressed during growth on *Pst* urediniospores. Thirteen of the top 100 most upregulated genes during *in situ* growth are putative CAZYs, eight of which are GHs, potentially secreted to break down the urediniospore coat or for protection against other microbes on the leaf. The most upregulated CAZY is annotated as a GH75 chitosanase. Chitosan is a modified form of chitin present in *Pst* infection structures (El Gueddari et al., 2002) so is a potential target for *P. coffeae* ANU01. However, as *Penicillium coffeae* ANU01 appears to target exposed urediniospores within pustules, it is unclear how it might access internal *Pst* structures. The second most upregulated CAZY gene encodes a β-1,3-glucanase, capable of destroying the cell walls of filamentous fungi (El-Shora et al., 2021). This may also target structural components of the *Pst* urediniospore. *Penicillium coffeae* ANU01 may also deploy CAZYs in targeting wheat tissue, using the third most upregulated gene, a GH43. Members of the GH43 family are commonly associated with breaking down pectin and other polysaccharides in the plant cell wall (Mewis et al., 2016). This GH43 may allow the fungus to exploit the weakened plant to feed on dead tissue. Polysaccharide lyases are a small but important group for parasitism, with all 3 PL genes upregulated and a PL within the top 50 most upregulated genes. These may be used to degrade *Pst* spore coats (Bowman and Free, 2006).

Penicillium coffeae ANU01 possesses 43 BGCs. Eight of the 50 genes most upregulated during growth on *Pst* urediniospores are members of BGCs. The upmost upregulated gene is a homolog of the *DEP3* efflux pump from a BGC classified as responsible for biosynthesis of depudecin. This cluster contains four additional biosynthetic genes by comparison to the characterised depudecin BGC from *Alternaria brassicola*. Homologs of the *DEP2* and *DEP4* genes were also highly upregulated. This modified BGC may secrete a related metabolite to inhibit rust germination and arrest associated depletion of spore nutrient stores, and to inactivate spore defences. A secreted member of a cluster with weak similarity to the aurofusarin BGC was also upregulated. Aurofusarin is an antibiotic active against mycelial fungi and yeasts (Medentsev et al., 1993). This modified version might act against other microbes on the leaf, including competing rust hyperparasites. Other upregulated BGC genes include an unannotated component of the ACR-toxin BGC from *Alternaria alternata,* which aids its pathogenesis on rough lemon (Gardner et al., 1985). An unknown fungal RiPP BGC unique to *P. coffeae* ANU01 was upregulated in 9 of 16 genes, suggesting importance in interaction with *Pst* spores. Its absence from the two comparators may also suggest a function in interaction with *Pst.* The most upregulated genes within the cluster encode a G-protein-coupled receptor and a major facilitator superfamily (MFS) transporter. The diversity of upregulated BGCs potentially with antimicrobial activity suggests the ability to antagonise other microorganisms within the microbiota.

The top upregulated *P. coffeae* ANU01 genes during growth on urediniospores indicate a bias towards secretion of enzymes and carbohydrate metabolism. A summary of the top 20 most upregulated genes is shown in Supplementary Table 5 [see Additional file 3]. Ten genes encode secreted proteins, three of which are GHs. This contrasts with the top genes upregulated during PDA growth (Supplementary Table 6, see Additional file 3) where only three proteins are predicted to be secreted and no CAZYs are present. The most upregulated gene during growth on *Pst* spores (*PenX_003989*-T2) is the *DEP3* homolog within the depudecin BGC described above. The second most upregulated gene (*PenX_004159*-T1) contains no annotation besides a secretion signal. Three of the other genes in the top 20 contain no annotation besides a secretion signal peptide (*PenX_010067-T1, PenX_000861-T1* and *PenX_008220-T1*). The secreted fungal chitosanase (*PenX_011559-T1*), secreted B-1,3-glucanase GH64 CAZY (*PenX_004154-T1)* and secreted GH43 (*PenX_003238*-T1) may be deployed to target host spores and other organisms. A putative transglycosylase (*PenX_010483-T1*) lacks a secretion signal peptide and its role is unclear. Thioredoxin peroxidases known as peroxiredoxins are essential enzymes for removal of damaging reactive oxygen species that arise *via* metabolism and host immune responses (Ross et al., 2000).

Concordantly, the peroxiredoxin genes *PRX5* (*PenX_007731-T1*) and *PRX7* (*PenX_007733-T1*) are upregulated during growth on urediniospores. Glycerol is a major component released during lipid break down, substrates highly abundant in rust spores (Chandel, 2021). The sugar transporter-like protein *STL1_1* (*PenX_007638-T1*) is responsible for glycerol uptake in *Saccharomyces cerevisiae* (Ferreira et al., 2005). Collectively, these genes that are highly upregulated during *in situ* growth offer insights into how *P. coffeae* ANU01 might antagonise and utilise *Pst* urediniospores for growth. Future work will examine the requirement of the top upregulated genes for hyperparasitic growth using gene depletion techniques. This will provide further insight into the extent of specialisation of this niche for *P. coffeae* ANU01.

There are several limitations associated with this study. Firstly, about 30 % of genes lack robust functional annotation, which means that our conclusions are based on partial data. Secondly, the fungal hyperparasite niche has been sparsely investigated from a genomic point of view, so we lack a solid point of comparison for benchmarking. Our high-quality genome assembly is a first step to addressing this lack of knowledge. Next, our study relies on growth on PDA as the sole instance of axenic growth. PDA is a relatively simple medium and it is likely that if we had used another medium for *in vitro* growth, the different chemical composition of the growth media would have influenced the results. Our growth *in situ* which approximates interaction with rust spores or parasitism used a single source of nutrient spores and was subject to several differences in growth conditions (light regime, temperature, presence of the rust host plant) which were not accounted for in our controls. Finally, we identified several *P. coffeae* ANU01 genes as important to growth associated with rust spores, based on massive upregulation and suggestive functional annotation. To confirm roles for these genes, further studies must exploit genetic deletion techniques to measure their impact on *P. coffeae* ANU01's ability to grow on *Pst* spores.

Availability of data and material

Data for this study has been deposited at NCBI under the BioProject number PRJNA1063332.

Ethics approval and consent to participate

Not applicable.

Adherence to national and international regulations

Not applicable.

Consent for publication

Not applicable.

Funding

This research did not receive any specific grant from funding agencies in the public, commercial or not-for-profit sectors.

CRediT authorship contribution statement

Jack Wess: Writing – review & editing, Writing – original draft, Visualization, Methodology, Investigation, Formal analysis, Data curation, Conceptualization. **Yiheng Hu:** Writing – review & editing, Methodology, Investigation, Conceptualization. **Sambasivam Periyannan:** Writing – review & editing, Methodology, Investigation, Conceptualization. **Ashley Jones:** Writing – review & editing, Methodology, Investigation, Conceptualization. **John P. Rathjen:** Writing – review & editing, Methodology, Conceptualization.

Declaration of competing interest

The authors declare that they have no known competing financial interests or personal relationships that could have appeared to influence the work reported in this paper.

Acknowledgments

S.P. acknowledges the Australian Research Council (ARC) for funding through Discovery Early Career Researcher Award (DE17010015).

Appendix A. Supplementary data

Supplementary data to this article can be found online at https://doi.org/10.1016/j.fgb.2024.103956.

Data availability

Data will be made available on request.

References

Aguileta, G., De Vienne, D.M., Ross, O.N., Hood, M.E., Giraud, T., Petit, E., Gabaldón, T., 2014. High variability of mitochondrial gene order among fungi. Genome Biology and Evolution 6 (2), 451–465. https://doi.org/10.1093/gbe/evu028.

Andrews, S., 2010. FastQC: A Quality Control Tool for High Throughput Sequence Data. Available online at https://www.bioinformatics.babraham.ac.uk/projects/fastqc/.

Barratt, B.I.P., Moran, V.C., Bigler, F., Van Lenteren, J.C., 2018. The status of biological control and recommendations for improving uptake for the future. BioControl 63 (1), 155–167. https://doi.org/10.1007/s10526-017-9831-y.

Bhargavi, S.D., Savitha, J., 2014. Arsenate resistant *Penicillium coffeae*: a potential fungus for soil bioremediation. Bulletin of Environmental Contamination and Toxicology 92 (3), 369–373. https://doi.org/10.1007/s00128-014-1212-y.

Bolger, A.M., Lohse, M., Usadel, B., 2014. Trimmomatic: a flexible trimmer for Illumina sequence data. Bioinformatics 30 (15), 2114–2120. https://doi.org/10.1093/bioinformatics/btu170.

Bonsch, B., Belt, V., Bartel, C., Duensing, N., Koziol, M., Lazarus, C.M., Bailey, A.M., Simpson, T.J., Cox, R.J., 2016. Identification of genes encoding squalestatin S1 biosynthesis and *in vitro* production of new squalestatin analogues. Chemical Communications 52 (41), 6777–6780. https://doi.org/10.1039/C6CC02130A.

Bowman, S.M., Free, S.J., 2006. The structure and synthesis of the fungal cell wall. BioEssays 28 (8), 799–808. https://doi.org/10.1002/bies.20441.

Cao, J., Li, X.-M., Li, X., Li, H.-L., Meng, L.-H., Wang, B.-G., 2019. New lactone and isocoumarin derivatives from the marine mangrove-derived endophytic fungus *Penicillium coffeae* MA-314. Phytochemistry Letters 32, 1–5. https://doi.org/10.1016/j.phytol.2019.04.018.

Chandel, N.S., 2021. Lipid metabolism. Cold Spring Harbor Perspectives in Biology 13 (9), a040576. https://doi.org/10.1101/cshperspect.a040576.

De Coster, W., D'Hert, S., Schultz, D.T., Cruts, M., Van Broeckhoven, C., 2018. NanoPack: visualizing and processing long-read sequencing data. Bioinformatics 34 (15), 2666–2669. https://doi.org/10.1093/bioinformatics/bty149.

Eitzen, K., Sengupta, P., Kroll, S., Kemen, E., Doehlemann, G., 2021. A fungal member of the *Arabidopsis thaliana* phyllosphere antagonizes *Albugo laibachii* via a GH25 lysozyme. eLife 10, e65306. https://doi.org/10.7554/eLife.65306.

El Gueddari, N.E., Rauchhaus, U., Moerschbacher, B.M., Deising, H.B., 2002. Developmentally regulated conversion of surface-exposed chitin to chitosan in cell walls of plant pathogenic fungi. The New Phytologist 156 (1), 103–112. https://doi.org/10.1046/j.1469-8137.2002.00487.x.

El-Shora, H.M., El-Sharkawy, R.M., Khateb, A.M., Darwish, D.B., 2021. Production and immobilization of β-glucanase from *Aspergillus niger* with its applications in bioethanol production and biocontrol of phytopathogenic fungi. Scientific Reports 11 (1), 21000. https://doi.org/10.1038/s41598-021-00237-2.

Esmail, S.M., Draz, I.S., Saleem, M.H., Mumtaz, S., Elsharkawy, M.M., 2022. *Penicillium simplicissimum* and *Trichoderma asperellum* counteract the challenge of *Puccinia striiformis* f. sp. *tritici* in wheat plants. Egyptian Journal Of Biological Pest Control 32 (1), 116. https://doi.org/10.1186/s41938-022-00614-7.

Estep, L.K., Torriani, S.F.F., Zala, M., Anderson, N.P., Flowers, M.D., McDonald, B.A., Mundt, C.C., Brunner, P.C., 2015. Emergence and early evolution of fungicide resistance in North American populations of *Zymoseptoria tritici*. Plant Pathology 64 (4), 961–971. https://doi.org/10.1111/ppa.12314.

European Food Safety Authority (EFSA), Arena, M., Auteri, D., Barmaz, S., Bellisai, G., Brancato, A., Brocca, D., Bura, L., Byers, H., Chiusolo, A., Court Marques, D., Crivellente, F., De Lentdecker, C., Egsmose, M., Erdos, Z., Fait, G., Ferreira, L., Goumenou, M., Greco, L., Ippolito, A., Istace, F., Jarrah, S., Kardassi, D., Leuschner, R., Lythgo, C., Magrans, J.O., Medina, P., Miron, I., Molnar, T., Nougadere, A., Padovani, L., Parra Morte, J.M., Pedersen, R., Reich, H., Sacchi, A., Santos, M., Serafimova, R., Sharp, R., Stanek, A., Streissl, F., Sturma, J., Szentes, C., Tarazona, J., Terron, A., Theobald, A., Vagenende, B., Verani, A., Villamar-Bouza, L.,

2018. Peer review of the pesticide risk assessment of the active substance chlorothalonil. EFSA Journal 16 (1). https://doi.org/10.2903/j.efsa.2018.5126.
Ferreira, C., Van Voorst, F., Martins, A., Neves, L., Oliveira, R., Kielland-Brandt, M.C., Lucas, C., Brandt, A., 2005. A member of the sugar transporter family, Stl1p is the glycerol/H^+ symporter in *Saccharomyces cerevisiae*. Molecular Biology of the Cell 16 (4), 2068–2076. https://doi.org/10.1091/mbc.e04-10-0884.
Figueroa, M., Hammond-Kosack, K.E., Solomon, P.S., 2018. A review of wheat diseases—a field perspective. Molecular Plant Pathology 19 (6), 1523–1536. https://doi.org/10.1111/mpp.12618.
Ford, R.E., Foster, G.D., Bailey, A.M., 2022. Exploring fungal RiPPs from the perspective of chemical ecology. Fungal Biology and Biotechnology 9 (1), 12. https://doi.org/10.1186/s40694-022-00144-9.
Galperin, M.Y., Kristensen, D.M., Makarova, K.S., Wolf, Y.I., Koonin, E.V., 2019. Microbial genome analysis: the COG approach. Briefings in Bioinformatics 20 (4), 1063–1070. https://doi.org/10.1093/bib/bbx117.
Gardner, J.M., Kono, Y., Tatum, J.H., Suzuki, Y., Takeuchi, S., 1985. Structure of the major component of ACRL-toxins, host-specific pathotoxic compounds produced by *Alternaria citri*. Agricultural and Biological Chemistry 49 (4), 1235–1238. https://doi.org/10.1080/00021369.1985.10866886.
Garnica, D.P., Upadhyaya, N.M., Dodds, P.N., Rathjen, J.P., 2013. Strategies for wheat stripe rust pathogenicity identified by transcriptome sequencing. PLoS One 8 (6), e67150. https://doi.org/10.1371/journal.pone.0067150.
Godfray, H.C.J., Mason-D'Croz, D., Robinson, S., 2016. Food system consequences of a fungal disease epidemic in a major crop. Philosophical Transactions of the Royal Society, B: Biological Sciences 371 (1709), 20150467. https://doi.org/10.1098/rstb.2015.0467.
Godio, R.P., Martín, J.F., 2009. Modified oxidosqualene cyclases in the formation of bioactive secondary metabolites: biosynthesis of the antitumor clavaric acid. Fungal Genetics and Biology 46 (3), 232–242. https://doi.org/10.1016/j.fgb.2008.12.002.
Green, M.R., Sambrook, J., 2019. Agarose gel electrophoresis. Cold Spring Harbor Protocols 2019 (1), pdb.prot100404. https://doi.org/10.1101/pdb.prot100404.
Griffith, G.W., Easton, G.L., Detheridge, A., Roderick, K., Edwards, A., Worgan, H.J., Nicholson, J., Perkins, W.T., 2007. Copper deficiency in potato dextrose agar causes reduced pigmentation in cultures of various fungi. FEMS Microbiology Letters 276 (2), 165–171. https://doi.org/10.1111/j.1574-6968.2007.00923.x.
Hartmann, F.E., Sánchez-Vallet, A., McDonald, B.A., Croll, D., 2017. A fungal wheat pathogen evolved host specialization by extensive chromosomal rearrangements. The ISME Journal 11 (5), 1189–1204. https://doi.org/10.1038/ismej.2016.196.
Howell, C.R., 2003. Mechanisms employed by *Trichoderma* species in the biological control of plant diseases: the history and evolution of current concepts. Plant Disease 87 (1), 4–10. https://doi.org/10.1094/PDIS.2003.87.1.4.
Jeleń, H., Błaszczyk, L., Chełkowski, J., Rogowicz, K., Strakowska, J., 2014. Formation of 6-n-pentyl-2H-pyran-2-one (6-PAP) and other volatiles by different *Trichoderma* species. Mycological Progress 13 (3), 589–600. https://doi.org/10.1007/s11557-013-0942-2.
Jones, A., Torkel, C., Stanley, D., Nasim, J., Borevitz, J., Schwessinger, B., 2021. High-molecular weight DNA extraction, clean-up and size selection for long-read sequencing. PLoS One 16 (7). https://doi.org/10.1371/journal.pone.0253830.
Kang, X., Liqin, H., Pengyuan, S., Rui, L., Dongbo, L., 2017. SMRT sequencing revealed mitogenome characteristics and mitogenome-wide DNA modification pattern in *Ophiocordyceps sinensis*. Frontiers in Microbiology 8. https://doi.org/10.3389/fmicb.2017.01422.
Kim, D., Paggi, J.M., Park, C., Bennett, C., Salzberg, S.L., 2019. Graph-based genome alignment and genotyping with HISAT2 and HISAT-genotype. Nature Biotechnology 37 (8), 907–915. https://doi.org/10.1038/s41587-019-0201-4.
King, J.C., Slavin, J.L., 2013. White potatoes, human health, and dietary guidance. Advances in Nutrition 4 (3), 393S–401S. https://doi.org/10.3945/an.112.003525.
Klein, M., Swinnen, S., Thevelein, J.M., Nevoigt, E., 2017. Glycerol metabolism and transport in yeast and fungi: established knowledge and ambiguities. Environmental Microbiology 19 (3), 878–893. https://doi.org/10.1111/1462-2920.13617.
Knight, S.A., Labbé, S., Kwon, L.F., Kosman, D.J., Thiele, D.J., 1996. A widespread transposable element masks expression of a yeast copper transport gene. Genes & Development 10 (15), 1917–1929. https://doi.org/10.1101/gad.10.15.1917.
Konzack, S., Rischitor, P.E., Enke, C., Fischer, R., 2005. The role of the kinesin motor KipA in microtubule organization and polarized growth of *Aspergillus nidulans*. Molecular Biology of the Cell 16 (2), 497–506. https://doi.org/10.1091/mbc.e04-02-0083.
Koren, S., Walenz, B.P., Berlin, K., Miller, J.R., Bergman, N.H., Phillippy, A.M., 2017. Canu: scalable and accurate long-read assembly via adaptive *k* -mer weighting and repeat separation. Genome Research 27 (5), 722–736. https://doi.org/10.1101/gr.215087.116.
Krumsiek, J., Arnold, R., Rattei, T., 2007. Gepard: a rapid and sensitive tool for creating dotplots on genome scale. Bioinformatics 23 (8), 1026–1028. https://doi.org/10.1093/bioinformatics/btm039.
Kwon, H.J., Kim, J.-H., Kim, M., Lee, J.-K., Hwang, W.-S., Kim, D.-Y., 2003. Anti-parasitic activity of depudecin on *Neospora caninum* via the inhibition of histone deacetylase. Veterinary Parasitology 112 (4), 269–276. https://doi.org/10.1016/S0304-4017(03)00035-9.
Lin, G., Li, D., Chidawanyika, T., Nathan, C., Li, H., 2010. Fellutamide B is a potent inhibitor of the *Mycobacterium tuberculosis* proteasome. Archives of Biochemistry and Biophysics 501 (2), 214–220. https://doi.org/10.1016/j.abb.2010.06.009.
Liu, D., Coloe, S., Baird, R., Pedersen, J., 2000. Rapid mini-preparation of fungal DNA for PCR. Journal of Clinical Microbiology 38 (1), 471. https://doi.org/10.1128/jcm.38.1.471-471.2000.
Lombard, V., Golaconda Ramulu, H., Drula, E., Coutinho, P.M., Henrissat, B., 2014. The carbohydrate-active enzymes database (CAZy) in 2013. Nucleic Acids Research 42 (D1), D490–D495. https://doi.org/10.1093/nar/gkt1178.
Mahdavian, E., Palyok, P., Adelmund, S., Williams-Hart, T., Furmanski, B.D., Kim, Y.-J., Gu, Y., Barzegar, M., Wu, Y., Bhinge, K.N., Kolluru, G.K., Quick, Q., Liu, Y.-Y., Kevil, C.G., Salvatore, B.A., Huang, S., Clifford, J.L., 2014. Biological activities of fusarochromanone: a potent anti-cancer agent. BMC Research Notes 7 (1), 601. https://doi.org/10.1186/1756-0500-7-601.
Marçais, G., Delcher, A.L., Phillippy, A.M., Coston, R., Salzberg, S.L., Zimin, A., 2018. MUMmer4: A fast and versatile genome alignment system. PLoS Computational Biology 14 (1), e1005944. https://doi.org/10.1371/journal.pcbi.1005944.
Medema, M.H., Kottmann, R., Yilmaz, P., Cummings, M., Biggins, J.B., Blin, K., De Bruijn, I., Chooi, Y.H., Claesen, J., Coates, R.C., Cruz-Morales, P., Duddela, S., Düsterhus, S., Edwards, D.J., Fewer, D.P., Garg, N., Geiger, C., Gomez-Escribano, J. P., Greule, A., Hadjithomas, M., Haines, A.S., Helfrich, E.J.N., Hillwig, M.L., Ishida, K., Jones, A.C., Jones, C.S., Jungmann, K., Kegler, C., Kim, H.U., Kötter, P., Krug, D., Masschelein, J., Melnik, A.V., Mantovani, S.M., Monroe, E.A., Moore, M., Moss, N., Nützmann, H.-W., Pan, G., Pati, A., Petras, D., Reen, F.J., Rosconi, F., Rui, Z., Tian, Z., Tobias, N.J., Tsunematsu, Y., Wiemann, P., Wyckoff, E., Yan, X., Yim, G., Yu, F., Xie, Y., Aigle, B., Apel, A.K., Balibar, C.J., Balskus, E.P., Barona-Gómez, F., Bechthold, A., Bode, H.B., Borriss, R., Brady, S.F., Brakhage, A.A., Caffrey, P., Cheng, Y.-Q., Clardy, J., Cox, R.J., De Mot, R., Donadio, S., Donia, M.S., Van Der Donk, W.A., Dorrestein, P.C., Doyle, S., Driessen, A.J.M., Ehling-Schulz, M., Entian, K.-D., Fischbach, M.A., Gerwick, L., Gerwick, W.H., Gross, H., Gust, B., Hertweck, C., Höfte, M., Jensen, S.E., Ju, J., Katz, L., Kaysser, L., Klassen, J.L., Keller, N.P., Kormanec, J., Kuipers, O.P., Kuzuyama, T., Kyrpides, N.C., Kwon, H.-J., Lautru, S., Lavigne, R., Lee, C.Y., Linquan, B., Liu, X., Liu, W., Luzhetskyy, A., Mahmud, T., Mast, Y., Méndez, C., Metsä-Ketelä, M., Micklefield, J., Mitchell, D.A., Moore, B.S., Moreira, L.M., Müller, R., Neilan, B.A., Nett, M., Nielsen, J., O'Gara, F., Oikawa, H., Osbourn, A., Osburne, M.S., Ostash, B., Payne, S.M., Pernodet, J.-L., Petricek, M., Piel, J., Ploux, O., Raaijmakers, J.M., Salas, J.A., Schmitt, E.K., Scott, B., Seipke, R.F., Shen, B., Sherman, D.H., Sivonen, K., Smanski, M.J., Sosio, M., Stegmann, E., Süssmuth, R.D., Tahlan, K., Thomas, C.M., Tang, Y., Truman, A.W., Viaud, M., Walton, J.D., Walsh, C.T., Weber, T., Van Wezel, G.P., Wilkinson, B., Willey, J.M., Wohlleben, W., Wright, G.D., Ziemert, N., Zhang, C., Zotchev, S.B., Breitling, R., Takano, E., Glöckner, F.O., 2015. Minimum information about a biosynthetic gene cluster. Nature Chemical Biology 11 (9), 625–631. https://doi.org/10.1038/nchembio.1890.
Medentsev, A., Kotik, A., Trufanova, V., Akimenko, V., 1993. Identification of aurofusarin in *fusarium graminearum* isolates, causing a syndrome of worsening of egg quality in chickens. Prikladnaia Biokhimiia i Mikrobiologiia 29 (4), 542–546.
Mewis, K., Lenfant, N., Lombard, V., Henrissat, B., 2016. Dividing the large glycoside hydrolase family 43 into subfamilies: a motivation for detailed enzyme characterization. Applied and Environmental Microbioly 82 (6), 1686–1692. https://doi.org/10.1128/AEM.03453-15.
Michaud, P., Da Costa, A., Courtois, B., Courtois, J., 2003. Polysaccharide lyases: recent developments as biotechnological tools. Critical Reviews in Biotechnology 23 (4), 233–266. https://doi.org/10.1080/07388550390447043.
Mikheenko, A., Prjibelski, A., Saveliev, V., Antipov, D., Gurevich, A., 2018. Versatile genome assembly evaluation with QUAST-LG. Bioinformatics 34 (13), i142–i150. https://doi.org/10.1093/bioinformatics/bty266.
Nattestad, M., 2023. Dot Software. Available online at https://github.com/MariaNattestad/dot.
Palmer, J., Stajich, J.. Funannotate v1.5.3. Available online at: https://github.com/nextgenusfs/funannotate/tree/1.5.3.
Parratt, S.R., Laine, A.-L., 2016. The role of hyperparasitism in microbial pathogen ecology and evolution. The ISME Journal 10 (8), 1815–1822. https://doi.org/10.1038/ismej.2015.247.
Patro, R., Duggal, G., Love, M.I., Irizarry, R.A., Kingsford, C., 2017. Salmon provides fast and bias-aware quantification of transcript expression. Nature Methods 14 (4), 417–419. https://doi.org/10.1038/nmeth.4197.
Petersen, C., Sørensen, T., Nielsen, M.R., Sondergaard, T.E., Sørensen, J.L., Fitzpatrick, D. A., Frisvad, J.C., Nielsen, K.L., 2023. Comparative genome study of the Penicillium genus elucidates a diverse pangenome and 15 lateral gene transfer events. IMA Fungus 14 (3). https://doi.org/10.1186/s43008-023-00108-7.
Peterson, S.W., Vega, F.E., Posada, F., Nagai, C., 2005. *Penicillium coffeae,* a new endophytic species isolated from a coffee plant and its phylogenetic relationship to *P. fellutanum, P. thiersii* and *P. brocae* based on parsimony analysis of multilocus DNA sequences. Mycologia 97 (3), 659–666. https://doi.org/10.1080/15572536.2006.11832796.
Pham, H.M., Le, D.T., Le, L.T., Chu, P.T.M., Tran, L.H., Pham, T.T., Nguyen, H.M., Luu, T. T., Hoang, H., Chu, H.H., 2023. A highly quality genome sequence of *Penicillium oxalicum* species isolated from the root of *Ixora chinensis* in Vietnam. G3: Genes, Genomes, Genetics 13 (2), jkac300. https://doi.org/10.1093/g3journal/jkac300.
Raffa, N., Keller, N.P., 2019. A call to arms: mustering secondary metabolites for success and survival of an opportunistic pathogen. PLoS Pathogens 15 (4), e1007606. https://doi.org/10.1371/journal.ppat.1007606.
Reynolds, H.T., Slot, J.C., Divon, H.H., Lysøe, E., Proctor, R.H., Brown, D.W., 2017. Differential retention of gene functions in a secondary metabolite cluster. Molecular Biology and Evolution 34 (8), 2002–2015. https://doi.org/10.1093/molbev/msx145.
Ritchie, M.E., Phipson, B., Wu, D., Hu, Y., Law, C.W., Shi, W., Smyth, G.K., 2015. Limma powers differential expression analyses for RNA-sequencing and microarray studies. Nucleic Acids Research 43 (7), e47. https://doi.org/10.1093/nar/gkv007.
Ross, S.J., Findlay, V.J., Malakasi, P., Morgan, B.A., 2000. Thioredoxin peroxidase is required for the transcriptional response to oxidative stress in budding yeast.

Molecular Biology of the Cell 11 (8), 2631–2642. https://doi.org/10.1091/mbc.11.8.2631.
Roux, I., Bowles, S., Kalaitzis, J.A., Vuong, D., Lacey, E., Chooi, Y.-H., Piggott, A.M., 2021. Characterisation and heterologous biosynthesis of burnettiene a, a new polyene-decalin polyketide from *Aspergillus burnettii*. Organic & Biomolecular Chemistry 19 (43), 9506–9513. https://doi.org/10.1039/D1OB01766G.
Schwessinger, B., 2017. Fundamental wheat stripe rust research in the 21st century. The New Phytologist 213 (4), 1625–1631. https://doi.org/10.1111/nph.14159.
Schwessinger, B., Sperschneider, J., Cuddy, W.S., Garnica, D.P., Miller, M.E., Taylor, J. M., Dodds, P.N., Figueroa, M., Park, R.F., Rathjen, J.P., 2018. A near-complete haplotype-phased genome of the dikaryotic wheat stripe rust fungus *Puccinia striiformis* f. sp. *tritici* reveals high interhaplotype diversity. mBio 9 (1). https://doi.org/10.1128/mBio.02275-17.
Shaw, M., 1964. The physiology of rust uredospores. Journal of Phytopathology 50 (2), 159–180. https://doi.org/10.1111/j.1439-0434.1964.tb02915.x.
Simão, F.A., Waterhouse, R.M., Ioannidis, P., Kriventseva, E.V., Zdobnov, E.M., 2015. BUSCO: assessing genome assembly and annotation completeness with single-copy orthologs. Bioinformatics 31 (19), 3210–3212. https://doi.org/10.1093/bioinformatics/btv351.
Sobhy Draz, I., 2019. Common ancestry of Egyptian *Puccinia striiformis* population along with effective and ineffective resistance genes. Asian Journal of Biological Sciences 12 (2), 217–221. https://doi.org/10.3923/ajbs.2019.217.221.
Sperschneider, J., 2020. FindTelomeres. Available online at https://github.com/JanaSperschneider/FindTelomeres.
Staples, R.C., Wynn, W.K., 1965. The physiology of uredospores of the rust fungi. The Botanical Review 31 (4), 537–564. https://doi.org/10.1007/BF02858608.
Summers, R.W., Brown, J.K.M., 2013. Constraints on breeding for disease resistance in commercially competitive wheat cultivars. Plant Pathology 62 (S1), 115–121. https://doi.org/10.1111/ppa.12165.
Tillich, M., Lehwark, P., Pellizzer, T., Ulbricht-Jones, E.S., Fischer, A., Bock, R., Greiner, S., 2017. GeSeq – versatile and accurate annotation of organelle genomes. Nucleic Acids Research 45 (W1), W6–W11. https://doi.org/10.1093/nar/gkx391.
Topolovec-Pintarić, S., 2019. *Trichoderma*: invisible partner for visible impact on agriculture. IntechOpen. https://doi.org/10.5772/intechopen.83363.
Tulloch, A.P., Craig, B.M., Ledingham, G.A., 1959. The oil of wheat stem rust uredospores: ii. The isolation of *cis* −9,10-epoxyoctadecanoic acid, and the fatty acid composition of the oil. Canadian Journal of Microbiology 5 (5), 485–491. https://doi.org/10.1139/m59-060.
Vandermeer, J., Perfecto, I., Liere, H., 2009. Evidence for hyperparasitism of coffee rust (*Hemileia vastatrix*) by the entomogenous fungus, *Lecanicillium lecanii*, through a complex ecological web. Plant Pathology 58 (4), 636–641. https://doi.org/10.1111/j.1365-3059.2009.02067.x.
Wang, N., Fan, X., Zhang, S., Liu, B., He, M., Chen, X., Tang, C., Kang, Z., Wang, X., 2020. Identification of a hyperparasitic *Simplicillium obclavatum* strain affecting the infection dynamics of *Puccinia striiformis* f. sp. *tritici* on wheat. Frontiers in Microbiology 11, 1277. https://doi.org/10.3389/fmicb.2020.01277.
Wang, M., Ruan, R., Li, H., 2021. The completed genome sequence of the pathogenic ascomycete fungus *Penicillium digitatum*. Genomics 113 (2), 439–446. https://doi.org/10.1016/j.ygeno.2021.01.001.
Wick, R., 2018. Porechop v0.2.4. Available online at: https://github.com/rrwick/Porechop.
Wight, W.D., Kim, K.-H., Lawrence, C.B., Walton, J.D., 2009. Biosynthesis and role in virulence of the histone deacetylase inhibitor depudecin from *Alternaria brassicicola*. Molecular Plant-Microbe Interactions 22 (10), 1258–1267. https://doi.org/10.1094/MPMI-22-10-1258.
Wilson, A., Cuddy, W.S., Park, R.F., Harm, G.F.S., Priest, M.J., Bailey, J., Moffitt, M.C., 2020. Investigating hyperparasites as potential biological control agents of rust pathogens on cereal crops. Australasian Plant Pathology 49 (3), 231–238. https://doi.org/10.1007/s13313-020-00695-8.
Xiao, M., Chen, D., Liu, S., Chen, A., Fang, A., Tian, B., Yu, Y., Bi, C., Kang, Z., Yang, Y., 2023. A chitin deacetylase *Ps*CDA2 from *Puccinia striiformis* f. sp. *tritici* confers disease pathogenicity by suppressing chitin-triggered immunity in wheat. Molecular Plant Pathology 24, 1467–1479. https://doi.org/10.1111/mpp.13381.
Yin, G., Zhao, H., Pennerman, K.K., Jurick, Fu, M., Bu, L., Guo, A., Bennett, J.W., 2021. Genomic Analyses of Penicillium species have revealed patulin and citrinin gene clusters and novel loci involved in oxylipin production. Journal of Fungi 7 (9), 743. https://doi.org/10.3390/jof7090743.
Zhan, G., Tian, Y., Wang, F., Chen, X., Guo, J., Jiao, M., Huang, L., Kang, Z., 2014. A novel fungal hyperparasite of *Puccinia striiformis* f. sp. *tritici*, the causal agent of wheat stripe rust. PLoS One 9 (11), e111484. https://doi.org/10.1371/journal.pone.0111484.
Zheng, L., Zhao, J., Liang, X., Zhan, G., Jiang, S., Kang, Z., 2017. Identification of a novel *Alternaria alternata* strain able to hyperparasitize *Puccinia striiformis* f. sp. *tritici*, the causal agent of wheat stripe rust. Frontiers in Microbiology 8. https://doi.org/10.3389/fmicb.2017.00071.
Zimin, A.V., Salzberg, S.L., 2020. The genome polishing tool POLCA makes fast and accurate corrections in genome assemblies. PLoS Computational Biology 16 (6), e1007981. https://doi.org/10.1371/journal.pcbi.1007981.

2.1 Supplementary material

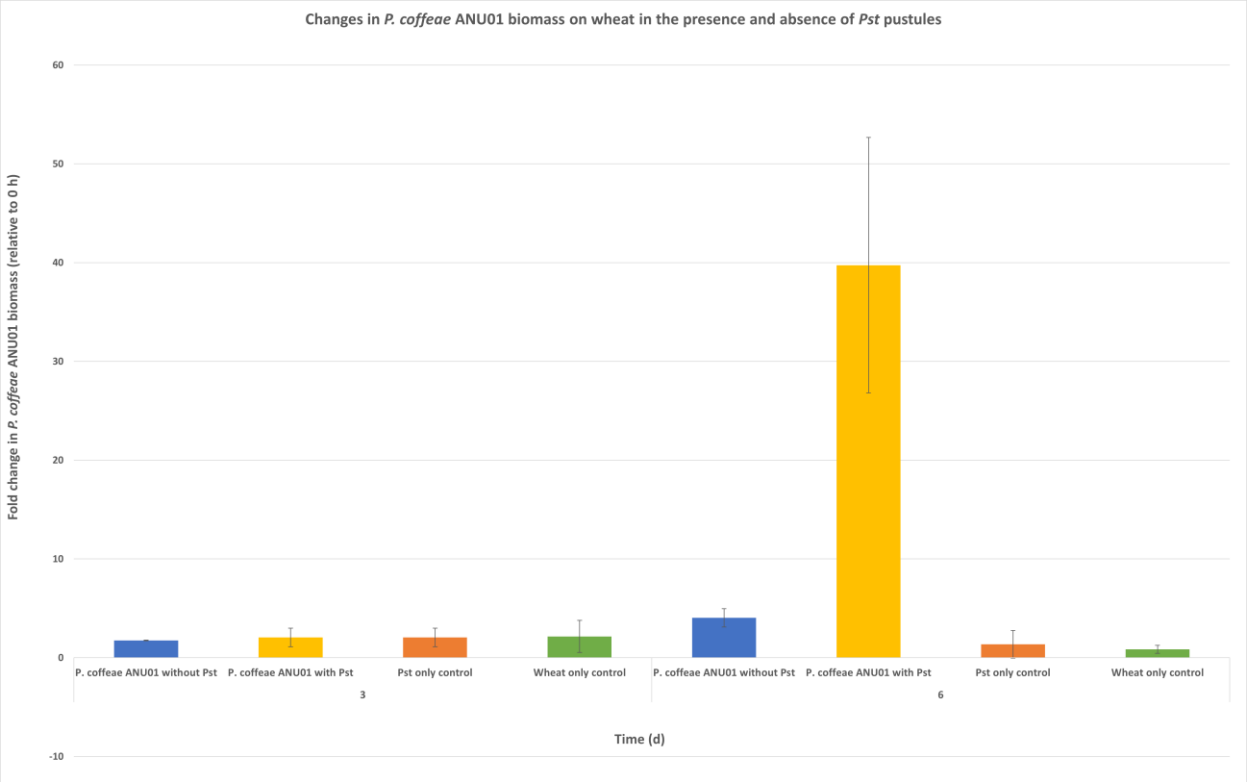

Supplementary Fig. 1. Bar graph showing changes in *P. coffeae* ANU01 biomass over time, in the presence and absence of *Pst* pustules on the surface of wheat leaves. Also included are a *Pst*-only and wheat-only control. Error bars represent standard deviation.

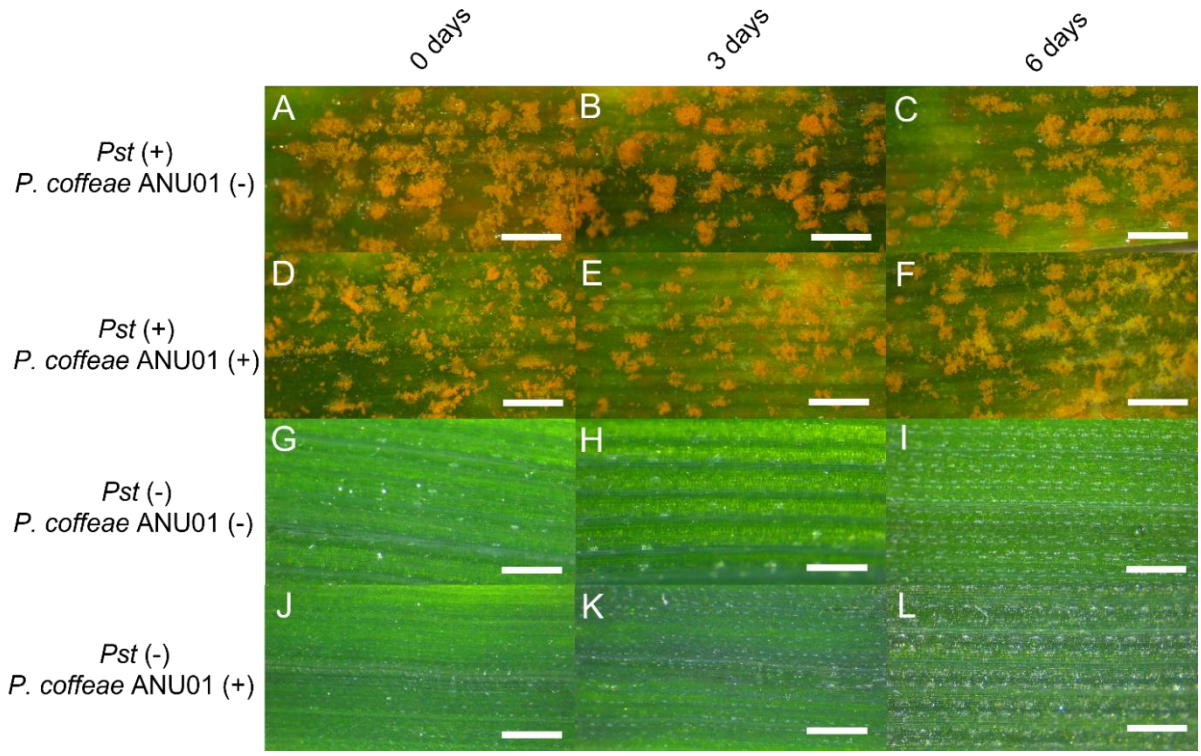

Supplementary Fig. 2. Microscope images of *P. coffeae* ANU01 growth on *Pst*-infected and uninfected wheat. A-C. Wheat infected with *Pst* and sprayed with sterile water (control). D-F. Wheat infected with *Pst* and sprayed with a *P. coffeae* ANU01 spore suspension, the pale fluffy tissue amongst pustules in F is *P. coffeae* ANU01 growth. G-I. Uninfected wheat sprayed with water (control). J-L. Uninfected wheat sprayed with a *P. coffeae* ANU01 spore suspension. Scale bars represent 0.5 mm.

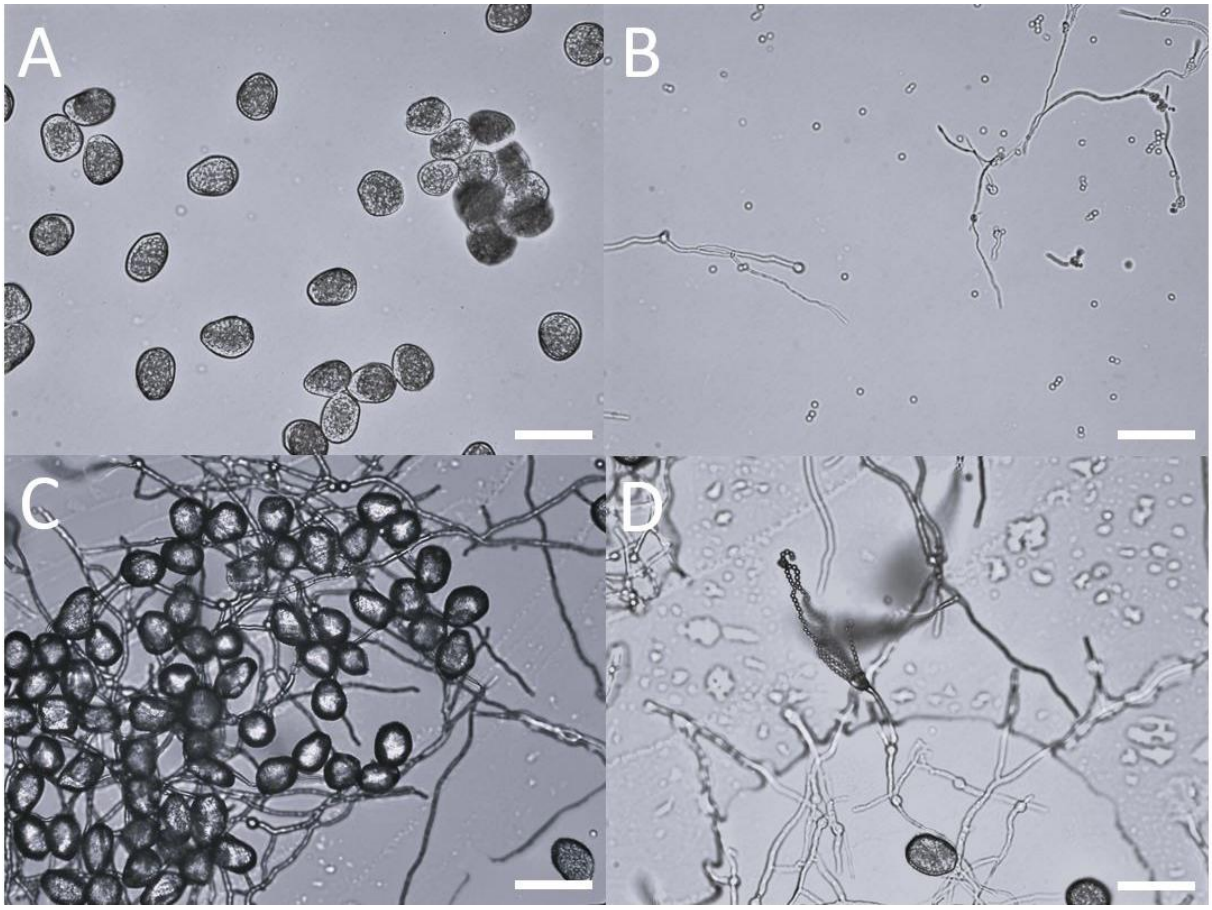

Supplementary Fig. 3. An experiment to measure the growth of *P. coffeae* ANU01 on glass microscope slides in the presence and absence of *Pst* urediniospores. A. Uninfected *Pst* urediniospores. B. Limited germination and growth of *P. coffeae* ANU01 spores in the absence of *Pst* urediniospores. C. Growth of *P. coffeae* ANU01 tissue to colonise *Pst* urediniospores. D. Sporulation of *P. coffeae* ANU01 in the presence of *Pst* urediniospores. The large ovate objects are *Pst* spores. The smaller paint brush-like sporulating structures are *Penicillium* fruiting bodies. Scale bars represent 35 µm.

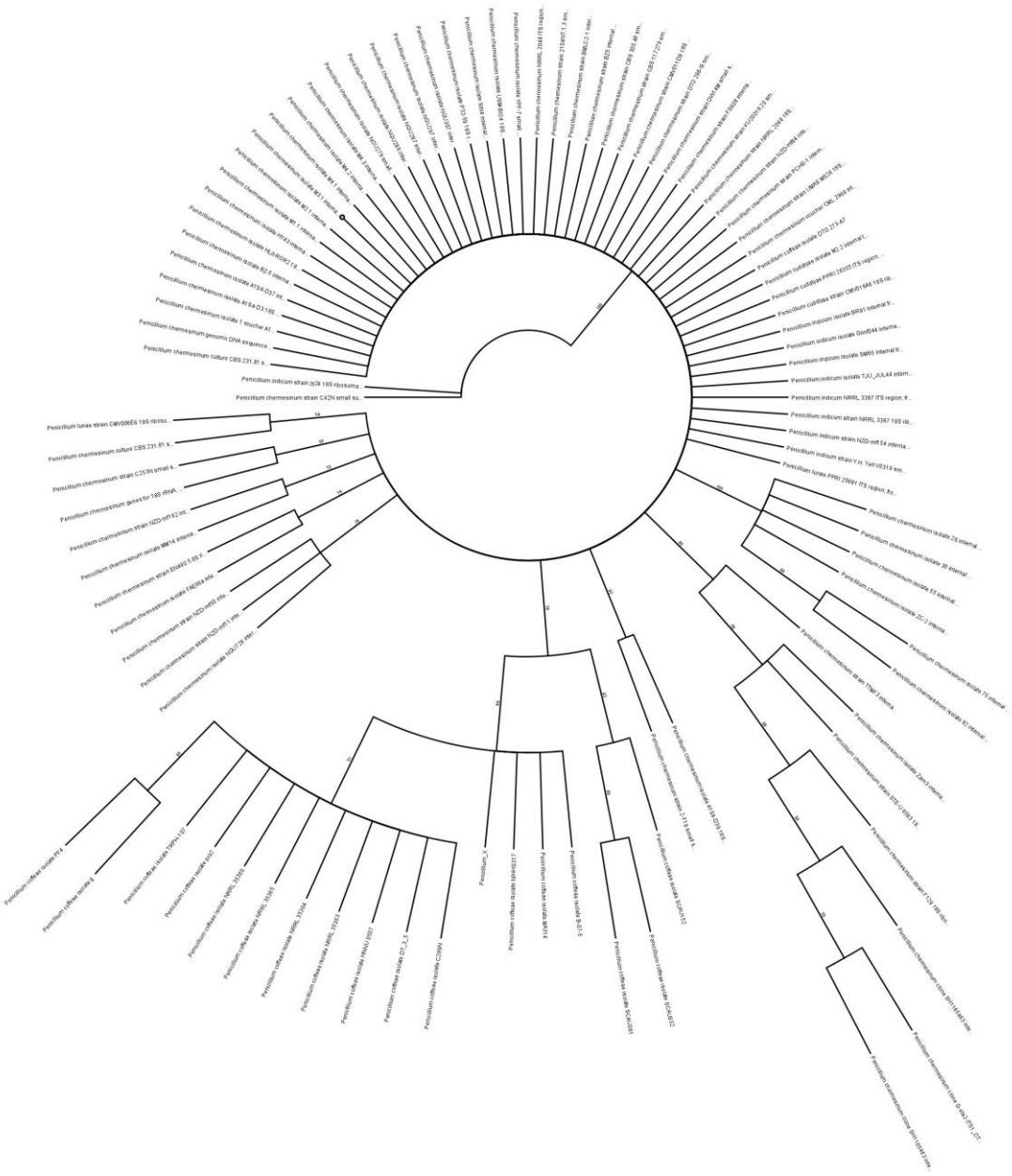

Supplementary Fig. 4. A phylogenetic tree of all available isolates of *Penicillium* within a clade including *Penicillium_X*. The tree was built from Geneious alignments of ITS sequences downloaded from the NCBI database, as well as the *Penicillium_X* amplicon generated here. The tree was constructed using the Tamura-Nei Neighbour-Joining method in Geneious.

Supplementary Table 2.1. Summary of *in planta* RNAseq readsets against the *Pst, Triticum aestivum* and *P. coffeae* ANU01 genomes

Sample_ID	# Total reads in sample	# Reads aligned to the *Pst* 104E-genome	# Reads aligned to the *Triticum aestivum* genome	# Reads aligned to *P. coffeae* ANU01 genome
RNAseq1	67,773,408	20,868,345 (30.8%)	525,306 (0.008%)	41,325,029 (60.9%)
RNAseq2	70,928,120	13,667,027 (19.3%)	442,268 (0.006%)	50,886,154 (71.7%)
RNAseq3	45,557,879	14,432,781 (31.7%)	254,290 (0.006%)	27,077,590 (59.4%)
Average (mean)	61,419,802	16,322,717 (27.3%)	407,288 (0.0067%)	39,762,924 (64%)

Supplementary Table 2.2. Summary statistics for the annotated *P. coffeae* ANU01 mitochondrial genome

Measurement	***Penicillium coffeae* ANU01 genome assembly**
Contig size	27,970 bp
Total number of protein coding genes	17
Number of fragmented protein coding genes	3
Gene content (*nad*)	*nad1-fragmented, nad2, nad3-fragmented, nad4, nad4L, nad5, nad6*
Gene content (*atp*)	*atp6, atp8, atp9*
Gene content (*cox*)	*cox1, cox2, cox3*
Gene content (*orf*)	*orf239, orf285*
Gene content (*rps*)	*rps3-fragmented*
Gene content (*cob*)	*cob*
Average CDS size (bp)	881.88
# tRNAs	39
# rRNAs	6
Gene content (rRNAs)	*rrnL, rnl, rrnS-fragment1, rrnS-fragment2, rrnS, rns*

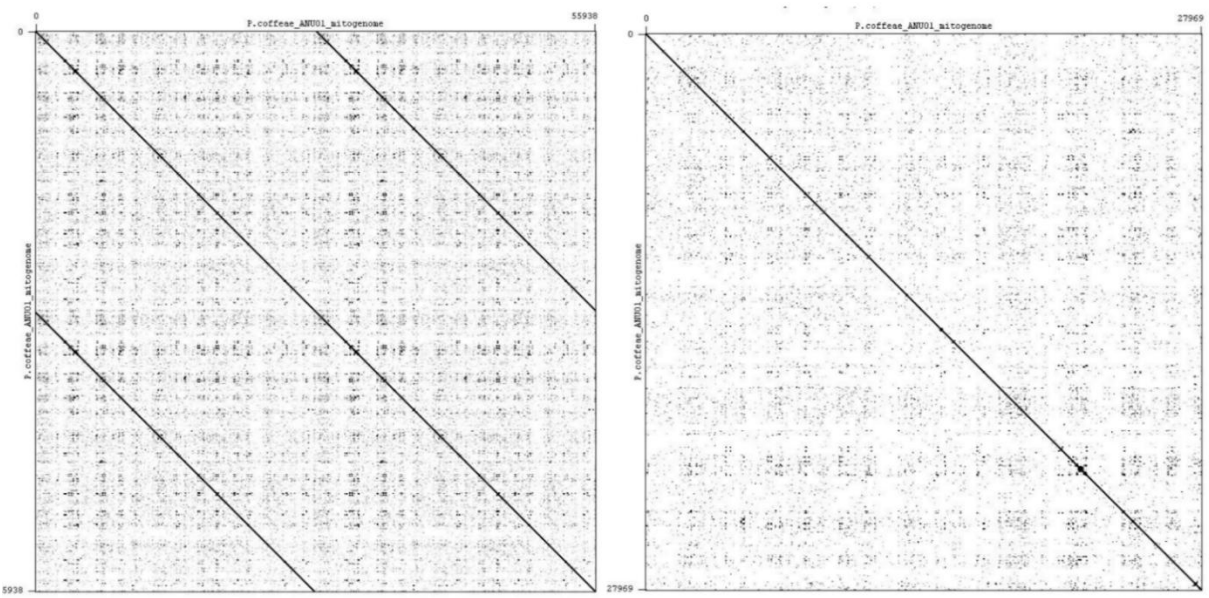

Supplementary Fig. 5. Two alignments of the *P. coffeae* ANU01 eighth contig to itself. A – Alignment of the original contig as output by the Canu assembly software. B – Alignment of the contig after removal of the second duplicated version of the contig.

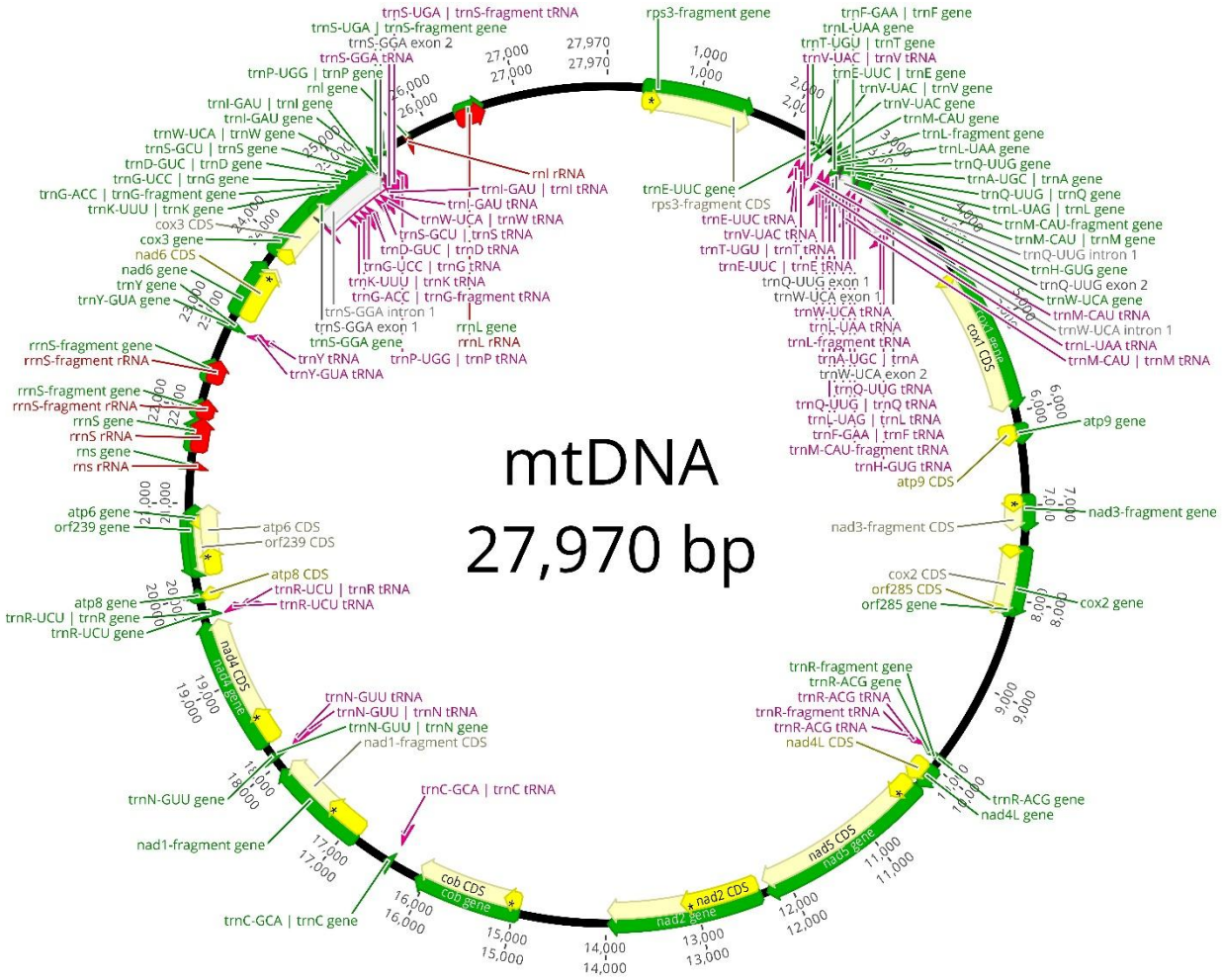

Supplementary Fig. 6. Visual representation of the *P. coffeae* ANU01 mitochondrial genome and all associated annotations. Genes are represented as green, CDS regions as yellow, tRNAs as pink and rRNAs as red.

Supplementary Table 2.3. Summary of the predicted *P. coffeae* ANU01 BGC content, alongside percentage similarity to characterised BGCs

Cluster ID	Type	Size (bp)	# Genes	Similarity to known cluster
Region_1_1	NRPS-like	39,446	20	-
Region_1_2	NRPS-like	135,278	51	BGC0001252 (100%)
Region_1_3	NRPS-like	43,057	17	Choline biosynthetic gene cluster (BGC0002276) (100%)
Region_1_4	T1PKS	45,180	18	Cytochalasin E/Cytochalasin K (BGC0000983) (15%)
Region_1_5	NRPS-like	54,221	21	Fusarochromanone (BGC0002256) (70%)
Region_1_6	T1PKS	38,494	10	-
Region_1_7	T1PKS	45,615	16	-
Region_1_8	Indole	21,306	15	-
Region_1_9	NRPS-like	43,339	15	-
Region_1_10	T1PKS	46,643	17	Aurofusarin (BGC0002709) (18%)
Region_1_11	Terpene	18,358	9	Clavaric acid (BGC0001248) (100%)
Region_1_12	Terpene	21,436	9	-
Region_2_1	NRPS	52,100	12	-
Region_2_2	Terpene	19,557	8	-
Region_2_3	Terpene	22,013	9	-
Region_2_4	T1PKS	45,913	21	-
Region_2_5	Fungal-RiPP	37,752	16	-
Region_2_6	T1PKS	47,352	15	ACR toxin (BGC0001252) (100%)
Region_2_7	T1PKS	45,701	19	Fusaric acid (BGC0001190) (10%)
Region_2_8	T1PKS	43,993	20	Depudecin (BGC0000046) (66%)
Region_2_9	T1PKS	42,296	16	-
Region_2_10	T1PKS	47,161	17	Aflatoxin (BGC0000007) (8%)
Region_2_11	NRPS	62,154	16	Aspercryptins (BGC0001515) (20%)
Region_2_12	NRPS-like	43,348	17	-
Region_3_1	NRPS-like	36,825	19	-
Region_3_2	NRPS	56,431	13	Nidulanin A (BGC0001699) (75%)
Region_3_3	T1PKS	41,836	20	2,4-dihydroxy-5,6-dimethyl benzaldehyde (BGC0002734) (28%)
Region_3_4	T1PKS-like	52,219	20	Curvupallide-B (BGC0001563) (22%)
Region_3_5	NRPS-like	41,402	24	-
Region_3_6	NRPS-like	43,756	22	-
Region_3_7	betalactone	31,501	11	-
Region_4_1	NRPS-like	37,958	19	-
Region_4_2	Terpene	18,993	11	Squalestatin S1 (BGC0001839) (60%)
Region_4_3	NRPS	41,143	14	-
Region_4_4	NRPS	47,505	18	-
Region_4_5	Terpene	22,862	10	-
Region_5_1	T1PKS	45,148	20	Burnettiene A/preburnettiene B/preburnettiene A (100%) (BGC0002139)

Region_5_2	NRPS	61,083	27	Imizoquin A/imizoquin B/ imizoquin C/ imizoquin D/TMC-2A/TMC-2B (BGC0001621) (40%)
Region_5_3	T1PKS	47,886	14	-
Region_6_1	NRPS	43,368	18	-
Region_6_2	NRPS	69,871	25	Fellutamide B (BGC0001399) (100%)
Region_7_1	Terpene	16,106	8	-
Region_7_2	Terpene	21,536	9	-

Note on the comparative transcriptomic experimental design

The comparative transcriptomic analysis I conducted in this chapter was based on tissue I sampled from *P. coffeae* ANU01 growing *in situ* on *Pst* pustules and axenically on PDA at eight and fifteen days respectively. I selected these time points as I considered they represented stages at which *P. coffeae* ANU01 was both sporulating, and actively producing new mycelial growth. Furthermore, at eight days, there was insufficient biomass in the PDA condition to conduct RNA-seq. However, the seven-day difference in growth between the two conditions may have introduced some confounding effects on the transcriptomic differences I observed. For example, after fifteen days of growth on PDA, compared with eight days, *P. coffeae* ANU01 may have upregulated additional genes associated with processes such as sporulation or maturation, potentially influencing the overall comparative transcriptomic analysis. Future experiments should therefore aim to carefully select time points that allow sampling from both conditions at comparable developmental stages, minimising background transcriptional differences that may not be directly attributable to growth on *Pst.*

Chapter Three

Which genes contribute to hyperparasitism? A CRISPR-mediated loss-of-function investigation of candidate *P. coffeae* ANU01 genes

3.1 Background

The molecular mechanisms underlying the parasitism of *Puccinia striiformis* f. sp. *tritici* (*Pst*) by fungal hyperparasites remain poorly understood. To date, investigations into how these mycoparasites antagonize and exploit *Pst* have largely been limited to observational studies. Microscopic analyses have revealed that hyperparasitic hyphae are capable of physically penetrating *Pst* urediniospores, indicating a direct mode of interaction (Wang *et al.,* 2020). *In vitro* assays and urediniospores isolated from infected pustules have demonstrated a marked reduction in the viability of *Pst* spores in the presence of hyperparasites (Zhan *et al.,* 2014; Zheng *et al.,* 2017). These findings suggest that, in addition to physical invasion, hyperparasites may secrete toxic secondary metabolites (SMs) that suppress or inhibit the growth of rust urediniospores (Wess *et al.*, 2025). Production of SMs in fungi is controlled by clusters of adjacent genes, referred to as biosynthetic gene clusters (BGCs) (Medema *et al.*, 2015). Carbohydrate-degrading enzymes play a pivotal role in the biology of rust hyperparasites, enabling the breakdown of cell walls and facilitating entry into rust urediniospores (Leinhos & Buchenauer 1992). The spore coat of rust fungi presents a significant barrier, being composed largely of polysaccharides such as chitin and various glucans, which serve as both structural and protective components (Xiao *et al.*, 2023). To breach this defence, mycoparasitic fungi secrete a suite of cell wall-degrading enzymes including chitinases, chitosanases, and β-glucanases that collectively act to soften and degrade the spore wall, thereby promoting hyphal penetration (Chatterton & Punja 2009). In addition to acting as a physical barrier, the spore coat also represents a nutrient-rich substrate. Hyperparasites may capitalize on this by using the polysaccharide-rich spore wall as a source of carbohydrates, further supporting their growth. *Pst* urediniospores are the most abundant form of the fungus, produced during the asexual infection cycle on wheat. *Pst* infects and replicates within wheat, ultimately culminating in the formation of pustules on the leaf surface, each containing thousands of individual urediniospores (Schwessinger 2017). *Pst* urediniospores are abundant in carbohydrates

(~22%), lipids (~20%) and ~25% protein (Staples and Wynn 1965; Tulloch *et al.*, 1959). Mycoparasites must possess secreted enzymes and nutrient transporters to exploit these nutrients (Wess *et al.*, 2025).

In Chapter Two, I investigated the transcriptional regulation of *P. coffeae* ANU01 genes during growth on *Pst* pustules. My analyses revealed a strong emphasis on the expression of secreted carbohydrate-active enzymes (CAZymes), antibiotic efflux pumps, nutrient transporters, and other infection-associated genes. Based on these observations, I hypothesised that *P. coffeae* ANU01 initially halts spore germination and suppresses *Pst* defence responses through the production of a toxic, depudecin-like secondary metabolite. Following this initial suppression, the hyperparasite likely proceeds to degrade the structural components of the rust spore using a suite of secreted hydrolytic enzymes. Once the spore coat is breached, *P. coffeae* ANU01 appears to exploit the host's internal stores, particularly lipids and amino acids through the action of nutrient importers and lipases. In addition to their role in breaching host defences, CAZymes may also enable *P. coffeae* to utilise host-derived carbohydrates as nutrient sources.

In this chapter, I describe the use of CRISPR-Cas9 genome editing to disrupt the function of several genes that were highly upregulated during parasitism. These gene knockouts were designed to challenge each stage of the infection model outlined above. To assess the phenotypic consequences of gene loss, I used quantitative PCR (qPCR) to measure *P. coffeae* ANU01 biomass and in effect its ability to grow on *Pst* urediniospores, comparing wild-type and mutant strains. These assays were designed to contextualise the importance of each gene to the parasitic process. This chapter serves as a direct expansion to Chapter Two, where I hypothesised which genes may lie at the core of how *P. coffeae* ANU01 parasitises *Pst*. Here I directly investigate those genes and attempt to determine their individual contribution to growth of *P. coffeae* ANU01 on *Pst* urediniospores.

3.2 Materials and methods

Fungal strains and media

Penicillium coffeae isolate ANU01 was maintained via subculturing onto potato dextrose agar plates (PDA; 25 g/L potato dextrose broth, 15 g/L agar) in a temperature-controlled room at 22 °C under a 12 hour day/night cycle and as 25 % glycerol stocks at -80 °C. Glycerol stocks were made by mixing 500 µL 50% glycerol (v/v) solution with 500 µL spore suspension (made as below) and storing at -80 °C. *Puccinia striiformis* f. sp. *tritici* (*Pst*) isolate 104 E137 A- (Schwessinger *et al.*, 2018) was used for all parts of this research and maintained via culturing on wheat cv. Morocco and storage as dried urediniospores stocks at -80 °C. *Escherichia coli* was used for maintenance of the pGpdGFP plasmid (Sexton & Howlett 2001) and was routinely grown on Luria-Bertaini plates (LB; yeast extract, 10 g/L,

tryptone, 16 g/L, NaCl, 5 g/L and agar 15 g/L) and liquid media (yeast extract, 10 g/l, tryptone, 16 g/L and NaCl, 5 g/L) at 37 °C and kept as 25% glycerol stocks at -80 °C.

Designing and synthesising gene-specific sgRNAs for CRISPR gene disruption

Target regions for gene-specific sgRNAs were decided by providing the gene sequence in fasta format to the Custom Alt-R CRISPR-Cas9 guide RNA tool (Integrated DNA Technologies), which generates a series of possible 20 bp target sequences for sgRNA binding. To generate total loss of function mutants, disruption was targeted towards the 5' end of the mRNA coding region of the gene. The resulting 20 bp sequences (one per gene) were uploaded to the EnGen sgRNA Template Oligo Designer v1.13.2 (New England Biolabs), which converts sequences into a DNA oligonucleotide usable with the EnGen™ sgRNA Synthesis Kit, *S. pyogenes* (New England Biolabs). After synthesis, sgRNAs were purified with the Monarch RNA Cleanup Kit (500 µg) (Monarch), eluted in 42 µL nuclease-free water and immediately frozen and stored at -80 °C until use.

Generating antibiotic resistance cassettes to disrupt gene function

Hygromycin resistance (hyg^+) cassettes for each specific gene were generated to include custom 50 bp homology arms that align to the regions either side of the Cas9 cut site (the 5' homology arm begins 3-5 bp upstream of the PAM site) and facilitate insertion via homology-directed repair (HDR) and therefore gene disruption. Primers were designed to include homology arms appended to universal primers PF (5' CTTGGCTGGAGCTAGTGGAG 3') and PR (5' GAGCGGATTCCTCAGTCTCG 3') and used to amplify the hyg^+ cassette from the pGpdGFP plasmid (Sexton and Howlett 2001). The resulting amplicons were cleaned using the Wizard® SV Gel and PCR Clean-Up System (Promega), eluted in 52 µL sorbitol-Tris-$CaCl_2$ buffer (STC; 1.2 M Sorbitol, and 10 mM Tris pH 7.5, 10mM $CaCl_2$) and quantified on a Quickdrop™ Micro-Volume Spectrometer (SpectraMax®).

Preliminary *in vitro* cleavage assays to test sgRNAs

In vitro cleavage assays were conducted as described by Khan *et al.* (2020). Briefly, to determine efficacy of sgRNAs in cleaving target genes, PCR amplicons were created for ~300 bp fragments of six of the target-genes, containing the region within 100-150 bp upstream and 100-150 bp downstream of the target cut site. To form Ribonucleoproteins (RNPs) for the *in vitro* cleavage assays, 1 µg of Cas9 protein was mixed with 1.5 µg of target-specific sgRNA and incubated at room temperature for 15 mins. After RNP assembly, 16 µL of cleavage buffer (10 mM $MgCl_2$, 0.1 mM EDTA, 20 mM HEPES pH 7.5, 150 mM KCl and 0.5 mM fresh DTT) was added, followed by approximately 100 ng of PCR product of the targeted gene or 100 ng of the gene-specific hyg^+ cassette PCR product. Samples were centrifuged briefly and incubated at 37°C for 90 min. After incubation, 3 µL of 0.25 M EDTA and 4

µL of 6X purple loading dye (New England Biolabs) were added to tubes, mixed well and incubated for a further 10 min at 60°C. The reaction mixtures were centrifuged for a final time for 5 min at 14,000 g and the supernatant was collected and run on a 0.5% agarose gel for visualisation.

Preparation of protoplasts

Mycelia were grown by inoculating 100 mL of PDB growth media in sterilised 250 mL conical flasks. with a *P. coffeae* ANU01 spore suspension and incubating at 22 °C and 140 rpm overnight (~16 hours). Protoplasts were prepared following a modified version of the protocol developed by Solomon *et al.*, (2003). Mycelia were removed from media via centrifugation for 5 min at 4,000 g and 4 °C, before being resuspended in 50 mL of 600 mM $MgSO_4$ wash buffer and centrifuged as before. At this time 400 mg of Extralyze enzyme (Laffort) was added to 25 mL of 1.2 M $MgSO_4$ solution buffered to pH 5.8 with 5M NaOH, and the solution was filter-sterilized. The mycelium pellet was resuspended in the enzymatic solution then the entire contents were transferred to a sterile conical flask, sealed with parafilm and incubated at 28 °C for 3 hours without agitation. The solution was poured into a 50 mL centrifuge tube and gently overlaid with 5 mL of protoplast overlay solution (600 mM sorbitol, 10 mM Tris pH 7.5), before centrifugation at 4,000 g for 15 min at 4°C. Protoplasts were very gently removed from the interface using a 1000 µL pipette and wide-bore filter tips and transferred to a 15 mL centrifuge tube. Protoplasts were gently mixed with an equal volume of 1 M sorbitol-Tris solution (1 M sorbitol, 10 mM Tris-HCl pH 7.5), then centrifuged at 1,500 g for 5 min at 4°C. The supernatant was removed, and protoplasts were washed with 3 mL STC buffer then centrifuged again as previous, once more removing the supernatant. Finally, protoplasts were resuspended in 0.5 mL STC buffer and kept on ice until transformation.

Generating RNPs and transforming protoplasts

Ribonucleoprotein (RNP) complexes were generated for each gene-target by combining 2 µg sgRNA and 6 µg of Cas9 protein and incubating at room temperature for 15 minutes. Each RNP complex was then combined with ~2 µg of gene-specific hyg^+ cassette DNA, and the RNP and donor DNA were added to 100 µL of protoplasts suspended in STC. The samples were gently mixed and incubated at room temperature for 15 minutes. After incubation, 200 µL of transformation buffer (60% polyethylene-glycol (PEG)-4000, 10 mM $CaCl_2$, 10 mM Tris-HCl pH 7.5) was added to the protoplasts and mixed via inversion, followed by a further 200 µL and a final 800 µL of buffer, mixing after every addition. Samples were then incubated at room temperature for 20 min. Control samples with sterile STC and transformation buffer added to protoplasts were also included. The transformation mixture was dispensed in 350 µL aliquots to tubes containing 5 mL of warm (60°C) top-PDA-agar (PDB, 25 g/L; sorbitol, 182.2g/L; agar, 7.5 g/L; adjusted to pH 6.0 with 5M NaOH), mixed via gentle inversion and poured onto the surface of thin proto-PDA-agar plates (PDB 25 g/L, sorbitol, 182.2 g/L; agar, 10 g/L; adjusted to pH 6.0 with 5M NaOH). Plates were sealed and covered with aluminium foil, then incubated

in a temperature-controlled room at 22°C. After 40 hours, 5 mL of warmed (60 °C) top-PDA agar containing 35 µL of Hygromycin B (100 mg/mL) (Invitrogen) was poured onto the media surfaces and they were again covered and left to grow until colonies grew through the overlay. Colonies were subcultured using a sterile blade as they emerged, transferred to individual PDA plates and grown without aluminium foil covering at 22°C in a controlled temperature room under 12 hour day/night cycles.

Confirming insertion of the hyg^+ cassette at the correct location

Insertion of the hyg^+ cassette into the target gene region was confirmed using PCR. Spores from transformant colonies were used to inoculate individual microcentrifuge tubes containing 1 mL of PDB and incubated at 22°C for 2 days to allow growth of mycelia. Mycelia were removed from media via centrifugation at 14,000 g for 10 min and disrupted using a Tissue Lyser II (QIAGEN). DNA was isolated from mycelium following the protocol of Liu *et al.* (2000). Primers to generate an amplicon that included the cut-site and 100-150 bp upstream and downstream of the cut-site were designed using the Primer3 software. Each 25 µL PCR reaction contained 12.5 µL of Onetaq Mastermix (New England Biolabs), 1.25 µL of each primer (10 µM), 2 µL of DNA and 8 µL of nuclease-free water. Amplicons were run on a 1 % agarose gel as per Lee *et al.* (2012), and size of the resulting amplicon was used to determine successful gene-targeting; if the hyg^+ cassette had been successfully inserted within the gene region (~2.1 kbp), or elsewhere in the genome and the gene had remained uninterrupted (~200-300 bp). Successful knockouts were given unique identifiers, subcultured onto PDA plates and maintained as 25% glycerol spore-stocks at -80 °C.

Phenotyping *P. coffeae* ANU01 target-gene knockouts

Measuring *P. coffeae* ANU01 biomass during growth on *Pst* pustules in wheat (*on planta* growth assays)

Impact of gene loss was originally quantified using an *on planta* set up. Spore suspensions were generated as described previously (Chapter Two) from colonies for mutants *ΔPenX_007638-T1*, *ΔPenX_000085-T1* and *ΔPenX_004154-T1* as well as wild type and standardised to 500,000 spores/mL. Wheat seedlings were grown and infected with *Pst* as described previously (Chapter Two) before being sprayed individually with *P. coffeae* ANU01 spores, again as described previously (Chapter Two). Three pots of wheat were infected with *P. coffeae* ANU01 spores for each genotype and were immediately covered with clear cellophane bags to promote humidity (Zhan *et al.*, 2014). Bagged plants were placed in open plastic tubs and grown for 264 hours at 22°C on a 12h day night cycle. One leaf was sampled from each plant at 96, 144 and 264 hours post inoculation and immediately snap frozen. Regions of leaves containing roughly comparable numbers of pustules were cut into two cm fragments and transferred to 2 mL microcentrifuge tubes containing two sterile metal ball bearings. Each

biological replicate consisted of one tube containing three 2 cm fragments and three biological replicates were included for each genotype at each time point. Samples were disrupted for four minutes at 50 Hz in a Tissuelyser II (QIAGEN) and DNA was isolated following the protocol of Liu *et al.* (2000). The resulting DNA pellets were resuspended in 400 µL of nuclease-free water and used in a biomass qPCR following the protocol described in Chapter Two. Briefly, each 10 µL qPCR reaction included 5 µL of Fast SYBR™ Green Master Mix (ThermoFisher), 1.5 µL each of the *P. coffeae* ANU01 specific primers (1 µM) FQ5 (5' ACCCTGAACGCTGTCTGAAG 3') and RQ6 (5' CGCTGCGTTCTTCATCGATG 3') and 2 µL of DNA sample. Three technical replicates were conducted for each sample. The resulting raw Ct values were used to generate a bar-chart shown in Figure 3.1, with lower Ct representing greater *P. coffeae* ANU01 biomass.

Measuring *P. coffeae* ANU01 biomass during growth on *Pst* on "synthetic leaves"

A second approach involved the use of "synthetic leaves" to create the first *in vitro* phenotyping method, in an effort to minimise the variation caused by humidity, spore count in both *P. coffeae* ANU01 mutants and *Pst*, as well as to reduce sampling bias. "Synthetic leaves" were prepared by cutting squares of tissue paper (Kleenex®) measuring 8 × 8 cm, followed by sterilisation by autoclaving. Nine circles of 0.5 cm diameter were drawn onto each square in a 3 × 3 grid format and the tissue paper sheets were secured to the bottom of plastic Petri dishes using laboratory tape. Approximately 5 mg of frozen *Pst* urediniospores were heat-shocked at 42°C for 3 minutes, then suspended in 2 mL of Novec™. The suspension was dispensed in 15 µL aliquots onto six of the drawn circles. Sterile Novec™ was applied to the remaining three to act as negative controls (*Pst* absent). Spore suspensions from a wild type and a *ΔPenX_000085-T1* knockout *P. coffeae* ANU01 colony were prepared as described above and normalised to 500,000 spores/mL. *Penicillium coffeae* ANU01 spore solutions were then dispensed in 5 µL aliquots onto three of the circles containing *Pst* and the three circles without to represent *P. coffeae* ANU01 growth in the presence and absence of *Pst* urediniospores respectively. 5 µL of sterile Milli-Q water was dispensed onto the remaining three circles containing *Pst* urediniospores. Following inoculation, each tissue paper square was wetted with 500 µL of sterile Milli-Q water to create even humidity between plates. Petri dishes were sealed with Parafilm (Amcor) and incubated in a controlled environment facility at 22 °C and 12-hour day/night cycles. Two synthetic leaves were included for each genotype, with one synthetic leaf harvested after 72 and 192 hours. The entire contents of each synthetic pustule were collected using a sterilised biopsy punch tool (KAI) and transferred to individual 2 mL Eppendorf microcentrifuge tubes containing two sterile steel ball bearings. DNA was isolated and used in a biomass qPCR as described above. Ability of wild type and *ΔPenX_000085-T1* mutant *P. coffeae* ANU01 to grow on *Pst* was estimated through measuring increase in biomass in samples which contained *Pst* urediniospores compared to ones where *P. coffeae* ANU01 grew alone. Relative growth for the genotypes was calculated at each time point by first subtracting the average Ct for samples with *Pst*, from samples where *Pst* was absent. This difference in Ct was converted to fold increase using the

formula 2^($Ct_{Pst\ absent}$-$Ct_{Pst\ present}$) and plotted as a bar graph for each genotype. The resulting bar graphs therefore represented how the presence of *Pst* influenced *P. coffeae* ANU01 ability to accumulate biomass (grow) and how loss of *PenX_000085-T1* affected that ability (Figure 3.2). A repeat assay was conducted with identical parameters except for sampling at different time points (96, 144 and 192 hours), (Figure 3.3).

Measuring *P. coffeae* ANU01 biomass during growth on *Pst* urediniospores in 2 mL Eppendorf microcentrifuge tubes

The final phenotyping approach involved a simplified method using synthetic pustules cultured directly within 2 mL Eppendorf tubes, and was attempted to reduce variation caused by sampling. Five mg of frozen *Pst* urediniospores were heat-shocked at 42°C for 3 minutes then suspended in 2 mL of Novec™ and dispensed in 10 µL aliquots to the bottom of sterile 2 mL Eppendorf microcentrifuge tubes. The Novec™ was allowed to evaporate and 5 µL of *P. coffeae* ANU01 spore solutions (made as described above) was aliquoted on top of the dried *Pst* urediniospores and again allowed to dry. Two sterile paper towels were put on the bottom of a clear plastic bag and wet with 10 mL of sterile Milli-Q water. Tubes were left open in a tube rack which was placed on the paper towels within the clear plastic bags. Bags were sealed and moved to a CEF growth chamber and incubated with the same parameters as the tissue paper assays. In all of the 2 mL Eppendorf tube assays, tubes were collected and flash frozen for each strain at zero hours (immediately after drying), then at later time points based on individual assays. Time points differed between runs of the assay in an attempt to find the optimal sampling time for detecting differences in biomass. In the first run of the assay, each tube represented a single replicate (3 tubes per time point). However, in subsequent assays this was changed to include three tubes per replicate, that were combined at the DNA isolation stage. DNA was isolated as described above, with sterile ball bearings added directly to the tubes. DNA was ultimately eluted in 400 µL of nuclease free water for use in qPCR, as described above. Briefly, cycle-threshold (Ct) values for samples collected at later time points were subtracted from the mean Ct for the strain at zero hours to calculate ΔCt for each time point. The ΔCt for each point was then converted into fold-change difference in biomass via the formula: 2^(ΔCt). As an example, the final formula to calculate fold-change difference in biomass for samples collected at 96 hours post inoculation was: 2^($Ct_{zero\ hours}$ -$Ct_{96\ hours}$). Fold-change values for biomass increase over time were plotted onto bar graphs.

3.3 Results

Choosing *P. coffeae* ANU01 candidate hyperparasitism genes for knockout experiments

I selected genes for knock out based on suggestive functional annotation and high upregulation during parasitism. I defined suggestive functional annotation as including genes possibly related to; antagonism and defence, cell-wall degradation, and nutrient acquisition, aspects I hypothesised were at the core of parasitism in Chapter Two. I ultimately selected 18 genes for knock out, which I will refer to as target or candidate genes throughout this report. It is important to note that although gene models were supported by RNA-seq evidence, each gene's functional annotation is the result of *de novo* annotation and is therefore still only a prediction.

During parasitism, *P. coffeae* ANU01 strongly upregulated a biosynthetic gene cluster (BGC) responsible for the production of the weakly antifungal metabolite depudecin. In Chapter Two, I proposed that this cluster may play a role in suppressing *Pst* urediniospore germination or weakening the host's defence responses. To investigate this, I selected two genes within the cluster: *PenX_003989-T2* (log_2 fold change: 14.4), encoding the depudecin efflux pump *DEP3,* and *PenX_003991-T1* (log_2 fold change: 6.3), encoding a depudecin monooxygenase required for compound biosynthesis. To further investigate the importance of BGCs I included the transcription factor *PenX_000085-T1* (log_2 fold change: 5.3), which belongs to an unannotated non-ribosomal peptide synthase (NRPS) BGC. Peroxiredoxins are enzymes that act in removing the harmful reactive oxygen species (ROS) that arise from metabolism and host immune response (Ross *et al.,* 2000). To test whether *P. coffeae* ANU01 uses its highly upregulated peroxiredoxin genes, *PRX5* (*PenX_007731-T1*) and *PRX7* (*PenX_007733-T1*) (log_2 fold change: 10.3 and 9.9 respectively) for a similar purpose, I decided to target them for knock out. The rust spore coat, rich in β-glucans, chitin, and other complex polysaccharides (Xiao *et al.,* 2023), presents a significant physical barrier to hyperparasites. In Chapter Two, I showed that *P. coffeae* ANU01 upregulates genes encoding secreted cell wall-degrading enzymes during infection. Based on this, I selected two genes encoding glycoside hydrolases in *PenX_004154-T1* (log_2 fold change: 9.2) a GH64 CAZyme and the highly upregulated GH5 secreted chitosanase *PenX_011559-T1* (log_2 fold change: 11.1). I also selected one of *P. coffeae* ANU01's three predicted polysaccharide lyase CAZyme genes in *PenX_000326-T1* (log_2 fold change: 3.5), which may assist in breaking down urediniospore coat polysaccharides. Since urediniospore coat polysaccharides may also serve as carbon sources, I included these genes to explore their importance in both penetration and nutrient acquisition.

To investigate nutrient acquisition further, I focused on genes associated with lipid and carbohydrate metabolism. I selected *PenX_000159-T1* (log_2 fold change: 6.4), a highly upregulated, secreted lipase encoding gene that may break down lipids in rust spores, and *PenX_007638-T1* (log_2 fold change: 8.9), encoding the *STL1*-like glycerol transporter gene, which could facilitate uptake of glycerol, a sugar

alcohol which is stored as a cryoprotectant by rust fungi and released from fatty acids during lipid catabolism (Klein *et al.,* 2017; Maclean & Scott 1976). I included the gene *PenX_001184-T1* (log_2 fold change: 8.6) a predicted L-galactonate dehydratase commonly associated with the breakdown of pectin, to measure if it is also used in consumption of *Pst* urediniospores. I also targeted a transcription factor with importance as a transcriptional activator of fatty acid utilisation in the *CTF1*-like gene *PenX_003326-T2* (log_2 fold change: 2.7).

In addition to my three predicted primary parasitic functions, I investigated other potentially important factors. I targeted a predicted kinesin motor protein gene in *PenX_008566-T1* (log_2 fold change: 2.5) that may assist *P. coffeae* ANU01 in growing across the wheat leaf surface towards its host. G protein-coupled receptors (GPCRs) are membrane-bound cell surface recognition proteins (Lara-Martinez *et al.,* 2025). I selected the predicted GPCR gene *PenX_003622-T1* (log_2 fold change: 5.8), a component of a BGC, to investigate if its loss had an effect on *P. coffeae* ANU01's ability to sense *Pst*. I selected a predicted ER-localised membrane protein gene in *PenX_011498-T1* (log_2 fold change: 11.5) for its potential importance in vesicle transport and secretion, and the fact that it is the third most upregulated gene during growth on rust spores. I targeted *PenX_010067-T1* (log_2 fold change: 9.9) and *PenX_004159-T1* (log_2 fold change: 12.3), two highly upregulated genes with no functional annotation beyond predicted secretion signals, to investigate whether they act as previously unrecognised contributors to parasitism. Finally, I chose to target the highly upregulated predicted transcription factor *PenX_010964-T1* (log_2 fold change: 6.5) in an attempt to affect several genes or processes through a single target gene. A summary of the target genes, their regulation during growth on *Pst* pustules, and their predicted function is presented below (Table 3.1).

Table 3.1. The eighteen target genes originally selected for knockout. Genes are listed with their log_2 fold change during parasitism and their predicted functional annotations

Target gene	Log_2 fold change during growth on *Pst*	Predicted protein
PenX_000085-T1	5.3	Transcription factor within a BGC (unknown function)
PenX_000159-T1	6.4	Secreted lipase
PenX_000326-T1	3.5	Secreted polysaccharide lyase (PL20 CAZyme)
PenX_001184-T1	8.6	LGD1 L-galactonate dehydratase (pectin breakdown)
PenX_003326-T2	2.7	CTF1, transcription factor involved in activating fatty acid metabolism
PenX_003622-T1	5.8	GPCR cell surface receptor within an unannotated BGC
PenX_003989-T2	14.4	Depudecin efflux transporter (Depudecin-like BGC)
PenX_003991-T1	6.3	Depudecin monooxygenase (biosynthesis gene) (Depudecin-like BGC)
PenX_004154-T1	9.2	Secreted β-glucanase (GH64 CAZyme)
PenX_004159-T1	12.3	Secreted protein (unknown function)
PenX_007638-T1	8.9	STL1 glycerol transporter
PenX_007731-T1	10.3	PRX5 peroxiredoxin
PenX_007733-T1	9.9	PRX7 peroxiredoxin
PenX_008566-T1	2.5	Kinesin movement protein
PenX_010067-T1	9.9	Secreted protein (unknown function)
PenX_010964-T1	6.5	Transcription factor (unknown function)
PenX_011498-T1	11.5	Secreted protein (intracellular trafficking)
PenX_011559-T1	11.1	Secreted chitosanase (GH75 CAZyme)

In vitro CRISPR cleavage assays to measure efficiency of gene-target disruption

To assess the quality of my sgRNA designs, I tested their ability to cleave gene-target PCR products *in vitro*. I incubated each gene-specific sgRNA with either an amplicon of the target gene region or the corresponding gene-specific hyg^+ cassette, both in the presence and absence of the Cas9 endonuclease.

I visualised the resulting DNA fragments on an agarose gel to evaluate cleavage efficiency and specificity. Due to limitations in sgRNA availability, I did not test every sgRNA *in vitro*. Instead, I selected a subset of six sgRNAs as a proof of concept to evaluate the general reliability of the design strategy. The results of these assays, shown in Supplementary Figure 3.2, demonstrate successful cleavage at the expected target sites. Specifically, I observed two smaller DNA fragments in reactions containing both the sgRNA and Cas9, consistent with targeted specific targeted cleavage. In contrast, the full-length 1.7 kb hyg^+ cassette remained intact in all reactions, indicating that the sgRNAs did not cleave within the cassette sequence. Based on these results, I proceeded with *in vivo* gene knockout in *P. coffeae* ANU01 protoplasts.

Transforming protoplasts to generate loss-of-function in individual gene-targets

I transformed a total of fifteen single-gene sgRNA and hygromycin resistance (hyg^+) cassettes individually into *P. coffeae* ANU01 protoplasts. To generate the protoplasts, I followed a modified version of the protocol described by Solomon *et al.* (2003), and introduced the sgRNA and hyg^+ cassettes using PEG-mediated transformation. After 40 hours of incubation, I overlaid the plates with hygromycin-containing media to select for resistant colonies. I then subcultured resistant colonies as they grew through the overlay. Transformation was highly efficient for eleven gene-targets: *PenX_007638-T1*, *PenX_000085-T1*, *PenX_010067-T1*, *PenX_001184-T1*, *PenX_011498-T1*, *PenX_000159-T1*, *PenX_008566-T1*, *PenX_011559-T1*, *PenX_003991-T1*, *PenX_000326-T1* and *PenX_03989-T2*. Each transformation produced between 30 and 50 hygromycin-resistant colonies. In contrast, transformations involving gene-targets *PenX_003326-T2* and *PenX_010964-T1* yielded fewer colonies, with approximately 15 resistant colonies each. I was unable to recover any resistant colonies for gene-targets *PenX_004154-T1* and *PenX_004159-T1*, despite repeating the transformations multiple times. To improve outcomes for *PenX_004154-T1* and *PenX_004159-T1*, I redesigned the sgRNA sequences and homology arms to target different regions of the same genes. Using these revised constructs, I obtained two resistant colonies for *PenX_004154-T1*. However, I still did not recover any resistant colonies for *PenX_004159-T1*. I did not perform transformations for gene targets *PenX_007731-T1*, *PenX_007733-T1* and *PenX_003622-T1* due to time constraints. All knockout strains displayed morphology and growth patterns indistinguishable from the wild type during growth on PDA plates.

To determine whether the hyg^+ cassette had integrated at the intended genomic loci, I carried out PCRs using primers that flanked the sgRNA cut-site. Successful insertions were expected to produce a ~2.1 kbp amplicon, reflecting the integration of the 1.7 kbp hyg^+ cassette. Unmodified loci were expected to yield a wild-type band of approximately 300 bp. I visualised the PCR products on agarose gels to distinguish between targeted insertions, wild type, and cases where no amplification occurred. For gene

targets *PenX_007638-T1*, *PenX_000085-T1*, *PenX_001184-T1*, *PenX_000159-T1*, *PenX_008566-T1*, *PenX_011559-T1*, *PenX_003991-T1*, and *PenX_000326-T1* I identified at least two to three independent transformants showing the expected ~2.1 kbp band, consistent with successful targeted insertions. Two colonies recovered from the *ΔPenX_004154-T1* transformation both showed correct insertion of the cassette at the target site. All colonies I screened for genes *PenX_003326-T1* and *PenX_010964-T1* displayed only the wild-type band, indicating that the cassette had inserted ectopically without disrupting the target loci. In several cases across various genes, the PCR failed to amplify any product. This may be the result of multiple insertions of the hyg^+ cassette making the target region not amplifiable by standard PCR. To investigate this, I conducted PCR using my gene-specific primers and internal primers within the hyg^+ cassette (both forwards and reverse) which all produced bands. This suggested that there were multiple hyg^+ inserts and thus the PCR I ran with the gene-specific primers was unable to bridge the overly large gap. A genotyping gel is presented in the Supplementary Material (Supplementary Figure 3.1). I was unable to screen transformants for gene-targets *PenX_010067-T1* and *PenX_011498-T1* due to time constraints.

Investigating the impact of loss-of-function in target genes on ability of *P. coffeae* ANU01 to grow on *Pst*

I measured the impact of loss-of-function in the target genes by using qPCR to compare the ability of mutant *P. coffeae* ANU01 strains to grow on *Pst* urediniospores, relative to the wild type. Changes in biomass were used as a proxy for changes in hyperparasitic fitness in the mutants. In all of my assays, I essentially grew *P. coffeae* ANU01 on *Pst* urediniospores and collected samples at different time points. I isolated DNA from the collected tissue and used qPCR with *P. coffeae* ANU01 specific primers to estimate how much *P. coffeae* ANU01 tissue existed within each sample at each time point. Cycle threshold (Ct) describes the number of PCR cycles taken for amplified DNA to raise fluorescence above the background detection threshold (Bonacorsi *et al.*, 2021). A lower Ct indicates a greater concentration of original DNA template, and therefore greater approximate *P. coffeae* ANU01 biomass. I used differences in Ct between genotypes to determine which grew more effectively on *Pst*, and used that as an approximation of its ability to act as a rust hyperparasite.

Phenotyping the knockout mutants was a lengthy process involving many changes to experimental design as well as the calculations I used to determine differences in growth. Set up for each phenotyping assay took a long time and it was not possible for me to extensively troubleshoot each approach, meaning elements such as timepoints often differ seemingly arbitrarily between approaches. Due to this, the results of individual assays cannot therefore be reliably compared to one another. Within this results section, I describe the reasoning behind each of the decisions I made regarding initial experimental design, time points for sampling and the method I took to approximate differences in biomass. Briefly, my first attempt to phenotype mutants involved growing wild type and knockout *P.*

coffeae ANU01 on *Pst* pustules on the leaves of wheat seedlings. This was the only assay where I reported raw Ct values as estimations of biomass. Issues with variability led me to move from there to a series of *in vitro* assays. I first attempted to troubleshoot an assay using tissue paper as "synthetic leaves" to co-inoculate *P. coffeae* ANU01 and *Pst* on, before settling on a similar assay using 2 mL Eppendorf tubes.

Overall, comparing relative biomass between mutants and the wild type allowed inference of whether loss-of-function in the target genes affected the ability of *P. coffeae* ANU01 to grow on *Pst*, and by extension, its hyperparasitic fitness.

Investigating the impact of loss-of-function in three target genes on growth of *P. coffeae* ANU01 on *Pst* pustules in wheat

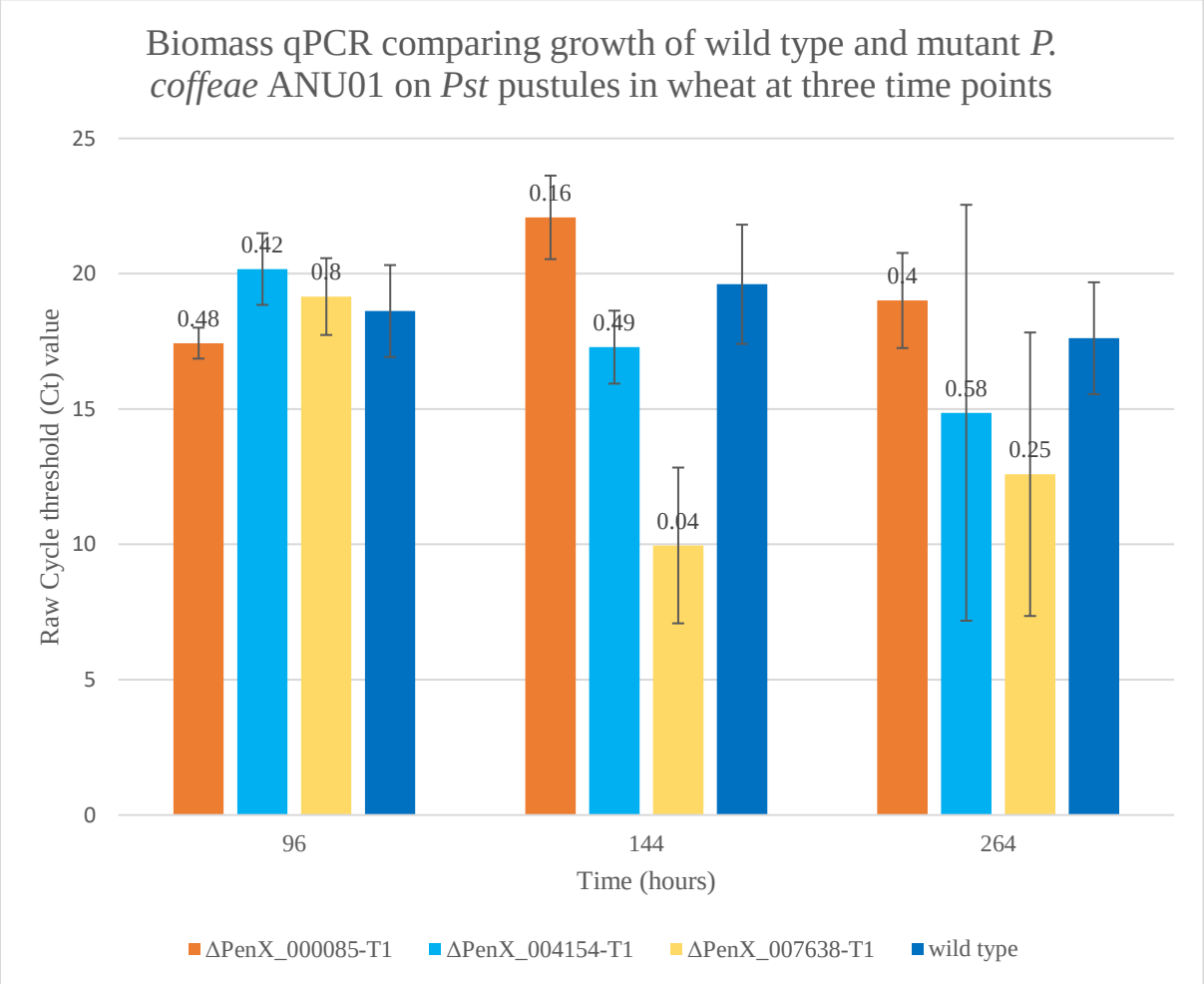

Figure 3.1. Bar graph showing raw quantitative PCR (qPCR) Ct values representing biomass of wild type and knockout (Δ*PenX_000085-T1* (BGC transcription factor), Δ*PenX_004154-T1* (secreted GH64 CAZyme) and Δ*PenX_007638-T1* (glycerol transporter)) *P. coffeae* ANU01 growing on *Pst* pustules in wheat at 96, 144, and 264 hours post-inoculation. Lower Ct values indicate higher DNA abundance.

Error bars represent mean ± standard deviation (n =3). Statistical significance was determined using a Welch's t-test comparing mutants individually to the wild type, individual *P* values are presented atop bars. The only statistically significant relationship was a lower Ct (indicating greater biomass) of the Δ*PenX_007638-T1* knockout, compared to the wild type at 144 hours (P = 0.04).

On planta (growth on the surface of pustules in infected plants) phenotyping produced highly variable results for the wild type and each of the first three mutants examined; Δ*PenX_000085-T1* (transcription factor within BGC), Δ*PenX_007638-T1* (glycerol transporter) and Δ*PenX_004154-T1* (secreted carbohydrate degrading enzyme). My initial approach to phenotyping was to use an experimental set-up as close to that of the initial *P. coffeae* ANU01 RNAseq experiment (Chapter Two) as possible. Briefly, I sprayed *P. coffeae* ANU01 spore suspensions onto wheat seedlings that had been infected with *Pst* and were presenting pustules (13 dpi), enclosed seedlings in plastic bags and isolated tissue (2 cm fragments of infected leaves) after 96, 144 and 264 hours for quantification with qPCR. Due to lack of understanding in the exact timeline of *P. coffeae* ANU01 parasitism, choosing these time points was somewhat arbitrary. However, I chose these time points to collect samples as *P. coffeae* ANU01 commonly presents as white fluffy growth atop pustules at 11 days (264 hours) (Chapter Two) and I believed that four (96 hours) and six days (144 hours) after spraying could serve as markers to investigate which genes were important at early, middle and late-stage infections. I chose these three genes in particular to investigate if they were important at certain times. For example, I chose the cell wall degrading enzyme encoding gene *PenX_004154-T1* to see if its loss would impact the early stage of infection where it might be used to break the urediniospore coat. The BGC transcription factor encoding gene *PenX_000085-T1* may also be used in earlier stages of infection to antagonise urediniospores, while the glycerol transporter encoding gene *PenX_007638-T1* might be used in later stages of the infection to transport nutrients into *P. coffeae* ANU01. Visual observation of pustules did not indicate a strong phenotype in any of the mutants, all appearing similar to the wild type. The beginnings of fluffy growth emerged on several pustules in all genotypes by 144 hours and I observed white fluffy growth on the surface of all *Pst* pustules by 264 hours in all plants regardless of *P. coffeae* ANU01 genotype. Over the course of the assay, I encountered several sources of variability that affected *P. coffeae* ANU01 growth. Stripe rust infections were not even, with pustule distribution on leaves often inconsistent between leaves and pots of seedlings. Condensation within the bags also appeared to vary greatly, suggesting higher humidity closer to the soil and the sides of the bag. In many cases, I observed increased *P. coffeae* ANU01 growth on leaf surfaces that were in direct contact with the inner surfaces of the plastic bags. This variability made it difficult to obtain unbiased samples that was ultimately manifest in the qPCR data (Figure 3.1). At this stage of my investigation, I had not yet developed a system to convert Ct values into more easily readable values (fold increase in biomass). The Ct values are therefore presented without any conversion, with lower Ct values indicating greater biomass and vice versa. Comparing growth profiles, Ct values across the three time points showed erratic patterns

for all strains apart from Δ*PenX_004154-T1* (secreted GH64 CAZyme). The qPCR showed decreased biomass at 264 hours compared to 144 hours in Δ*PenX_007638-T1* (glycerol transporter), and a slight increase in biomass at 144 hours compared to 96 hours for the wild type. The highest (lowest biomass) and lowest (greatest biomass) Ct values were both observed at 144 hours in Δ*PenX_007638-T1* (glycerol transporter) and Δ*PenX_000085-T1* (BGC transcription factor) respectively. The only genotype to show steady increase in biomass was Δ*PenX_004154-T1* (secreted GH64 CAZyme), which showed steady decrease in Ct as time progressed. At 144 hours Δ*PenX_004154-T1* showed significantly lower Ct (greater biomass) than the biomass, the only statistically significant relationship across the assay. Otherwise, I found no statistically significant relationship between the mutants and the wild type at any of the time points using individual t-tests. Knocking out the genes *PenX_004154-T1*, *PenX_007638-T1* and *PenX_000085-T1* clearly did not halt the ability of *P. coffeae* ANU01 to use *Pst* urediniospores for growth. However, I was unable to quantify whether a difference in fitness exists between the mutants and wild type using the *on planta* system. I decided that the variability in this set up was too high to warrant repeating the assay or using it to investigate other genes and moved on to developing an *in vitro* system where I could more easily control variables such as the amount of *Pst* urediniospores and humidity. Importantly, although Ct differences may appear small, amplification in qPCR is exponential, meaning each 1-2 shift in Ct corresponds to a 2-4-fold difference in biomass (Bonacorsi *et al.*, 2021). Ultimately meaning that raw Ct values that may seem close can in fact mask large differences in *P. coffeae* ANU01 biomass. It was therefore imperative that I come up with a better method to compare differences between mutants and the wild type in terms of growth.

Developing a "synthetic leaf" system on tissue paper to phenotype loss-of-function mutants in growth on *Pst* urediniospores

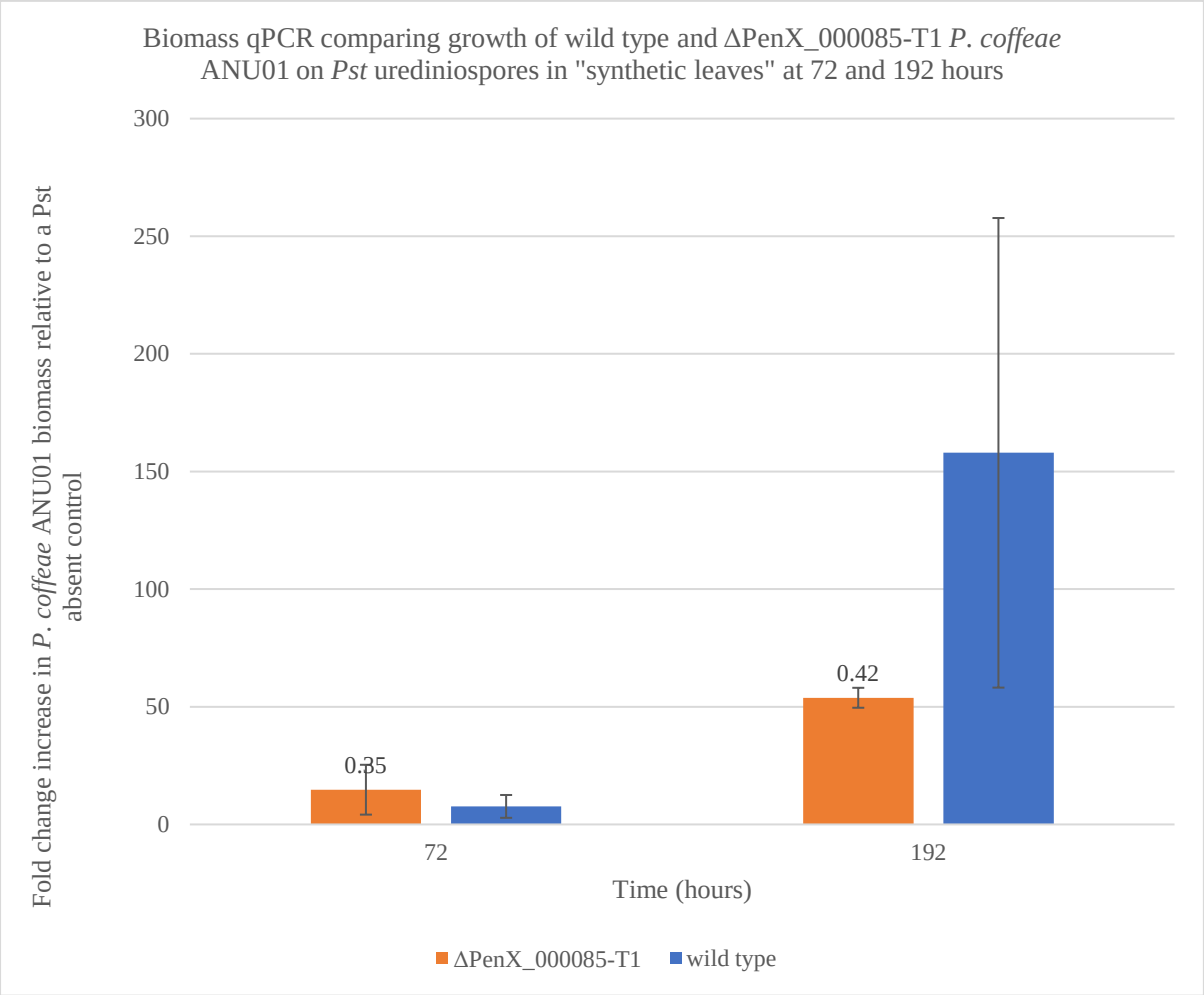

Figure 3.2. Bar graph showing relative biomass change of *PenX_000085-T1* and wild-type *P. coffeae* ANU01 when grown on *Pst* urediniospores on "synthetic leaves". Bars show the fold increase in fungal biomass in the presence of *Pst* compared with growth in the absence of *Pst* at 72 and 192 hours. Error bars represent mean ± standard deviation (n =3). Statistical significance was determined using a Welch's t-test comparing the mutant to the wild type at each time point and the resulting *P* values are presented above the bars, the relationship was not significant at any time point.

My first attempt to develop an *in vitro* phenotyping system involved growing wild type and Δ*PenX_000085-T1* (BGC transcription factor) *P. coffeae* ANU01 on patches of *Pst* urediniospores on a piece of tissue paper acting as a "synthetic leaf". Briefly, I first aliquoted *Pst* urediniospores in small circles on tissue paper to simulate pustules each with an identical amount of *Pst* spores. I then aliquoted 5 µL of *P. coffeae* ANU01 spores on top of the *Pst* urediniospores, and allowed all liquid to evaporate before adding fresh sterile water to the paper to facilitate even humidity and sealing "synthetic leaves"

in petri dishes. I calculated that each sample contained approximately 0.025 mg of *Pst* urediniospores and 2,500 individual *P. coffeae* ANU01 spores for all of the *in vitro* assays in this report. I chose this ratio as I hoped that it would measure *P. coffeae* ANU01 growing from a small initial input with *Pst* as the only source of nutrients, as I hypothesise it does on the wheat leaf. Importantly, in this assay I estimated changes in *P. coffeae* ANU01 biomass by comparing samples with *Pst* present, to samples with *Pst* absent for each genotype at each time point. This allowed for a more appropriate calculation (fold-change increase due to presence of *Pst* spores) of impact of gene-loss than raw Ct values. However, this experiment and the repeat displayed below (Figure 3.3) were the only two times I used this calculation. In subsequent experiments (2 mL Eppendorf tube assays) I approximated changes in biomass by comparing samples at later time points to samples collected at hour zero. The first time I ran this assay, loss-of-function in *PenX_000085-T1* (BGC transcription factor) appeared to perhaps have an impact on the ability of *P. coffeae* ANU01 to grow on *Pst* (Figure 3.2) at 192 hours. Growth between wild type and Δ*PenX_000085-T1 P. coffeae* ANU01 was approximately equal at 72 hours (7.7 ± 4.8-fold increase and 14.8 ± 10.6-fold increase respectively). However, the wild type showed a (non-statistically significant) greater increase in biomass (158 ± 99.8-fold increase) than the knockout (53.8 ± 4.2-fold increase) after 192 hours, suggesting the gene may be important to growth on *Pst.* I believe the failure to garner a result that was statistically significant was in part due to two of the tubes containing wild type samples exploding during the disruption step, resulting in a partial loss of input tissue, lower biomass values and therefore high variation. The low variation between Δ*PenX_000085-T1* replicates suggested to me that the issue lay not in experimental design but in those disrupted wild type tubes and that a repeat assay would support my hypothesis that loss of function in *PenX_000085-T1* (BGC transcription factor) was in fact leading to decreased biomass. Not only did this approach initially yield data that might support identification of a potentially important gene to parasitism, the tighter error bars suggested that my movement from *on planta* to a more controlled *in vitro* set up had at least reduced my previous issues with variability. Based on this possible success, I decided to run a repeat of the assay, however due to the time required to run each assay, I decided to try and include more data by changing the times I collected tissue to 96, 144 and 192 hours.

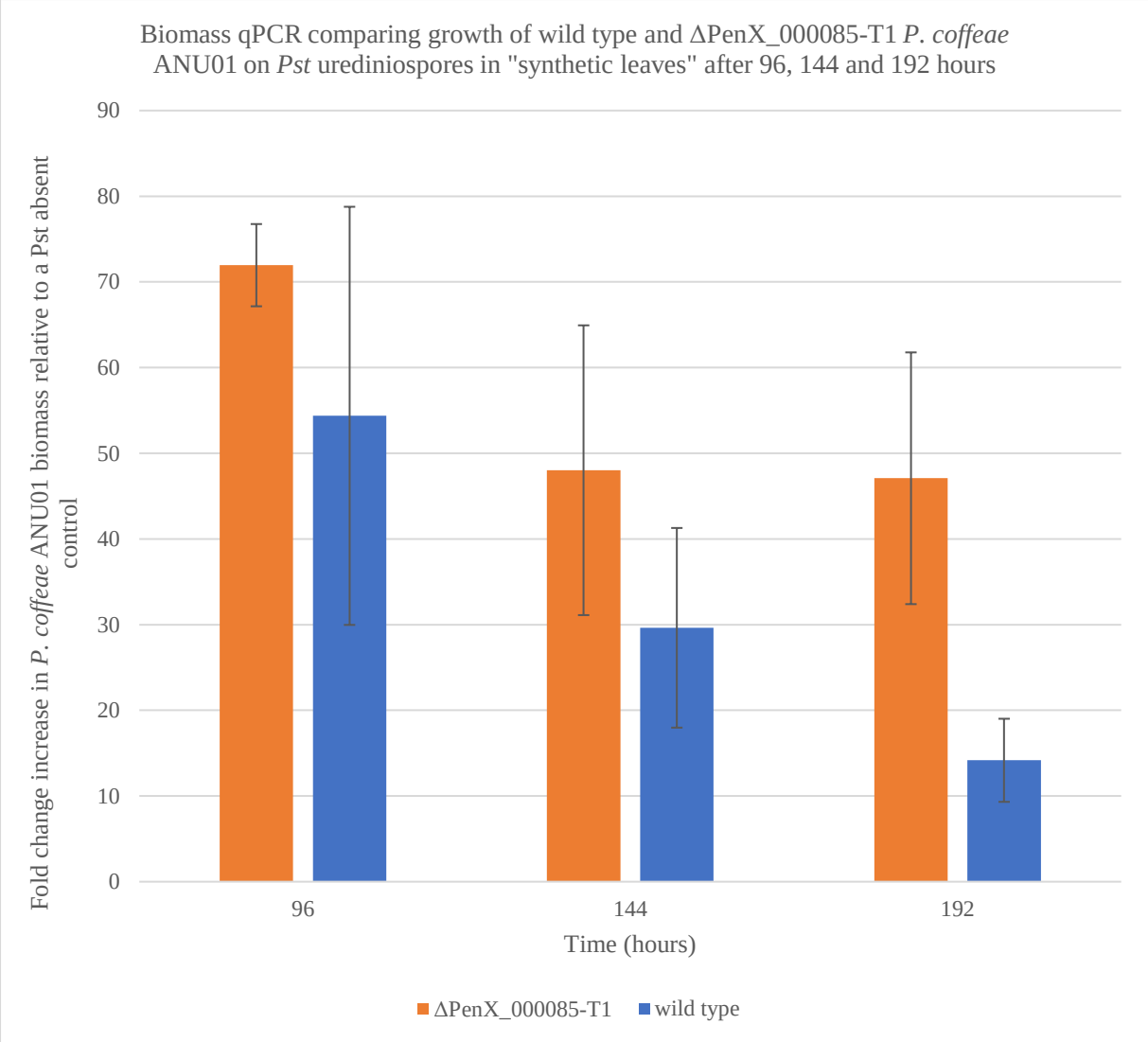

Figure 3.3. Bar graph showing relative biomass change of *PenX_000085-T1* and wild-type *P. coffeae* ANU01 when grown on *Pst* urediniospores on "synthetic leaves" made from tissue paper. Bars show the fold increase in *P. coffeae* ANU01 biomass in the presence of *Pst* compared with growth in the absence of *Pst* at 96, 144 and 192 hours. Error bars represent mean ± standard deviation (n =3). Statistical significance was determined using a Welch's t-test comparing the mutant to the wild type, the relationship was not significant at any time point (96 hours, P = 0.34, 144 hours, P = 0.2 and 192 hours, P = 0.06).

My initial observation in decreased biomass due to loss-of-function in the predicted BGC transcription factor gene *PenX_000085-T1* did not repeat in the second run-through of my "synthetic leaf" set up. I measured increase in biomass at 96, 144 and 192 hours. In both the wild type and Δ*PenX_000085-T1* knockout, *P. coffeae* ANU01 biomass appeared to decrease as time progressed (Figure 3.3). At each time point, the knockout showed greater biomass than the wild type, with the highest biomass observed at 96 hours in the knockout (71 ± 4.8-fold increase). Unexpectedly, I observed the lowest biomass at

192 hours in the wild type (14.2 ± 4.8-fold increase). Variation between replicates was much greater in this assay compared to the initial "synthetic leaf" assay and according to t tests comparing mutant and wild type at each time point, there were no statistically significant relationships. Ultimately the repeat assay did not replicate the initially promising data of my preliminary assay with Δ*PenX_000085-T1* (BGC transcription factor) and therefore the results of the preliminary assay cannot be considered valid. I hypothesise that the issues with variability in this assay predominantly came from sampling, where I again used a hole punch to collect samples from the tissue paper, which was often messy and prone to partial loss of samples. I decided that the most effective plan to move forward was to focus on a similar approach but this time in a closed system where I could directly lyse and measure samples without the need to transfer tissue. This led me to develop a system where I used a similar procedure but in the bottom of 2 mL Eppendorf tubes in place of on the surface of tissue paper.

Transitioning to measuring growth of loss-of-function *P. coffeae* ANU01 mutants on *Pst* urediniospores in a novel 2 mL Eppendorf tube assay

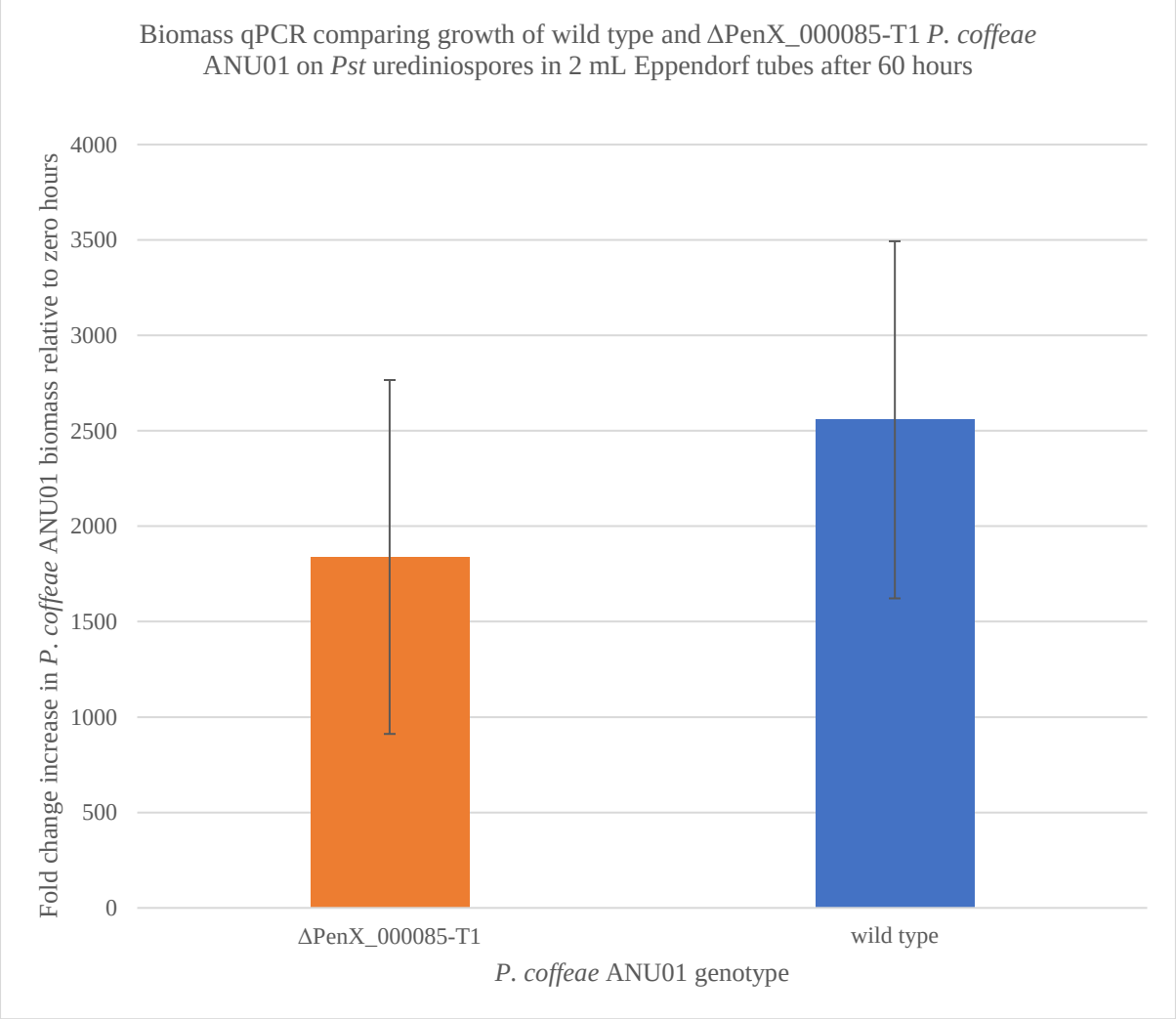

Figure 3.4. Bar graph showing fold change in *P. coffeae* ANU01 biomass in wild-type and

Δ*PenX_000085-T1 (*BGC transcription factor knockout) strains following co-incubation with *Pst* urediniospores in 2 mL Eppendorf tubes at 72 hours. Error bars represent mean ± standard deviation (n =3). Statistical significance was determined using a Welch's t-test comparing the mutant to the wild type, the relationship was not significant (P = 0.48).

Briefly, the new set up involved dispensing 10 µL *Pst* urediniospores suspended in Novec™ into the bottom of 2 mL Eppendorf tubes, allowing the Novec™ to evaporate before adding 5 µL of *P. coffeae* ANU01 spores suspended in water and again waiting for all liquid to evaporate. Eppendorf tubes were left open and upright for the course of the assay in a tube rack. To simulate the high humidity needed for parasitism I placed the tube rack on top of two sterile paper towels soaked with 10 mL of Milli-Q water and sealed the apparatus within a clear plastic bag. Each replicate was represented by a single 2 mL Eppendorf tube, with three replicates per time point for each genotype. As mentioned above, this experimental set up also differed from the previous in the way that I calculated increases in biomass. Rather than comparing *P. coffeae* ANU01 in the presence of *Pst* to the absence of *Pst,* I calculated increase in biomass at each time point by comparing it to the initial biomass of the strain at zero hours. I felt this method more accurately represented the changes in *P. coffeae* ANU01 biomass over time and continued using it for the remainder of this report. To test the set up I again used Δ*PenX_000085-T1* (BGC transcription factor) and captured samples after 72 hours. Both the wild type and the knockout were capable of growth in this set up with *Pst* urediniospores as the sole source of nutrition (Figure 3.4). Though the wild type appeared to show greater biomass at 72 hours (2557.5 ± 935.6-fold increase) than the Δ*PenX_000085-T1* mutant (1838.8 ± 927.1- fold increase) it was not statistically significant (P = 0.38) due to the high degree of variability between replicates. In comparison to all of the assays I conducted in this report, this was the greatest increase in *P. coffeae* ANU01 biomass. I was unable to decern why changing to the 2 mL Eppendorf tube system would lead to this radical increase, especially given it was unique to this specific run. In a final attempt to reduce variability in this set up, I decided to increase the number of 2 mL Eppendorf tubes per replicate from one to three.

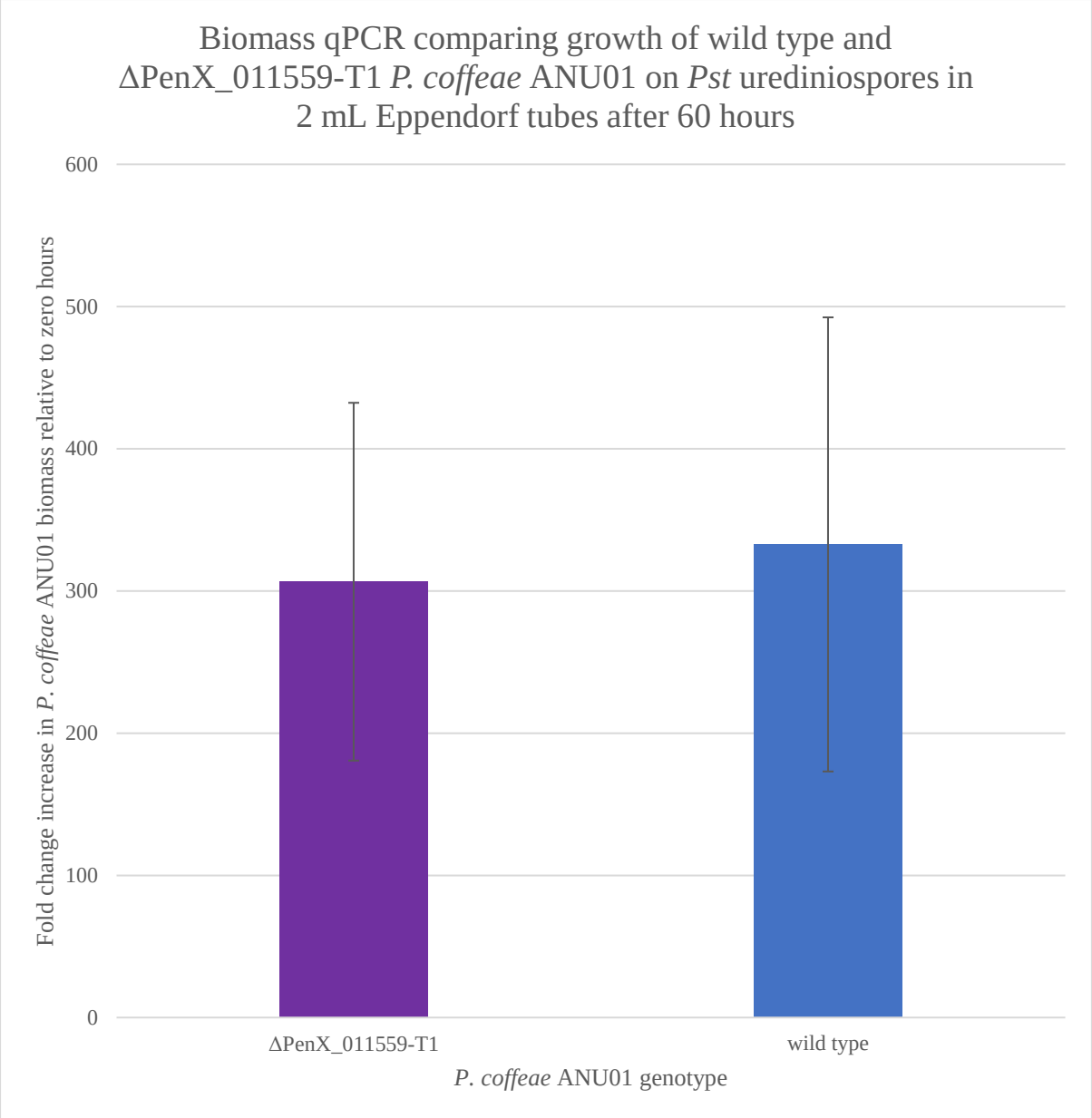

Figure 3.5. Bar graph showing fold change in *P. coffeae* ANU01 biomass in wild-type and Δ*PenX_011559-T1* (secreted chitosanase) strains following co-incubation with *Pst* urediniospores in 2 mL tubes at 60 hours. Error bars represent mean ± standard deviation (n =3). Statistical significance was determined using a Welch's t-test comparing the mutant to the wild type, the relationship was not significant (P = 0.83).

Briefly, I made a final attempt to reduce variability in my *in vitro* 2 mL Eppendorf tube set up by increasing the number of tubes per replicate from one to three. Due to the previous unpredictability of Δ*PenX_000085-T1*, I also switched to investigating Δ*PenX_011559-T1* (secreted chitosanase), and compared increase in biomass with the wild type at 60 hours rather than 72 to see if a difference existed at that stage of the interaction. As with Δ*PenX_000085-T1* (BGC transcription factor), loss-of-function in *PenX_011559-T1* (secreted chitosanase) did not completely eliminate the ability of *P. coffeae*

ANU01 to grow on *Pst* urediniospores (Figure 3.5). Unfortunately, increasing the number of tubes within each replicate did not significantly reduce variability and the phenotyping remained unreliable. I observed no statistically significant difference (P = 0.83) in biomass between the wild type (332.7 ± 159.7-fold increase) and the Δ*PenX_011559-T1* knockout (306.5 ± 125.8-fold increase) after 60 hours of growth. Despite the high variability, I decided to use this phenotyping approach to do a final phenotyping of 9 mutants, with the logic that I would at least be able to determine if loss of function in any of the genes lead to complete inability to grow on *Pst*.

A final attempt to measure growth of nine loss-of-function *P. coffeae* ANU01 mutants on *Pst* urediniospores in a novel Eppendorf tube system

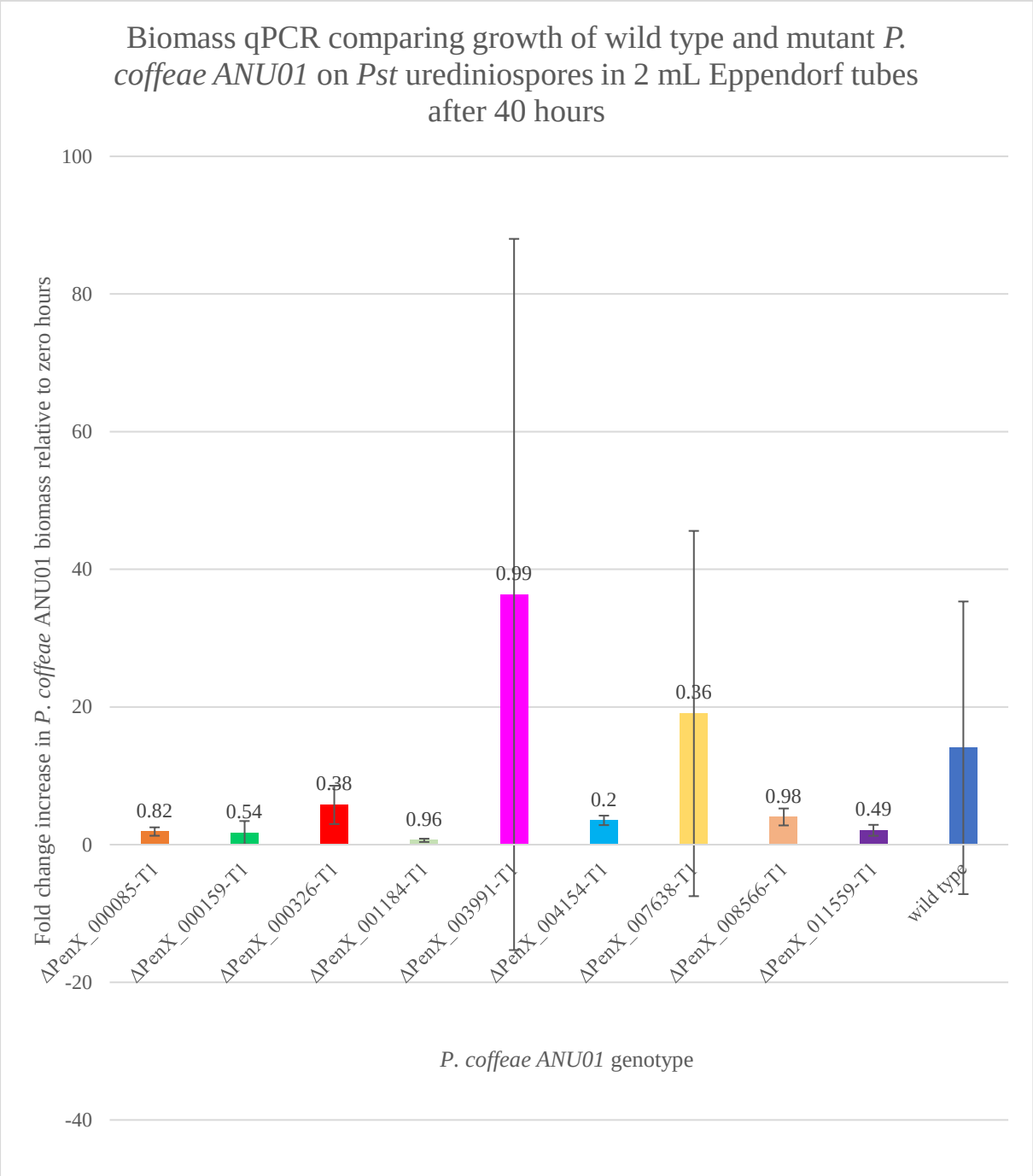

Figure 3.6. Bar graph showing fold change in *P. coffeae* ANU01 biomass in wild-type and nine mutant strains following co-incubation with *Pst* urediniospores in 2 mL Eppendorf tubes at 40 hours. Error bars represent mean ± standard deviation (n =3). Statistical significance was determined using a Welch's t-test comparing each mutant individually to the wild type (individual *P* values are presented at the top of bars), none of the differences were statistically significant. Descriptions of predicted mutant loss-of-function genes are as follows; Δ*PenX_000085-T1* (transcription factor from unannotated BGC),

Δ*PenX_000159-T1* (secreted lipase), Δ*PenX_000326-T1* (secreted polysaccharide lyase), Δ*PenX_001184-T1* (L-galactonate dehydratase), Δ*PenX_003991-T1* (depudecin biosynthesis gene), Δ*PenX_004154-T1* (secreted GH64 CAZyme), Δ*PenX_007638-T1* (*STL1* glycerol transporter), Δ*PenX_008566-T1* (kinesin motor protein) and Δ*PenX_011559-T1* (secreted chitosanase).

I used the 2 mL Eppendorf tube set up to measure fold change increase in biomass in nine mutants at 40 and 70 hours post inoculation. I chose these two time points as a final attempt to investigate both a new time point (40 hours) and a time point similar to those I had investigated previously (70 hours). None of the nine knockout mutants showed a statistically significant difference in phenotype compared to the wild type in my final attempt to phenotype the impact of gene loss. As described previously, I was unable to develop a reliable method to detect subtle differences in fitness between the knockouts and the wild type. Thus, the aim of this final assay was to determine whether any of the mutants were completely unable to grow with *Pst* urediniospores as the sole nutrient source, or if any mutants exhibited distinct phenotypes. All genotypes showed an increase in biomass relative to the zero-hour samples at 40 hours (Figure 3.6). However, I observed substantial variability between replicates, particularly in the strains with the largest increases in biomass. I observed the greatest increase in biomass in the Δ*PenX_003991-T1* (depudecin biosynthesis gene) knockout, which showed a 36 ± 51.6-fold increase, followed by the Δ*PenX_007638-T1* (*STL1* glycerol transporter) knockout (19 ± 26.5-fold increase) and the wild type (14 ± 21.3-fold increase). In contrast, the smallest biomass increases were observed in the Δ*PenX_001184-T1* (L-galactonate dehydratase) knockout, which showed a minimal increase (0.6 ± 0.2-fold increase) and Δ*PenX_000159-T1* (secreted lipase), with only a 1.7 ± 1.7-fold increase in biomass. The data were highly variable, with certain genotypes (Δ*PenX_003991-T1*, Δ*PenX_007638-T1*, and the wild type) exhibiting one replicate with significantly higher biomass than the other two replicates. Due to this variability, individual t-tests comparing each mutant to the wild type revealed no statistically significant differences in biomass accumulation between any of the genotypes.

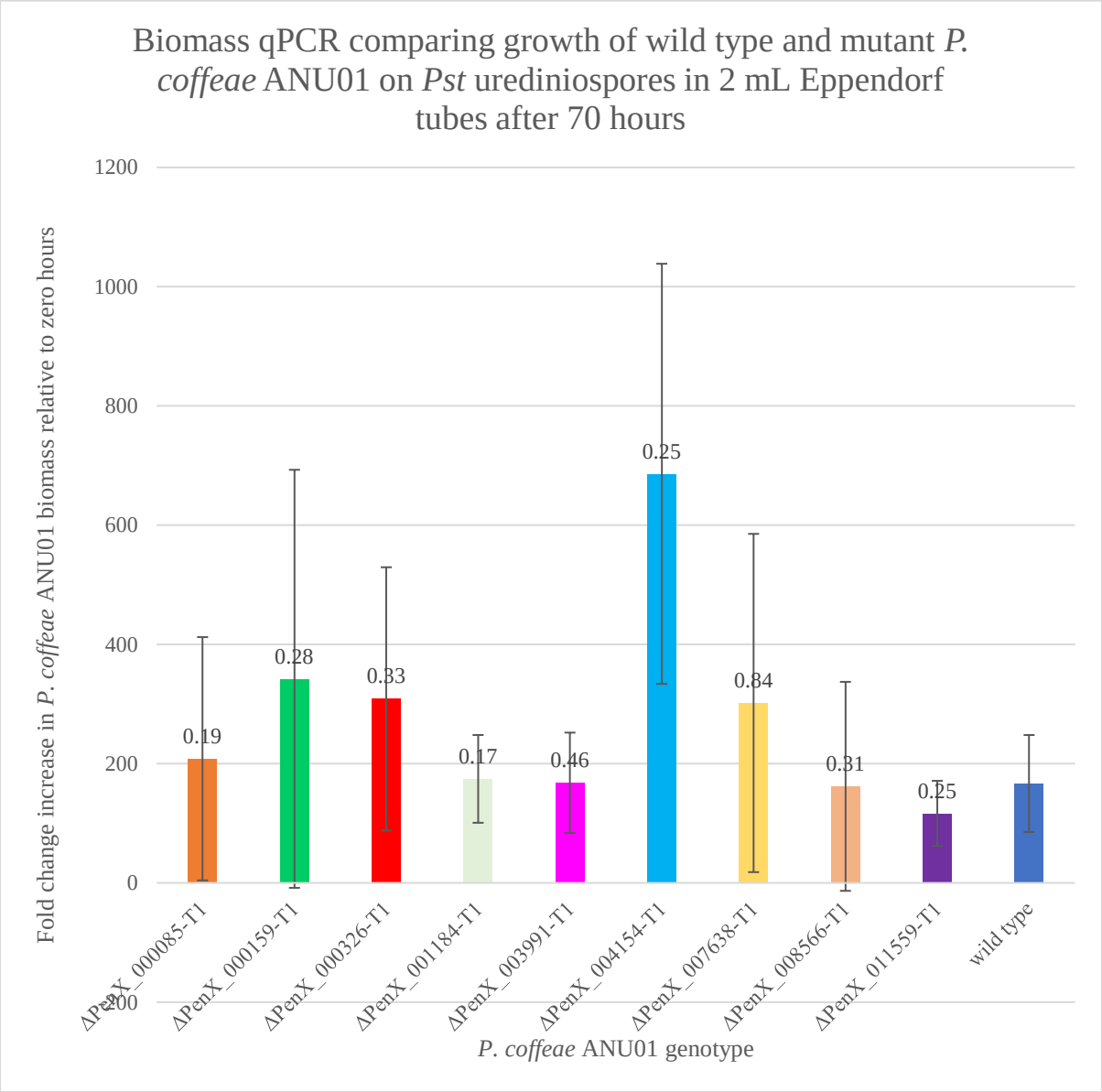

Figure 3.7. Bar graph showing fold change in *P. coffeae* ANU01 biomass in wild-type and nine mutant strains following co-incubation with *Pst* urediniospores in 2 mL Eppendorf tubes at 70 hours. Error bars represent mean ± standard deviation (n =3). Statistical significance was determined using a Welch's t-test comparing each mutant individually to the wild type (individual *P* values are presented at the top of bars), none of the differences were statistically significant. Descriptions of predicted mutant loss-of-function genes are as follows; Δ*PenX_000085-T1* (transcription factor from unannotated BGC), Δ*PenX_000159-T1* (secreted lipase), Δ*PenX_000326-T1* (secreted polysaccharide lyase), Δ*PenX_001184-T1* (L-galactonate dehydratase), Δ*PenX_003991-T1* (depudecin biosynthesis gene), Δ*PenX_004154-T1* (secreted GH64 CAZyme), Δ*PenX_007638-T1* (*STL1* glycerol transporter), Δ*PenX_008566-T1* (kinesin motor protein) and Δ*PenX_011559-T1* (secreted chitosanase).

All genotypes of *P. coffeae* ANU01 exhibited increased biomass at the 70 hour time point compared to the 40 hour time point (Figure 3.7). None of the mutant strains showed a complete loss of ability to grow on *Pst* urediniospores, nor was there any statistically significant difference from the wild type after 70 hours of incubation. The greatest increase in biomass was observed in loss-of-function mutants for Δ*PenX_004154-T1* (secreted GH64 CAZyme) (686.1 ± 352.3-fold increase), followed by Δ*PenX_000159-T1* (secreted lipase) (342.3 ± 350.5-fold increase) and Δ*PenX_000326-T1* (secreted polysaccharide lyase) (308.7 ± 220.7-fold increase). In contrast, the lowest biomass values were recorded for the mutants with loss-of-function in Δ*PenX_011559-T1* (secreted chitosanase) (116.5 ± 54.7-fold increase), Δ*PenX_008566-T1* (kinesin motor protein) (162.0 ± 175.2-fold increase), and the wild type (166.7 ± 81.3-fold increase). Statistical analysis using individual t-tests comparing each mutant to the wild type revealed no significant differences in biomass accumulation across any of the genotypes.

Ultimately, I was unable to establish a phenotyping method reliable enough to detect fitness differences between mutant and wild type *P. coffeae* ANU01 growing on *Pst* urediniospores. My results nevertheless demonstrate that loss-of-function in the targeted genes did not eliminate ability to grow on *Pst* urediniospores. This suggests that these genes are not individually essential for this phenotype.

3.4 Discussion

In this study, I aimed to identify genes essential for the growth of *P. coffeae* ANU01 on *Pst* urediniospores by knocking out several candidate genes. The results did not yield clear phenotypes for any knockout mutants despite selecting genes based on expression profiles during infection and functional annotations potentially linked to parasitism. None of the gene knockouts led to a complete loss of growth on *Pst* urediniospores, suggesting that these genes are either non-essential or redundant for hyperparasitism. This outcome raises important questions about the functional redundancy in the *P. coffeae* genome and the potential for compensatory mechanisms that may obscure the contribution of individual genes. Additionally, phenotyping mutants in this study proved challenging due to the complex nature of the parasitic process, the variability in experimental conditions, and limitations in the phenotyping methods I employed.

Assumed deletion of the genes *PenX_007638-T1 (*glycerol transporter*), PenX_000085-T1 (BGC transcription factor),* and *PenX_004154-T1* (secreted GH64 CAZyme) did not result in a reliably measurable impact on the ability of *P. coffeae* ANU01 to grow on *Pst* urediniospores in pustules on wheat. The fact that each of these three mutants were still able to utilise rust urediniospores for growth suggests that these genes are not essential for growth on *Pst*. However, accurately assessing the impact of gene loss on growth was complicated by several challenges related to standardisation of experimental

conditions and sampling. Humidity plays a critical role in the effectiveness of rust hyperparasites (Zhan *et al.*, 2014). *Penicillium coffeae* ANU01 was originally isolated from *Pst* pustules in cellophane bagged wheat (Wess *et al.*, 2025), suggesting it also requires a high degree of relative humidity for optimal growth. Within bagged pots of wheat, I observed both condensation and significantly higher *P. coffeae* ANU01 growth on leaves that were in contact with the plastic sleeve or near the moist soil at the base of the pot, introducing spatial variability. Additionally, the degree of *Pst* infection varied across leaves, meaning that some had fewer *Pst* pustules and thus fewer urediniospores. Given that pustules are not identical and can each contain thousands of urediniospores (Schwessinger 2017), this led to differing nutrient availability for *P. coffeae* ANU01 across the leaves and genotypes. A third confounding factor was the variability in the number of *P. coffeae* ANU01 spores on each leaf, as spraying infected plants with *P. coffeae* ANU01 spore suspensions may have resulted in unequal spore distribution across the samples. These variables not only complicated the standardisation of growth conditions between replicates and strains but also made unbiased selection of infection sites on leaves difficult. Moreover, dissecting infected leaves without disrupting *P. coffeae* ANU01 growth on pustules presented further challenges. Despite multiple attempts to troubleshoot the setup, these issues persisted, prompting the need to move beyond *on planta* phenotyping. To mitigate the effects of variability in input spore quantity and humidity, I spent over a year designing and troubleshooting an *in vitro* system to phenotype the mutants.

In vitro phenotyping using an "synthetic leaf" set up showed early promise in addressing the issues of variability, using the Δ*PenX_000085-T1* (BGC transcription factor) knockout mutant. The "synthetic leaf" theoretically allowed for identical amounts of *Pst* and *P. coffeae* ANU01 spores to be incubated together and ultimately sampled. The first assay suggested that loss of *PenX_000085-T1* might have a negative impact on the ability of *P. coffeae* ANU01 to grow on *Pst* spores compared to the wild type. This initial result was rejected by a repeat assay in which the qPCR showed reduced biomass at 144 and 192 hours compared to 96 hours for both the wild type and the Δ*PenX_000085-T1* mutant, with the wild type showing less biomass than the mutant at all time points. I also observed a high degree of variability between replicates. I hypothesise that these changes are due to two factors. Firstly, I collected all tissue samples using a tissue biopsy punch. Tissue within the samples may have been lost due to static electricity causing tissue to adhere to the hole punch or over time as the implement became blunter, both of which I did observe. However, this would not explain the tight distribution I observed in the initial assay. A second factor to consider is that *Pst* urediniospores were suspended in Novec™, due to the severely hydrophobic nature of *Pst* urediniospores (Sale *et al.*, 2026). Novec™ evaporates very quickly, making it difficult to ensure that the concentration of urediniospores being aliquoted onto each spot was always equal. Secondly, in Novec™ urediniospores quickly rise and clump at the top, meaning a need for almost constant shaking and opening of tubes, a process difficult when dealing with so many samples. A qPCR using primers I designed specifically for *Pst* showed similar biomass

between spots in a secondary assay, however in larger experiments with hundreds of samples it is harder to ensure an even distribution. Differing amounts of available nutrients might be a limiting factor that halted growth in samples and lead to the strange results I observed at 144 and 192 hours in the repeat assay.

To avoid the sampling issues that may have affected the "synthetic leaf" approach, I attempted to apply the same logic regarding spore-to-spore ratio but in a closed system using 2 mL Eppendorf tubes. I believed that co-inoculation of *P. coffeae* ANU01 and *Pst* spores at the bottom of these tubes would allow both interaction of the two fungi and easier collection of tissue in its entirety for lysis and downstream processing. Unfortunately, even with further troubleshooting, this final approach to phenotyping remained time-consuming and did not reduce the high variation between replicates. Despite my best efforts in developing a phenotyping method that could detect subtle differences between mutant and wild type *P. coffeae* ANU01 in growth on *Pst,* I was ultimately unable to do so. In the end, I hypothesise that the constant variation between samples may simply be a result of the unpredictable nature of fungus-fungus interactions.

None of the nine mutant genotypes that I investigated using the 2 mL Eppendorf tube set up showed statistically significant differences to the wild type at any time point. The ability of all mutants to grow on *Pst* urediniospores in this set up suggests that loss of none of the genes was sufficient to eliminate the ability to consume *Pst* and therefore the genes can be considered not essential for hyperparasitic growth. This may be due to the presence of functional homologs, or unrelated genes with similar function, that can complement the phenotype. Here I describe the results for each target gene in the final 2 mL Eppendorf tube assay, as well as individual assays the mutants were used in. For ease of reading, I describe the impact of knockouts within three paragraphs based on predicted function of the target genes; cell wall degradation, nutrient acquisition and finally antagonism of urediniospores.

Knocking out the secreted predicted chitosanase gene *PenX_011559-T1* had no statistically significant impact on growth at 40, 60 or 70 hours and did not prevent growth on *Pst* urediniospores in 2 mL Eppendorf tubes. Chitosan is a key component polysaccharide in the rust urediniospore germ tube but is not present in the rust urediniospore coat (El Gueddari *et al.,* 2002). Secretion of an enzyme that breaks down chitosan may therefore be relevant in growth on pustules *on planta* but not in a situation where *P. coffeae* ANU01 grows on isolated *Pst* urediniospores. The L-galactonate dehydratase gene *PenX_001184-T1* was not required for growth on *Pst* urediniospores. Its absence had a small but not significant impact on biomass at 40 hours but not at 70 hours. This is possibly due to the fact that *P. coffeae* ANU01 has a direct homolog in the secreted L-galactonate dehydratase encoding gene *PenX_003130-T1*. *PenX_003130-T1* was slightly upregulated during parasitism (0.46 Log_2 fold change) but may be further upregulated to adjust for loss-of-function in *PenX_001184-T1*. I hypothesise a similar situation for the secreted polysaccharide lyase 20 encoding gene *PenX_000326-T1*. Knockout

of this gene caused no significant difference in growth to the wild type at 40 or 70 hours. *Penicillium coffeae* ANU01 contains only 3 polysaccharide lyases, a PL1 (*PenX_004689-T1,* 2.6 Log_2 fold change), PL20 (*PenX_000324-T1,* 6.8 Log_2 fold change) and PL26 (*PenX_004509-T1,* 3.9 Log_2 fold change). It is possible that one or more of these similar PLs were co-opted in the *PenX_000326-T1* knockout. Alternatively, the importance of PL20s in targeting pectin (Mayans *et al.,* 1997) may indicate that the enzyme encoded by *PenX_000326-T1* acts on plant-derived carbohydrates released during pustulation. These carbohydrates would not be present when *P. coffeae* ANU01 is grown on isolated *Pst* urediniospores, making the loss of *PenX_000326-T1* irrelevant. The depudecin synthesis gene *PenX_003991-T1* knockout showed increased growth that was highly variable and not significant compared to the wild type at 40 hours but similar to the wild type at 70 hours. *Penicillium coffeae* ANU01 with knockout of the secreted glycoside hydrolase *PenX_004154-T1* showed no statistically significant difference to the wild type at 40 or 70 hours *in vitro*. Disruption of the *PenX_004154-T1* gene was difficult and involved re-design of the sgRNA and hyg^+ cassette, ultimately yielding only two viable colonies. I did observe a large increase in biomass of Δ*PenX_004154-T1* compared to all other strains at 70 hours, though it was not statistically significant. It is possible that loss-of-function in *PenX_004154-T1* lead to a rapid growth on urediniospores, that I never observed on PDA. *PenX_004154-T1* showed very low expression on PDA (0.29 transcripts per million) compared to growth on *Pst* pustules (147.1) (Chapter Two). Alternatively, the inherent variability of the 2 mL Eppendorf tube phenotyping method may simply mean that the vastly increased growth I observed at 70 hours was an anomaly.

Knockout of the secreted lipase gene *PenX_000159-T1* had no significant impact on growth at 40 or 70 hours. In Chapter Two, I posit that lipids are a major nutrient target for *P. coffeae* ANU01 (Wess *et al.,* 2025) and that as a result its genome contains many genes related to lipid metabolism. *Penicillium coffeae* ANU01 contains 18 genes related to lipid metabolism, 10 of which are predicted to encode secreted lipases, including the highly upregulated *PenX_004063-T1* (6.2 Log_2 fold change). It is possible that other lipase genes are upregulated to adjust to the loss-of-function in *PenX_000159-T1.* The STL1 glycerol transporter encoding gene *PenX_007638-T1* knockout showed no significant difference from the wild type at either 40 or 70 hours. *Penicillium coffeae* ANU01 contains a very close *STL1* homolog in *PenX_011265-T1,* which is also upregulated during growth on urediniospores (3.9 Log_2 fold change). This second *STL1* gene may allow uptake of glycerol in the absence of *PenX_007638-T1,* although the upregulation of *PenX_011265-T1* during parasitism suggests that they already work in combination. Loss of *PenX_007638-T1* may therefore have a mild effect unable to be quantified by my approach.

In a previous chapter I hypothesise that depudecin, through the action of the synthesis monooxygenase gene *PenX_003991-T1,* is deployed as a toxic SM to inhibit germination, limit defence responses or even kill urediniospores. This function may be redundant or less important in a setting where *P. coffeae*

ANU01 is growing on *Pst* urediniospores that may be weakened, slow or dead due to repeated freeze-thaw cycles during storage. The *Pst* urediniospores used in all aspects of the *in vitro* phenotyping process were heat-shocked before use, however are likely to still be less viable than fresh urediniospores in a pustule on an infected plant. Deletion of the predicted kinesin motor protein encoding gene *PenX_008566-T1* did not inhibit the growth of *P. coffeae* ANU01 on *Pst* urediniospores. *Penicillium coffeae* ANU01 possesses 15 genes predicted to be related to microtubule-based growth, 9 of which are significantly upregulated during parasitism (Chapter Two). *Penicillium coffeae* ANU01 may upregulate any of these other genes to account for the loss of *PenX_008566-T1*. Alternatively, the gene may simply be less important in a scenario in which *P. coffeae* ANU01 is directly incubated with *Pst* urediniospores in a tube compared to possible polar growth towards them on a much larger wheat leaf. Finally, loss-of-function of the BGC transcription factor gene *PenX_000085-T1* initially suggested a negative impact on phenotype on "synthetic leaves". However, in all subsequent assays, including the final assay in 2 mL Eppendorf tubes, *ΔPenX_000085-T1* showed no significant difference in biomass compared to the wild type. Ultimately, none of the gene knockouts I investigated eliminated the ability of *P. coffeae* ANU01 to use *Pst* urediniospores for growth. I was unable to develop an effective phenotyping method to investigate whether loss-of-function in the target genes reduced fitness in parasitism to any measurable degree. Future studies should focus on investigating the small but significant impacts that loss-of-function in these genes could have on fitness. Developing a reliable, repeatable and functional phenotyping method will be integral to this.

Three of my original target-genes appeared to be essential for *P. coffeae* ANU01 viability. Multiple attempts to knockout the transcription factors *PenX_003326-T1* and *PenX_010964-T1* yielded only ectopic mutants. Multiple attempts including a complete re-design of the sgRNA and hyg^+ cassette for the *PenX_004159-T1* (unannotated secreted protein) knockout yielded no viable colonies at all. *PenX_003326-T1* is predicted to encode a transcriptional activator that regulates fatty acid metabolism, I selected it to investigate whether it plays a critical role in metabolising the fatty acids abundant in *Pst* urediniospores (Staples and Wynn, 1965; Tulloch *et al.*, 1959). The inability to generate viable *PenX_003326-T1* knockouts suggests that this gene is required for more fundamental processes, perhaps the utilisation of self-derived fatty acids during sporulation and growth. Given that PDA media is relatively poor in fatty acids (Kohn and Grenville 1987), an importance in utilising external fatty acids is likely not the reason that Δ*PenX_003326-T1* did not grow on the media. Alternatively, the gene might simply possess some role not related to fatty acid utilisation, which cannot be excluded as a possibility. I chose the transcription factor encoding gene *PenX_010964-T1* as a target due to its strong upregulation during infection, despite its lack of functional annotation. My failure to obtain Δ*PenX_010964-T1* knockouts indicates that the gene may regulate processes necessary for general fungal growth that are simply enhanced during parasitism, rather than specialised for growth on urediniospores. Alternatively, it may control a function that is critical in both axenic and parasitic

growth. Finally, *PenX_004159-T1*, an unannotated gene encoding a predicted secreted protein, also appeared to be required for growth. Its importance may also reflect a role in fundamental cellular processes rather than parasitism. Fungal secreted proteins are known to contribute towards cell wall remodelling (Gow *et al.*, 2017), a fundamental process that could explain this result. However, *P. coffeae* ANU01 possesses several genes related to cell wall remodelling (Wess *et al.*, 2025). Another possible explanation for the failure to generate knockouts is that the designed sgRNAs targeted homologous regions in other genes which are essential, leading to off-target lethality. I observed lethality with the original design for Δ*PenX_004154-T1*, which was somewhat relieved with redesign which produced 2 colonies, both of which had insertions in the correct position. However, the Δ*PenX_004159-T1* re-design did not work, suggesting it is not an off-target effect and that the gene may be truly necessary for survival. Overall, these findings suggest that *PenX_003326-T1*, *PenX_010964-T1* and *PenX_004159-T1* are required for fungal survival, highlighting their potential involvement in essential cellular functions that are not entirely specific to parasitism. This discovery somewhat highlights the arbitrary nature of selecting genes for knockout based on supposed importance specifically to parasitism.

An important consideration when interpreting the absence of a clear phenotype is whether the target genes were truly disrupted. I validated insertion of the hyg^+ cassette at the intended locus by colony PCR. Insertion of the 1.7 kb cassette should be sufficient to eliminate gene function, as demonstrated in previous studies (Khan *et al.*, 2020). In all cases, target sites were chosen near the 5′ end of each gene to minimise the possibility of leaving truncated but partially functional protein-coding regions. A further concern is that all genes in the *P. coffeae* ANU01 genome were annotated *de novo*. It is therefore possible that reading frames or coding sequences were inaccurately defined, resulting in target sites falling outside essential regions of the gene. Additional RT-qPCR assays or western blots would help confirm loss of transcripts or proteins, respectively. Moreover, qPCR comparing copy number of the hyg^+ cassette to a single-copy housekeeping gene or whole genome sequencing would allow detection of unintended additional insertions elsewhere in the genome, which could also influence phenotypes.

A major limitation of this study is that each strain carried a loss-of-function mutation in only a single gene. As discussed above, with the exception of the transcription factor target genes, *P. coffeae* ANU01 possesses multiple genes with overlapping or redundant functions for each gene examined. These homologs which were less upregulated than each gene may be used by *P. coffeae* ANU01 to compensate for loss-of-function in knockouts by increased expression. Future assays should therefore target multiple closely related genes, or entire gene families, to assess the importance of a biological function rather than the contribution of an individual gene. For example, knocking out all genes predicted to encode secreted lipases would allow assessment of how loss of lipid degradation affects growth on *Pst* urediniospores. Combinatorial knockouts may also be informative; for instance, simultaneously

disrupting representatives from the GH and PL cell wall–degrading enzyme families together with an unannotated secreted enzyme to test for synergistic effects or functional redundancy.

Measuring impact of gene-loss solely by estimating biomass via qPCR may have overlooked key aspects of parasitism. I largely phenotyped mutants using qPCR to measure their growth compared to the wild type. This neglects other aspects such as impact on *Pst* urediniospore viability and integrity. I attempted to use the co-inoculation protocol described by Wilson *et al.* (2020) to investigate the impact of *P. coffeae* ANU01 on *Pst* spore viability but was unable to establish it for *P. coffeae* ANU01 (data not shown). If I had more time to develop the protocol, I would have preferred to investigate whether loss-of-function in genes that underly antagonistic processes, such as the depudecin monooxygenase or secreted polysaccharide lyase reduced any ability of *P. coffeae* ANU01 to antagonise and kill *Pst* urediniospores. To investigate the impact of *P. coffeae* ANU01 on urediniospore integrity, I would use scanning electron microscopy to determine invasion capability of the mutants, in particular those deficient in cell wall degrading enzymes. It could also be the case that increased growth is not directly correlated to increased fitness, as an increase in biomass could reflect a vigorous search for nutrients as opposed to an improved capacity to utilise nutrients.

In conclusion, this chapter highlights the difficulty of phenotyping *P. coffeae* ANU01 knockouts and the challenges in pinpointing specific genes critical for hyperparasitic growth on *Pst* urediniospores. While no single gene knockout resulted in a complete loss of growth, the findings suggest that functional redundancy, variability in environmental factors, and limitations in phenotyping methods may have masked more subtle effects. Future studies should explore combinatorial knockouts, refine phenotyping techniques, and assess additional aspects of parasitism, such as impact on rust spore viability and integrity, to better understand the role of these genes in *P. coffeae* ANU01's hyperparasitic strategy.

3.5 Bibliography

Bonacorsi, S., Visseaux, B., Bouzid, D., Pareja, J., Rao, S. N., Manissero, D., Hansen, G., & Vila, J. (2021). Systematic review on the correlation of quantitative PCR cycle threshold values of gastrointestinal pathogens with patient clinical presentation and outcomes. Frontiers in Medicine, 8. https://doi.org/10.3389/fmed.2021.711809

Chatterton, S., & Punja, Z. K. (2009). Chitinase and β-1,3-glucanase enzyme production by the mycoparasite *Clonostachys rosea* f. *catenulata* against fungal plant pathogens. Canadian Journal of Microbiology, 55(4), 356-367. https://doi.org/10.1139/W08-156

El Gueddari, N. E., Rauchhaus, U., Moerschbacher, B. M., & Deising, H. B. (2002). Developmentally regulated conversion of surface-exposed chitin to chitosan in cell walls of plant pathogenic fungi. New Phytologist, 156(1), 103-112. https://doi.org/10.1046/j.1469-8137.2002.00487.x

Gow Neil, A. R., Latge, J.-P., & Munro Carol, A. (2017). The fungal cell wall: structure, biosynthesis, and function. Microbiology Spectrum, 5(3), 10.1128/microbiolspec.funk-0035-2016. https://doi.org/10.1128/microbiolspec.funk-0035-2016

Khan, H., McDonald, M. C., Williams, S. J., & Solomon, P. S. (2020). Assessing the efficacy of CRISPR/Cas9 genome editing in the wheat pathogen *Parastagonspora nodorum*. Fungal Biology and Biotechnology, 7(1). https://doi.org/10.1186/s40694-020-00094-0

Klein, M., Swinnen, S., Thevelein, J. M., & Nevoigt, E. (2017). Glycerol metabolism and transport in yeast and fungi: established knowledge and ambiguities. Environmental Microbiology, 19(3), 878-893. https://doi.org/https://doi.org/10.1111/1462-2920.13617

Kohn, L. M., & Grenville, D. (1987). Some factors influencing lipid storage in sclerotia of *Sclerotinia minor*. Mycologia, 79(6), 907-909. https://doi.org/10.1080/00275514.1987.12025483

Lara-Martínez, D., Tristán-Flores, F. E., Cervantes-Montelongo, J. A., & Silva-Martínez, G. A. (2025). Fungal stress responses and the importance of GPCRs. Journal of Fungi, 11(3), 213. https://doi.org/10.3390/jof11030213

Lee, P. Y., Costumbrado, J., Hsu, C. Y., & Kim, Y. H. (2012). Agarose gel electrophoresis for the separation of DNA fragments. Journal of Visualized Experiments (62). https://doi.org/10.3791/3923

Leinhos, G. M. E., & Buchenauer, H. (1992). Inhibition of rust diseases of cereals by metabolic products of *Verticillium chlamydosporium*. Journal of Phytopathology, 136(3), 177-193. https://doi.org/https://doi.org/10.1111/j.1439-0434.1992.tb01296.x

Liu, D., Coloe, S., Baird, R., & Pedersen, J. (2000). Rapid mini-preparation of fungal DNA for PCR. Journal of clinical microbiology, 38, 471. https://doi.org/10.1128/JCM.38.1.471-471.2000

Maclean, D. J., & Scott, K. J. (1976). Identification of glucitol (sorbitol) and ribitol in a rust fungus, *Puccinia graminis* f. sp. *tritici*. Microbiology, 97(1), 83-89. https://doi.org/https://doi.org/10.1099/00221287-97-1-83

Mayans, O., Scott, M., Connerton, I., Gravesen, T., Benen, J., Visser, J., Pickersgill, R., & Jenkins, J. (1997). Two crystal structures of pectin lyase A from *Aspergillus* reveal a pH driven conformational change and striking divergence in the substrate-binding clefts of pectin and pectate lyases. Structure, 5(5), 677-689. https://doi.org/10.1016/s0969-2126(97)00222-0

Medema, M. H., Kottmann, R., Yilmaz, P., Cummings, M., Biggins, J. B., Blin, K., De Bruijn, I., Chooi, Y. H., Claesen, J., Coates, R. C., Cruz-Morales, P., Duddela, S., Düsterhus, S., Edwards, D. J., Fewer, D. P., Garg, N., Geiger, C., Gomez-Escribano, J. P., Greule, A., . . . Glöckner, F. O. (2015).

Minimum information about a biosynthetic gene cluster. Nature Chemical Biology, 11(9), 625-631. https://doi.org/10.1038/nchembio.1890

Ross, S. J., Findlay, V. J., Malakasi, P., & Morgan, B. A. (2000). Thioredoxin peroxidase is required for the transcriptional response to oxidative stress in budding yeast. Molecular Biology of the Cell, 11(8), 2631-2642.

Sale, S., Nock, V., & Garrill, A. (2026). Physical and chemical considerations for successful *in vitro* culture of rust fungi: challenges, insights and novel strategies. Physical Biology, 23(1), 011002.

Schwessinger, B. (2017). Fundamental wheat stripe rust research in the 21st century. New Phytologist, 213(4), 1625-1631. https://doi.org/10.1111/nph.14159

Schwessinger, B., Sperschneider, J., Cuddy, W. S., Garnica, D. P., Miller, M. E., Taylor, J. M., Dodds, P. N., Figueroa, M., Park, R. F., & Rathjen, J. P. (2018). A near-complete haplotype-phased genome of the dikaryotic wheat stripe rust fungus *Puccinia striiformis* f. sp. *tritici* reveals high interhaplotype diversity. mBio, 9(1), e02275-02217. https://doi.org/10.1128/mbio.02275-17

Sexton, A. C., & Howlett, B. J. (2001). Green fluorescent protein as a reporter in the *Brassica–Leptosphaeria maculans* interaction. Physiological and Molecular Plant Pathology, 58(1), 13-21. https://doi.org/https://doi.org/10.1006/pmpp.2000.0307

Solomon, P. S., Thomas, S. W., Spanu, P., & Oliver, R. P. (2003). The utilisation of di/tripeptides by *Stagonospora nodorum* is dispensable for wheat infection. Physiological and Molecular Plant Pathology, 63(4), 191-199. https://doi.org/https://doi.org/10.1016/j.pmpp.2003.12.003

Staples, R. C., & Wynn, W. K. (1965). The physiology of uredospores of the rust fungi. The Botanical Review, 31(4), 537-564. https://doi.org/10.1007/BF02858608

Tulloch, A. P., Craig, B. M., & Ledingham, G. A. (1959). The oil of wheat stem rust uredospores: II. The isolation of *cis*-9,10-epoxyoctadecanoic acid, and the fatty acid composition of the oil. Canadian Journal of Microbiology, 5(5), 485-491. https://doi.org/10.1139/m59-060

Wang, N., Fan, X., Zhang, S., Liu, B., He, M., Chen, X., Tang, C., Kang, Z., & Wang, X. (2020). Identification of a hyperparasitic *Simplicillium obclavatum* strain affecting the infection dynamics of *Puccinia striiformis* f. sp. *tritici* on wheat. Frontiers in Microbiology, 11. https://doi.org/10.3389/fmicb.2020.01277

Wess, J., Hu, Y., Periyannan, S., Jones, A., & Rathjen, J. P. (2025). Global transcriptome changes during growth of a novel *Penicillium coffeae* isolate on the wheat stripe rust fungus, *Puccinia striiformis* f. sp. *tritici*. Fungal Genetics and Biology, 176, 103956. https://doi.org/https://doi.org/10.1016/j.fgb.2024.103956

Wilson, A., Cuddy, W. S., Park, R. F., Harm, G. F. S., Priest, M. J., Bailey, J., & Moffitt, M. C. (2020). Investigating hyperparasites as potential biological control agents of rust pathogens on cereal crops. Australasian Plant Pathology, 49(3), 231-238. https://doi.org/10.1007/s13313-020-00695-8

Xiao, M., Chen, D., Liu, S., Chen, A., Fang, A., Tian, B., Yu, Y., Bi, C., Kang, Z., & Yang, Y. (2023). A chitin deacetylase Ps CDA2 from *Puccinia striiformis* f. sp. *tritici* confers disease pathogenicity by suppressing chitin-triggered immunity in wheat. Molecular Plant Pathology, 24(12), 1467-1479.

Zhan, G., Tian, Y., Wang, F., Chen, X., Guo, J., Jiao, M., Huang, L., & Kang, Z. (2014). A novel fungal hyperparasite of *Puccinia striiformis* f. sp. *tritici*, the causal agent of wheat stripe rust. PLoS One, 9(11), e111484. https://doi.org/10.1371/journal.pone.0111484

Zheng, L., Zhao, J., Liang, X., Zhan, G., Jiang, S., & Kang, Z. (2017). Identification of a Novel *Alternaria alternata* strain able to hyperparasitize *Puccinia striiformis* f. sp. *tritici*, the causal agent of wheat stripe rust. Frontiers in Microbiology, 8. https://doi.org/10.3389/fmicb.2017.00071

3.6 Supplementary material

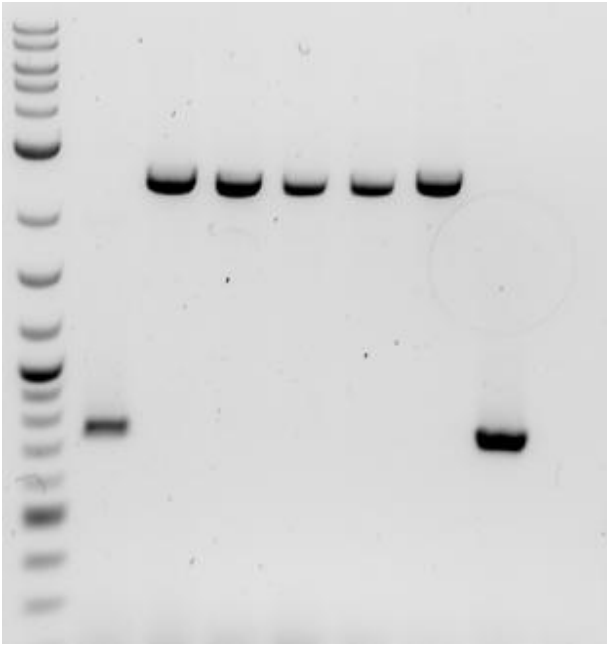

Supplementary Figure 3.1. Agarose gel showing amplicons from a PCR to genotype *PenX_011559-T1* mutants. From left to right; 1kbp+ ladder (NEB) ladder, an amplicon from a potentially ectopic *PenX_011559-T1* mutant showing an undisrupted *PenX_011559-T1* gene (hyg^+ resistance cassette inserted at a random location in the genome), five amplicons from individual mutants showing successful insertion of the hyg^+ resistance cassette at target-site, one wild type control amplicon and a water-only control well.

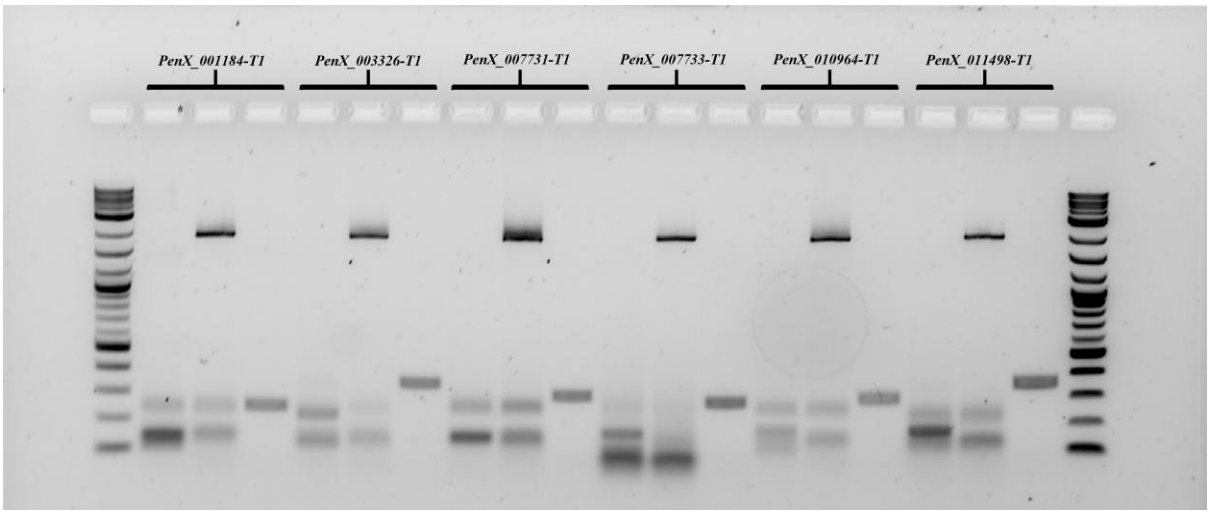

Supplementary Figure 3.2. Agarose gel showing the results of *in vitro* cleavage assays (3 wells each) for six target genes from left to right, flanked on either side by wells containing 1kbp+ ladder (NEB). Each *in vitro* cleavage assay consisted of one reaction containing; gene amplicon, sgRNA and Cas9

protein (left well), hyg^+ resistance cassette, sgRNA and Cas9 protein (middle well) and gene amplicon and sgRNA only (right well).

Chapter Four

A hidden defence: Investigating rust hyperparasitism from the perspective of *Pst*

4.1 Background

The majority of *Puccinia striiformis f. sp. tritici* (*Pst*) research, the causative agent of wheat stripe rust, focuses on the genomic and pathogenic strategies employed by this fungus to establish infection (Chen *et al.,* 2014; Schwessinger 2017). Fungal hyperparasites offer the opportunity to understand how *Puccinia striiformis* f. sp. *tritici* (*Pst*) responds when it is forced to defend itself against pathogenic attack. Beyond its tough spore coat, little is known about the defensive capabilities of *Pst* against other fungi. In this study, I reanalyse existing transcriptomic data to investigate potential mechanisms employed by *Pst* to detect and respond to attack by the rust hyperparasite *Penicillium coffeae* ANU01.

The asexual infection cycle of *Pst* on wheat enables rapid colonisation and repeated spore production during the growing season. The infection begins when urediniospores land on a susceptible leaf and germinate under favourable moisture and temperature conditions, producing elongating germ tubes (Garnica *et al.,* 2014). Germ tubes penetrate the leaf via the stomata and once inside, the fungus rapidly colonises the space between plant cells, extracting nutrients from mesophyll cells through specialised feeding structures called haustoria. Approximately 12 days after infection, newly replicated urediniospores erupt through the leaf surface in lesions called pustules (Chen *et al.,* 2014). Pustules can produce approximately 1,000 urediniospores per day and initiate secondary infection cycles, allowing rapid disease amplification under favourable conditions (Roelfs 1985). However, while these urediniospores remain within pustules, they present a rich potential nutrient source for foliar hyperparasites. Urediniospores are rich in lipids, amino acids, and carbohydrates when ungerminated, yet active defence mechanisms beyond the urediniospore coat have not been described (Shaw 1964; Staples and Wynn, 1965; Tulloch *et al.,* 1959). Existing literature suggests that ungerminated *Pst* urediniospores are dormant until the point of germination (Staples and Wynn, 1965; Wiese & Ravenscroft 1979). If this is true, it implies that prior to germination, *Pst* is largely incapable of responding to its environment and is defenceless apart from its spore coat, its sole protection against hyperparasitic attack. The thick spore wall composed primarily of chitin and glucans is the first line of defence for *Pst* urediniospores (Xiao *et al.,* 2023). These polysaccharides are structurally robust and

typically require enzymatic degradation to break down (Srivastava *et al.,* 1985). Beyond this physical barrier, little is known regarding the defensive capabilities of *Pst* urediniospores as they lie within pustules on the leaf surface.

Rust hyperparasites are capable of degrading spore structures and killing rust urediniospores. Several fungal species have been shown to reduce or completely inhibit *Pst* germination (Wang *et al.,* 2020; Zhan *et al.,* 2014; Zheng *et al.,* 2017). *Penicillium brevicompactum*, for example, can halt *Pst* germination without the need for physical colonisation (Wilson *et al.,* 2020). This inhibition is often mediated by toxic secondary metabolites (SMs), such as cladosporols, produced by certain *Cladosporium* species (Nasini *et al.,* 2004). Direct invasion of *Pst* urediniospores within pustules by hyperparasitic fungal hyphae has been observed many times and appears to be a very common aspect of *Pst* parasitism (Wang *et al.,* 2020; Zhan *et al.,* 2014; Zheng *et al.,* 2017). Direct invasion is often assisted by cell wall degrading enzymes, including chitinases and β-glucanases, which have also been shown to degrade the rust urediniospore coat and disrupt the cell wall (Srivastava *et al.,* 1985). Hyperparasites therefore employ a diverse range of mechanisms to target rust fungi, but the literature regarding a response simply does not exist.

The intensity of antagonistic approaches deployed by rust hyperparasites, suggested to me that the commonly considered inert *Pst* urediniospores (Wiese & Ravenscroft 1979) were capable of mounting a defence response. The literature regarding a response from *Pst* to hyperparasitism simply does not exist, making this report the first investigation. If a defence response exists, it may be the evolutionary pressure driving the diversity of approaches to consuming *Pst* that I observed in Chapter Five. *Penicillium coffeae* ANU01 is a hyperparasite that attacks *Pst* urediniospores within pustules. In Chapter Two, I investigated the genetic mechanisms deployed by *P. coffeae* ANU01 to attack and extract nutrients from ungerminated *Pst* urediniospores in pustules. I hypothesised that *P. coffeae* ANU01 uses a depudecin-like toxic SM to attack host urediniospore gene regulation, before using cell-wall degrading enzymes to degrade host structures and access nutrients. Here, I present an investigation of the transcriptomic profile of *Pst* in response to this attack. This is the first study of its kind and reveals a previously completely unknown feature of host-pathogen dynamics in rust hyperparasitism.

4.2 Materials and methods

Genomic and transcriptomic materials

The *Pst* 104E- genome and associated transcriptome were built by Rita Tam of the Schwessinger Laboratory (RSB, ANU). The assembly and annotation of the *Pst* 104E- genome is described in detail here (Tam *et al.,* 2025).

Description of the discovery of *P. coffeae* ANU01 acting as a hyperparasite, RNA isolated from colonised *Pst* pustules, and the assembly of its genome and transcriptome is presented in Chapter Two (Wess *et al.,* 2025). The genome assembly, transcriptome and RNAseq data for the infected pustule condition (see below) are all described in that Chapter.

RNAseq datasets

This analysis used six RNAseq datasets; three replicates of *Pst* pustules colonised by *P. coffeae* ANU01 (hereafter referred to as infected pustules) and three replicates of healthy *Pst* pustules alone on the wheat leaf (hereafter referred to as uninfected pustules). For the infected pustule condition, total RNA was extracted from colonised *Pst* pustules on the surface of wheat leaves, described in detail in Chapter Two (Wess *et al.,* 2025). Sampling at this stage of infection meant that *P. coffeae* ANU01 was already colonising and feeding on *Pst* urediniospores as they sat in the pustules.

The uninfected pustule RNAseq datasets were generated by Dr. Mareike Möller of the Schwessinger Laboratory (RSB, ANU). A detailed description of the RNA isolation and sequencing is presented here (Tam *et al.*, 2025). Briefly, at 12 dpi, whole infected wheat leaves showing pustules were collected and ground to fine powder using a TissueLyser II (QIAGEN). Total RNA was extracted from disrupted tissue using the Zymo Research Direct-zol RNA Miniprep Plus Kit (Zymo Research) and shipped to Genewiz (Suzhou, China) for paired-end Illumina sequencing. Sequenced reads were trimmed of adapters using the fastp (v0.23.4) software (Chen *et al.,* 2018). Sampling at this stage of infection meant that *Pst* had already formed dense pustules on the wheat leaf, full of urediniospores.

Bioinformatic analyses

RNAseq experiments covering the different rust pustule infection conditions were designed to investigate *P. coffeae* ANU01 gene expression during parasitism. Therefore, the majority of reads belonged to *P. coffeae* ANU01 and needed to be removed. *Penicillium* reads were removed by aligning to the *P. coffeae* ANU01 genome using the hisat2 software (Kim *et al.*, 2019). RNA reads from the uninfected pustule datasets and filtered reads from the infected pustule datasets were quantified by aligning against the *Pst104E*- transcriptome using the Salmon (v1.4.0) software (Patro *et al.,* 2017). Quantified reads were imported into R-studio for gene expression analysis using the Limma package (Ritchie *et al.,* 2015). All of the code used to generate the Volcano Plot and the GO enrichment Violin plot is presented in the GitHub page for this project: https://github.com/Jack-WessANU/*Pst*_under_attack.

4.3 Results and Discussion

Global changes in the *Pst* transcriptome when under attack by *P. coffeae* ANU01

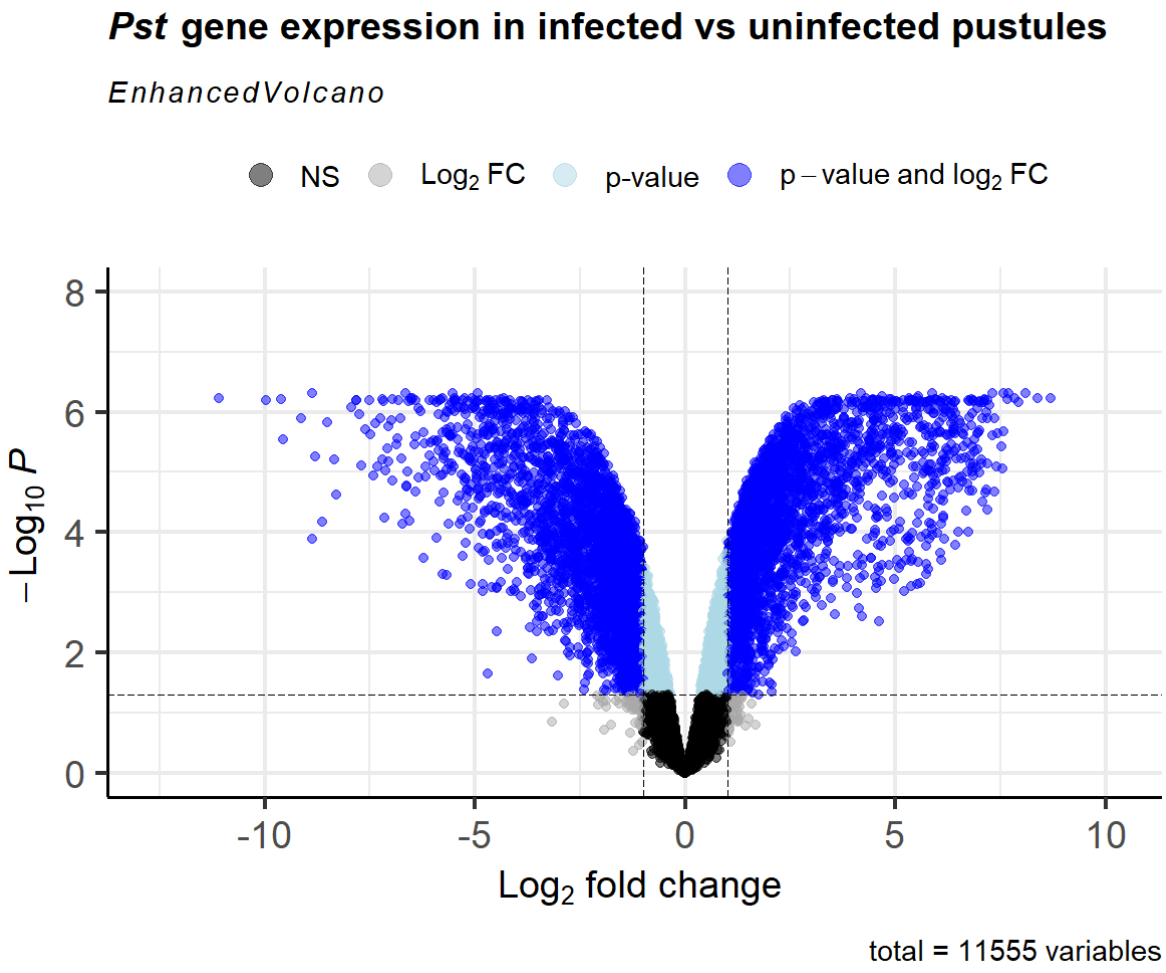

Figure 4.1. Volcano plot of differentially expressed *Pst* genes during hyperparasitic attack versus normal growth in pustules. The dashed line on the Y axis indicates an adjusted *P* value of 0.05. On the X axis, dashed lines indicate log_2fold changes of -1 and 1 respectively. Each dark blue dot represents a gene that is significantly differentially expressed, downregulated on the left and upregulated on the right. Each grey dot represents a gene that is differentially expressed but not statistically significant. Pale blue dots represent genes that are statistically significantly expressed but are not considered sufficiently differentially expressed. Each black dot represents a gene that was neither sufficiently differential nor statistically significant in their expression.

I conducted a comparative transcriptomic analysis to identify *Pst* genes upregulated during hyperparasitic attack. Transcripts were quantified with Salmon (Patro *et al.*, 2017) then loaded into Limma (Ritchie *et al.*, 2015) to calculate relative gene expression values. The output of this analysis is shown in a volcano plot in Figure 4.1. Genes that exhibited an adjusted *P* value of < 0.05 were

considered differentially expressed. Of those genes, I considered those that also possessed a $\log_2$ fold change of >1 as upregulated, and a $\log_2$ fold change of < -1 as downregulated. I found that 2,898 genes were upregulated and 3,030 genes were downregulated when *Pst* was under attack by *P. coffeae* ANU01. The *Pst* transcriptome consists of 31,064 unique transcripts (Tam *et al.*, 2025), meaning that 9.33% of genes and 9.75% of genes were up- and down-regulated during parasitism respectively. Therefore, the *Pst* transcriptome undergoes significant expressional change during hyperparasitic attack, supporting my hypothesis that urediniospores are not as inert in pustules as previously believed (Wiese & Ravenscroft 1979). The exact differential expression values for these genes and their associated functional annotations are presented in Supplementary Table 3.1.

GO enrichment during parasitic attack

I conducted a gene ontology (GO) enrichment analysis to identify the functional pathways upregulated in *Pst* urediniospores when attacked by *P. coffeae* ANU01. The results of the topmost significantly enriched terms ($p < 0.05$) according to a weighted adjusted Fisher's exact test for each condition are presented in a dotplot in (Figure 4.2). Adjustment of the raw p-values for Fisher's exact test can be very stringent leading to loss of transcriptomic signals, often leaving only fundamental processes as enriched (Alexa & Rahnenführer 2016). In this analysis I aimed to develop a comprehensive understanding of how *Pst* reacts to attack by *P. coffeae* ANU01 so have included the results of the most significantly enriched weighted GO terms (without adjustment) in Figure 4.3. Importantly, the findings presented in this report are based solely on transcriptomic data. Consequently, the functional roles and biological processes I discuss are inferred from patterns of gene expression and annotation, and therefore remain hypothetical. These interpretations should be regarded as putative explanations of the observed transcriptional responses within the context of parasitic attack, rather than definitive evidence of gene function or biological activity. These results serve as a first step before more extensive transcriptomic analyses that may be performed by future researchers.

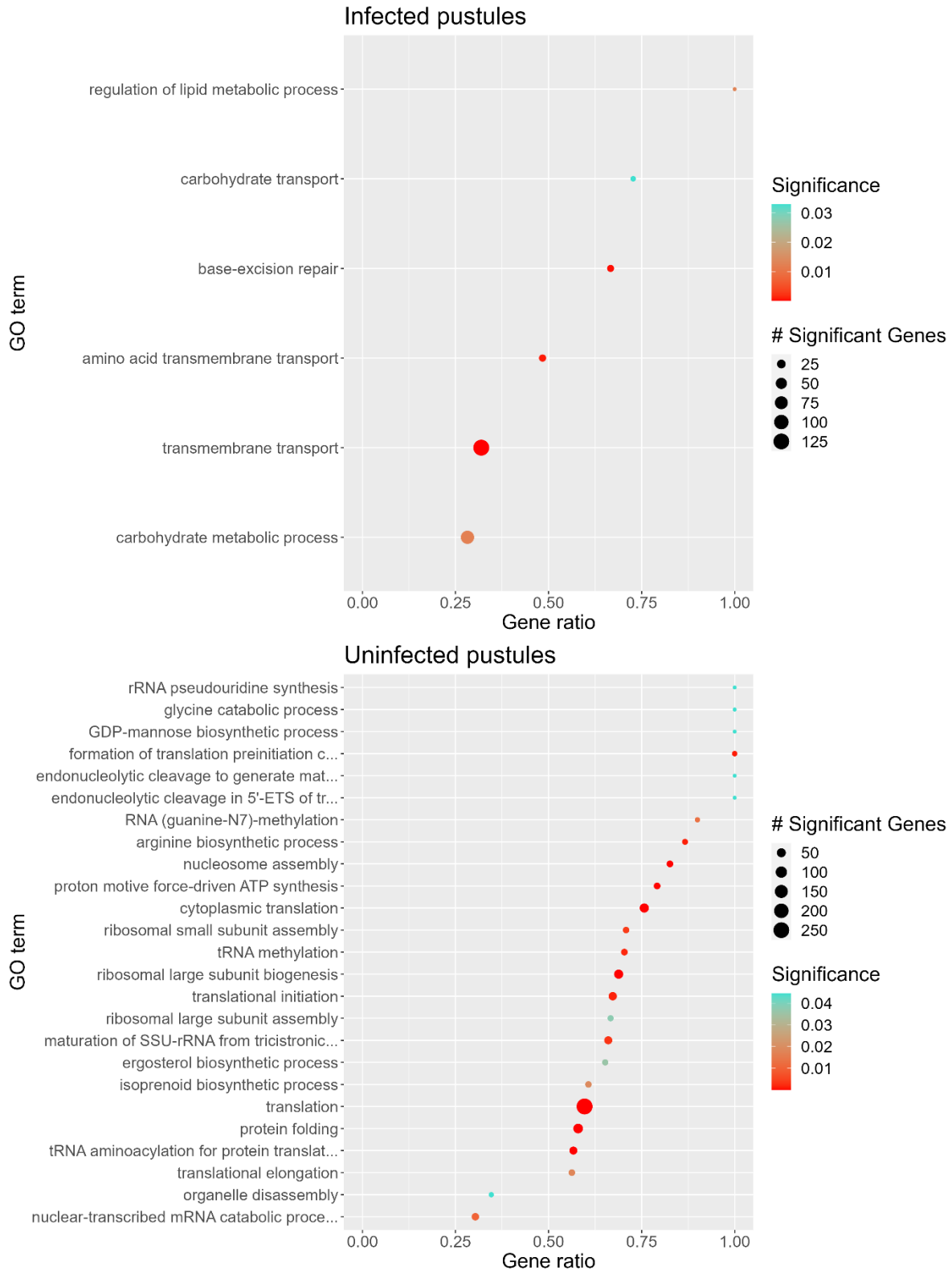

Figure 4.2. Dotplots representing the results of a gene ontology (GO) enrichment analysis. Top, GO terms significantly upregulated during antagonism by the hyperparasite *P. coffeae* ANU01. Bottom, GO terms significantly upregulated during normal growth in pustules (can also be described as downregulated in infected pustules). In both dotplots, the dot size is calculated by the total number of

significant genes within the GO term. Dot colour represents the degree of significance assigned to the GO term according to an adjusted Fisher's exact test. Position along the "Gene ratio" X axis represents the ratio of significant to total genes in the GO term. The shortened GO terms on the Y axis are: formation of translation preinitiation complex, endonucleolytic cleavage to generate mature 5'-end of SSU-rRNA from (SSU-rRNA, 5.8S rRNA, LSU-rRNA), endonucleolytic cleavage in 5'-ETS of tricistronic rRNA transcript (SSU-rRNA, 5.8S rRNA, LSU-rRNA), maturation of LSU-rRNA from tricistronic rRNA transcript (SSU-rRNA, 5.8S rRNA, LSU-rRNA), tRNA aminoacylation for protein translation and nuclear-transcribed mRNA catabolic process.

The most significantly (adjusted) enriched GO terms during attack by *P. coffeae* ANU01 (Figure 4.2) were transmembrane transport (128 genes, 32% of genes in GO term), base-excision repair (14 genes, 66.67%), amino acid transmembrane transport (15 genes, 48.39%), carbohydrate metabolic process (79 genes, 28.2%), regulation of lipid metabolic process (6 genes, 100%) and carbohydrate transport (8 genes, 72.72%). A significant upregulation in overall transmembrane transport and specifically amino acid transmembrane transport could imply an attempt to export toxins or antifungal compounds and an attempt to import or scavenge nutrients and important ions during competitive stress. Rust urediniospores are abundant in lipids (20%) and carbohydrates (21.9%) (Shaw 1964; Staples and Wynn, 1965; Tulloch *et al.,* 1959). The upregulation of genes related to mobilisation of these substrates through metabolism and transport suggest that *Pst* might be utilising its nutrients to mount a defence response that can be energetically expensive (Heil 2001). The high degree of genes related to base-excision repair that were significantly upregulated suggests that potentially the attacking *P. coffeae* ANU01 produces toxins or aims to accumulate ROS in *Pst* urediniospores that in turn target and cause lesions on DNA. In Chapter Two, I showed that *P. coffeae* ANU01 likely produces a depudecin-like (histone deacetylase inhibitor) metabolite during interaction with *Pst*. Thus, mobilisation of a DNA repair pathway might be in response to its action. It is important to note that these conclusions and all of the conclusions I draw from the transcriptomic signals I detected in these datasets remain speculative. This is the first report of a possible response of *Pst* to hyperparasitic attack and as a result it is difficult to reliably interpret signals in this new context, even if at first, they may suggest clear pathways. The interpretations I made in Chapter Two regarding how *P. coffeae* ANU01 might parasitise *Pst* are also purely speculative, further reducing the veracity of the proposed *Pst* response.

In uninfected pustules, the top five most significantly enriched GO terms were translation (256 genes, 59.67%), protein folding (62 genes, 57.94%), cytoplasmic translation (53 genes, 75.7%), ribosomal large subunit biogenesis (53 genes, 68.8%) and tRNA aminoacylation for protein translation (34 genes, 56.6%). Terms that were enriched in uninfected pustules, were by definition unenriched or absent in pustules that were under attack by *P. coffeae* ANU01. The marked enrichment of genes related to cellular and biosynthetic activity therefore suggest that these processes were negatively affected by the presence of *P. coffeae* ANU01. Decreased cellular and biosynthetic activity during parasitic attack

suggests that the nutrients which are normally abundant in rust urediniospores and used to mobilise those processes were either being exploited by *P. coffeae* ANU01 or were mobilised instead to mount a defence response.

An unadjusted Fisher's exact test determines significance from the raw *P* value from a 2x2 contingency table, adjustment involves correcting those *P* values for multiple testing (Alexa & Rahnenführer 2016). Therefore, those GO terms that remained significant after adjustment are more robustly significant and therefore more likely to be at the core of defence against *P. coffeae* ANU01 attack. I consider GO terms that were only significant before adjustment (unadjusted significant terms) to be secondary aspects of the defence, they should be considered important but perhaps less integral than those that remain after adjustment. Before adjustment there were 85 significantly enriched terms, this dropped to six after adjustment. To investigate less-significantly enriched terms, I continued my analysis by looking at those 85 unadjusted significantly enriched GO terms in pustules under attack by *P. coffeae* ANU01 (Figure 4.3). Importantly, though it provides a more robust confidence in the enrichment of a GO term, and I hypothesise that core terms are more integral to rust defence, retaining statistical significance after adjustment does not necessarily mean that the associated biological process is more important during parasitism than a term that did not retain significance after adjustment.

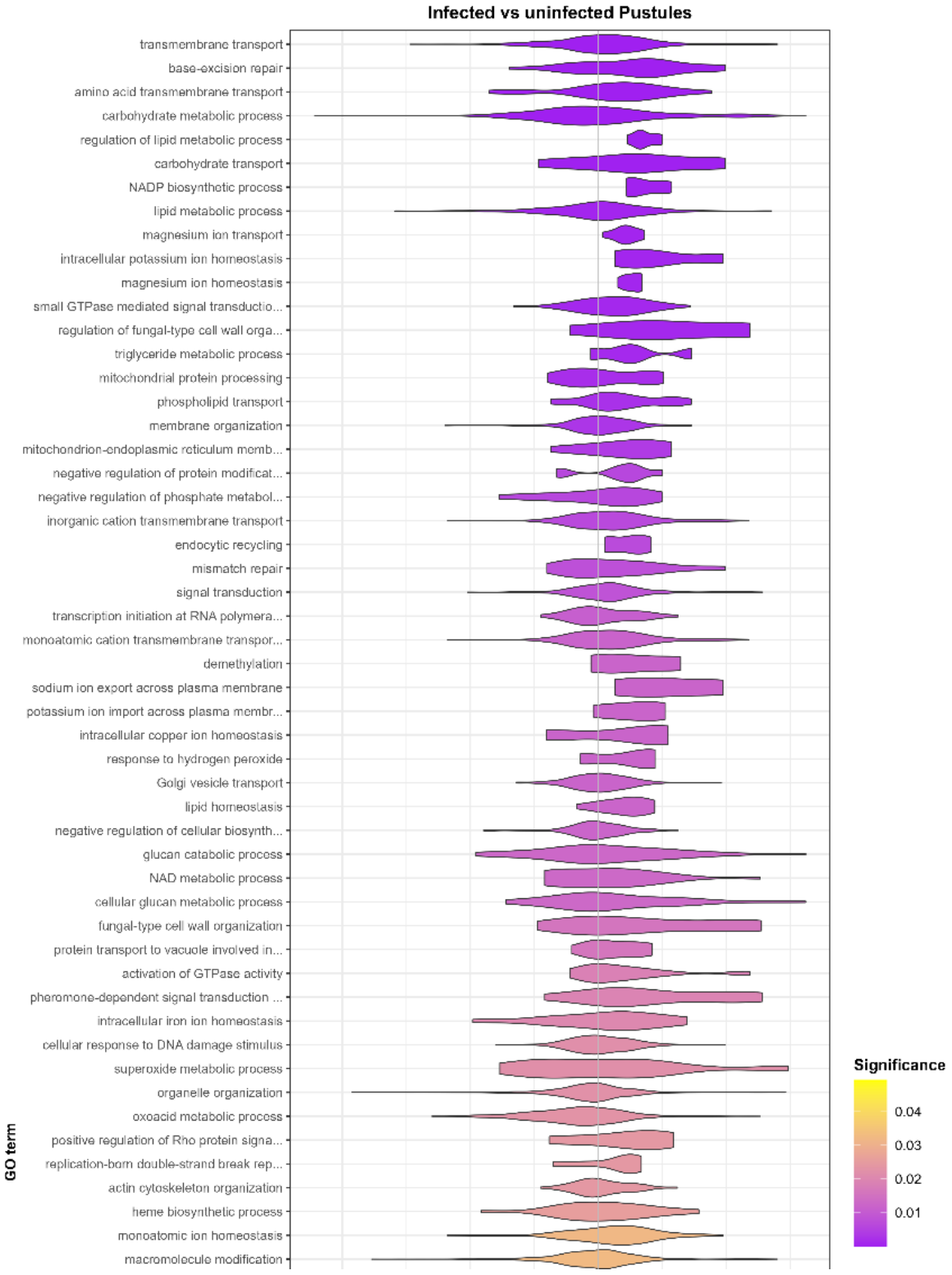
Infected vs uninfected Pustules
transmembrane transport
base-excision repair
amino acid transmembrane transport
carbohydrate metabolic process
regulation of lipid metabolic process
carbohydrate transport
NADP biosynthetic process
lipid metabolic process
magnesium ion transport
intracellular potassium ion homeostasis
magnesium ion homeostasis
small GTPase mediated signal transductio...
regulation of fungal-type cell wall orga...
triglyceride metabolic process
mitochondrial protein processing
phospholipid transport
membrane organization
mitochondrion-endoplasmic reticulum memb...
negative regulation of protein modificat...
negative regulation of phosphate metabol...
inorganic cation transmembrane transport
endocytic recycling
mismatch repair
signal transduction
transcription initiation at RNA polymera...
monoatomic cation transmembrane transpor...
demethylation
sodium ion export across plasma membrane
potassium ion import across plasma membr...
intracellular copper ion homeostasis
response to hydrogen peroxide
Golgi vesicle transport
lipid homeostasis
negative regulation of cellular biosynth...
glucan catabolic process
NAD metabolic process
cellular glucan metabolic process
fungal-type cell wall organization
protein transport to vacuole involved in...
activation of GTPase activity
pheromone-dependent signal transduction ...
intracellular iron ion homeostasis
cellular response to DNA damage stimulus
superoxide metabolic process
organelle organization
oxoacid metabolic process
positive regulation of Rho protein signa...
replication-born double-strand break rep...
actin cytoskeleton organization
heme biosynthetic process
monoatomic ion homeostasis
macromolecule modification
GO term
Significance
0.04
0.03
0.02
0.01



Figure 4.3. Violin plot (split into two sections for readability) representing processes enriched in *Pst* when under attack by *P. coffeae* ANU01. Each violin represents a process (GO term) that was significantly enriched in *Pst* when under attack by the hyperparasite. Terms are ranked from top to bottom by significance according to an unadjusted Fisher's exact test with all terms meeting the cut off of p=>0.05. The X axis represents the distribution of genes within each term with respect to up-down regulation (Log_2 fold change) during parasitic attack. The shortened GO terms on the Y axis are: small GTPase-mediated signal transduction, regulation of fungal-type cell wall organization, mitochondrion-endoplasmic reticulum membrane tethering, negative regulation of protein modification process, negative regulation of phosphate metabolic process, transcription initiation at RNA polymerase II gene promoter, monoatomic cation transmembrane transport, potassium ion import across plasma membrane, negative regulation of cellular biosynthetic process, protein transport to vacuole involved in ubiquitin-

dependent protein catabolic process via the multivesicular body sorting pathway, pheromone-dependent signal transduction involved in conjugation with cellular fusion, positive regulation of Rho protein signal transduction, replication-born double-strand break repair via sister chromatid exchange, negative regulation of amide metabolic process, regulation of macromolecule biosynthetic process, regulation of cyclin-dependent protein serine/threonine kinase activity, dolichol-linked oligosaccharide biosynthetic process, pyrimidine nucleotide-sugar transmembrane transport, DNA-templated DNA replication maintenance of fidelity, cellular nitrogen compound metabolic process, regulation of cellular component organization, intracellular monoatomic cation homeostasis. tRNA aminoacylation for protein translation, formation of translation preinitiation complex, maturation of SSU-rRNA from tricistronic rRNA transcript (SSU-rRNA, 5.8S rRNA, LSU-rRNA), nuclear-transcribed mRNA catabolic process, endonucleolytic cleavage in 5'-ETS of tricistronic rRNA transcript (SSU-rRNA, 5.8S rRNA, LSU-rRNA), endonucleolytic cleavage to generate mature 5'-end of SSU-rRNA from (SSU-rRNA, 5.8S rRNA, LSU-rRNA), endonucleolytic cleavage in ITS1 to separate SSU-rRNA from 5.8 rRNA and LSU-rRNA from tricistronic rRNA transcript (SSU-rRNA, 5.8S rRNA, LSU-rRNA), formation of cytoplasmic translation initiation complex, positive regulation of translational fidelity, long-chain fatty acid biosynthetic process, ribosomal large subunit export from nucleus, pyrmidine ribonucleotide biosynthetic process, ER-associated misfolded protein catabolic process, 'de novo' pyrmidine nucleobase biosynthetic process, organonitrogen compound biosynthetic process, ribosomal small subunit export from nucleus, ribonucleoside monophosphate biosynthetic process, maturation of 5.8S rRNA from tricistronic rRNA transcript (SSU-rRNA, 5.8S rRNA, LSU-rRNA), nonribosomal peptide biosynthetic process and maturation of LSU-rRNA from tricistronic rRNA transcript (SSU-rRNA, 5.8S rRNA, LSU-rRNA).

Expanding my analysis to include GO terms that were only significantly enriched before adjustment suggested that *Pst* mounts a more complex response than the core enriched terms would indicate. The 85 enriched terms suggests that *Pst* urediniospores are not dormant or defenceless but instead mobilise a diverse range of processes in response to hyperparasitic attack. The upregulation of signalling-related genes suggests that *Pst* activates complex intracellular communication networks upon detection of *P. coffeae* ANU01. Broadly, 94 of the 361 genes (26% of genes) related to signal transduction were upregulated, indicating recognition of stimuli. An increase in GPI anchor biosynthesis (14 genes upregulated, 31.8% of the total genes related to GPI anchor biosynthesis) may indicate multiple functions in cell wall remodelling and extracellular recognition. Glycosylphosphatidylinositol (GPI)-anchored proteins serve diverse functions, are integral components of the cell wall and can be used in sensing environmental cues, in this context, potentially damage due to hyperparasite enzymes (De Groot *et al.,* 2003). Rho proteins are internal "cellular switches" commonly associated with inducing large metabolic changes during stress response (Xu *et al.,* 2026). The induction of Rho proteins (4 genes, 57%) may be paired with increased GTPase activity to induce responses in vesicle trafficking and cell

wall biogenesis (Oliveira-Garcia *et al.*, 2022). Pheromone-dependent signalling genes (6 genes, 46%) are commonly associated with processes such as mating (Raudaskoski & Kothe 2010), however, in this case may be co-opted for stress signalling during defence, especially with the upregulation of several G-proteins (Supplementary Table 3.1). Stripe rust urediniospores are densely packed together within pustules, so it is possible that urediniospores may communicate with one another to coordinate defence against invading hyperparasites. Finally, an upregulation in general cellular response to abiotic stimulus (7 genes, 29%) suggests that while *Pst* recognises it is under stress and upregulates downstream pathways, it may not be a specifically tailored response to a hyperparasite. Overall, *Pst* appears to be capable of recognising signals associated with hyperparasitic attack and of mobilising defence responses and pathways.

The GO enrichment data suggests that *Pst* appears to fortify its urediniospore coat and cellular membranes to protect against hyperparasitic attack. Fungal hyperparasites deploy direct hyphal puncturing and invasion as well as the action of cell-wall degrading enzymes to break through the tough fungal urediniospore coat (Srivastava *et al.*, 1985). Ascomycete hyperparasite hyphae have been repeatedly observed physically invading *Pst* urediniospores in pustules (Wang *et al.*, 2020, Zhan *et al.*, 2014). The upregulation of several secreted *P. coffeae* ANU01 glycoside hydrolase CAZymes during growth on *Pst* suggests it might deploy them in a similar way (Chapter Two). I observed an upregulation in 7 *Pst* genes (29%) related to fungal-type cell wall biogenesis. GO enrichment showed a specific upregulation in chitin and glucan cell wall metabolism (7 genes (26.9%) and 13 genes (35.1%) respectively), both chitin and glucan are key defensive structural components of the urediniospore coat (Fesel & Zuccaro 2016). β-glucans are common targets of mycoparasitic fungi (Archambault *et al.*, 1998); *Penicillium coffeae* ANU01 may degrade *Pst* cell-wall glucans through its highly upregulated and secreted β-1,3-glucanase (*PenX_011559-T1*). Remodelling of the *Pst* cell wall may be a response to degradation by it and similar enzymes. This potential remodelling is reinforced by upregulation of further genes in the actin (18 genes, 21%) and cortical (3 genes, 17.6%) cytoskeleton organisation category. These may maintain overall cellular composition and reduce the chance of crumbling as often seen after parasitic attack (Wang *et al.*, 2020, Zhan *et al.*, 2014). Overall, we observed a shift towards reinforcing the physical barriers to entry during parasitic attack, indicating fortification is a key component of the defence strategy.

Maintaining homeostasis appears integral to survival during parasitic attack, seemingly mediated through transmembrane transport of important ions. An upregulation in copper ion homeostasis (4 genes, 66.6%), specifically *Ctr* and *CUP* (copper uptake proteins) genes in *Pst*, indicates an increased need for copper import into the cell (Knight *et al.*, 1996). Copper is essential as a cofactor in redox enzymes such as superoxide dismutases (McCord & Fridovich 1969) which are highly upregulated genes in *Pst* defence (Supplementary Table 3.1). Importantly, copper importers, specifically *Ctr* genes, were dramatically downregulated in *P. coffeae* ANU01 when parasitising *Pst* (Wess *et al.*, 2025). This

may suggest that *P. coffeae* ANU01 can not only source all of its copper requirements from urediniospores but limits influx to avoid accumulating toxic amounts. Genes related to potassium ion homeostasis (6 genes, 75%), specifically potassium import genes (4 genes, 66.6%) were significantly upregulated in *Pst* during attack. Controlling potassium ion concentration is important to maintaining osmotic balance and turgor pressure (Lew and Nasserifar, 2009). Potassium is also important in protein synthesis and enzyme action; all of these processes are crucial in a rapidly changing cell environment (Rodríguez-Navarro 2000). An upregulation in intracellular iron ion homeostasis (9 genes, 37.5%) may be crucial to scavenging rare iron ions from the environment for use in heme-dependent enzymes. The heme biosynthetic process was also highly upregulated (8 genes, 38.1%); heme-dependent enzymes serve crucial roles in defence including tasks such as ROS detoxification (Misslinger *et al.*, 2017). Inability to acquire iron is highly detrimental to filamentous fungi (Robinson *et al.*, 2021) as Iron (Fe2+) is commonly limiting for microbes, often sequestered by the host in order to reduce pathogen growth (Hood & Skaar 2012). Accordingly, *Pst* urediniospores may therefore also rapidly import iron to sequester it from *P. coffeae* ANU01. Sodium appeared to be the only ion solely exported during hyperparasite attack (4 genes, 66.6%). Maintaining homeostasis of important inorganic ions may be crucial not only to survival of *Pst* but also to reducing the strength of *P. coffeae* ANU01 by limiting its growth.

Detoxification of reactive oxygen species (ROS) and SMs appears to be important to survival of *Pst* during hyperparasite attack. ROS are an important aspect of pathogen-host interactions in fungi, often accumulating as a result of stress or mechanical damage (Fester & Hause 2005). An upregulation in genes related to superoxide metabolism (9 genes, 47.4%) and response to hydrogen peroxide (4 genes, 66.6%) suggests protection against a possible offensive ROS burst from *P. coffeae* ANU01 or overaccumulation of ROS produced in defence and increased metabolism from mitochondria. Upregulation of all five of the genes related to NADP biosynthesis may be due to the molecule being a precursor to nicotinamide adenine dinucleotide phosphate (NADPH), a critical reducing equivalent used by many ROS detox mechanisms (Chandel 2021). The upregulation of genes related to "Protein transport to the vacuole involved in ubiquitin-dependent protein catabolic process" (7 genes, 43.8%) points to the vacuole's role in degrading proteins (Klionsky *et al.*, 1990). The vacuole may be used to degrade damaged or misfolded proteins that could arise from oxidative stress, or alternatively, proteins such as cell wall degrading enzymes or toxic SMs secreted by *P. coffeae* ANU01. Increased vesicle fusion (10 genes, 28.6%) might be related to exocytotic export of toxic metabolites such as the depudecin-like SM produced by *P. coffeae* ANU01, or the export of defensive SMs produced by *Pst* (Chanda *et al.*, 2009). Thus, protection against hyperparasite-derived damage appears to be a critical component of the *Pst* defence system.

Pst appears to mobilise repair mechanisms to protect itself against DNA damage. The upregulation of genes related to "cellular response to DNA damage stimulus" (64 genes, 24%) first suggests that *Pst* is

responding to DNA stress. This is supported by a number of upregulated genes related to base-excision (14 genes, 66.7%), UV-damage excision (3 genes, 60%), nucleotide excision (15 genes, 34.9%), mismatch (12 genes, 37.5%) and replication-born double strand break repair (4 genes, 57.1%). These genes are likely upregulated to repair DNA damage done by SMs or the ROS described in the previous paragraph. Depudecin is a toxic SM predicted to act as a histone deactylase inhibitor (Kwon *et al.,* 2003). A depudecin-like biosynthetic gene cluster was highly upregulated in *P. coffeae* ANU01 (Wess *et al.,* 2025). The potential action of this SM may be reflected by the upregulation of *Pst* histone h3 acetylation (3 genes, 60%). The mobilisation of repair mechanisms suggests that DNA repair and maintaining genomic stability is a vital aspect of defence against *P. coffeae* ANU01.

Finally, a comprehensive defence response would likely place high energy demands on *Pst* urediniospores, which could be addressed by mobilisation of their abundant energy stores. During parasitism, infected pustules showed genetic upregulation of several metabolic pathways; cellular lipid catabolic process (23 genes, 33.8%), glycerophospholid catabolic process (5 genes, 45.45%), triglyceride metabolic process (6 genes, 66.67%) and carbohydrate metabolism (79 genes, 28.2%). Lipids and carbohydrates are rich sources of energy for fungi and in *Pst* are the major nutrients mobilised to fuel germination and invasion (Staples & Wynn, 1965; Tulloch *et al.,* 1959). Defence responses such as cell wall remodelling, ion homeostasis and DNA repair are energetically expensive (Heil 2001). The transcriptomic data suggests that *Pst* appears to utilise its abundant lipids, nutrients it would usually use in germination and colonisation, to fuel the defence response. Triggering mobilisation of *Pst* nutrients that normally would be used to infect plants may enhance *P. coffeae* ANU01's usefulness as a potential biocontrol.

My GO enrichment analysis revealed a diverse functional transcriptional reprogramming during pathogen attack (Figure 4.3). The GO terms enriched in infected pustules can be divided into six key components; sensing and signalling, fortification, maintenance of homeostasis, detoxification, repair and metabolism. I hypothesise that *Pst* defends itself against the hyperparasite on the leaf surface through these mechanisms.

Investigating the COG categories upregulated during parasitic attack reinforces the possible components of defence I observed in GO enrichment

Table 3.2. Summary of the number of upregulated (>1 Log_2 fold change) genes related to each COG (Clusters of Orthologous Genes) category during parasitic attack

COG category	Total # Genes in Category	# Upregulated Genes	% Upregulated Genes
RNA processing and modification	726	53	7.3
Chromatin structure and dynamics	319	23	7.2
Energy production and conversion	499	62	12.4
Cell cycle control, cell division, chromosome partitioning	435	49	11.3
Amino acid transport and metabolism	644	61	9.5
Nucleotide transport and metabolism	158	18	11.4
Carbohydrate transport and metabolism	833	137	16.5
Coenzyme transport and metabolism	311	38	12.2
Lipid transport and metabolism	538	81	15.1
Translation, ribosomal structure and biogenesis	843	37	4.4
Transcription	653	60	9.2
Replication, recombination and repair	573	73	12.7
Cell wall/membrane/envelope biogenesis	153	23	15.0
Cell motility	56	8	14.3
Posttranslational modification, protein turnover, chaperones	1348	133	9.9
Inorganic ion transport and metabolism	347	84	24.2
Secondary metabolites biosynthesis, transport and metabolism	326	53	16.3
Function unknown	3060	536	17.5
Signal transduction mechanisms	863	155	18
Intracellular trafficking, secretion and vesicular transport	820	113	13.8
Defence mechanisms	64	14	21.9

Extracellular structures	13	3	23.1
Nuclear structure	67	1	1.5
Cytoskeleton	300	38	12.7

I further explored the *Pst* genes upregulated during response to *P. coffeae* ANU01 by exploring a second functional annotation grouping, COGs. COG terms assign genes to groups of shared predicted function based on similarity to a database of proteins of known function (Galperin *et al.,* 2019). The emphasis on fortification, homeostasis and signalling that I observed in enriched GO terms, was reinforced in the COG categories upregulated in infected pustules (Table 3.2). The five most represented COG terms in upregulated (>1 Log_2 fold change) genes were; Inorganic ion transport and metabolism (84 genes, 24.2% of genes within this term were upregulated), extracellular structures (3 genes, 23.1%), Defence mechanisms (14 genes, 21.9%), Signal transduction mechanisms (155 genes, 18%) and finally genes for which function is unknown (536 genes, 17.5%).

The position of inorganic ion transport as the most proportionally upregulated COG category, and the previously stated significant enrichment of GO terms related to ion transport, suggest its importance for *Pst* in maintaining cellular homeostasis during parasitic attack. All three of the upregulated genes related to extracellular structures encode Twinfilins, actin-binding proteins that act in coordinating remodelling of the cytoskeleton (Xu *et al.,* 2021). These proteins may help stabilise the cytoskeleton and support membrane repair in response to invasion or cell wall degrading enzymes, produced by *P. coffeae* ANU01 (Chapter Two). Unsurprisingly, genes specific to defence mechanisms were upregulated. Genes encoding tyrosine phosphatases accounted for 43% (6 genes) of these, while three Ras and Rho GTPases genes were upregulated. These proteins work as switches at the apex of complex downstream pathways involved in stress response and survival (Macara *et al.,* 1996; Soriano *et al.,* 2021). The emphasis on stress signalling was supported by the upregulation of a large proportion of genes related to signal transduction mechanisms, which reinforces the presence of a complex and coordinated stress response by *Pst* to *P. coffeae* ANU01 attack. Finally, the high proportion of genes upregulated with unknown function may suggest a yet uncharacterised defensive response to parasitic attack. However, without further annotation or characterisation it is impossible to ascribe meaning to this. Interestingly, 53 genes (16.3%) related to secondary metabolism were upregulated, suggesting that the *Pst* response may extend into active attack against the invading *Penicillium.*

Investigating the top 20 most upregulated *Pst* genes during parasitic attack

I investigated the top 20 upregulated genes in infected pustules to gain insight into what *Pst* might prioritise when under attack. Five of the top 20 genes encode enzymes, including *Pst104E137_016797-T1* (8.7 Log_2 fold change), a glucan endo-1,6-beta-glucosidase lacking a secretion signal peptide that is potentially used to reinforce and/or remodel the cell wall in response to *P. coffeae* ANU01 attack

(Volkov *et al.,* 2021). The absence of a secretion signal peptide may be due to a mis annotation. Cutin is a polymer abundant in the waxy cuticle layer on the surface of leaves (Nawrath 2002), while pectin is a polysaccharide in the plant cell wall (Voragen *et al.,* 2009). The genes encoding the predicted pectin lyase *Pst104E137_006947-T1* (7.56 Log_2 fold change) and cutinase *Pst104E137_019167-T1* (7.37 Log_2 fold change) both contain an SP and may be upregulated to scavenge nutrients from damaged plant cell walls and fuel the energetically expensive defence response. It is difficult to speculate on the possible function of these two enzymes, an alternative possibility is that these secreted enzymes target substrates similar to pectin or cutin in the hyperparasite hyphal walls. Superoxide dismutases (SODs) are enzymes responsible for detoxification of superoxide to less harmful ROS (McCord & Fridovich 1995). The two superoxide dismutase encoding genes *Pst104E137_002289-T1* (7.41 Log_2 fold change) and *Pst104E137_017851-T1* (7.2 Log_2 fold change) may be upregulated to help protect against oxidative stress, reinforcing the importance of protection against ROS I observed in the GO enrichment. *Pst* has been shown to use superoxide dismutases to defend against plant-derived defences (Zheng *et al.,* 2020), however as these SOD genes are upregulated in the infected pustule dataset relative to the uninfected dataset, I suspect that they are directly related to ROS-induced stress from the parasite. *Pst104E137_020473-T1* (7.32 Log_2 fold change) which encodes the mitochondrial ATPase complex subunit ATP10, involved in the assembly and maintenance of the main enzyme responsible for synthesising ATP in mitochondria (Ackerman & Tzagoloff 1990). Reactive oxidative stress can damage mitochondrial components (Kowaltowski 2019); upregulating ATP10 may help replace degraded mitochondrial components, but may also help with the increased energy demand associated with mounting a complex defence response. Eight of the top 20 upregulated genes encode secretion signal peptides. Six of those genes, including the most upregulated secreted gene (*Pst104E137_017520*-T1, 7.7 Log_2 fold change), contain no other annotation. These unannotated secreted proteins may be enzymes produced and secreted to target hyperparasite structures or interact with proteins produced by *P. coffeae* ANU01. Unfortunately, several of the most upregulated genes contain no functional annotation whatsoever, including the most upregulated gene (*Pst104E137_016179-T1,* 8.7 Log_2 fold change). This is also the case for the fourth (*Pst104E137_024098-T1,* 7.92 Log_2 fold change), fifth (*Pst104E137_027547-T1,* 7.83 Log_2 fold change) and sixth (*Pst104E137_012029-T1,* 7.68 Log_2 fold change) most upregulated genes. The lack of homology to known genes may suggest these highly upregulated genes encode novel mechanisms to defend against parasitic attack. Finally, the 10th most upregulated gene (*Pst104E137_016911-T1,* 7.54 Log_2 fold change) is predicted to encode a secreted effector. Effector is a broad definition meaning a protein secreted to interact with host immunity, through manipulating host cell structure and function (Li *et al.*, 2024, Todd *et al.,* 2022), such as LysM proteins which may protect *Meloidogyne graminicola* hyphae against cell wall degrading enzymes produced by the host (Kombrink & Thomma 2013). The EffectorP software predicts effectors based on their possession of a secretion signal peptide and sequence-derived features such as cysteine enrichment or N-terminal features after the signal peptide (Sperschneider & Dodds 2022). A total of 129 predicted

Pst effectors were upregulated (> 1 Log_2 fold change) during parasitic attack, compared to 34 in uninfected pustules. This broad increase in the expression of secreted effectors during interaction with *P. coffeae* ANU01 suggests that they are potentially important in the defence response. The most upregulated effector candidates with functional annotation encode RlpA-like proteins (*Pst104E137_004173-T1* (7.05 Log_2 fold change) and *Pst104E137_019691-T1* (6.83 Log_2 fold change)). *Rhizoctonia solani* RlpA proteins suppress proteolytic activity and ROS burst from the plant host (Charova *et al.*, 2020). In the context of *Pst*, its RlpA-like proteins may protect against similar activity by *P. coffeae* ANU01 beyond simply passive measures.

There are several limitations associated with this study, primarily with regards to experimental differences between the two RNAseq conditions. Firstly, for uninfected pustules, RNA was isolated from pustules that emerged 12 days after plants were first inoculated with rust urediniospores. In the infected pustule condition, pustules were sprayed with *P. coffeae* ANU01 spores at 14 dpi and then harvested ~9 days later, making them substantially older than the uninfected condition. Future experiments should take samples at identical time points between treatments, I was unable to match time points as I conducted this experiment simply using the only ungerminated *Pst* pustule dataset that was available. The infected pustules had also experienced high relative humidity for 9 days due to the cellophane bags, which uninfected pustules did not. Finally, as the original RNA sampling was conducted to investigate *P. coffeae* ANU01 gene expression, tissue was scraped firmly from the surface of the infected pustules, as opposed to the whole leaf sampling approach taken for uninfected pustules. This difference in sampling could affect downstream analysis if deeper components of the pustule express genes differentially and were not collected in infected pustules. However, this analysis was done retrospectively, future experiments should focus on isolating RNA from *Pst* pustules under attack by *P. coffeae* ANU01 at numerous time points during colonisation.

The transcriptomic data suggest that *Pst* urediniospores are not simply sitting dormant and defenceless in pustules, but are capable of recognising the presence of a parasite and coordinating a complex defence response. I propose that the defence response can be divided into six key aspects; sensing the hyperparasite and engaging downstream signalling, fortification of the rust urediniospore coat to protect against enzymatic and mechanical damage, maintenance of homeostasis to protect *Pst* in a rapidly changing environment, detoxification of SMs and harmful ROS induced by *P. coffeae* ANU01, repair of damage to DNA, potentially inflicted by SMs from *P. coffeae* ANU01 and finally a mobilisation of metabolites, primarily lipids, to fuel the defence.

4.4 Bibliography

Ackerman, S. H., & Tzagoloff, A. (1990). *ATP10*, a yeast nuclear gene required for the assembly of the mitochondrial F1-F0 complex. Journal of Biological Chemistry, 265(17), 9952-9959. https://doi.org/https://doi.org/10.1016/S0021-9258(19)38763-0

Alexa, A., & Rahnenfuhrer, J. (2016). topGO: Enrichment analysis for Gene Ontology. R package version 2.28. 0. Cranio, 2, 289-300.

Archambault, C., Coloccia, G., Kermasha, S., & Jabaji-Hare, S. (1998). Characterization of an endo-1,3-β-D-glucanase produced during the interaction between the mycoparasite *Stachybotrys elegans* and its host *Rhizoctonia solani*. Canadian Journal of Microbiology, 44(10), 989-997. https://doi.org/10.1139/w98-088

Chanda, A., Roze, L. V., Kang, S., Artymovich, K. A., Hicks, G. R., Raikhel, N. V., Calvo, A. M., & Linz, J. E. (2009). A key role for vesicles in fungal secondary metabolism. Proceedings of the National Academy of Sciences, 106(46), 19533-19538. https://doi.org/10.1073/pnas.0907416106

Chandel, N. S. (2021). NADPH—The Forgotten Reducing Equivalent. Cold Spring Harbor Perspectives in Biology, 13(6), a040550. https://doi.org/10.1101/cshperspect.a040550

Charova, S. N., Dölfors, F., Holmquist, L., Moschou, P. N., Dixelius, C., & Tzelepis, G. (2020). The RsRlpA effector is a protease inhibitor promoting *Rhizoctonia solani* virulence through suppression of the hypersensitive response. International Journal of Molecular Sciences, 21(21), 8070.

Chen, S., Zhou, Y., Chen, Y., & Gu, J. (2018). fastp: an ultra-fast all-in-one FASTQ preprocessor. Bioinformatics, 34(17), i884-i890. https://doi.org/10.1093/bioinformatics/bty560

Chen, W., Wellings, C., Chen, X., Kang, Z., & Liu, T. (2014). Wheat stripe (yellow) rust caused by *Puccinia striiformis* f. sp. *tritici*. Molecular Plant Pathology, 15(5), 433-446. https://doi.org/10.1111/mpp.12116

De Groot, P. W. J., Hellingwerf, K. J., & Klis, F. M. (2003). Genome-wide identification of fungal GPI proteins. Yeast, 20(9), 781-796. https://doi.org/10.1002/yea.1007

Fesel, P. H., & Zuccaro, A. (2016). β-glucan: Crucial component of the fungal cell wall and elusive MAMP in plants. Fungal Genetics and Biology, 90, 53-60. https://doi.org/https://doi.org/10.1016/j.fgb.2015.12.004

Fester, T., & Hause, G. (2005). Accumulation of reactive oxygen species in arbuscular mycorrhizal roots. Mycorrhiza, 15(5), 373-379. https://doi.org/10.1007/s00572-005-0363-4

Galperin, M. Y., Wolf, Y. I., Makarova, K. S., Vera Alvarez, R., Landsman, D., & Koonin, E. V. (2021). COG database update: focus on microbial diversity, model organisms, and widespread pathogens. Nucleic Acids Research, 49(D1), D274-D281.

Garnica, D. P., Nemri, A., Upadhyaya, N. M., Rathjen, J. P., & Dodds, P. N. (2014). The ins and outs of rust haustoria. PLOS Pathogens, 10(9), e1004329. https://doi.org/10.1371/journal.ppat.1004329

Heil, M. (2001). The ecological concept of costs of induced systemic resistance (ISR). European Journal of Plant Pathology, 107(1), 137-146. https://doi.org/10.1023/a:1008793009517

Hood, M. I., & Skaar, E. P. (2012). Nutritional immunity: transition metals at the pathogen–host interface. Nature Reviews Microbiology, 10(8), 525-537. https://doi.org/10.1038/nrmicro2836

Kim, D., Paggi, J. M., Park, C., Bennett, C., & Salzberg, S. L. (2019). Graph-based genome alignment and genotyping with HISAT2 and HISAT-genotype. Nature Biotechnology, 37(8), 907-915. https://doi.org/10.1038/s41587-019-0201-4

Klionsky, D. J., Herman, P. K., & Emr, S. D. (1990). The fungal vacuole: composition, function, and biogenesis. Microbiological Reviews, 54(3), 266-292. https://doi.org/10.1128/mr.54.3.266-292.1990

Knight, S. A., Labbé, S., Kwon, L. F., Kosman, D. J., & Thiele, D. J. (1996). A widespread transposable element masks expression of a yeast copper transport gene. Genes & Development, 10(15), 1917-1929. https://doi.org/10.1101/gad.10.15.1917

Kombrink, A., & Thomma, B. P. H. J. (2013). LysM effectors: secreted proteins supporting fungal life. PLOS Pathogens, 9(12), e1003769. https://doi.org/10.1371/journal.ppat.1003769

Kowaltowski, A. J. (2019). Strategies to detect mitochondrial oxidants. Redox Biology, 21, 101065. https://doi.org/https://doi.org/10.1016/j.redox.2018.101065

Kwon, H. J., Kim, J.-H., Kim, M., Lee, J.-K., Hwang, W.-S., & Kim, D.-Y. (2003). Anti-parasitic activity of depudecin on *Neospora caninum* via the inhibition of histone deacetylase. Veterinary Parasitology, 112(4), 269-276. https://doi.org/https://doi.org/10.1016/S0304-4017(03)00035-9

Lew, R. R., & Nasserifar, S. (2009). Transient responses during hyperosmotic shock in the filamentous fungus *Neurospora crassa*. Microbiology, 155(3), 903-911. https://doi.org/https://doi.org/10.1099/mic.0.023507-0

Li, G., Newman, M., Yu, H., Rashidzade, M., Martínez-Soto, D., Caicedo, A., Allen, K. S., & Ma, L.-J. (2024). Fungal effectors: past, present, and future. Current Opinion in Microbiology, 81, 102526. https://doi.org/https://doi.org/10.1016/j.mib.2024.102526

McCord, J. M., & Fridovich, I. (1969). Superoxide dismutase. Journal of Biological Chemistry, 244(22), 6049-6055. https://doi.org/10.1016/s0021-9258(18)63504-5

Misslinger, M., Gsaller, F., Hortschansky, P., Müller, C., Bracher, F., Bromley, M. J., & Haas, H. (2017). The cytochrome b5CybE is regulated by iron availability and is crucial for azole resistance in *A. fumigatus*. Metallomics, 9(11), 1655-1665. https://doi.org/10.1039/c7mt00110j

Nasini, G., Arnone, A., Assante, G., Bava, A., Moricca, S., & Ragazzi, A. (2004). Secondary mould metabolites of *Cladosporium tenuissimum*, a hyperparasite of rust fungi. Phytochemistry, 65(14), 2107-2111. https://doi.org/10.1016/j.phytochem.2004.03.013

Nawrath, C. (2002). The Biopolymers Cutin and Suberin. The Arabidopsis Book, 1, e0021. https://doi.org/10.1199/tab.0021

Oliveira-Garcia, E., Aliyeva-Schnorr, L., De Oliveira Silva, A., El Din Ghanem, S., Thor, K., Peiter, E., & Deising, H. B. (2022). The small Ras superfamily GTPase Rho4 of the maize anthracnose fungus *Colletotrichum graminicola* is required for β-1,3-glucan synthesis, cell wall integrity, and full virulence. Journal of Fungi, 8(10), 997. https://doi.org/10.3390/jof8100997

Patro, R., Duggal, G., Love, M. I., Irizarry, R. A., & Kingsford, C. (2017). Salmon provides fast and bias-aware quantification of transcript expression. Nature Methods, 14(4), 417-419. https://doi.org/10.1038/nmeth.4197

Raudaskoski, M., & Kothe, E. (2010). Basidiomycete mating type genes and pheromone signaling. Eukaryotic Cell, 9(6), 847-859. https://doi.org/10.1128/ec.00319-09

Ritchie, M. E., Phipson, B., Wu, D., Hu, Y., Law, C. W., Shi, W., & Smyth, G. K. (2015). limma powers differential expression analyses for RNA-sequencing and microarray studies. Nucleic Acids Research, 43(7), e47-e47. https://doi.org/10.1093/nar/gkv007

Robinson, J. R., Isikhuemhen, O. S., & Anike, F. N. (2021). Fungal–metal interactions: a review of toxicity and homeostasis. Journal of Fungi, 7(3), 225.

Rodríguez-Navarro, A. (2000). Potassium transport in fungi and plants. Biochimica et Biophysica Acta (BBA) - Reviews on Biomembranes, 1469(1), 1-30. https://doi.org/https://doi.org/10.1016/S0304-4157(99)00013-1

Roelfs, A. P. (1985). 1 - Wheat and Rye Stem Rust. In A. P. Roelfs & W. R. Bushnell, Diseases, distribution, epidemiology, and control. Academic Press. 3-37. https://doi.org/https://doi.org/10.1016/B978-0-12-148402-6.50009-2

Schwessinger, B. (2017). Fundamental wheat stripe rust research in the 21st century. New Phytologist, 213(4), 1625-1631. https://doi.org/10.1111/nph.14159

Shaw, M. (1964). The physiology of rust uredospores. Journal of Phytopathology, 50(2), 159-180. https://doi.org/10.1111/j.1439-0434.1964.tb02915.x

Soriano, O., Alcón-Pérez, M., Vicente-Manzanares, M., & Castellano, E. (2021). The crossroads between RAS and RHO signaling pathways in cellular transformation, motility and contraction. Genes, 12(6), 819. https://doi.org/10.3390/genes12060819

Sperschneider, J., & Dodds, P. N. (2022). EffectorP 3.0: prediction of apoplastic and cytoplasmic effectors in fungi and oomycetes. Molecular plant-microbe interactions, 35(2), 146-156.

Srivastava, A. K., Défago, G., & Kern, H. (1985). Hyperparasitism of *Puccinia horiana* and other microcyclic rusts. Journal of Phytopathology, 114(1), 73-78. https://doi.org/10.1111/j.1439-0434.1985.tb04338.x

Staples, R. C., & Wynn, W. K. (1965). The physiology of uredospores of the rust fungi. The Botanical Review, 31(4), 537-564. https://doi.org/10.1007/BF02858608

Tam, R., Möller, M., Luo, R., Luo, Z., Jones, A., Periyannan, S., Rathjen, J. P., & Schwessinger, B. (2025). Long-read genomics reveal extensive nuclear-specific evolution and allele-specific expression in a dikaryotic fungus. Genome Research, 35(6), 1364-1376. https://doi.org/10.1101/gr.280359.124

Todd, J. N., Carreón-Anguiano, K. G., Islas-Flores, I., & Canto-Canché, B. (2022). Microbial effectors: key determinants in plant health and disease. Microorganisms, 10(10), 1980.

Tulloch, A. P., Craig, B. M., & Ledingham, G. A. (1959). The oil of wheat stem rust uredospores: II. The isolation of *cis*-9,10-epoxyoctadecanoic acid, and the fatty acid composition of the oil. Canadian Journal of Microbiology, 5(5), 485-491. https://doi.org/10.1139/m59-060

Volkov, P. V., Rubtsova, E. A., Rozhkova, A. M., Sinitsyna, O. A., Zorov, I. N., Kondratyeva, E. G., & Sinitsyn, A. P. (2021). Properties of recombinant endo-β-1,6-glucanase from *Trichoderma harzianum* and its application in the pustulan hydrolysis. Carbohydrate Research, 499, 108211. https://doi.org/https://doi.org/10.1016/j.carres.2020.108211

Voragen, A. G. J., Coenen, G.-J., Verhoef, R. P., & Schols, H. A. (2009). Pectin, a versatile polysaccharide present in plant cell walls. Structural Chemistry, 20(2), 263-275. https://doi.org/10.1007/s11224-009-9442-z

Wang, N., Fan, X., Zhang, S., Liu, B., He, M., Chen, X., Tang, C., Kang, Z., & Wang, X. (2020). Identification of a hyperparasitic *Simplicillium obclavatum* strain affecting the infection dynamics of

Puccinia striiformis f. sp. *tritici* on wheat. Front Microbiol, 11, 1277. https://doi.org/10.3389/fmicb.2020.01277

Wess, J., Hu, Y., Periyannan, S., Jones, A., & Rathjen, J. P. (2025). Global transcriptome changes during growth of a novel *Penicillium coffeae* isolate on the wheat stripe rust fungus, *Puccinia striiformis* f. sp. *tritici*. Fungal Genetics and Biology, 176, 103956. https://doi.org/https://doi.org/10.1016/j.fgb.2024.103956

Wiese, M., & Ravenscroft, A. (1979). Environmental effects on inoculum quality of dormant rust uredospores. Phytopathology, 69(10), 1106.

Wilson, A., Cuddy, W. S., Park, R. F., Harm, G. F. S., Priest, M. J., Bailey, J., & Moffitt, M. C. (2020). Investigating hyperparasites as potential biological control agents of rust pathogens on cereal crops. Australasian Plant Pathology, 49(3), 231-238. https://doi.org/10.1007/s13313-020-00695-8

Xiao, M., Chen, D., Liu, S., Chen, A., Fang, A., Tian, B., Yu, Y., Bi, C., Kang, Z., & Yang, Y. (2023). A chitin deacetylase Ps CDA2 from *Puccinia striiformis* f. sp. *tritici* confers disease pathogenicity by suppressing chitin-triggered immunity in wheat. Molecular Plant Pathology, 24(12), 1467-1479.

Xu, J., Zhang, Y., Ren, J., Liu, M., Huo, Y., & Kong, Q. (2026). Rho GTPase RhoD interacts with the Rho GEF Bud3 and is involved in aflatoxin biosynthesis, cell wall integrity, and pathogenicity in *Aspergillus flavus*. Microbiological Research, 307, 128486. https://doi.org/https://doi.org/10.1016/j.micres.2026.128486

Xu, R., Li, Y.-B., Liu, C., Shen, N., Zhang, Q., Cao, T., Qin, M., Han, L.-B., & Tang, D. (2021). Twinfilin regulates actin assembly and Hexagonal peroxisome 1 (Hex1) localization in the pathogenesis of rice blast fungus *Magnaporthe oryzae*. Molecular Plant Pathology, 22(12), 1641-1655. https://doi.org/https://doi.org/10.1111/mpp.13136

Zhan, G., Tian, Y., Wang, F., Chen, X., Guo, J., Jiao, M., Huang, L., & Kang, Z. (2014). A novel fungal hyperparasite of *Puccinia striiformis* f. sp. *tritici*, the causal agent of wheat stripe rust. PLoS One, 9(11), e111484. https://doi.org/10.1371/journal.pone.0111484

Zheng, L., Zhao, J., Liang, X., Zhan, G., Jiang, S., & Kang, Z. (2017). Identification of a Novel *Alternaria alternata* strain able to hyperparasitize *Puccinia striiformis* f. sp. *tritici*, the causal agent of wheat stripe rust. Frontiers in Microbiology, 8. https://doi.org/10.3389/fmicb.2017.00071

Zheng, P., Chen, L., Zhong, S., Wei, X., Zhao, Q., Pan, Q., Kang, Z., & Liu, J. (2020). A Cu-only superoxide dismutase from stripe rust fungi functions as a virulence factor deployed for counter defense against host-derived oxidative stress. Environmental Microbiology, 22(12), 5309-5326. https://doi.org/https://doi.org/10.1111/1462-2920.15236

Chapter Five

Beyond *P. coffeae* ANU01: Identifying and Investigating further rust hyperparasites

5.1 Background

Fungi capable of parasitising rust fungi are taxonomically diverse and infect a wide variety of rust hosts. Owing to the importance of stripe rust in global agriculture, much research on rust hyperparasites has focused on *P. striiformis* f. sp. *tritici* (*Pst*) antagonists. Isolates belonging to the genera *Alternaria*, *Cladosporium*, *Simplicillium*, and *Penicillium* have been observed acting as hyperparasites of stripe rust (Wang *et al.*, 2020; Wess *et al.*, 2025; Zhan *et al.*, 2014; Zheng *et al.*, 2017;). *Verticillium lecanii* has been shown to antagonise the stripe rust, chrysanthemum rust (*Puccinia horiana*), and coffee rust pathogens (*Hemileia vastatrix*) (Mendgen 1981; Whipps 1993). Isolates of *Verticillium lecanii* and *Ramichloridium* act as natural hyperparasites of the leek rust pathogen (*Puccinia allii*) (Uma & Taylor 1987). Species belonging to the genus *Darluca* have been observed parasitising *Puccinia amphigena* and groundnut rust (*Puccinia arachidis*) (Zambettakis *et al.*, 1985). These natural antagonists have been shown to reduce rust spore viability and overall disease severity in host plants. Despite their potential agricultural and ecological significance, the genetic basis of rust hyperparasitism remains poorly understood. Little is known about the genes required for antagonism and nutrient acquisition from rust spores, or whether such genes are shared with generalist saprophytic fungi or represent specialised adaptations to the hyperparasitic niche. Furthermore, the extent of host specificity and nutrient targeting within rust fungi remains largely unexplored.

In Chapter Two I investigated genes possibly involved in growth of *P. coffeae* ANU01 on *Pst* urediniospores. I found that it mobilised a gene set rich in BGCs, cell wall degrading enzymes, secreted lipases and nutrient transporters. I hypothesise that parasitism in *P. coffeae* ANU01 and in a broader context the majority of hyperparasites occurs in three major stages; recognition and antagonism, degradation of the cell wall and uptake and metabolism of nutrients. As per my hypothesis, after recognition of the rust host, *P. coffeae* ANU01 antagonises *Pst* through the action of SMs to disable germination and possible defence responses. It then uses cell wall degrading enzymes to break through the polysaccharide-rich urediniospore coat, and deploys a wealth of secreted catabolic proteins and nutrient transporters to exploit the abundant nutrients within urediniospores. Here, I went beyond *P.*

coffeae ANU01 to better understand the genes behind parasitism and potentially confirm my hypothesis on the major components of rust parasitism.

In this chapter, I describe the discovery, identification, and genetic investigation of nine novel rust hyperparasites. I isolated a diverse group of ascomycete fungi that appeared to act as hyperparasites of different rust species and confirmed their ability to grow on *Pst* urediniospores. I assembled reference genomes for each hyperparasite and used comparative transcriptomics and context from the *P. coffeae* ANU01 growth pattern to identify shared and unique genetic features associated with growth on *Pst*. The primary focus of my PhD is the genomics underlying fungal hyperparasitism of wheat stripe rust. Therefore, even though I aimed to isolate candidates from a diversity of rust species, I investigated their transcriptomes during growth on *Pst*. I hoped that by investigating hyperparasites of *Pst* and other rust species, I would discover differences that may address the severe lack of information regarding host range and specificity.

5.2 Materials and methods

Fungal strains and media

An isolate of the wheat stripe rust pathogen *Puccinia striiformis* f. sp. *tritici* (*Pst*) 104 E137 A- (Schwessinger *et al.*, 2018) was used for all aspects of this research and maintained as dried stocks at -80 °C. All candidate hyperparasite fungi were maintained on PDA (potato dextrose broth 25 g/l and agar 15 g/l) plates at 22 °C with 12 hour day night cycles in a temperature-controlled room and as 25% glycerol stocks. Candidate spore suspensions were made by flooding mature colonies with 10 mL of sterile Milli-Q water and scraping the colony surface with a sterile blade to suspend spores in the water. Glycerol stocks were generated by mixing 500 µL of a 50% glycerol solution (v/v) and 500 µL of the spore suspensions and storing at -80 °C.

Isolating new hyperparasite candidates

Rust-infected leaves were collected from plants across the Australian National University (ANU) campus and placed into clear plastic bags. To maintain the high humidity required for hyperparasite development, the interior surfaces of the bags were misted with sterile Milli-Q water prior to sealing. The bags were then incubated at 22 °C in a temperature-controlled room under 12 hour day night cycles. As pale fluffy fungal growth emerged from pustules on the leaf surfaces, the material was collected using a sterile scalpel and transferred onto PDA plates, which were subsequently incubated at 22 °C. When mixed cultures were observed, individual colonies were selected based on morphological differences and subcultured onto fresh PDA plates to obtain pure isolates. Once axenic cultures were established, each isolate was assigned a unique identifier and preserved in long-term storage as 25% glycerol stocks, prepared as described above. The ability of each fungal isolate to grow on *Pst*

urediniospores was tested using the same *in vitro* method on glass microscope slides described in Chapter Two.

Internal transcribed spacer (ITS) phylogenies

Genomic DNA was isolated from spore and mycelial tissue of each isolate growing on PDA plates using the DNeasy Plant Mini Kit (QIAGEN). The fungal ITS region was amplified from fungal DNA using the primers ITS1F (5' CTTGGTCATTTAGAGGAAGTAA 3') and LR6 (5' CGCCAGTTCTGCTTACC 3'). Amplicons were sequenced using Sanger technology and the resulting data imported into Geneious Prime (Dotmatics). A preliminary BLAST search (blastn) was performed to identify candidates to the genus level. ITS sequences for all available isolates within the identified genera were imported manually from the National Center for Biotechnology Information (NCBI) nucleotide database to Geneious Prime. Alignments were generated using each candidates ITS sequence against all sequences in its respective genera using the default 'Geneious alignment' algorithm. From these alignments, individual phylogenetic trees for each represented genus were built using the Tamura-Nei Neighbor-Joining method, with trees built using the bootstrap resampling method and 100 replicates.

Long read DNA isolation

Spore suspensions were made by flooding mature (~6.5 cm diameter) fungal colonies with 10 mL sterile MQ water and were used to inoculate 100 mL Potato Dextrose Broth (PDB) in conical flasks. Fungal mycelium was grown for 3-4 days at 22°C with shaking at 140 rpm. Mycelium was isolated from liquid culture by centrifuging samples at 5,000 g for 5 minutes, resuspending the fungal pellet in 30 mL sterile Milli-Q water then centrifuging again, removing the supernatant and flash freezing the pellet until use. Due to the challenging nature of isolating DNA from filamentous fungi, three methods of DNA isolation were used across the candidates. Tissue was disrupted for all samples by combining ~750 mg of fungal tissue with 1-2 g of acid-washed sand in individual mortars sitting in liquid nitrogen and grinding until tissue became a fine powder. For *Sarocladium terricola* SRSh, high molecular weight DNA was isolated following a CTAB-lysis protocol (Jones & Schwessinger 2021). DNA was isolated from *Penicillium brevicompactum* FRF and *Penicillium copticola* SRB by following the optimised "SDS method 4" developed by Xia *et al.* (2019). Finally, DNA was isolated from the remaining six candidates following a high molecular weight extraction method developed by McDonald & Schwessinger (2017). The DNA was quantified using a Qubit Fluorometer (Thermo Fisher Scientific) and purity was assessed on a Quickdrop spectrophotometer (SpectraMax). Crude DNA samples were taken to the BRF, JCSMR (Biomolecular Resource Facility, John Curtin School of Medical Research) for purification and size selection (10 kbp+) on a BluePippin system (Sage Science). Native barcodes were added to samples by BRF staff using the SQK-NBD114-24 Ligation sequencing kit and samples were loaded onto a FLO-

PRO114M flow cell and sequenced on an Oxford Nanopore Technology Promethion sequencing device. Reads were base called using the Dorado basecalling software (ONT).

RNA isolation and sequencing from *in vitro* and *in situ* samples

For *in vitro* samples, total RNA was isolated from mature fungal colonies grown on the surface of PDA plates. For each biological replicate, a single colony was grown on an individual PDA plate. Three plates (i.e., three biological replicates) were incubated in a temperature-controlled room at 22°C under a 12-h light/dark cycle for fourteen days. Mycelial and spore tissue was scraped from the surface of plates and transferred to 2 mL tubes containing two steel ball bearings, then immediately frozen in liquid nitrogen. Tissue was disrupted with eight rounds of shaking for 30 s at 50 Hz on a Tissuelyser II (QIAGEN) and total RNA was isolated using the RNeasy Plant Mini Kit (Qiagen). RNA was eluted in 46 µL of RNase-free water and concentration and purity ratios were assessed using a Quickdrop Spectrophotometer (SpectraMax). RNA integrity was assessed using a Tapestation 4200 (Agilent), and samples were submitted to the BRF at JCSMR, ANU for library preparation and Illumina paired-end sequencing.

For *in situ* samples, total RNA was isolated from fungal tissue growing on the surface of *Pst* urediniospores in 2 mL Eppendorf tubes. Approximately 15 mg of frozen *Pst* urediniospores were heat shocked at 42 °C for three minutes and then suspended in 2 mL Novec™ solution (3M). The spores were then dispensed in 15 µL aliquots into the bottom of 2 mL centrifuge tubes and allowed to dry. After the Novec evaporated, 5 µL of hyperparasite spore suspension (prepared as described above then filtered through sterile Miracloth (Millipore) and diluted to 1:100) was added and again allowed to dry. Tubes were then placed upright and open in racks and racks were enclosed in sterile plastic bags alongside a sterile tissue paper moistened with 10 mL of sterile Milli-Q water to maintain humidity. Samples were incubated at 22°C and 16-hour day/night cycles for five days. Each biological replicate consisted of four tubes; tissue within each tube was snap frozen, ground individually using the Tissuelyser II (Qiagen) and then combined at the chemical lysis step. Total RNA was isolated using the RNeasy Plant Mini Kit (Qiagen). RNA was eluted in 46 µL of RNase-free water, and concentration and purity ratios were assessed using a Quickdrop Spectrophotometer (SpectraMax). RNA integrity was assessed using a Tapestation 4200 (Agilent), and samples were submitted to the BRF at JCSMR, ANU for library preparation and Illumina paired-end sequencing.

Genome assembly

Read length and quality were assessed using Nanoplot (De Coster *et al.*, 2018). Reads longer than 10 kbp were retained using Filtlong (Wick 2025) and then built into assemblies using Flye (Kolmogorov *et al.*, 2019). Preliminary assemblies were originally polished with two rounds of Racon (v0.5.2) (Vaser *et al.*, 2017) and one round of Medaka (v1.2.1) (Oxford Nanopore Technologies), however polishing

steps were ultimately rejected after they were found to decrease genome completeness. Basic assembly statistics were generated using the Quast software (Gurevich *et al.,* 2013) and manual curation was used to remove repeat and artifact contigs (<100 kbp but not circular). Contiguity was evaluated by identifying telomeric repeat regions at contig ends using the FindTelomeres script (Sperschneider 2020). Completeness of the final unpolished assemblies was assessed using a BUSCO analysis and the Ascomycota dataset (Simão *et al.*, 2015).

Genome annotation using a bioinformatics pipeline

Raw Illumina RNA-seq reads (see RNA isolation section above) were trimmed to remove adapters using fastp (v1.3.4) (Chen *et al.,* 2018). Genomes were functionally annotated using the Funannotate (v1.8.1) pipeline (Palmer & Stajich 2020), incorporating all six corresponding RNA-seq datasets as additional evidence. The pipeline was run using the 'predict', 'update', and 'annotate' steps to generate protein-coding predictions and integrate additional functional information. Protein sequences generated by Funannotate 'update' (protein.fasta) were used as input for InterProScan (v5.0) (Jones *et al.,* 2014), Phobius (Käll *et al.,* 2004) and SignalP (v5.0) (Almagro *et al.,* 2019) to predict protein domains, transmembrane regions and secretion signal peptides respectively. GenBank files (.gbk) produced by Funannotate 'update' were mined for biosynthetic gene clusters using antiSMASH (v6.0) (Blin *et al.,* 2021). The outputs from these additional annotation tools were integrated into Funannotate for the final 'annotate' step. Transcriptomes generated through Funannotate annotation were used for all downstream analyses.

Comparative transcriptomics analysis

For the comparative transcriptomics analysis, contaminant *Pst* reads were removed from *in situ* read sets by aligning reads to the *Pst* 104E137 A- genome (PRJNA1195871) using hisat2 (Kim *et al.,* 2019). Reads from all data sets were then quantified by alignment to their respective hyperparasite transcriptomes using Salmon (v1.4.0) (Patro *et al.,* 2017). Salmon output files were imported into RStudio and differential gene expression analyses were conducted using the Limma package (Ritchie *et al.,* 2015). Volcano plots for each isolate were generated with the Enhanced volcano package (Blighe *et al.,* 2020) and gene ontology enrichments were determined using topGO (v2.52.0) (Alexa & Rahnenführer 2009). All code used for this analysis is presented in the associated github page for this project: https://github.com/Jack-WessANU.

5.3 Results and Discussion

Isolating and identifying new hyperparasite candidates

I isolated all fungal samples described in this report from rust-infected plant tissue collected within the ACT region. I incubated rust-infected tissue at 100% humidity and collected fluffy tissue as it appeared, before purifying samples into individual fungal isolates. In all cases, the putative hyperparasitic fluffy tissue was pale and soft and stood in stark contrast to the orange/brown rust urediniospores. In total, I obtained 40 distinct fungal isolates. From these, I selected nine candidates for genomic and transcriptomic analysis. Apart from stripe rust (*Puccinia striiformis* f. sp. *tritici*) and stem rust (*Puccinia graminis* f. sp. *tritici*), I did not formally identify the specific rust species present, however predicted the species based on the host plant. Thus, I predict that the fungus I isolated from pustules on flax plants (*Linum usitatissimum*) was growing on flax rust (*Melampsora lini*) and the fungi I isolated from pustules on poplar trees (*Populus spp.*) were growing on the most common poplar rust species (*Melampsora larici-populina*). I selected candidates based on diversity in their colony morphology, making sure to select candidates from a variety of host rusts, especially those with agricultural or ecological importance. Below, I provide brief descriptions of the nine candidates, along with their taxonomic identifications based on ITS barcode sequencing.

I grew pure spores from each candidate hyperparasite on ungerminated *Pst* urediniospores on glass microscope slides under 100% relative humidity. I observed candidate hyperparasite spores germinate and grow hyphae that began to cover *Pst* urediniospores in thick webbed mycelial masses in all cases. After seven days all candidate hyperparasites had produced fruiting bodies, indicating that all were capable of completing their lifecycles with *Pst* urediniospores as the sole source of nutrients. In all *Pst*-absent control slides I observed candidate spores germinate and produce short hyphae before they stopped growing, indicating the candidates were reliant on the *Pst* spores for growth. Stripe Rust Sinister (SRSi), a candidate I isolated from *Pst* infected wheat, was the sole candidate to produce a unique phenotype. I observed *Epicoccum italicum* SRSi (see identification section below) hyphae seemingly penetrate and lyse *Pst* urediniospores (Supplementary Figure 5.1). The large ovate *Pst* spores were left wrinkled and punctured after incubation with the fungus. *Epicoccum italicum* SRSi was the only candidate for which I observed this phenotype.

I identified all of the candidate hyperparasitic fungi to species level using an internal transcribed spacer region (ITS) barcoding approach. The ITS region is a highly variable section of the fungal genome that is commonly used as a molecular barcode for species identification (Schoch *et al.*, 2012). Prior to formal identification, I gave each of the candidate hyperparasites an informal placeholder name based on the predicted rust species it was identified from and an inspiration I took from their colony morphology. Table 5.1 presents placeholder names, predicted host species (the rust species from which I isolated

each candidate), and the predicted genus of each candidate based on a preliminary BLAST analysis of their ITS regions.

Table 5.1. Placeholder names, predicted genus and predicted host species for nine novel rust hyperparasite candidates

Placeholder name	Predicted genus	Predicted host species
Flax Rust Faroes (FRF)	*Penicillium*	Flax rust (*Melampsora lini*)
Poplar Blue (PBLUE)	*Cladosporium*	Poplar rust (*Melampsora larici-populina*)
Poplar Brown (PBROWN)	*Alternaria*	Poplar rust (*Melampsora larici-populina*)
Poplar Mud (PMUD)	*Alternaria*	Poplar rust (*Melampsora larici-populina*)
Poplar Cherry Blossom (PCB)	*Trichothecium*	Poplar rust (*Melampsora larici-populina*)
Stem Rust Bullseye (SRB)	*Penicillium*	Wheat stem rust (*Puccinia graminis* f. sp. *tritici*)
Stripe Rust Meat (SRM)	*Fusarium*	Wheat stripe rust (*Puccinia striiformis* f. sp. *tritici*)
Stripe Rust Sherbet (SRSh)	*Sarocladium*	Wheat stripe rust (*Puccinia striiformis* f. sp. *tritici*)
Stripe Rust Sinister (SRSi)	*Epicoccum*	Wheat stripe rust (*Puccinia striiformis* f. sp. *tritici*)

Identification of all nine candidates to species level using an ITS barcoding approach and species from genera unrelated to the candidate's predicted genus as outgroups

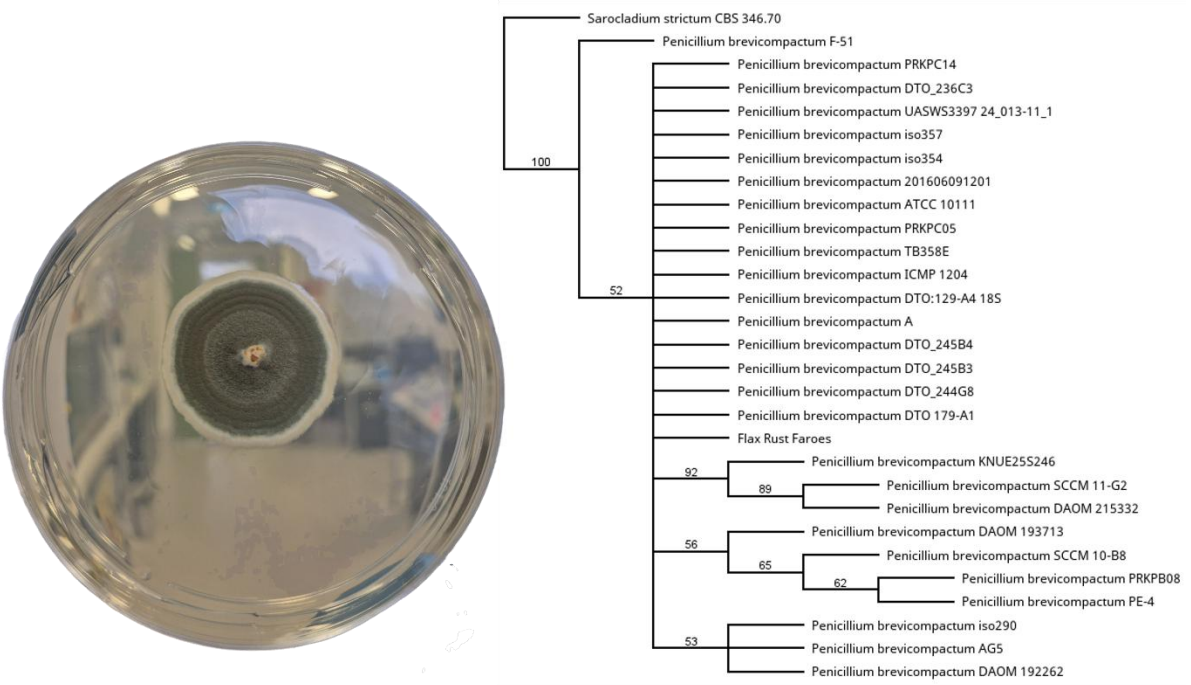

Figure 5.1. Morphology and phylogenetic placement of Flax Rust Faroes (FRF). Left: Single mature colony morphology of Flax Rust Faroes grown on PDA for 14 days at 22°C on a 12 hour day/night

cycle. Right: A rooted phylogenetic tree built from Geneious superalignments of *P. brevicompactum* ITS sequences downloaded from NCBI and the Flax Rust Faroes ITS amplicon generated here. The tree was constructed using the Tamura-Nei Neighbor-Joining method in Geneious, with *Sarocladium strictum* as an outgroup. Numbers on nodes represent confidence in bootstrapping statistical analysis.

I isolated "Flax Rust Faroes" from flax rust (predicted) infected flax leaves in a growth chamber at the CEF at ANU. Colonies were blue-green and irregular with aerial grey spores arranged in alternating rings of dark greenish-grey and paler grey (Figure 5.1, Left). The colony surface was velvety and showed heavy sporulation. The underside of colonies was a pale blue. I conducted a preliminary blast of the Flax Rust Faroes ITS region which suggested the hyperparasite belonged to the genus *Penicillium*. An initial tree built using ITS sequences from Flax Rust Faroes and type material for all available species of *Penicillium* placed Flax Rust Faroes on a branch alongside *P. brevicompactum*. I constructed a second tree including Flax Rust Faroes and 27 isolates of *P. brevicompactum*, which placed the candidate amongst the isolates (Figure 5.1, Right), suggesting it is a novel isolate of the species. For the remainder of this report, I will refer to Flax Rust Faroes as *P. brevicompactum* FRF. An isolate of *P. brevicompactum* has previously been observed supressing the germination of *P. coronata* var *avenae* (oat crown rust) urediniospores without colonising rust pustules, suggesting it produces antifungal secondary metabolites (Wilson *et al.*, 2020). This is the first observation of *P. brevicompactum* specifically growing on flax and stripe rust spores.

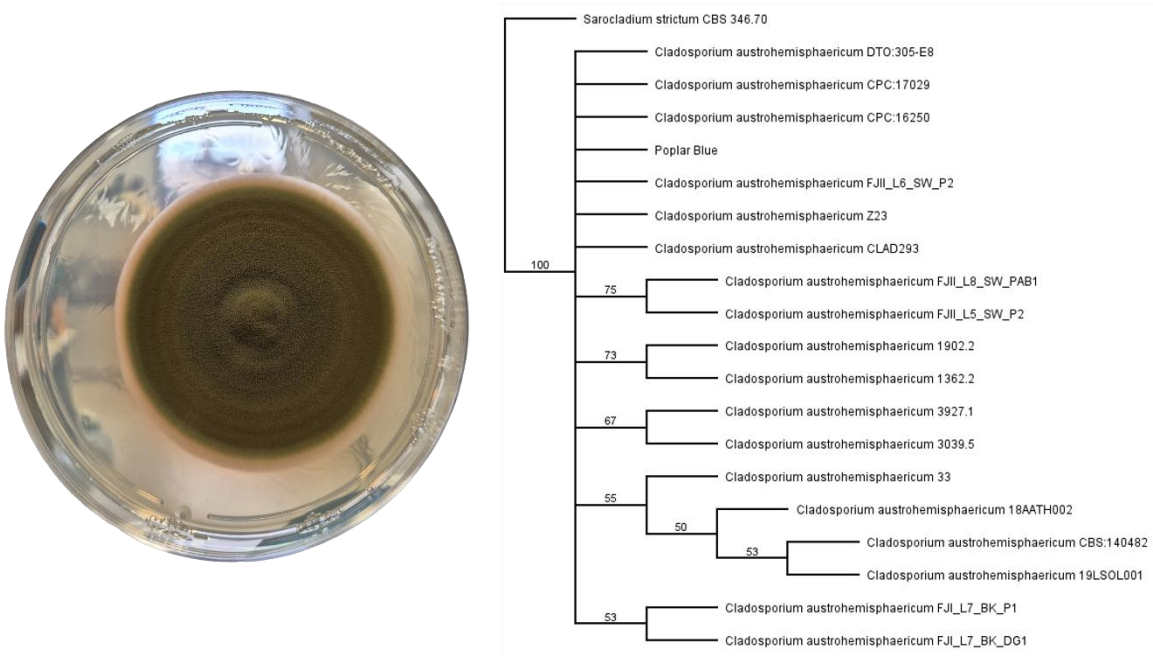

Figure 5.2. Morphology and phylogenetic placement of Poplar Blue (PBLUE). Left: Single mature colony morphology of Poplar Blue grown on PDA for 14 days at 22°C on a 12 hour day night cycle.

Right: A rooted phylogenetic tree built from Geneious superalignments of *C. austrohemisphaericum* ITS sequences downloaded from NCBI and the Poplar Blue ITS amplicon generated here. The tree was constructed using the Tamura-Nei Neighbor-Joining method in Geneious, with *Sarocladium* strictum as an outgroup. Numbers on nodes represent confidence in bootstrapping statistical analysis.

I isolated "Poplar Blue" from a poplar rust (predicted) infected leaf on a poplar tree growing along the bank of Sullivans Creek on the ANU campus. Colonies were slow growing, powdery, flat and dark blue-green on PDA, with blue aerial spores (Figure 5.2, Left). Colony margins were smooth and tinted deep red on the underside. There appeared to be a slight diffusion of red pigment into the media immediately surrounding the margin and underneath the colony. An initial BLAST of the Poplar Blue ITS sequence suggested the fungus belonged to the genus *Cladosporium*. A first phylogenetic tree constructed using ITS sequences from all available *Cladosporium* species placed Poplar Blue on a branch alongside *C. austrohemisphaericum*. I constructed a second tree using ITS sequences from Poplar Blue and all available isolates of the species, which placed Poplar Blue firmly amongst them (Figure 5.2, Right). For the remainder of this report, I refer to Poplar Blue as *C. austrohemisphaericum* PBLUE. The first description of *C. austrohemisphaericum* was as a black mould on the fruit of *L. patersonia* in New Zealand (Bensch *et al.*, 2015). While an isolate of *C. cladosporoides* has been observed acting as a hyperparasite of *Pst* (Zhang *et al.*, 2022), this is the first observation of *C. austrohemisphaericum* growing on rust spores.

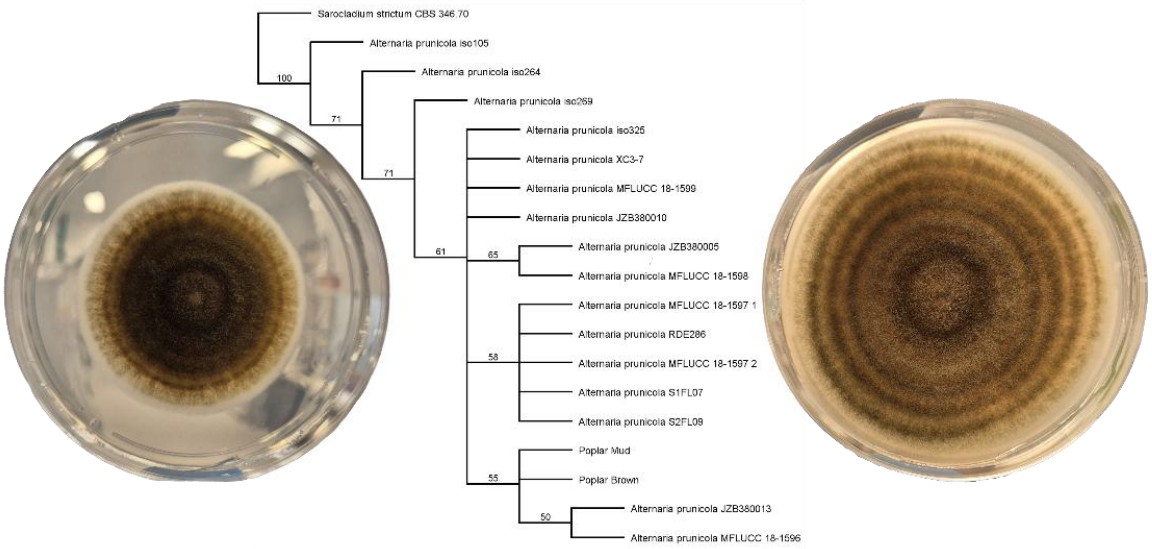

Figure 5.3. Morphology and phylogenetic placement of Poplar Brown (PBROWN) and Poplar Mud (PMUD). Left: Single mature colony morphology of *A. prunicola* PBROWN grown on PDA for 14 days at 22°C on a 12h day night cycle. Middle: A rooted phylogenetic tree built from Geneious superalignments of *A. prunicola* isolates ITS sequences downloaded from NCBI and the Poplar Brown and Poplar Mud ITS amplicon generated here. The tree was constructed using the Tamura-Nei Neighbor-Joining method in Geneious, with *Sarocladium* strictum as an outgroup. Numbers on nodes

represent confidence in bootstrapping statistical analysis. Right: Single mature colony morphology of *A. prunicola* PMUD grown on PDA for 14 days at 22 °C on a 12h day night cycle.

I isolated "Poplar Brown" from a rust infected leaf on a Poplar tree growing along the bank of Sullivans Creek on the ANU campus. Colonies were dark brown in the centre, and light brown or tan in younger regions. Colonies were flat and powdery with dense aerial spores (Figure 5.3, Left). Margins were white and regular and colony undersides were a dark tan/brown with no diffusion of pigment into the media. I isolated "Poplar Mud" from a rust infected leaf on a Poplar tree growing in an open space surrounding a fire pit again on the ANU campus, approximately 150 metres from the site I collected Poplar Brown. Poplar Mud produced flat circular colonies with alternating rings of olive-brown, tan and darker brown pigmentation radiating from the centre outward (Figure 5.3, Right). The surface texture was powdery and hairy, with dense aerial spores. Colony margins were round, well defined and lighter in colour, indicating less sporulation than more central parts of the colony. The underside of colonies were a dark brown and there was no pigment diffusion into the agar. Though colonies looked significantly different to the naked eye and were isolated from different places, my identification analysis suggested that Poplar Mud and Poplar Brown were different isolates of the same species. Firstly, ITS sequences for the two candidates showed 100% pairwise identity. A preliminary blast of said ITS sequences suggested they were from a species of *Alternaria*. I first constructed a phylogenetic tree using the ITS sequences from Poplar Brown, Poplar Mud and all available species of *Alternaria*, which placed Poplar Brown and Poplar Mud together besides *A. prunicola*. A second ITS tree including Poplar Brown, Poplar Mud and all isolates of *A. prunicola*, placed the two firmly amongst the isolates (Figure 5.3, Middle), indicating they are both isolates of *A. prunicola*. To further investigate the similarity between the two candidates, I conducted a genome-to-genome (see genome assembly section below) alignment and dotplot, presented in the Supplementary Material (Supplementary Figure 5.2). The continuous diagonal line in the plot indicated that the genomes are almost entirely syntenous with one another, suggesting they are in fact the same species. For the remainder of this report, I refer to the candidates as *A. prunicola* PBROWN and *A. prunicola* PMUD. *Alternaria prunicola* is the primary cause of sweet cherry leaf spot diseases in China (Şimşek *et al.,* 2022) and has been detected as a potential pathogen in grapevine and mandarin samples (Baramidze *et al.,* 2025). Though an isolate of *Alternaria alternata* has been observed acting as a hyperparasite of *Pst* (Zheng *et al.,* 2017), this is the first recorded incident of *A. prunicola* growing on rust spores.

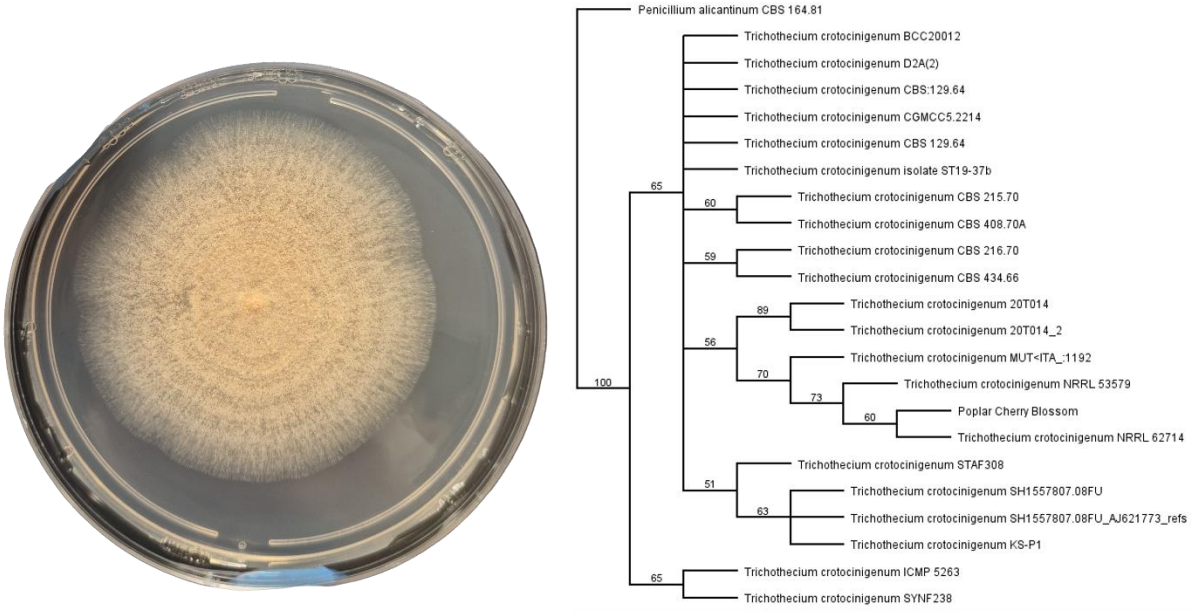

Figure 5.4. Morphology and phylogenetic placement of Poplar Cherry Blossom (PCB). Left: Single mature colony morphology of Poplar Cherry Blossom grown on PDA for 14 days at 22 °C on a 12h day night cycle. Right: A rooted phylogenetic tree built from Geneious superalignments of *T. crotocingenum* ITS sequences downloaded from NCBI and the Poplar Cherry Blossom ITS amplicon generated here. The tree was constructed using the Tamura-Nei Neighbor-Joining method in Geneious, with *Penicillium alicantinum* as an outgroup. Numbers on nodes represent confidence in bootstrapping statistical analysis.

I isolated "Poplar Cherry Blossom" from a rust infected leaf on a poplar tree growing along the road outside the JCSMR on the ANU campus. Colonies were light pink, flat and semi-irregular with slightly raised rings extending from the centre towards the margin (Figure 5.4, left). Surfaces of colonies were powdery with dense aerial spores. Colony margins were a lighter pink and filamentous, with no pigment diffusion into the surrounding agar and colony undersides were a pale pink. A preliminary BLAST using the Poplar Cherry Blossom ITS sequence suggested the fungus belonged to the genus *Trichothecium*. A preliminary phylogeny I built using ITS sequences from Poplar Cherry Blossom and all available species of *Trichothecium* placed Poplar Cherry Blossom next to *T. crotocingenum*. I constructed a second phylogeny using the ITS of Poplar Cherry Blossom and all available isolates of *T. crotocingenum*, which placed the candidate amongst the isolates (Figure 5.4, Right) suggesting it is an isolate of the species. For the remainder of this report, I will refer to Poplar Cherry Blossom as *T. crotocingenum* PCB. An isolate of *T. crotocingenum* which acts as a potato endophyte produces antifungal SMs against several potato pathogenic fungi (Yang *et al.*, 2018). *Trichothecium crotocingenum* CBS 129.64 acts as a parasite of cordyceps fungi, growing on mycelia and fruiting bodies of the fungus (Liu and Dong 2020). However, this is the first observation of *T. crotocingenum* growing on rust spores.

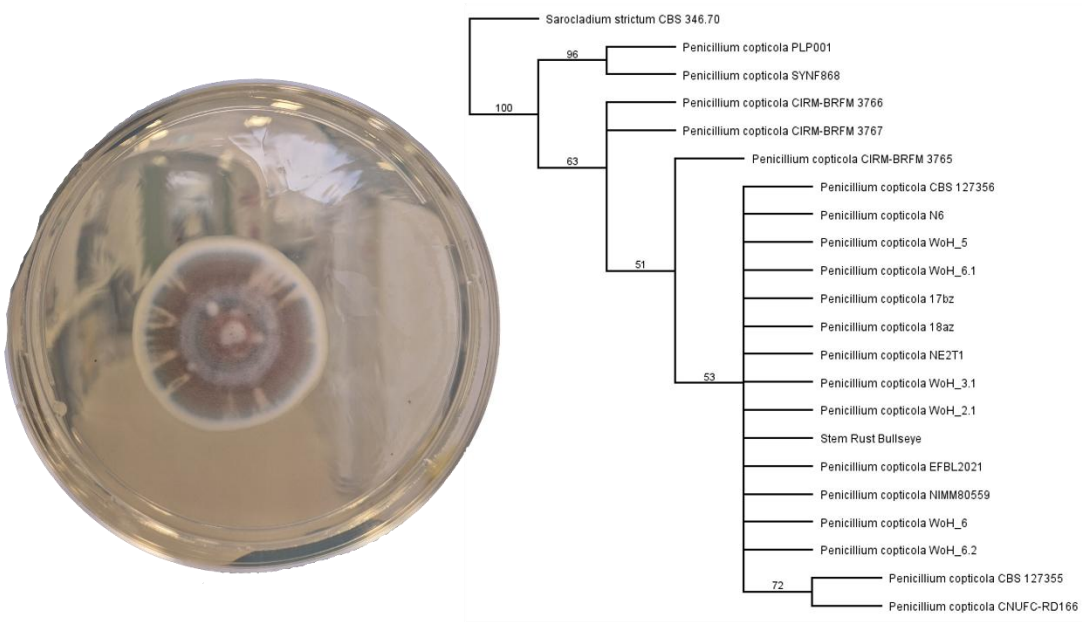

Figure 5.5. Morphology and phylogenetic placement of Stem Rust Bullseye. Left: Single mature colony morphology of Stem Rust Bullseye grown on PDA for 14 days at 22°C on a 12h day night cycle. Right: A rooted phylogenetic tree built from Geneious superalignments of *P. copticola ITS* sequences downloaded from NCBI and the Stem Rust Bullseye ITS amplicon generated here. The tree was constructed using the Tamura-Nei Neighbor-Joining method in Geneious, with *Sarocladium* strictum as an outgroup. Numbers on nodes represent confidence in bootstrapping statistical analysis.

I isolated "Stem Rust Bullseye" from stem rust (*Puccinia graminis triticina*) infected wheat (*Triticum aestivum*) cv. Rangcoo in a growth chamber at the Controlled Environment Facility (CEF) at ANU. Stem Rust Bullseye produced raised circular colonies with alternating streaks of red, blue and white pigmentation, extending from the centre towards the margin. Colony surfaces were velvety/powdery with dense aerial spores (Figure 5.5, Left). Colony margins were even and well defined, with narrow whitish edges and no pigment diffusion into the surrounding media. Colony undersides were a pale red. A preliminary BLAST of the Stem Rust Bullseye ITS region suggested it was a *Penicillium*. I constructed a preliminary tree using the Stem Rust Bullseye ITS and all available ITS sequences from type material for all *Penicillium* species. This tree placed Stem Rust Bullseye on a branch alongside *Penicillium copticola*. A second tree constructed using ITS sequences from Stem Rust Bullseye and all available isolates of *P. copticola* placed the candidate amongst the isolates (Figure 5.5, Right). For the remainder of this report Stem Rust Bullseye will be referred to as *P. copticola* SRB. An isolate of *Penicillium copticola* exhibited inhibitory activity against the fungus *Mucorhiemalis* (Bu *et al.,* 2015), and in cannabis (*Cannabis sativa*) an endophytic isolate was observed dominating the associated microbiome (Kusari *et al.,* 2013). This is the first report of an isolate of *P. copticola* growing on rust spores.

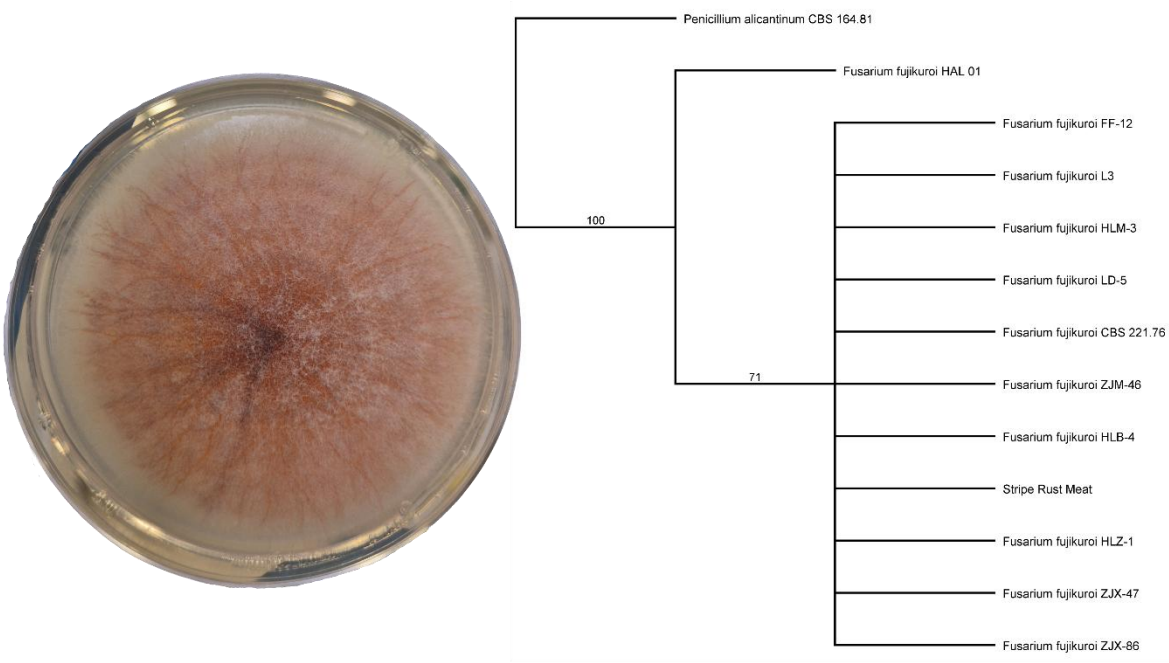

Figure 5.6. Morphology and phylogenetic placement of Stripe Rust Meat. Left: Single mature colony morphology of Stripe Rust Meat grown on PDA for 14 days at 22 °C on 12h day night cycle. Right: A rooted phylogenetic tree built from Geneious superalignments of *F. fujikuroi* ITS sequences downloaded from NCBI and the Stripe Rust Meat ITS amplicon generated here. The tree was constructed using the Tamura-Nei Neighbor-Joining method in Geneious, with *Penicillium alicantinum* as an outgroup. Numbers on nodes represent confidence in bootstrapping statistical analysis.

I isolated "Stripe Rust Meat" from *Pst* infected wheat cv. Morocco in a growth chamber at the CEF at ANU. It produced fluffy, pink-red, filamentous colonies on PDA, with pink-white spores (Figure 5.6, Left). Colony margins were filamentous and the underside of colonies are pink with deep red veins spread throughout. An initial blast of the Stripe Rust Meat ITS region suggested the fungus was a *Fusarium*. A tree built from an alignment of Stripe Rust Meat and all available *Fusarium* species ITS regions, placed Stripe Rust Meat on a branch alongside *F. fujikuroi*. I built a second tree using the Stripe Rust Meat ITS sequence and all available ITS sequences for isolates of *F. fujikuroi*, which placed Stripe Rust Meat amongst the isolates (Figure 5.6, Right), suggesting it is a novel isolate of the species. For the remainder of this report the isolate will be referred to as *F. fujikuroi* SRM. *Fusarium fujikuroi* is the causative agent of bakanae disease in rice (Cen *et al.*, 2020), and is a rich source of antibiotic pigments such as Bikaverun (Wiemann *et al.*, 2009). This is the first observation of an isolate of *F. fujikuroi* growing on rust fungi.

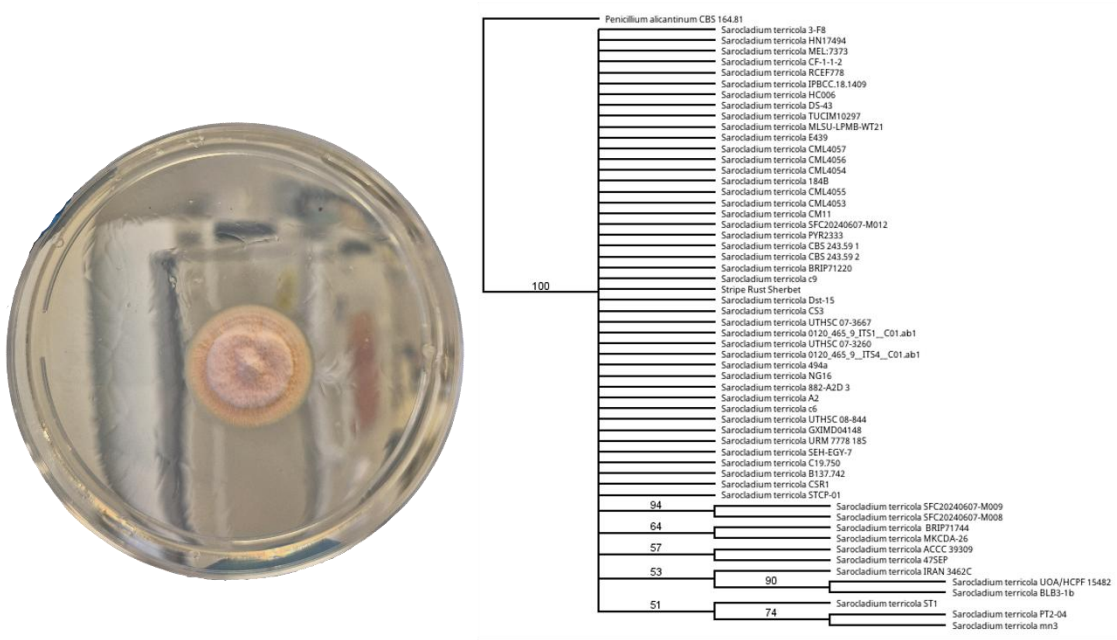

Figure 5.7. Morphology and phylogenetic placement of Stripe Rust Sherbet. Left: Single mature colony morphology of Stripe Rust Sherbet grown on PDA for 14 days at 22 °C on a 12h day night cycle. Right: A rooted phylogenetic tree built from Geneious superalignments of *S. terricola* ITS sequences downloaded from NCBI and the Stripe Rust Sherbet ITS amplicon generated here. The tree was constructed using the Tamura-Nei Neighbor-Joining method in Geneious, with *Penicillium alicantinum* as an outgroup. Numbers on nodes represent confidence in bootstrapping statistical analysis.

I isolated "Stripe Rust Sherbet" from *Pst* infected wheat cv. Morocco growing in a growth chamber at the CEF at ANU. Stripe Rust Sherbet produced vibrant pink, raised and circular colonies. Colony surfaces were velvety and dense with pink aerial spores (Figure 5.7, Left). Colony margins were noticeably flatter than regions immediately surrounding the colony centre and presented pink rings that grew to be raised after maturation. Colonies produced large hairs sprouting from the colony centre at maturation and colony undersides were pink with no pigment diffusion into the surrounding agar. An initial BLAST of the Stripe Rust Sherbet ITS sequence suggested the fungus was a *Sarocladium*, and an initial phylogeny placed it most closely to *Sarocladium terricola*. I built a second tree from the ITS sequence of Stripe Rust Sherbet and all available isolates of *S. terricola*, which suggested it is an isolate of the species (Figure 5.7, Right). For the remainder of this report, the candidate will be referred to as *S. terricola* SRSh. Isolates of *S. terricola* have been reported as capable of bioremediation in petrochemical-contaminated soils (Ge *et al.*, 2024), and been identified as capable of biocontrol of the southern root-nematode (*Meloidogyne incognita*) (Tian *et al.*, 2022). This is the first observation of *S. terricola* growing in association with rust fungi.

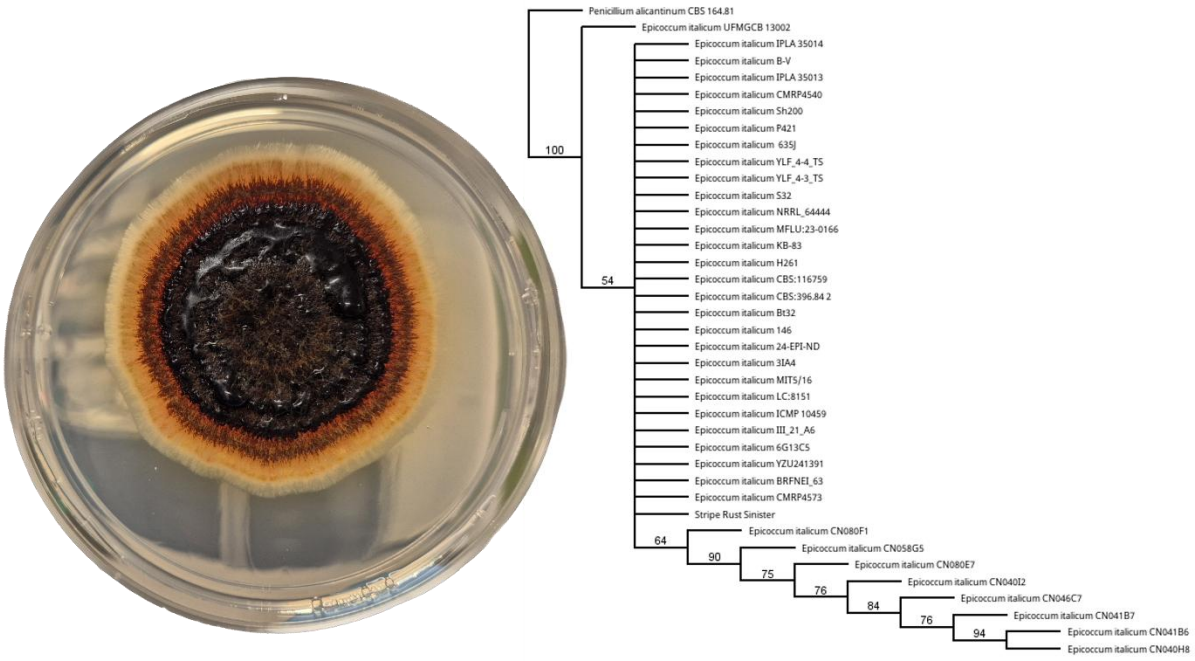

Figure 5.8. Morphology and phylogenetic placement of Stripe Rust Sinister. Left: Single mature colony morphology of Stripe Rust Sinister grown on PDA for 14 days at 22 °C on a 12h day night cycle. Right: A rooted phylogenetic tree built from Geneious superalignments of *S. terricola* ITS sequences downloaded from NCBI and the Stripe Rust Sinister ITS amplicon generated here. The tree was constructed using the Tamura-Nei Neighbor-Joining method in Geneious, with *Penicillium alicantinum* as an outgroup. Numbers on nodes represent confidence in bootstrapping statistical analysis.

I isolated "Stripe Rust Sinister" from *Pst* infected wheat cv. Morocco in a growth chamber at the CEF at ANU. Stripe Rust Sinister produced colonies that were a deep red/black when mature (Figure 5.8, Left). Colonies showed rings that extended from the colony centre outwards and darkened as they matured. The surface of mature regions of colonies were covered in a thick dark black exudate and hairs. Younger regions were a lighter orange and colour was almost white in the filamentous margins. Underside of colonies were black and there was no pigment diffusion into the media. A preliminary blast of the Stripe Rust Sinister ITS sequence suggested it was an *Epicoccum*. I constructed a preliminary first tree using ITS sequences from Stripe Rust Sinister and all available *Epicoccum* species, which placed the candidate close to *E. italicum*. I then constructed a second tree using the ITS sequence from Stripe Rust Sinister and all available isolates of *E. italicum*, which put Stripe Rust Sinister firmly amongst the isolates (Figure 5.8, Right). My analysis suggests Stripe Rust Sinister is a novel isolate of *E. italicum*, for the remainder of this report it will be referred to as *E. italicum* SRSi. *Epicoccum italicum* has most commonly been isolated as a plant pathogen, causing leaf spots on *Eugenia uniflora* fruit frees in Brazil (Falk De Avila *et al.,* 2025), postharvest rot in pear fruit in Italy (Cortiello *et al.,* 2026) and seed disease in soybeans in the US (George *et al.,* 2025). However, the *E. italicum* isolate HE20 is

capable of reducing the severity of *Pst* in wheat, potentially through triggering an upregulation in wheat genes related to the production of polyphenols (Rashad *et al.,* 2025). *Epicoccum italicum* SRSi was the only candidate in my experiments that belonged to a species which had been previously reported to grow in association with or control *Pst*.

I uncovered a small snapshot of the diversity in fungi potentially acting as hyperparasites of rust species around the ANU. Prior to identification, selecting candidates for downstream analysis was somewhat arbitrary as I simply aimed for diversity in the genera and species I would investigate. I isolated a highly diverse group of fungi spanning seven genera. The majority of isolates had not been observed growing on rust spores. *Epicoccum italicum* was the sole species to previously be observed interacting with *Pst*, controlling severity of the disease, potentially through inducing defence responses in wheat, rather than direct action (Rashad *et al.,* 2025). Other species of *Alternaria* and *Cladosporium* have been observed acting as *Pst* hyperparasites (Zhang *et al.,* 2022; Zheng *et al.,* 2017), but not the species that I identified in my analysis. I isolated *A. prunicola* PBROWN and *A. prunicola* PMUD from the same predicted host species, both growing on poplar rust infected leaves in locations approximately 350 metres apart. This suggests that a lineage of *A. prunicola* might be well specialised and may have colonised a small portion of Poplar trees across the ANU campus. Alternatively, *A. prunicola* is a common endophyte of poplar trees and simply makes use of *Pst* spores when they are present as an opportunistic hyperparasite. I hope that with further phenotyping, the identification of the species in this report will go towards addressing the critical lack of information regarding diversity of rust hyperparasites in the literature.

All candidates, regardless of the rust species I originally isolated them from, were capable of growing on *Pst* urediniospores. I did not notice observable differences in growth rate between candidates during growth on *Pst*. I would have preferred to use biomass qPCR, as I have previously (Chapter Two), to compare growth rate in candidates I isolated from *Pst*, to those I isolated from other predicted rust species. I expect that an increased growth rate in *E. italicum* SRSi, *S. terricola* SRSh and *F. fujikuroi* SRM, would suggest that those candidates are more adapted to grow on *Pst* spores specifically. I did observe what appeared to be mechanical lysis of urediniospores in *E. italicum* SRSi (Supplementary Figure 5.1), a unique trait it may have evolved from evolution alongside stripe rust. The ability of the majority of candidates to grow on *Pst* urediniospores suggests that for at least these candidates they are not limited to growth on one species of rust, a trait which is not investigated at all in literature.

However, my analysis did not confirm that the candidates are true rust hyperparasites. Screening the fungi for their ability to complete their lifecycle with *Pst* urediniospores as the sole source of nutrients reveals only that they can antagonise and consume *Pst* urediniospores. To confirm the isolates are true rust hyperparasites, Koch's postulates would need to be fulfilled, as was done with *P. coffeae* ANU01 (Chapter Two). However, this was beyond the scope of the present research. For this report I therefore refer to the fungi as putative or candidate hyperparasites and any conclusions I draw regarding their

interaction with rust fungi should not immediately be considered one of parasite and host without further phenotyping. As with the transcriptomic data (see below), candidates were all grown on *Pst* urediniospores in 2 mL Eppendorf tubes, separate from the host plant. Future experiments should focus on comprehensively phenotyping candidates *on planta* to best understand their veracity as true rust hyperparasites, and to ultimately contextualise their downstream genomic and transcriptomic traits.

Generation of highly complete genome assemblies

I generated high-quality reference genome assemblies for the nine candidate hyperparasites. Sequencing was performed on an Oxford Nanopore MinION device, yielding approximately 11 GB of data per candidate, corresponding to an average ~300× estimated coverage. I found that the most contiguous and complete assemblies resulted from using reads subset to ≥10 kbp in length and assembling them with Flye (Kolmogorov *et al.*, 2019), which produced an average genome coverage of 168.5. Although I initially polished assemblies with two rounds of Racon (Vaser *et al.*, 2017) followed by one round of Medaka (Oxford Nanopore Technologies), this approach consistently led to a loss of approximately 50% of telomeric sequences without improving genome completeness. As a result, I excluded polishing from the final assemblies. I manually inspected each assembly and removed redundant contigs. To minimise the risk of discarding accessory chromosomes, potentially important for opportunistic hyperparasitism, I only removed linear contigs shorter than 100 kbp, those flagged as repetitive by Flye and those with zero gene content. I removed a total of 42 contigs from the nine genomes. Final assemblies contained an average of 14.8 contigs. *Epicoccum italicum* SRSi possessed the highest number of contigs (26), while *P. brevicompactum* FRF possessed the fewest (8). The largest genome was that of *F. fujikuroi* SRM at 43.6 Mbp, whilst the smallest was *S. terricola* SRSh at 30.8 Mbp, the average genome size across candidates was 34.5 Mbp. I assessed completeness of the assembled genomes using a BUSCO analysis and the *Ascomycota* dataset (Simão *et al.*, 2015). My assemblies contained an average of 99.04% complete BUSCOs, indicating a high level of completeness. The *P. brevicompactum* FRF and *S. terricola* SRSh assemblies were the least complete (98.7%), while *E. italicum* SRSi was the most complete (99.5%). Despite their completeness, most assemblies lacked contiguity, with few contigs containing both forward and reverse telomeric repeats (Table 5.2). However, given my focus on identifying genes and pathways relevant to rust parasitism, I prioritised genome completeness over contiguity.

Table 5.2. Basic genome assembly statistics for nine rust hyperparasite candidate genomes.

Statistic	**FRF**	**PBLUE**	**PBROWN**	**PCB**	**PMUD**	**SRB**	**SRM**	**SRSh**	**SRSi**
Coverage	261 X	191 X	87 X	250 X	136 X	152 X	192 X	120 X	127 X
# Total contigs	8	24	12	12	15	11	14	11	26
# Circular contigs	1	1	1	1	1	1	1	1	1
Total length (bp)	30,942,442	34,859,616	33,723,775	32,388,692	33,540,653	35,384,811	43,672,825	30,813,703	34,781,166
Largest contig (bp)	6,826,810	2,809,821	6,774,811	4,641,645	3,956,572	6,392,638	6,101,707	4,517,545	3,890,046
N50	5,372,917	1,950,996	5,273,287	4,147,659	2,820,223	4,976,829	4,321,891	4,049,054	1,441,224
N90	3,253,929	1,249,514	2,449,930	2,090,193	1,831,271	3,382,824	2,484,796	1,810,490	1,077,252
GC content (%)	49.44	52.50	50.99	51.44	51.03	46.83	48.30	53.88	52.03
BUSCO completeness - *Ascomycota*	98.7%	98.9%	99.1%	99.1%	99.0%	99.4%	99.1%	98.7%	99.5%
# Complete BUSCOs	1,684	1,688	1,691	1,691	1,689	1,696	1,690	1,684	1,697
# Complete and single copy BUSCOs	1,679	1,683	1,689	1,689	1,688	1,690	1,680	1,682	1,694
# Complete and duplicated BUSCOs	5	5	2	2	1	6	10	2	3
# Fragmented BUSCOs	1	2	2	2	1	1	1	2	2
# Missing BUSCOs	21	16	13	13	16	9	15	20	7
# Telomeres									
Forward	4	8	5	4	6	4	10	7	5
Reverse	4	14	6	5	6	5	9	8	5

High quality functional annotation of the candidate hyperparasite genomes

I used the Funannotate pipeline and individual RNAseq datasets (see below) to generate highly complete and functionally rich *de novo* gene annotations for the nine candidate genomes. Basic statistics regarding the gene sets of each candidate are presented in Table 5.3. Funannotate predicted an average of 13,318 protein-coding genes, 14,112 mRNA transcripts, and 148 tRNA genes per genome. The average gene length was 1,886 bp, while exons averaged 599.7 bp in length. To assess the completeness of the annotated gene sets, I performed a BUSCO analysis using the *Ascomycota* dataset. The results showed that the gene sets contained an average of 99.06% conserved single-copy orthologs, indicating a high degree of annotation completeness (Table 5.4). Among the candidates, *E. italicum* SRSi showed the highest completeness (99.5%), while *P. brevicompactum* FRF and *S. terricola* SRSh had the lowest (98.7%), a result consistent with my analysis of genome completeness. Importantly, I did not have the funding to sequence RNA from *A. prunicola* PBROWN growing axenically on PDA, and therefore the *A. prunicola* PBROWN annotations were generated with only three replicates of *in situ* RNAseq.

Table 5.3. Basic statistics on the gene sets of nine fungal rust hyperparasites

Statistic	FRF	PBLUE	PBROWN	PCB	PMUD	SRB	SRM	SRSh	SRSi
# Total genes	12,470	14,834	13,570	10,339	13,888	13,258	16,729	11,900	12,873
# Transcripts	13,344	15,415	14,292	11,246	14,652	14,289	17,662	12,520	13,586
Average gene length (bp)	1,854.9	1,797.3	1,850.4	2,122.1	1,834.0	1,908.6	1,831.9	1,944.6	1,829.9
Average exon length (bp)	535.3	635.0	605.4	671.5	613.87	535.2	572.5	599.2	629.6
# CAZymes	500	644	640	437	628	556	636	538	544
# Proteases	381	427	423	369	426	408	536	407	378
# BGCs	68	44	43	41	40	58	66	38	40
# Interproscan terms	10,864	11,186	10,816	8,901	10,767	11,485	13,401	9,803	10,090
# Eggnog terms	12,278	12,749	12,866	10,107	12,873	12,980	16,397	11,115	11,875
# PFAM terms	9,710	9,778	9,580	7,864	9,494	10,265	11,864	8,766	8,860
# Secreted proteins	986	1,339	1,430	856	1,463	1,156	1,577	1,184	1,230

# GO Terms	8,926	8,815	8,287	7,348	8,264	9,321	10,498	8,018	7,979
# tRNAs	176	191	117	104	115	152	255	92	134

Table 5.4. Completeness of the candidate gene sets according to a BUSCO analysis

Measurement	**FRF**	**PBLUE**	**PBROWN**	**PCB**	**PMUD**	**SRB**	**SRM**	**SRSh**	**SRSi**
Completeness	98.7 %	98.9 %	99.1 %	99.1 %	99.0 %	99.4 %	99.1 %	98.7 %	99.5 %
# Complete BUSCOs	1684	1688	1690	1691	1689	1696	1690	1684	1697
# Complete and single copy BUSCOs	1679	1683	1688	1689	1688	1690	1680	1682	1694
# Complete and duplicated BUSCOs	5	5	2	2	1	6	10	2	3
# Fragmented BUSCOs	1	2	1	2	1	1	1	2	2
# Missing BUSCOs	21	16	15	13	16	9	15	20	7

Investigating the proportion of candidate genomes dedicated to genes potentially important to rust hyperparasitism; CAZymes, proteases and BGCs

Hyperparasite genomes contained an average of 560.4 carbohydrate-active enzymes (CAZymes), making up an average of 4% of the overall gene sets. Proportionally to their gene sets, *A. prunicola* PBROWN was the most enriched in CAZymes (640 genes, 4.48% of genes), followed by *S. terricola* SRSh (538, 4.30%), *A. prunicola* PMUD (628, 4.29%), *C. austrohaemisphericum* PBLUE (644, 4.18%), *E. italicum* SRSi (544, 4.00%), *P. copticola* SRB (556, 3.89%), *T. crotocingenum* PCB (437, 3.89%), *P. brevicompactum* FRF (500, 3.75%) and finally *F. fujikuroi* SRM (636, 3.60%). Among the CAZyme classes, Glycoside Hydrolases (GHs) were the most abundant in all candidate genomes, with an average of 287.5 genes per genome. This was followed by Auxiliary Activities (AAs; 120.9 genes), Glycosyl Transferases (GTs; 88.5 genes), Carbohydrate Esterases (CEs; 41.6 genes), Carbohydrate-Binding Modules (CBMs; 22.1 genes), and Polysaccharide Lyases (PLs), which were the least represented with an average of 17.8 per genome.

The hyperparasite genomes encoded a diverse repertoire of proteases, with an average of 416.5 protease genes per genome, an average of 3.0% of the total gene sets. Proportionally to their gene sets, *T. crotocingenum* PCB was the most enriched in proteases (369 genes, 3.28%), followed by *S. terricola*

SRSh (407, 3.25%), *F. fujikuroi* SRM (536, 3.03%), *A. prunicola* PBROWN (423, 2.96%), *A. prunicola* PMUD (426, 2.91%), *P. brevicompactum* FRF (381, 2.86%), *P. copticola* SRB (408, 2.86%), *E. italicum* SRSi (378, 2.78%) and finally *C. austrohaemisphericum* PBLUE (427, 2.77%). The most represented catalytic class was the serine proteases (S), averaging 188 genes per genome. This was followed by metalloproteases (M) with 108.1, cysteine proteases (C) with 73, threonine proteases (T) with 21.3, aspartic proteases (A) with 16.5, inhibitors (I) with 6.1, glutamic proteases (G) with 2.6, and proline proteases (P) with 0.9 genes per genome.

I used antiSMASH to identify biosynthetic gene clusters (BGCs) within the candidate genomes. I identified a total of 438 clusters across the nine genomes, an average of 48.7 clusters per isolate. Due to the varying sizes of BGCs, I present raw counts of BGCs in place of values proportional to each gene set. *Penicillium brevicompactum* FRF was the richest in BGC content, possessing 68 individual clusters. An isolate of *P. brevicompactum* was previously observed inhibiting germination of *P. coronata* urediniospores, without physically colonising pustules (Wilson *et al.*, 2020). The rich BGC content of the species may be a driving factor behind this potential chemical antagonism. *Penicillium brevicompactum* FRF was followed by *F. fujikuroi* SRM (66 BGCs), *P. copticola* SRB (58 BGCs), *C. austrohaemisphericum* PBLUE (44 BGCs), *A. prunicola* PBROWN (43 BGCs), *T. crotocingenum* PCB (41 BGCs), *E. italicum* SRSi (40 BGCs), *A. prunicola* PMUD (40 BGCs) and finally *S. terricola* SRSh (38 BGCs). Not including hybrid clusters, the most common BGC type was terpene (102 total BGCs), the rarest were CDPS, phosphonate-like, phosphonate and NI-siderophore which were each found only once across the entire 9 genomes, the CDPS in *F. fujikuroi* SRM, the phosphonate-like in *S. terricola* SRSh and the others in *P. copticola* SRB. The antiSMASH software annotated a total of 68 hybrid clusters across the nine genomes. Clusters responsible for production of the SMs clavaric acid and choline were the only clusters (with similarity to known clusters) present in all 9 genomes. In Chapter Two I posited the importance of a highly upregulated BGC with similarity to depudecin, a known histone deactylase inhibitor, to antagonism of *Pst* by *P. coffeae* ANU01. Here, the depudecin cluster was only present in the *P. copticola* SRB genome.

Differences between candidates in enrichment of key gene types such as CAZymes, proteases and BGCs help understand possible strategies for antagonism, and possible nutrient targets. The *Pst* urediniospore is rich in carbohydrates, particularly in the tough spore coat (Xiao *et al.*, 2023). Enrichment in CAZymes was fairly similar between candidates, roughly 4% of their total gene sets. However, with 4.5% of its total genes being CAZymes, *A. prunicola* PBROWN exhibited a slightly expanded tool kit regarding carbohydrate degradation, compared to the other candidates. Only 3.6% of *F. fujikuroi* SRM genes were predicted to encode CAZymes, suggesting breaking down and using carbohydrates is potentially less important to *F. fujikuroi* SRM compared to other candidates. Rust spores are composed of approximately 25% protein (Staples & Wynn 1965), making it a rich nutrient source for fungi equipped to break down amino acids. Protease content was more similar between

candidates than CAZymes, clustering tightly around the 3% average. *Trichothecium crotocingenum* PCB possessed one of the lowest proportions of CAZymes, but was the most enriched in proteases of any candidate (3.28%), suggesting amino acids may be its primary nutrient target in *Pst*. Exactly 2.77% of *C. austrohaemisphericum* PBLUE genes were proteases, placing it below the 2.97% average, suggesting the candidate might not prioritise breaking down proteins. Interestingly, *S. terricola* SRSh was the candidate with the second most enrichment in both CAZymes and proteases, suggesting it possesses an expansive toolkit to make use of both nutrients. In Chapter Two I explored the importance of BGCs in producing antifungal metabolites to possibly target and disable *Pst*. *Penicillium brevicompactum* FRF (68 BGCs) and *F. fujikuroi* SRM (66 BGCs) were enriched in BGC content compared to the average across candidates (48.7 BGCs). An expanded set of BGCs suggests that a fungus is capable of production of more antibiotic secondary metabolites, in the context of rust parasitism, this might be to better target and disable *Pst* and facilitate invasion. Interestingly, even though *A. prunicola* PBROWN and *A. prunicola* PMUD appear to be two isolates of the same species, they did not possess identical gene sets regarding CAZymes, proteases or BGCs. It is possible this difference is a result of poor annotation in *A. prunicola* PBROWN due to less RNAseq evidence than was given to *A. prunicola* PMUD. However, *A. prunicola* PBROWN was predicted to possess a greater number of genes than *A. prunicola* PMUD, suggesting the difference might be a real result. The difference between the two candidates may be a result of divergence due to differences in the microbiomes they exist in or evolution to target slightly different substrates in rust spores. Alternatively, the two isolates of *A. prunicola* evolved different gene sets without any influence of rust and are simply two saprophytes which are capable of making use of rust spores when they are present,

Although possession of a diverse repertoire of these three gene classes may suggest an enhanced capacity to antagonise or exploit *Pst* spores, their presence alone does not confirm that they contribute to hyperparasitism. To better understand the genetic basis of rust hyperparasitism, I next examined how these genes were expressed during growth on *Pst* urediniospores.

To do this I conducted a comparative transcriptomic analysis, comparing growth on *Pst* spores (*in situ*) to axenic growth (*in vitro*), to investigate the potential substrates targeted by each candidate and the strategies they might deploy to access them. Unfortunately, due to financial constraints, only *in planta* RNA seq samples for *A. prunicola* PBROWN were sequenced and therefore it was not included in this aspect of the analysis.

Candidate hyperparasites showed mobilisation of their transcriptomes during growth on *Pst* urediniospores

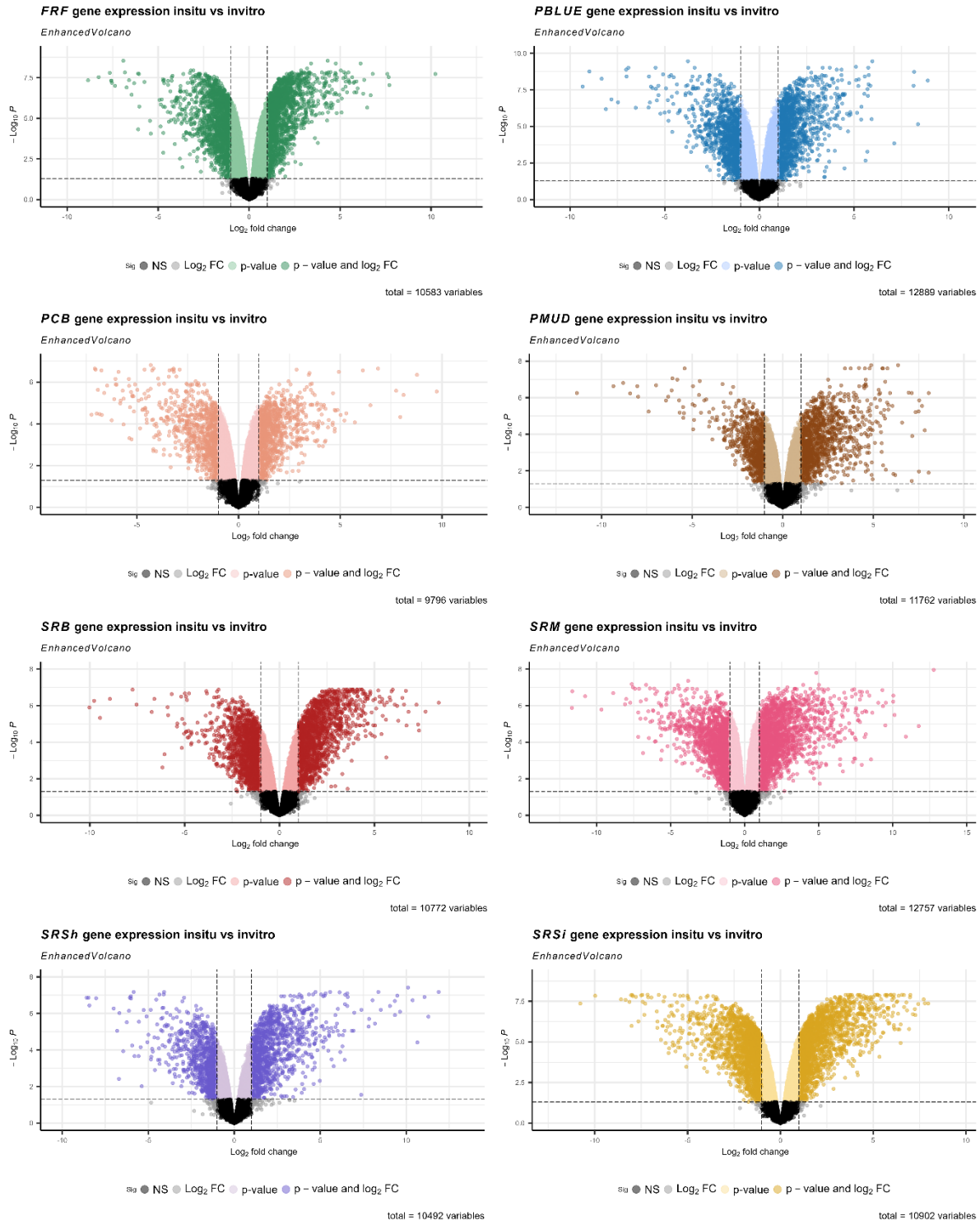

Figure 5.9. Eight individual volcano plots of differentially expressed genes for 8 individual fungal isolates growing on *Pst* urediniospores (*in situ*) versus on PDA (*in vitro*). Dashed lines on the X axis indicate log2fold changes of -1 and 1 respectively, the dashed line on the Y axis indicates adjusted *P* value of 0.05. Darker colour dots above the dashed line on the Y axis represent genes that are both

differentially and significantly expressed. Lighter dots above the dotted line on the Y axis represent genes that are significantly but not sufficiently differentially expressed. Grey dots represent genes that are differentially but not significantly expressed and black dots represent genes that are neither differentially nor significantly expressed.

Table 5.5. Number and proportion of upregulated and downregulated genes in each candidate during growth on *Pst*

Candidate	Upregulated	Upregulated (%)	Downregulated	Downregulated (%)	Difference (%)
SRSi	2040	15.01546	2096	15.42765	-0.41219
FRF	1759	13.18195	1691	12.67236	0.509592
SRB	1733	12.12821	1769	12.38015	-0.25194
SRM	1929	10.92175	1680	9.511947	1.409806
SRSh	1191	9.51278	918	7.332268	2.180511
PCB	1032	9.176596	846	7.522675	1.653921
PBLUE	1357	8.803114	1201	7.791113	1.012001
PMUD	1237	8.442533	851	5.808081	2.634453

I observed major changes in gene expression in all eight transcriptomes while growing on *Pst* spores compared to PDA (Table 5.5). I defined a gene as significantly upregulated if it exhibited an adjusted *P* value of <0.05 and a $\log_2$ fold change of >1, I defined a gene as significantly downregulated if it exhibited an adjusted *P* value of <0.05 and a $\log_2$ fold change of < -1. The results of this analysis are presented in the form of Volcano plots in Figure 5.9.

Across the candidates, the average number of upregulated genes was 1,534, while the average number of downregulated genes was 1,381. I observed the highest proportion of upregulated genes in *E. italicum* SRSi, which upregulated 2040 genes (15%) of its total gene set. This was followed by the *P. brevicompactum* FRF (1759 genes, 13.2%), *P. copticola* SRB (1733 genes, 12.1%), *F. fujikuroi* SRM (1929 genes, 10.9%), *S. terricola* SRSh (1191 genes, 9.51%), *T. crotocingenum* PCB (1032 genes, 9.2%), *C. austrohaemisphericum* PBLUE (1357 genes, 8.8%) and finally *A. prunicola* PMUD which upregulated 1,237 genes, only 8.4% of its total gene set.

Interestingly, *E. italicum* SRSi also downregulated the greatest proportion of its gene set in 2096 genes, 15.4%. In descending order followed by FRF (1691 genes, 12.7%), *P. copticola* SRB (1769 genes, 12.4%), *F. fujikuroi* SRM (1680 genes, 9.5%), *C. austrohaemisphericum* PBLUE (1201, 7.8%), *T. crotocingenum* PCB (846 genes, 7.5%), *S. terricola* SRSh (918 genes, 7.3%) and finally *A. prunicola* PMUD (851 genes, 5.8%). *Alternaria prunicola* PMUD exhibited the biggest difference in growth on the two substrates, upregulating 2.6% more genes than it downregulated, followed by *S. terricola* SRSh (2.2%). All of the candidates showed significant mobilisation of their gene sets during growth on *Pst* spores.

The proportion of genes upregulated during *in situ* growth raises interesting questions regarding specialisation. As all candidates were capable of completing their lifecycles with *Pst* urediniospores as the sole source of nutrition, it remains unclear whether mobilisation of a larger proportion of the genome reflects the evolution of an expanded parasitic toolkit, or whether mobilisation of fewer genes represents a more streamlined and efficient strategy for exploiting *Pst* spores. Without extensive phenotypic characterisation, these questions could not be resolved in the present study.

All candidates were capable of readily completing their lifecycles on *Pst*, although *E. italicum* SRSi was the only candidate to exhibit a distinct phenotype (Supplementary Figure 5.1). The comparatively large proportion of genes upregulated in *E. italicum* SRSi may contribute to this phenotype by supporting multiple aspects of the interaction, including nutrient acquisition, antagonism and mechanical lysis. However, the similarly large proportion of genes upregulated during *in vitro* growth suggests that *E. italicum* SRSi may simply transcribe a greater proportion of its genome during growth, irrespective of substrate. During growth on *Pst* pustules, *P. coffeae* ANU01 upregulated 19% and downregulated 18.2% of its gene set (Chapter Two). This increased mobilisation of genes may be due to the additional element of growth on pustules *on planta.* The presence of the plant as a third element in the hyperparasite-rust interaction therefore may play a major role in influencing the genes upregulated during growth *in situ.* Future studies should investigate the candidate transcriptome during growth on *Pst* urediniospores, as described in this chapter, and during *on planta* growth, as described in Chapter Two. Comparing gene expression across these conditions would help identify processes specifically associated with interactions with *Pst* and distinguish them from those involved in possible saprophytic growth on the plant host.

Future work should also incorporate detailed phenotypic analyses to better understand the degree of specialisation among these candidates. Biomass qPCR could be used to determine relative growth rates on *Pst*, tests that measure impact on *Pst* germination, such as those described by Wilson *et al.* (2020) could assess antagonistic activity against urediniospores, and chitin catabolism assays could evaluate the capacity of each candidate to degrade the polysaccharides that comprise the *Pst* spore coat. Although the present data do not permit definitive conclusions regarding specialisation, functional annotation of the differentially expressed genes provides insight into the mechanisms by which each fungus may antagonise *Pst* and the substrates it may target during exploitation of the rust.

I conducted a Gene Ontology (GO) enrichment analysis to identify both shared traits and differences among the candidates in their transcriptomic response to growth on *Pst* compared with axenic growth on PDA. I initially focused on GO terms that remained significant following stringent statistical correction, as these were considered to represent the core components of each candidate's parasitic response (Figure 5.10).

Importantly, the findings I present in this report are based solely on gene expression data. As a result, the functional roles and biological processes I discuss are predicted from patterns of gene expression and annotation, and are therefore all hypothetical. My interpretations should be regarded as putative explanations of how each candidate hyperparasite interacts with *Pst*, rather than definitive evidence of gene function or biological activity.

Analysis of the most significantly enriched (core) GO terms during growth on *Pst* provides insight into the possible major elements of rust hyperparasitism

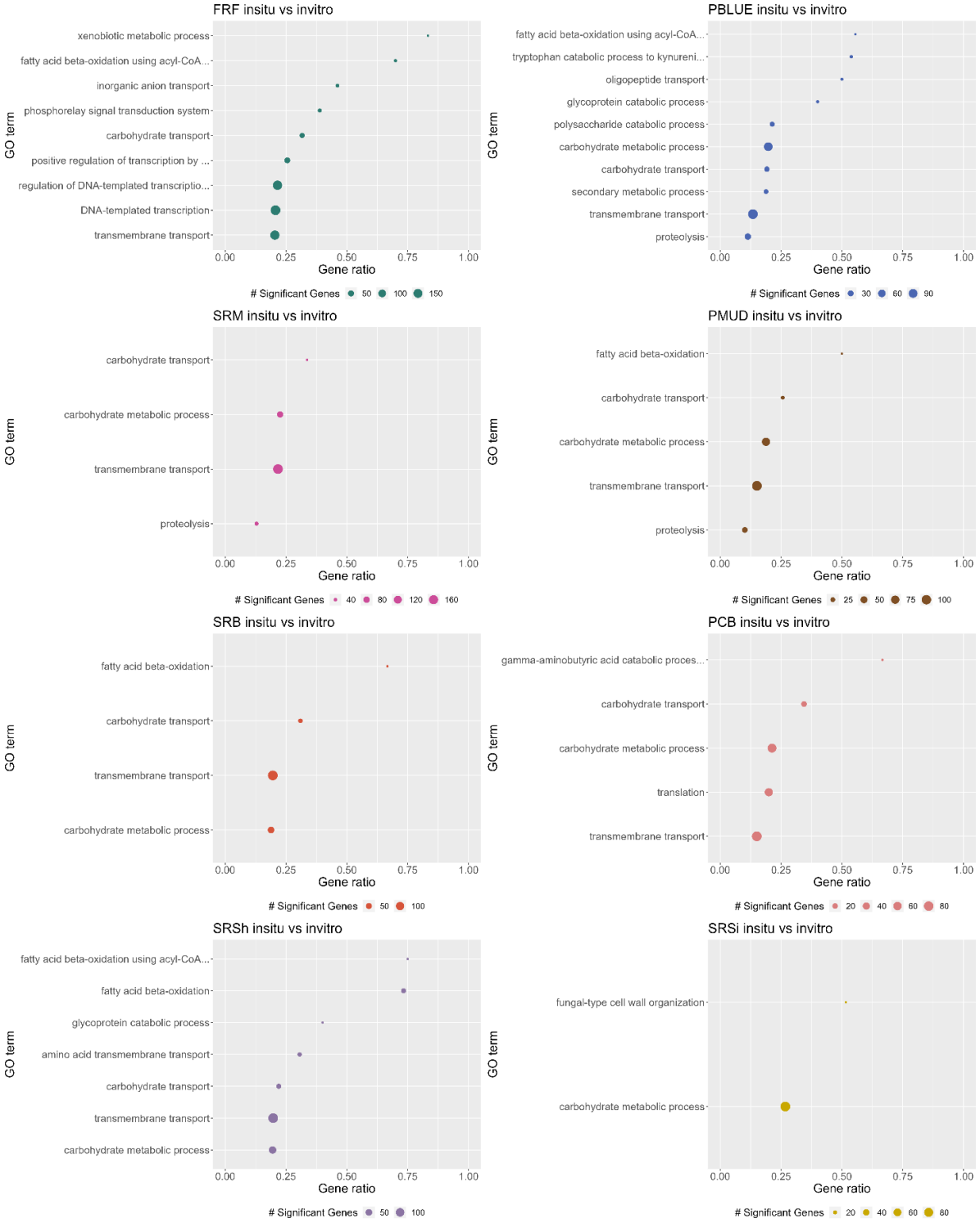

Figure 5.10. Dotplots representing the most significantly enriched (core) gene ontology (GO terms) according to an adjusted Fisher's exact test. The size of each dot represents the number of significant genes within the GO term, whilst position along the X axis represents the number of significant genes, as a fraction of the total genes within the term. Only GO terms that showed an adjusted *P* value <0.05

were included in this analysis. To include all enriched GO terms, representations of the GO analysis before *P* value adjustment are presented in Figures 5.11-5.18.

Metabolism of substrates abundant within *Pst* urediniospores was among the most significantly enriched (core) biological processes during *in situ* growth (Figure 5.10). Rust urediniospores are composed of approximately 22% carbohydrate, 20% lipid and 25% protein (Staples & Wynn, Tulloch 1959), and I observed differences among the candidates in how they appeared to target these substrates. Several GO terms were significantly enriched across multiple candidates, including transmembrane transport (7 candidates), carbohydrate metabolism (7 candidates), carbohydrate transport (6 candidates), fatty acid β-oxidation (5 candidates), and proteolysis (3 candidates).

Transmembrane transport was the joint most frequently enriched GO term. Although this category was significantly enriched, only a modest proportion of the associated genes were significantly upregulated across the candidates (average: 17.8%). *Fusarium fujikuroi* SRM exhibited the highest proportion of upregulated genes within this category, with 21.7% (183 genes), while *C. austrohaemisphericum* PBLUE exhibited the lowest proportion, with 13.4% (117 genes). These genes are likely involved in the uptake of degraded nutrients and the export of secondary metabolites that may antagonise *Pst*.

Genes involved in carbohydrate metabolism were also widely and significantly upregulated across the candidates. The *Pst* urediniospore wall is rich in protective polysaccharides, which present a barrier to invading hyperparasites (Xiao *et al.,* 2023). *Epicoccum italicum* SRSi exhibited the greatest emphasis on carbohydrate metabolism, upregulating 26.7% (96 genes) of its genes associated with this GO term, compared with an overall average of 21%. In contrast, *A. prunicola* PMUD and *P. copticola* SRB exhibited the lowest proportions, each upregulating 18.8% of their associated genes (73 and 59 genes, respectively). The increased emphasis on carbohydrate metabolism in *E. italicum* SRSi may be related to its distinct phenotype of growing around and mechanically lysing *Pst* urediniospores. Enhanced production of cell wall-degrading enzymes may facilitate penetration of the robust spore coat, while increased carbohydrate anabolism may contribute to strengthening the fungal cell wall during mechanical invasion.

The related GO term carbohydrate transport was significantly enriched in six candidates, with an average of 28.1% of associated genes upregulated. *Trichothecium crotocingenum* PCB exhibited the highest proportional upregulation (34.4%, 21 genes), whereas *C. austrohaemisphericum* PBLUE exhibited the lowest proportion (19.2%, 23 genes). I hypothesise that, in some candidates, carbohydrate metabolism is primarily directed towards degradation of the *Pst* spore coat, whereas others deploy a broader carbohydrate metabolic and transport repertoire to both degrade structural polysaccharides and exploit the abundant carbohydrates within *Pst* as a nutrient source. This distinction may be most evident in *C. austrohaemisphericum* PBLUE, which specifically enriched polysaccharide catabolism (19 genes,

21.3%) but upregulated the lowest proportion of genes associated with carbohydrate transport. This pattern suggests that the candidate may efficiently degrade the polysaccharides abundant within the urediniospore wall but may place less emphasis on carbohydrates as a primary nutritional target than the other candidates.

Fatty acid β-oxidation facilitates the breakdown of fatty acids to generate acetyl-CoA and, ultimately, cellular energy (Schulz, 1991). Significant enrichment of the GO terms fatty acid β-oxidation and fatty acid β-oxidation using acyl-CoA dehydrogenase in five candidates suggests that lipids are an important nutrient target for these fungi. On average, candidates possessed only 10.25 genes associated with this pathway, of which an average of 5.1 genes were significantly upregulated (49.7%). *Sarocladium terricola* SRSh exhibited the greatest proportional upregulation, with six of its eight associated genes upregulated (75%), followed by *P. brevicompactum* FRF (7 genes, 70%), *P. copticola* SRB (20 genes, 60%), and *C. austrohaemisphericum* PBLUE (5 genes, 55.5%). Fatty acid β-oxidation was also a core component of growth on *Pst* for *A. prunicola* PMUD, although only three of its associated genes were significantly upregulated (27.7%). In contrast, this pathway was not a core feature of growth on *Pst* for *F. fujikuroi* SRM or *T. crotocingenum* PCB and was not enriched, even before statistical correction, in *E. italicum* SRSi (see secondary GO terms below) (Figure 5.18).

Lipids account for approximately 20% of the dry weight of rust urediniospores (Tulloch *et al.*, 1959), making it unsurprising that they represent a major nutrient target for several candidates. Although the candidates possessed far fewer genes associated with fatty acid β-oxidation (10.25 genes on average) than with carbohydrate metabolism (357 genes on average), they upregulated a substantially greater proportion of them during growth on *Pst* (49.7% versus 21%). I hypothesise that candidates which strongly target fatty acids have evolved a relatively small but specialised set of genes for exploiting this nutrient source, whereas more generalist candidates either place less emphasis on lipid utilisation or rely on broader metabolic strategies.

Proteolysis was significantly enriched in only three candidates: *F. fujikuroi* SRM (43 genes, 12.9%), *C. austrohaemisphericum* PBLUE (38 genes, 11.3%), and *A. prunicola* PMUD (33 genes, 10.1%). These findings suggest that protein degradation is a core component of growth on *Pst* urediniospores for only a subset of candidates, particularly when compared with the more commonly targeted substrates of carbohydrates and fatty acids. Furthermore, candidates that targeted protein upregulated only a modest proportion of the genes associated with this GO term, suggesting that this aspect of their metabolic repertoire may not be highly specialised for growth on *Pst*. Proteins account for approximately 25% of the composition of rust urediniospores (Staples & Wynn 1965), making the limited enrichment of proteolysis somewhat unexpected. The requirement to degrade the carbohydrate-rich spore wall, together with the potential energetic value of fatty acids, may reduce the relative importance of protein

as a nutritional target for many candidates. Glycoproteins, which consist of proteins with one or more attached carbohydrate chains (Zhang *et al.*, 2023), may represent a more specialised substrate. Glycoprotein catabolism was significantly enriched only in *S. terricola* SRSh and *C. austrohaemisphericum* PBLUE, with both candidates upregulating six associated genes (15%). The enrichment of this pathway in only two candidates suggests that these fungi may possess specialised mechanisms for exploiting this comparatively niche substrate.

Core GO terms that were only enriched in individual candidates reflected possible differences in the strategies employed during growth on *Pst*. *Penicillium brevicompactum* FRF exhibited the most diverse enrichment profile, with 10 significantly enriched GO terms, including phosphorelay signal transduction (14 genes; 38.9%). Enrichment of signal transduction pathways suggests a more coordinated response to encountering *Pst* compared with other candidates. Together with enrichment of regulation of DNA-templated transcription (168 genes, 21.5%), these results indicate that *P. brevicompactum* FRF may mount a broad transcriptional response during interaction with *Pst*. This candidate was also the only candidate to show enrichment in xenobiotic metabolism (5 genes, 83.3%), suggesting potential production of secondary metabolites that may act in chemical antagonism against *Pst* or interfere with host defences. A similar emphasis on secondary metabolism was observed in *C. austrohaemisphericum* PBLUE, which showed significant enrichment of secondary metabolic processes (16 genes, 18.9%). Together, these patterns suggest that chemical antagonism may be a feature of *P. brevicompactum* FRF and *C. austrohaemisphericum* PBLUE, but is not a core element shared across all candidates. In contrast, *Epicoccum italicum* SRSi showed enrichment of solely fungal-type cell wall organisation (16 genes, 51.6%) and carbohydrate metabolic processes (96 genes, 26.7%). These processes likely underpin the observed aggressive phenotype *in vitro*, including mechanical interaction with and lysis of *Pst* urediniospores, supported by coordinated cell wall modification and carbohydrate-degrading activity. Finally, *T. crotocingenum* PCB uniquely enriched genes associated with gamma-aminobutyric acid (GABA) catabolism (6 genes, 66.6%), suggesting use of nitrogen and carbon within *Pst* (Dhakal *et al.*, 2012).

During growth on *Pst* urediniospores, GO enrichment was dominated by metabolic processes targeting substrates abundant within rust urediniospores. Transmembrane transport and carbohydrate metabolism were the most consistently enriched terms, followed by carbohydrate transport, fatty acid β-oxidation, and proteolysis, indicating that carbohydrates, lipids, and proteins represent the principal nutrient targets during parasitism. The widespread enrichment of carbohydrate metabolism likely reflects both the need to breach the polysaccharide-rich spore wall and to exploit carbohydrates as a primary carbon source, whereas lipid and protein utilisation appeared more candidate-specific. Differences in enrichment profiles therefore suggest distinct parasitic strategies among hyperparasites. Some candidates, such as *E. italicum* SRSi and *T. crotocingenum* PCB, appeared to preferentially target

carbohydrates, while others, including *P. brevicompactum* FRF, *P. copticola* SRB, and *S. terricola* SRSh, showed a stronger emphasis on fatty acid metabolism. Proteolysis was restricted to *C. austrohaemisphericum* PBLUE, *A. prunicola* PMUD, and *F. fujikuroi* SRM, indicating that protein utilisation is a more secondary or perhaps specialised strategy. *Cladosporium austrohaemisphericum* PBLUE and *A. prunicola* PMUD were the only candidates to show core enrichment in genes related to all three major nutrient classes. They were the candidates to upregulate the smallest portion of their genes during *in situ* growth, raising questions regarding the balance between generalist and specialist strategies in rust hyperparasites. Specifically, does growth and completion of the fungal lifecycle on *Pst* spores with fewer upregulated genes mean those genes are more effective or streamlined and therefore more specialised? Or does mobilisation of a greater number of genes mean the fungus has evolved to possess more genes to aid them in growing on *Pst.* Variation in GO term enrichment highlights divergent metabolic strategies among candidates. Additional unique enrichments, including secondary metabolism, signal transduction, and cell wall organisation, likely reflect candidate-specific adaptations related to host invasion, antagonism, and mechanical penetration. Collectively, these results suggest that while fungi capable of growing on rust spores share a common reliance on host-derived nutrients, variation in substrate preference and metabolic strategy underpins divergent modes of potential parasitism on *Pst* urediniospores.

The statistical adjustment applied in this analysis preferentially retained what were considered the core features of growth on *Pst* for each candidate. I present a detailed explanation of the stringent topGO statistical adjustment in Chapter Four. As a result, processes that were less statistically significant, but potentially still biologically relevant, fell below the significance threshold. However, my examination of secondary GO terms below this cut-off revealed additional aspects of growth *in situ* that further distinguished each candidate in its interaction with *Pst*, and these are discussed below. Importantly, adjustment provides a more robust confidence in the enrichment of a GO term during hyperparasitism. However, as I discuss in Chapter Three, retaining statistical significance after adjustment can not guarantee that the associated biological process is more important during parasitism than a term that did not retain significance after adjustment.

Analysis of less significantly enriched (secondary) GO terms during growth on *Pst* provides further insight into potential parasitic strategies of individual candidates

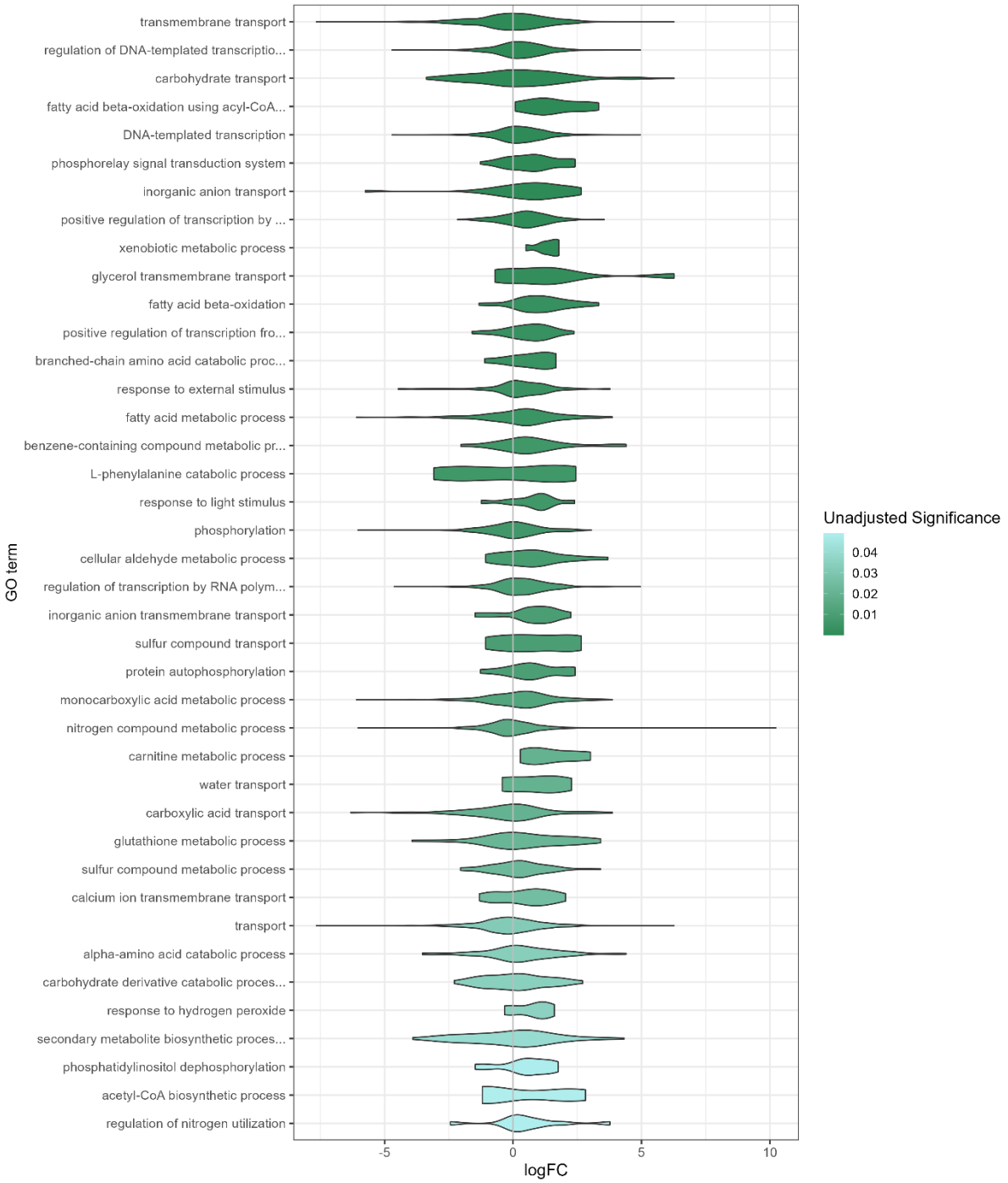

Figure 5.11. Violin plot representing the distribution of genes within significant ($P < 0.05$ before statistical adjustment) GO terms during *in situ* growth of *P. brevicompactum* FRF on *Pst* urediniospores. Terms are ordered from top to bottom in terms of significance according to an unadjusted Fisher's exact test. Each violin represents the density distribution of $\log_2$ fold change values for all differentially expressed genes within the corresponding GO term. The width of the violin indicates the number of

genes at a given log_2 fold change value. The shortened GO terms on the Y axis are: regulation of DNA-templated transcription, fatty acid beta-oxidation using acyl-CoA dehydrogenase, positive regulation of transcription by RNA polymerase II, positive regulation of transcription from RNA polymerase II promoter by galactose, branched-chain amino acid catabolic process, benzene-containing compound metabolic process, regulation of transcription by RNA polymerase II, carbohydrate derivative catabolic process and secondary metabolite biosynthetic process.

The core features of *P. brevicompactum* FRF growth on *Pst* were the production of secondary metabolites, extensive transcriptional and signalling activity, and a primary reliance on lipids as a nutrient source (Figure 5.10). Secondary GO terms provide further insight into the molecular mechanisms and additional nutrient sources underpinning this parasitic strategy (Figure 5.11).

Although lipid utilisation appeared to be the dominant nutritional strategy, enrichment of carbohydrate derivative catabolic process (10 genes, 22.7%), branched-chain amino acid catabolism (5 genes, 55.5%), and alpha-amino acid catabolism (19 genes, 30.1%) indicates that *P. brevicompactum* FRF also exploits carbohydrate and protein substrates during growth on *Pst*. Enrichment of acetyl-CoA biosynthesis (4 genes, 44.4%) may facilitate the integration of these carbon sources into central metabolism (Shi & Tu 2015). The importance of lipids was further emphasised by enrichment of the fatty acid metabolic process (36 genes, 27.9%) and by the upregulation of glycerol transmembrane transport (5 genes, 62.5%). Glycerol is released during fatty acid degradation (Garnica *et al.*, 2014), suggesting that lipid catabolism contributes substantially to nutrient acquisition during growth on *Pst*.

Metabolism can generate reactive oxygen species and other free radicals (Li *et al.*, 2023), potentially explaining the enrichment of genes involved in the response to hydrogen peroxide (3 genes, 50%). These genes may function in detoxification of metabolic by-products or in protection against oxidative stress generated during antagonistic interactions with *Pst*. The importance of chemical antagonism was further supported by enrichment of genes associated with secondary metabolism (14 genes, 22.2%).

Signalling and transcriptional regulation also appeared to play major roles during parasitism. *P. brevicompactum* FRF upregulated seven of its 23 genes related to calcium ion transmembrane transport (30.4%), potentially enhancing calcium-mediated signalling pathways (Roy *et al.*, 2021). In addition, phosphorelay signal transduction systems (14 genes, 38.9%), response to light stimulus (5 genes, 50%), and response to external stimulus (18 genes, 23.3%) were all significantly enriched. The combined enrichment of transcriptional regulation, environmental sensing, and downstream signalling pathways suggests that *P. brevicompactum* FRF mounts a highly coordinated response during interaction with *Pst* urediniospores.

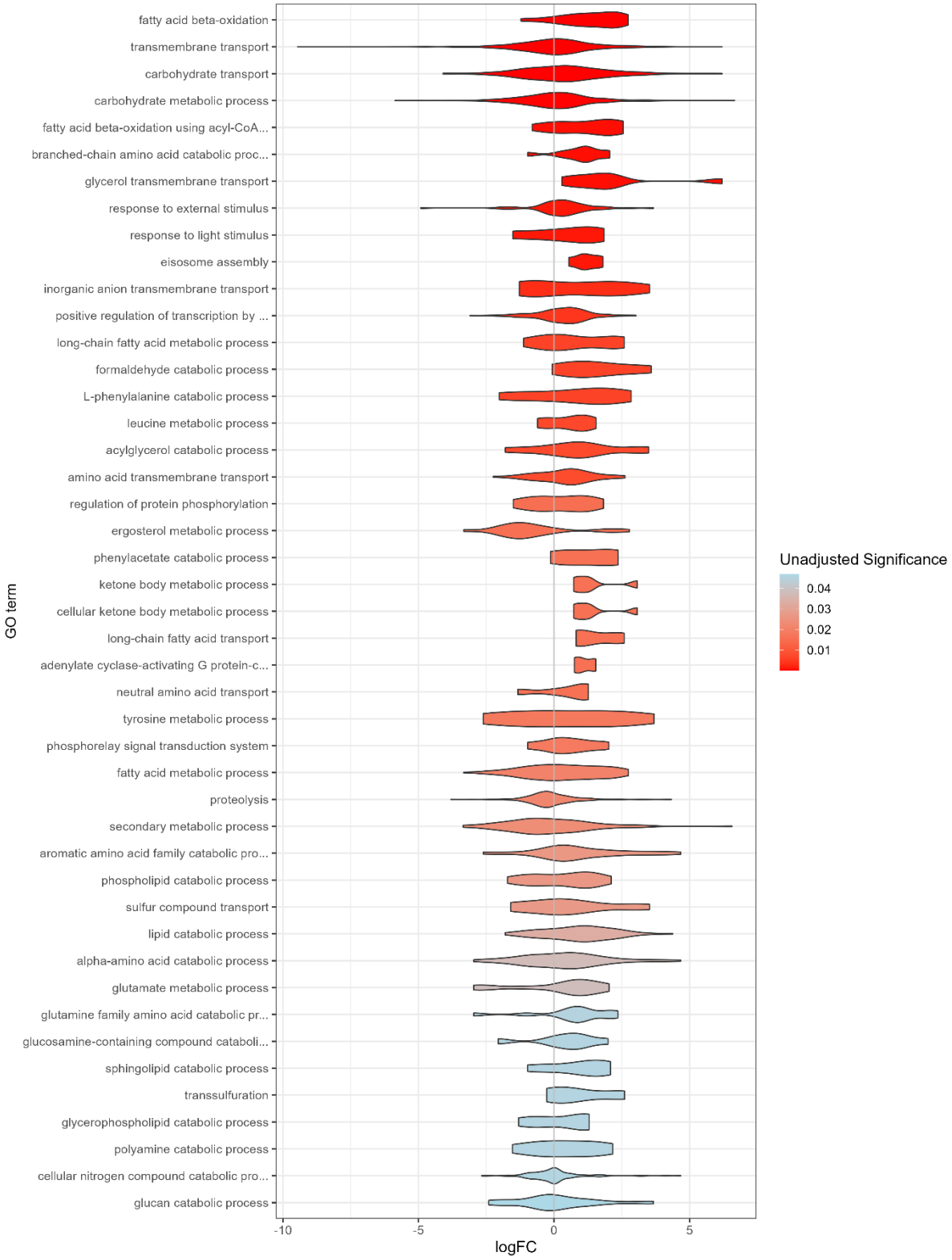

Figure 5.12. Violin plot representing the distribution of genes within significant ($P < 0.05$ before statistical adjustment) GO terms during *in situ* growth of *P. copticola* SRB on *Pst* urediniospores. Terms are ordered from top to bottom in terms of significance according to an unadjusted Fisher's exact test. Each violin represents the density distribution of $\log_2$ fold change values for all differentially expressed genes within the corresponding GO term. The width of the violin indicates the number of genes at a

given log_2 fold change value. The shortened GO terms on the Y axis are: branched-chain amino acid catabolic process, fatty acid beta-oxidation using acyl-CoA dehydrogenase, positive regulation of transcription by RNA polymerase II, adenylate cyclase-activating G protein-coupled receptor signalling pathway, aromatic amino acid family catabolic process, glutamine family amino acid catabolic process, glucosamine-containing compound catabolic process and cellular nitrogen compound catabolic process.

The core features of *P. copticola* SRB growth on *Pst* spores were the degradation of fatty acids and carbohydrates (Figure 5.10). Investigation of secondary GO terms revealed an even greater emphasis on lipid utilisation, signalling, cell wall degradation, and the acquisition of secondary nutrients such as protein and glycerol (Figure 5.12).

Lipid metabolism was the dominant feature of growth *in situ*, with enrichment of fatty acid beta-oxidation using acyl-CoA dehydrogenase (6 genes, 60%), fatty acid metabolic process (40 genes, 33.9%), long-chain fatty acid metabolic process (5 genes, 35.7%), lipid catabolic process (42 genes, 49.4%), sphingolipid catabolic process (3 genes, 42.9%), and glycerophospholipid catabolic process (3 genes, 42.9%). *Penicillium copticola* SRB was the only candidate to show such extensive investment in lipid utilisation, suggesting that it may possess specialised mechanisms for exploiting this nutrient source within *Pst* spores.

Protein appeared to be a secondary nutrient target, potentially accessed through proteolysis (28 genes, 9.4%) and branched-chain amino acid catabolism (6 genes, 60%), with uptake facilitated by genes involved in neutral amino acid transport (3 genes, 60%). Similar to *P. brevicompactum* FRF, *P. copticola* SRB also upregulated genes related to glycerol transmembrane transport (5 genes, 71.4%), suggesting that glycerol released during lipid degradation is an additional nutrient source. Enrichment of acylglycerol catabolism (5 genes, 45.4%) further supports the hypothesis that this candidate targets lipid droplets within *Pst* urediniospores (Lösel & Sancholle 2017).

As with *P. brevicompactum* FRF, I observed environmental sensing and downstream signalling as prominent features of growth *in situ*, with enrichment of response to external stimulus (13 genes, 19.1%), response to light stimulus (5 genes, 50%), and phosphorelay signal transduction (7 genes, 30.4%). Coordinated signalling of this nature was primarily observed in the two *Penicillium* candidates and *F. fujikuroi*, suggesting either a degree of specialisation or that these fungi possess regulatory networks particularly suited to growth in the presence of rust spores.

Antagonism of *Pst* may be facilitated through enrichment of genes associated with secondary metabolism (11 genes, 18.3%). In addition, upregulation of four of its five genes (80%) related to eisosome assembly may contribute to protection against self-produced secondary metabolites or compounds produced by *Pst*. Unlike *P. brevicompactum* FRF, *P. copticola* SRB enriched glucan

metabolism (7 genes, 25%), potentially reflecting the secretion of cell wall degrading enzymes that target glucans within the *Pst* spore coat.

Together, these results suggest that *P. copticola* SRB adopts a highly lipid-focused parasitic strategy, supported by coordinated signalling, secondary metabolism, and targeted degradation of the *Pst* spore wall.

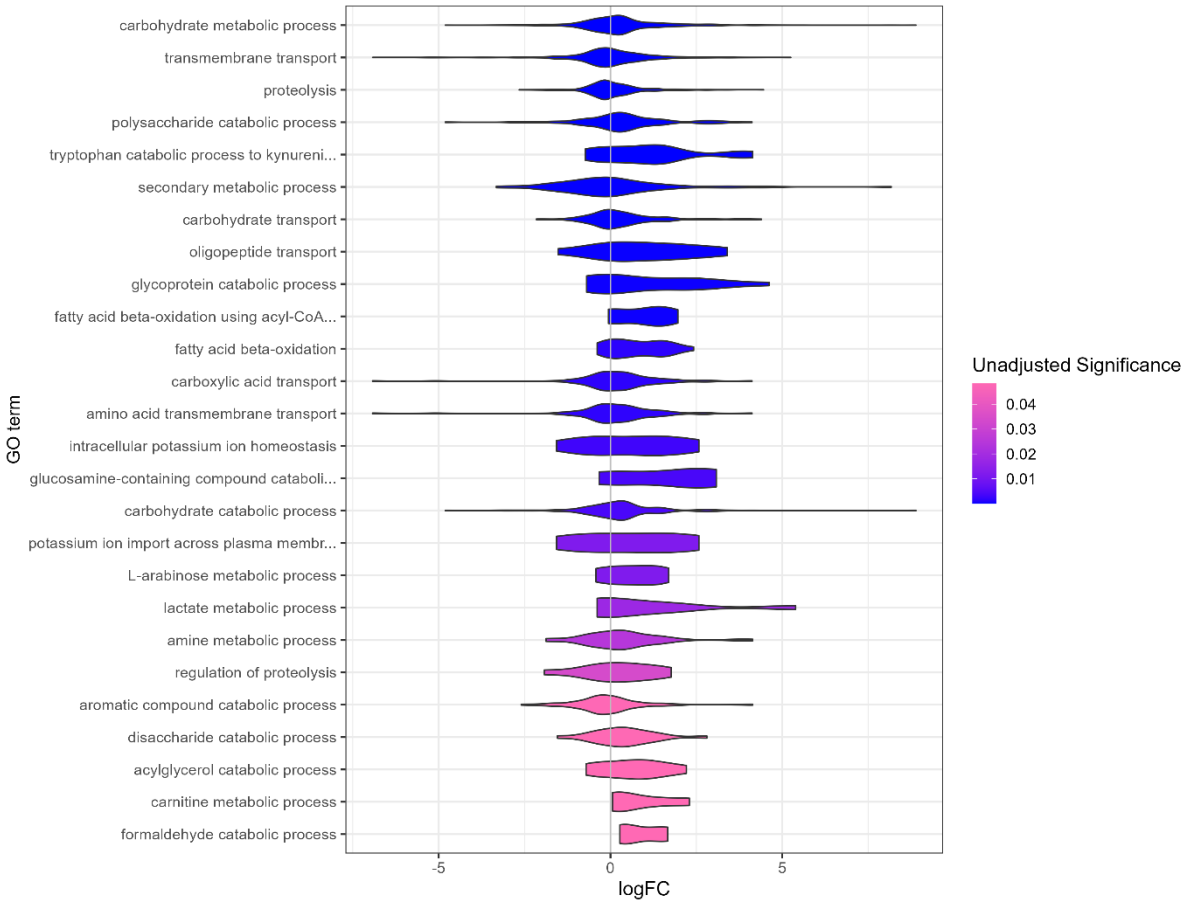

Figure 5.13. Violin plot representing the distribution of genes within significant ($P < 0.05$ before statistical adjustment) GO terms during *in situ* growth of *C. austrohaemisphericum* PBLUE on *Pst* urediniospores. Terms are ranked from top to bottom in terms of significance according to an unadjusted Fisher's exact test. Each violin represents the density distribution of $\log_2$ fold change values for all differentially expressed genes within the corresponding GO term. The width of the violin indicates the number of genes at a given $\log_2$ fold change value. The shortened GO terms on the Y axis are: tryptophan catabolic process to kynurenine, fatty acid beta-oxidation using acyl-CoA dehydrogenase, glucosamine-containing compound catabolic process and potassium ion import across plasma membrane.

The core GO terms enriched during *in situ* growth of *C. austrohaemisphericum* PBLUE involved the targeting of lipids, carbohydrates, and protein, together with the production of secondary metabolites

and secretion of cell wall degrading enzymes (Figure 5.10). *C. austrohaemisphericum* PBLUE was the only candidate to include all of these seemingly characteristic parasitic functions within its core GO terms, suggesting that it may represent a more specialised hyperparasitic strategy than the other candidates.

Beyond the core enriched terms, I observed several additional nutrient targets in its secondary GO terms (Figure 5.13). *C. austrohaemisphericum* PBLUE was one of only four candidates to enrich acylglycerol catabolism, upregulating three of its ten associated genes (30%). Catabolism of formaldehyde (2 genes, 40%) and carnitine (2 genes, 40%) was also enriched, indicating the utilisation of secondary nutrient sources during parasitism. Potassium is important in osmotic regulation and protein synthesis, elements particularly important under stressful conditions (Rodriguez-Navarro 2000). Enrichment of potassium ion import across the plasma membrane (3 genes, 42.9%) and maintenance of intracellular potassium ion homeostasis (4 genes, 44.4%) may therefore assist *C. austrohaemisphericum* PBLUE in maintaining cellular integrity during antagonistic interactions with *Pst*. I also observed that *C. austrohaemisphericum* PBLUE was the only candidate to enrich catabolism of aromatic compounds (14 genes, 10%). These pathways may facilitate exploitation of a specialised nutrient source or contribute to detoxification of secondary metabolites produced by *Pst*.

The core aspects of parasitism in *C. austrohaemisphericum* PBLUE appear to involve the deployment of secondary metabolites and cell wall degrading enzymes to inhibit and penetrate the host before utilisation of all three major nutrient classes. Despite upregulating only 8.8% of its genes during *in situ* growth (Table 5.5), the second fewest of all candidates, I observed enrichment of nearly all functions that I consider characteristic of an adapted rust hyperparasite. Together with the similarly streamlined response observed in *A. prunicola* PMUD, these findings suggest that a smaller transcriptional response may reflect a more efficient or highly specialised hyperparasitic strategy rather than reduced biological complexity.

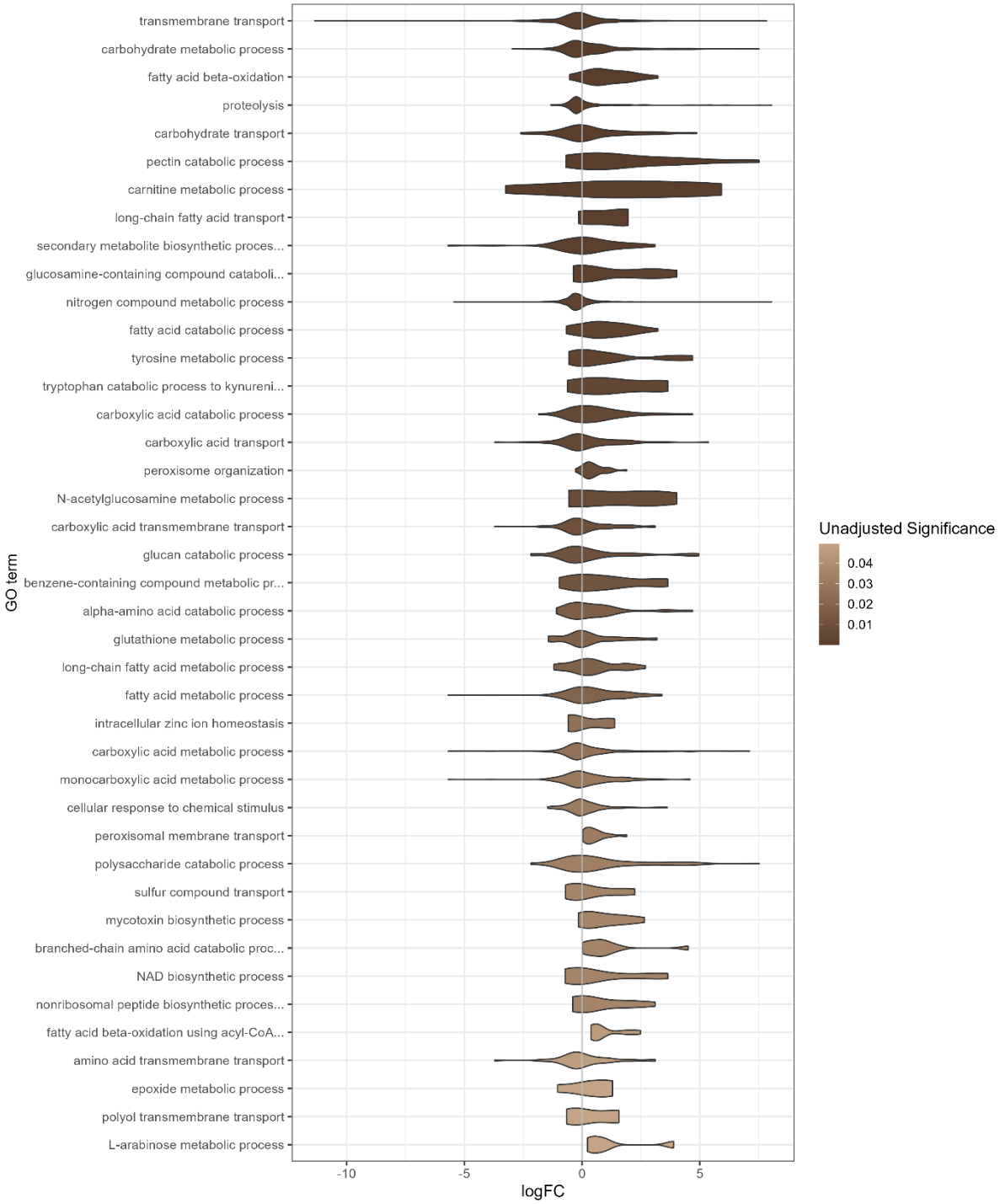

Figure 5.14. Violin plot representing the distribution of genes within significant ($P < 0.05$ before statistical adjustment) GO terms during *in situ* growth of *A. prunicola* PMUD on *Pst* urediniospores. Terms are ordered from top to bottom in terms of significance according to an unadjusted Fisher's exact test. Each violin represents the density distribution of $\log_2$ fold change values for all differentially expressed genes within the corresponding GO term. The width of the violin indicates the number of genes at a given $\log_2$ fold change value. The shortened GO terms on the Y axis are: secondary metabolite biosynthetic process, glucosamine-containing compound catabolic process, tryptophan catabolic process to kynurenine, benzene-containing compound metabolic process, nonribosomal peptide

biosynthetic process, branched-chain amino acid catabolic process and fatty acid beta-oxidation using acyl-CoA dehydrogenase.

The core elements of *A. prunicola* PMUD growth *in situ* were the metabolism of all three major nutrient targets; carbohydrates, lipids, and protein (Figure 5.10). Alongside *C. austrohaemisphericum* PBLUE, *A. prunicola* PMUD was one of only two candidates to show metabolism of all three major nutrients within its core enriched terms. Investigation of secondary GO terms revealed a strong emphasis on the production of secondary metabolites and the deployment of cell wall degrading enzymes (Figure 5.14).

I observed enrichment of secondary metabolite biosynthesis (13 genes, 24.5%), mycotoxin biosynthesis (3 genes, 30%), and nonribosomal peptide biosynthesis (3 genes, 30%), suggesting that *A. prunicola* PMUD deploys a diverse suite of secondary metabolites during interaction with *Pst*. I also observed enrichment of glucan catabolic process (7 genes, 21.2%), polysaccharide catabolic process (17 genes, 27.4%), and glucosamine-containing compound catabolism (4 genes, 40%), suggesting an emphasis on degradation of the *Pst* spore wall. Glucosamine is a derivative of chitin (Rudall & Kenchington, 1973), a major component of the *Pst* spore coat.

Interestingly, *A. prunicola* PMUD also upregulated pectin catabolism (6 genes, 46.2%). Pectin is not present in *Pst* urediniospores (Xiao *et al.*, 2023) but is present in plant tissue (Schultz & Coleman 2021). It is possible that genes involved in pectin degradation are co-opted to exploit structurally similar carbohydrates present in *Pst*. Alternatively, pectin catabolism may represent a general response to the recognition of rust spores, as *on planta* they would indicate pustules and therefore the presence of disrupted host tissue. If this is the case, *A. prunicola* PMUD may function as an opportunistic plant-associated fungus capable of acting as both a pathogen and a rust hyperparasite. However, the apparent ability to employ such a diverse genetic toolkit against *Pst* may also indicate a degree of specialisation for this ecological niche.

A. prunicola PMUD deployed the smallest proportion of its genes during parasitism of any candidate (Table 5.5). Despite this, I observed a potent and multifaceted response characterised by the production of secondary metabolites, deployment of cell wall degrading enzymes, and acquisition of all three major nutrient classes. Together, these findings suggest that *A. prunicola* PMUD relies on a relatively small but highly specialised or streamlined set of genes during potential hyperparasitism.

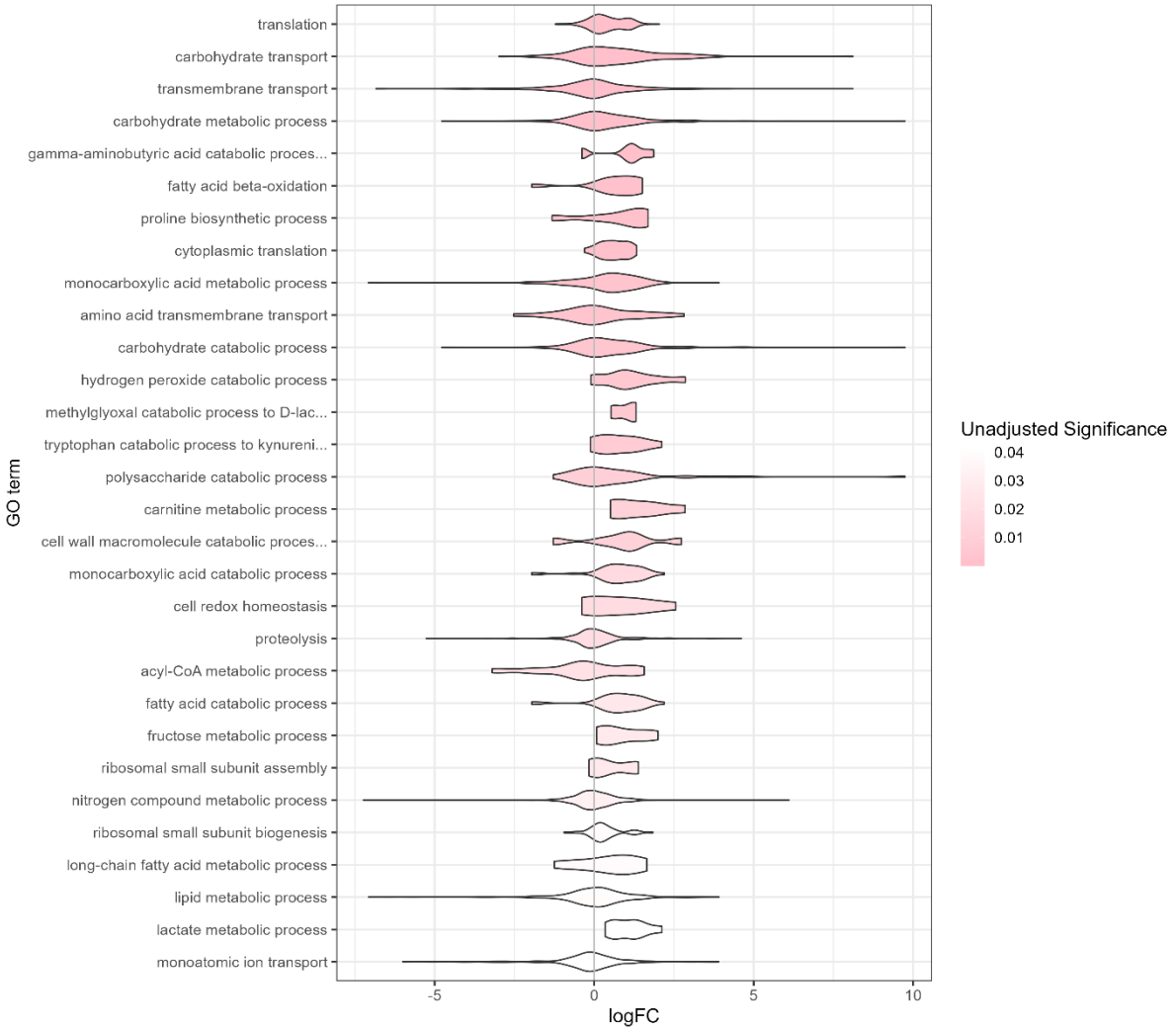

Figure 5.15. Violin plot representing the distribution of genes within significant ($P < 0.05$ before statistical adjustment) GO terms during *in situ* growth of *T. crotocingenum* PCB on *Pst* urediniospores. Terms are ordered from top to bottom in terms of significance according to an unadjusted Fisher's exact test. Each violin represents the density distribution of $\log_2$ fold change values for all differentially expressed genes within the corresponding GO term. The width of the violin indicates the number of genes at a given $\log_2$ fold change value. The shortened GO terms on the Y axis are: gamma-aminobutyric acid catabolic process, methylglyoxal catabolic process to D-lactate via S-lactoyl-glutathione, tryptophan catabolic process to kynurenine and cell wall macromolecule catabolic process.

The core aspects of *T. crotocingenum* PCB growth on *Pst* spores reflected a primary focus on carbohydrate utilisation, together with catabolism of GABA and increased translational activity (Figure 5.10). Investigation of secondary enriched GO terms revealed additional nutrient targets and a strong emphasis on the deployment of cell wall degrading enzymes (Figure 5.15).

Beyond carbohydrates and GABA, I observed enrichment of fatty acid beta-oxidation (9 genes, 36%) and proteolysis (29 genes, 9%), suggesting that lipids and amino acids function as secondary nutrient

sources. Additional nutrient targets included methylglyoxal (3 genes, 60%), tryptophan (4 genes, 40%), monocarboxylic acid (15 genes, 37.5%), lactate (5 genes, 55.6%), fructose (3 genes, 38%), and carnitine (3 genes, 50%), indicating a broad capacity for nutrient utilisation.

Trichotheium crotocingenum PCB upregulated polysaccharide catabolism (10 genes, 22.3%) and was the only candidate to enrich cell wall macromolecule catabolism (3 genes, 50%), suggesting that secretion of cell wall degrading enzymes might be a particularly important aspect of its parasitic strategy. In contrast to the majority of the other candidates, I did not observe enrichment of any GO term related to secondary metabolism or mycotoxin production, suggesting that chemical antagonism may play a lesser role during growth on *Pst*.

Protection against oxidative stress appeared to be important during parasitism, with enrichment of hydrogen peroxide catabolism (4 genes, 44.4%) and cell redox homeostasis (3 genes, 43%). These findings may indicate that growth on *Pst* imposes some physiological stress on *T. crotocingenum* PCB.

Overall, my results suggest that *T. crotocingenum* PCB primarily exploits carbohydrates while making secondary use of lipids and proteins. Rather than relying heavily on secondary metabolites, this candidate may preferentially deploy cell wall degrading enzymes to penetrate the *Pst* spore coat and facilitate nutrient acquisition. The enrichment of multiple stress-related pathways may indicate that this strategy is physiologically demanding, that the candidates is less specialised for growth on *Pst* than some of the other candidates, or that nutrients within the urediniospores had become limiting by the time samples were collected. Further phenotypic investigation would be required to distinguish between these possibilities.

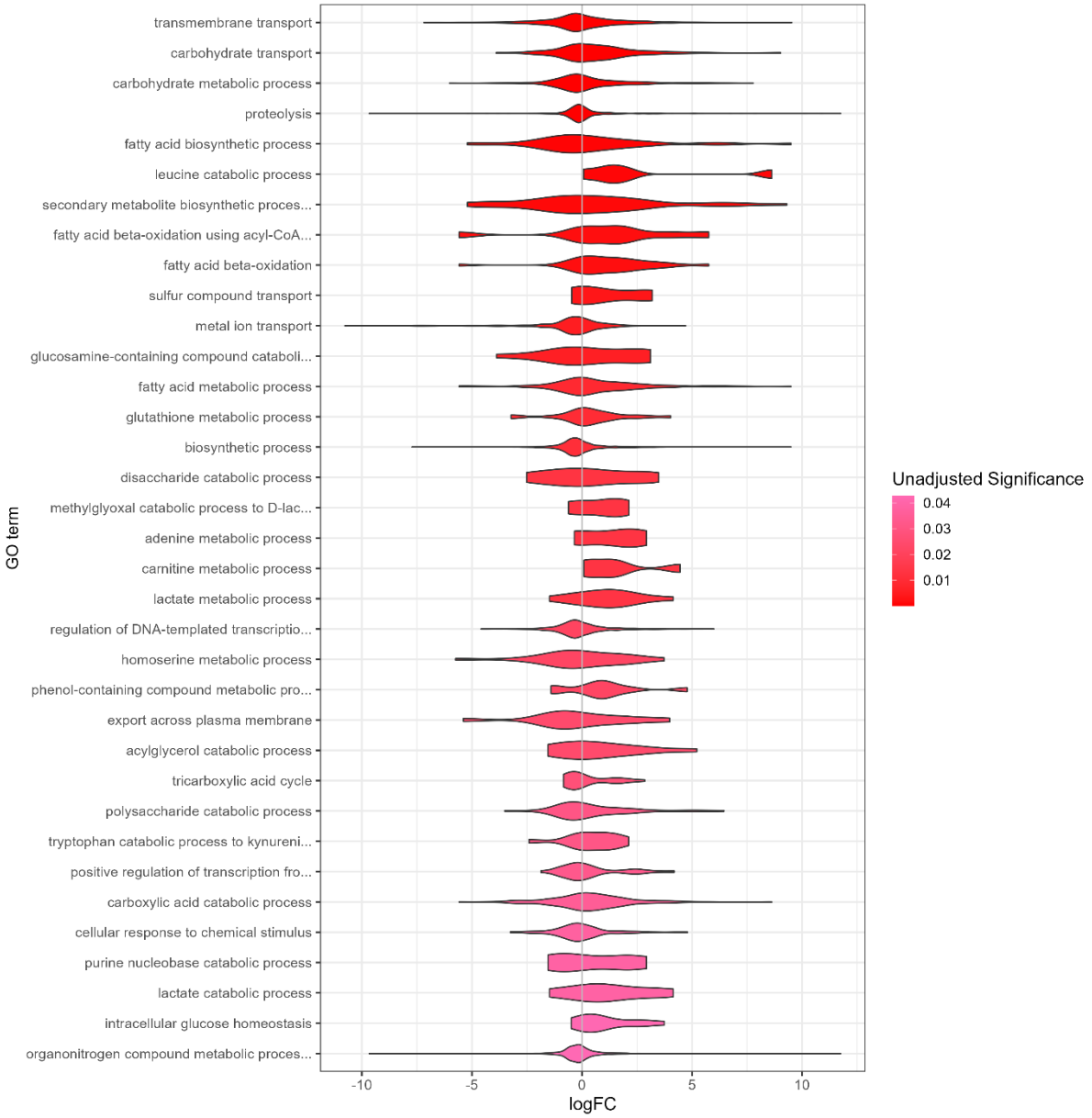

Figure 5.16. Violin plot representing the distribution of genes within significant ($P < 0.05$ before statistical adjustment) GO terms during *in situ* growth of *F. fujikuroi* SRM on *Pst* urediniospores. Terms are ordered from top to bottom in terms of significance according to an unadjusted Fisher's exact test. Each violin represents the density distribution of $\log_2$ fold change values for all differentially expressed genes within the corresponding GO term. The width of the violin indicates the number of genes at a given $\log_2$ fold change value. The shortened GO terms on the Y axis are: secondary metabolite biosynthetic process, fatty acid beta-oxidation using acyl-CoA dehydrogenase, glucosamine-containing compound catabolic process, methylgloxal catabolic process to D-lactate via S-lactoyl-glutathione, regulation of DNA-templated transcription, phenol-containing compound metabolic process, tryptophan catabolic process to kynurenine, positive regulation of transcription from RNA polymerase II promoter by galactose and organonitrogen compound metabolic process.

Carbohydrate and protein metabolism formed the core of *F. fujikuroi* SRM growth on *Pst* urediniospores (Figure 5.10). My investigation of secondary enriched GO terms revealed additional nutrient targets, together with an emphasis on transcriptional regulation, secondary metabolism, and the deployment of carbohydrate degrading enzymes (Figure 5.16).

Lipids were the only major nutrient class not represented within the core enriched terms of *F. fujikuroi* SRM. However, here I observed enrichment of fatty acid beta-oxidation (12 genes, 46.2%) and fatty acid beta-oxidation using acyl-CoA dehydrogenase (5 genes, 55.6%), indicating that lipids may also function as secondary nutrient targets during parasitism.

F. fujikuroi SRM shared several characteristics with the two *Penicillium* candidates. Alongside *P. brevicompactum* FRF and *P. copticola* SRB, it was one of the few candidates to enrich acylglycerol catabolism (4 genes, 30.1%), suggesting that this substrate may represent a more specialised nutrient source. I also observed enrichment of regulation of DNA-templated transcription (120 genes, 12.2%) and positive regulation of transcription from RNA polymerase II promoter by galactose (8 genes, 24.2%), indicating a substantial investment in transcriptional control during growth on *Pst* spores. Further enrichment of metal ion transport (13 genes, 11.5%) and cellular response to chemical stimulus (15 genes, 14.2%) suggests that *F. fujikuroi* SRM is capable of mounting a coordinated response following recognition of *Pst*.

Enrichment of secondary metabolite biosynthetic process (11 genes, 32.3%) suggests that production of potentially toxic metabolites contributes to the parasitic interaction. In addition, I observed enrichment of polysaccharide catabolic process (12 genes, 26.1%), indicating the deployment of cell wall degrading enzymes that may facilitate penetration of the *Pst* spore coat.

Together, these findings suggest that *F. fujikuroi* SRM primarily exploits carbohydrates and proteins while also making secondary use of lipid substrates. My results indicate that this candidate employs coordinated transcriptional regulation and environmental sensing to direct the production of secondary metabolites and carbohydrate degrading enzymes during parasitism. The strong similarities with the two *Penicillium* candidate hyperparasites, particularly in transcriptional regulation, stimulus response, and acylglycerol utilisation, may reflect convergent adaptation to exploitation of rust spores or the deployment of broadly conserved genetic programmes in response to their presence.

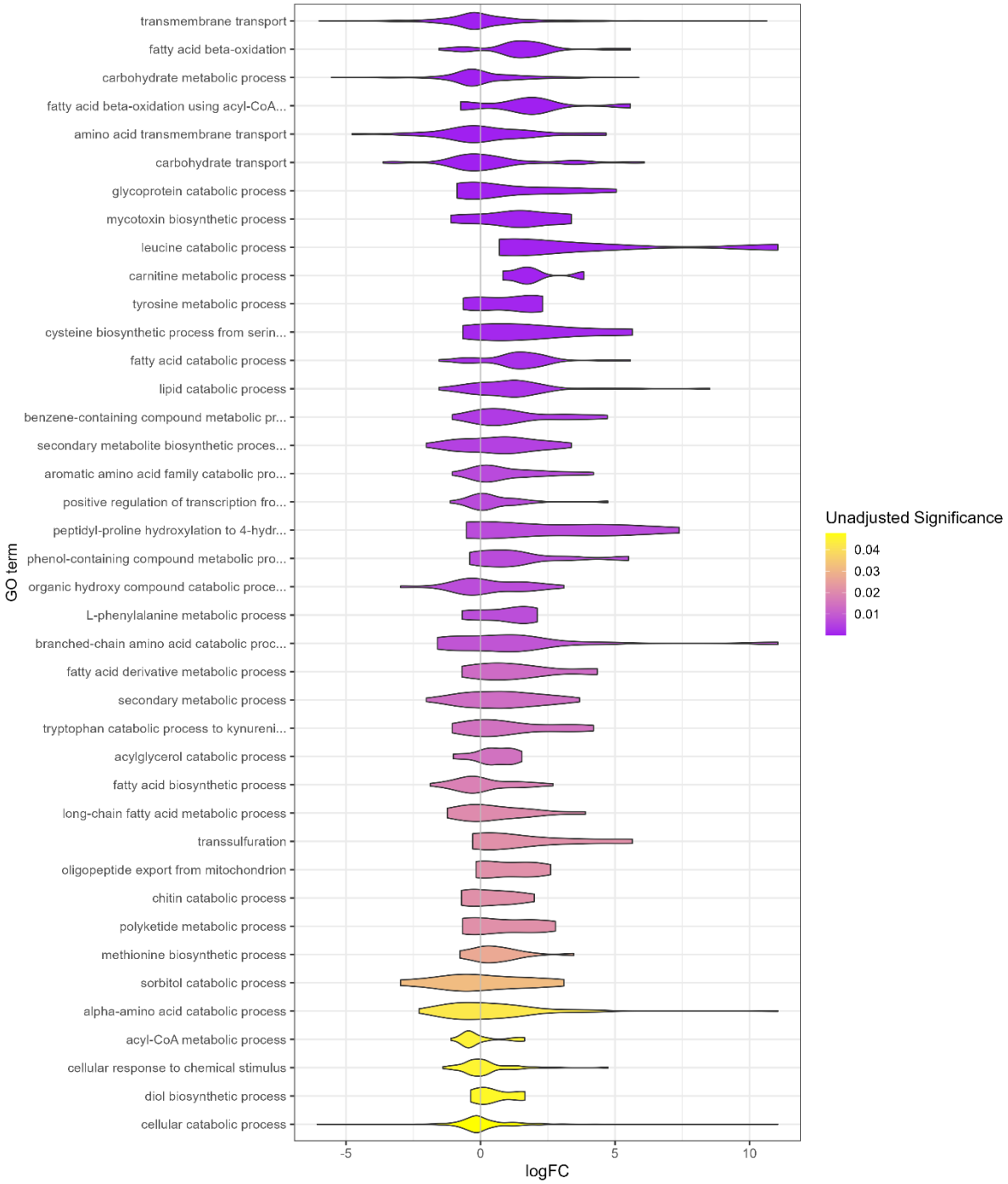

Figure 5.17. Violin plot representing the distribution of genes within significant ($P < 0.05$ before statistical adjustment) GO terms during *in situ* growth of *S. terricola* SRSh on *Pst* urediniospores. Terms are ordered from top to bottom in terms of significance according to an unadjusted Fisher's exact test. Each violin represents the density distribution of $\log_2$ fold change values for all differentially expressed genes within the corresponding GO term. The width of the violin indicates the number of genes at a given $\log_2$ fold change value. The shortened GO terms on the Y axis are: fatty acid beta-oxidation using acyl-CoA dehydrogenase, cysteine biosynthetic process from serine, benzene-containing compound metabolic process, secondary metabolite biosynthetic process, aromatic amino acid family catabolic

process, positive regulation of transcription from RNA polymerase II promoter by galactose, peptidyl-proline hydroxylation to 4-hydroxy-L-proline, phenol-containing compound metabolic process, organic hydroxy compound catabolic process and tryptophan catabolic process to kynureinine.

The core elements of *S. terricola* SRSh growth on *Pst* included metabolism of lipids and carbohydrates, together with the more specialised nutrient target of glycoproteins (Figure 5.10). Investigation of secondary GO terms revealed a strong emphasis on the production of secondary metabolites and deployment of cell wall degrading enzymes during *in situ* growth (Figure 5.17).

Lipids emerged as the dominant nutrient source for *S. terricola* SRSh, with enrichment of fatty acid catabolic process (26 genes, 70.2%), lipid catabolic process (36 genes, 53%), fatty acid derivative metabolic process (3 genes, 50%), and long-chain fatty acid metabolic process (4 genes, 33.3%). I also observed enrichment of leucine metabolism (4 genes, 80%), carnitine metabolism (4 genes, 80%), tyrosine metabolism (5 genes, 55.5%), and L-phenylalanine metabolism (3 genes, 60%), suggesting that these amino acids may function as secondary nutrient sources. *S. terricola* SRSh was one of the few candidates to enrich acylglycerol catabolism (4 genes, 36.4%), further supporting the idea that acylglycerol represents a specialised nutrient source available to fungi equipped to exploit it.

Secondary metabolism appeared to be a major component of the possible parasitic strategy. I observed enrichment of mycotoxin biosynthesis (5 genes, 62.5%), secondary metabolite biosynthesis (12 genes, 37.5%), secondary metabolic process (19 genes, 38.8%), and polyketide metabolic process (3 genes, 42.3%), suggesting extensive production of potentially antagonistic compounds during interaction with *Pst*. As with most of the other candidates, *S. terricola* SRSh also appeared to invest in cell wall degradation, upregulating three of its seven genes related to chitin catabolism (42.9%).

Interestingly, I also observed enrichment of cellular response to chemical stimulus (15 genes, 16.9%), a GO term that was primarily associated with candidates that targeted glycerol or acylglycerol. This relationship may simply be coincidental, but it may also reflect adaptation for recognising and exploiting these specialised substrates or a response to metabolites generated during their degradation.

Overall, my results suggest that *S. terricola* SRSh adopts a strongly antagonistic parasitic strategy centred on lipid utilisation. Carbohydrates and proteins appear to function as additional nutrient sources, while extensive secondary metabolite production may inhibit *Pst* prior to invasion mediated through the secretion of cell wall degrading enzymes.

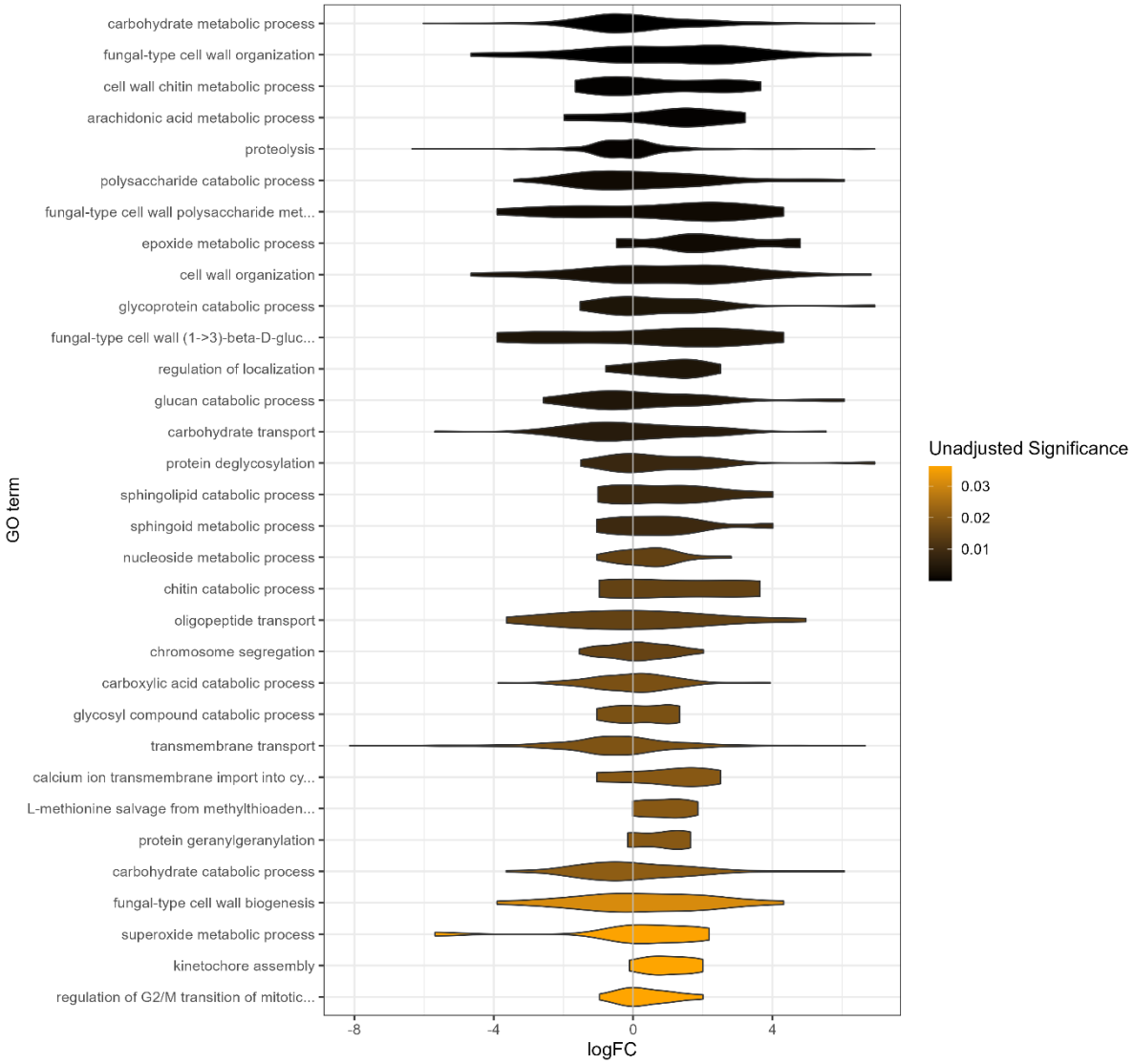

Figure 5.18. Violin plot representing the distribution of genes within significant (P < 0.05 before statistical adjustment) GO terms during *in situ* growth of *E. italicum* SRSi on *Pst* urediniospores. Terms are ranked from top to bottom in terms of significance according to an unadjusted Fisher's exact test. Each violin represents the density distribution of $\log_2$ fold change values for all differentially expressed genes within the corresponding GO term. The width of the violin indicates the number of genes at a given $\log_2$ fold change value. The shortened GO terms on the Y axis are: fungal-type cell wall polysaccharide metabolic process, fungal-type cell wall (1->3)-beta-D-glucan biosynthetic process, calcium ion transmembrane transport into cytosol, L-methionine salvage from methylthioadenosine and regulation of G2/M transition of mitotic cell cycle.

The core aspects of growth of *E. italicum* SRSi on *Pst* spores were fungal-type cell wall organisation and carbohydrate metabolism (Figure 5.10). This unique GO enrichment profile suggested that reinforcement of the fungal cell wall and production of cell wall degrading enzymes were the principal

drivers behind its distinctive phenotype. Investigation of secondary enriched GO terms revealed further expansion of both processes, together with the catabolism of additional nutrient sources (Figure 5.18).

Epicoccum italicum SRSi primarily focused on the breakdown and utilisation of carbohydrates, although I also observed enrichment of proteolysis (46 genes, 13.7%), indicating that amino acids may function as secondary nutrient sources. Lipid utilisation appeared to play only a minor role, with enrichment limited to sphingolipid catabolic process (5 genes, 55.5%). Additional nutrient targets included glycoproteins (9 genes, 42.9%), glycosyl compounds (3 genes, 33.3%), and arachidonic acid (6 genes, 66.6%).

Importantly, I did not observe enrichment of any GO terms related to secondary metabolism or the production of toxic metabolites. Instead, the transcriptomic profile of *E. italicum* SRSi suggested a strategy centred on degradation of the host cell wall and remodelling of its own cell wall to facilitate mechanical penetration of *Pst* spores. I observed enrichment of polysaccharide catabolism (19 genes, 35.8%), glucan catabolism (10 genes, 33.3%), chitin catabolism (4 genes, 50%), and carbohydrate catabolism (32 genes, 28.1%), indicating extensive investment in degradation of the *Pst* spore coat.

This was accompanied by substantial enrichment of pathways associated with fungal cell wall growth and reinforcement, including fungal-type cell wall organisation (16 genes, 51.6%), cell wall chitin metabolic process (6 genes, 40%), fungal-type cell wall polysaccharide metabolism (9 genes, 56.3%), cell wall organisation (22 genes, 51.2%), fungal-type cell wall (1→3)-beta-D-glucan biosynthetic process (5 genes, 55.6%), and fungal-type cell wall biogenesis (10 genes, 40%). I observed enrichment of kinetochore assembly (3 genes, 50%) and regulation of G2/M transition of the mitotic cell cycle (4 genes, 23.6%), which may facilitate rapid hyphal growth.

Overall, *E. italicum* SRSi displayed the most distinctive potential parasitic strategy of any candidate. In contrast to the majority of the other isolates, it showed limited investment in lipid and protein utilisation and was one of only two candidates that did not enrich pathways related to toxic secondary metabolite production. Instead, my results suggest that *E. italicum* SRSi relies primarily on enzymatic weakening of the *Pst* spore coat followed by mechanical penetration supported by reinforcement and remodelling of its own cell wall, with carbohydrates serving as the principal nutrient source. This interpretation is consistent with the phenotype I observed during *in vitro* assays of *E. italicum* SRSi growing on *Pst* (Supplementary Figure 5.1).

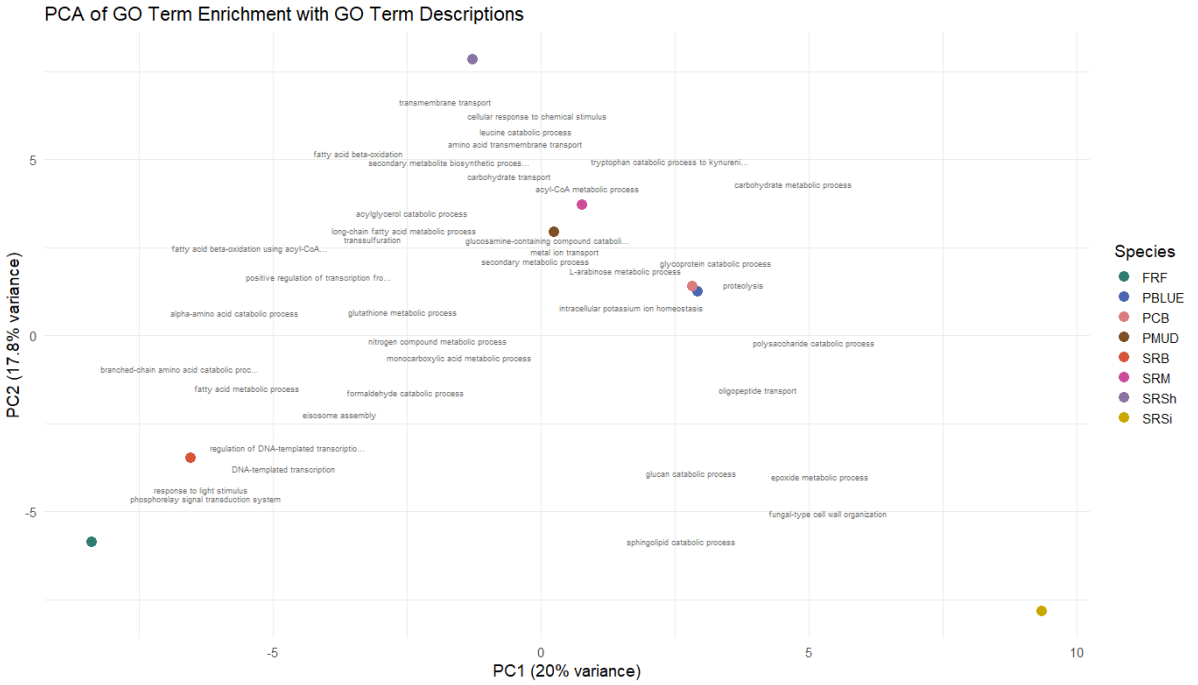

Figure 5.19. Principal Component Analysis (PCA) of GO term enrichment profiles across eight putative hyperparasitic fungi during growth on *Pst* urediniospores, compared to growth on PDA. Each point represents an individual fungal isolate, coloured uniquely. Overlaid GO term labels correspond to loadings that contribute to variation among candidates, scaled to fit within the PCA space.

A Principal Component Analysis (PCA) of all GO terms enriched during growth on *Pst* urediniospores revealed distinct clustering patterns among the eight candidates (Figure 5.19). The first two principal components accounted for approximately 38% of the total variance (PC1: 20.0%, PC2: 17.8%), capturing the major axes of functional differentiation.

Alternaria prunicola PMUD, *F. fujikuroi* SRM, *T. crotocingenum* PCB, and *C. austrohaemisphericum* PBLUE clustered towards the centre of the plot. I hypothesise that this clustering reflects the sharing of traits that appear characteristic of rust hyperparasitism, including moderate production of secondary metabolites, deployment of cell wall degrading enzymes, utilisation of carbohydrates, lipids, and proteins, and transmembrane transport processes.

The more distinctly separated candidates appear to possess additional specialised features beyond these common traits. *P. brevicompactum* FRF and *P. copticola* SRB clustered together, likely reflecting their shared emphasis on environmental sensing, signalling, and transcriptional regulation. These features were particularly prominent in the two *Penicillium* isolates and may represent an important component of their parasitic strategy.

S. terricola SRSh was separated from the remaining candidates, potentially reflecting its strong emphasis on secondary metabolite biosynthesis and suggesting a greater reliance on chemical antagonism during interaction with *Pst* spores. *E. italicum* SRSi displayed the most distinct GO enrichment profile, which was also reflected in the PCA. Its separation from the other candidates likely reflects its extensive investment in glucan catabolism and fungal cell wall remodelling, processes that were uniquely emphasised by this isolate and are consistent with its distinctive mechanical mode of parasitism.

The results of the GO enrichment analysis further support the conclusions I draw in Chapter Two regarding the importance of cell wall degradation, production of secondary metabolites, and predicted nutrient targets during rust hyperparasitism. I observed strong and consistent patterns in both nutrient acquisition and parasitic strategies during *in situ* growth on *Pst* urediniospores.

Pst spores consist of approximately 22% carbohydrates, 20% lipids, and 25% protein (Staples & Wynn 1965; Tulloch *et al.,* 1959), making these the major nutrient resources available to hyperparasites. Accordingly, I observed metabolism of these three substrates across the majority of candidates. Importantly, metabolism of all three major nutrient classes was only represented within the core enriched terms of *C. austrohaemisphericum* PBLUE and *A. prunicola* PMUD. These were also the two candidates that mobilised the smallest proportion of their gene sets during *in situ* growth, suggesting that they may possess relatively streamlined and highly specialised transcriptional programmes capable of efficiently exploiting all major nutrient sources. In contrast, the remaining candidates appeared to preferentially target one or two major nutrients, with the others acting as secondary nutrient sources.

As was the case for *P. coffeae* ANU01 (Chapter Two), *P. brevicompactum* FRF and *P. copticola* SRB showed a strong preference for lipid utilisation during growth on *Pst*. The repeated observation of this pattern across three *Penicillium* isolates suggests that members of this genus may preferentially exploit fatty acids during rust parasitism. Other distinctive nutritional strategies included the strong reliance on carbohydrates displayed by *E. italicum* SRSi and the emphasis on protein metabolism observed in *F. fujikuroi* SRM.

The molecular mechanisms deployed during parasitism also showed consistent patterns across candidates. I observed enrichment of secondary metabolite production in all isolates except *E. italicum* SRSi and *T. crotocingenum* PCB. *S. terricola* SRSh and *A. prunicola* PMUD showed particularly strong emphasis on the production of potentially toxic metabolites, suggesting that chemical antagonism may play an important role in their interaction with *Pst*. This also represents the second report of *P. brevicompactum* potentially using secondary metabolites during growth on rust fungi, following observations that the species can inhibit germination of *P. coronata* (Wilson *et al.,* 2020).

The absence of enriched secondary metabolism pathways in *E. italicum* SRSi and *T. crotocingenum* PCB suggests that these candidates may rely on alternative mechanisms of antagonism. *T. crotocingenum* PCB was the only isolate to specifically enrich cell wall macromolecule catabolism, while the distinctive transcriptomic profile and phenotype of *E. italicum* SRSi suggest that it may rely more heavily on mechanical penetration than chemical inhibition. Production of secondary metabolites is energetically expensive, and their widespread enrichment across the majority of candidates suggests that there may be strong selective pressure to inhibit *Pst* prior to invasion. Such inhibition may prevent the rust from germinating and exhausting its nutrient reserves or may suppress active defence responses that could interfere with hyperparasitism. Following antagonism, degradation of carbohydrates, including glucans and chitin, was a common feature across all candidates, highlighting the importance of penetrating the carbohydrate-rich *Pst* spore coat before access to internal nutrient reserves can occur.

I further explored broad functions important to parasitism by investigating the upregulation of genes within Clusters of Orthologous Genes (COG) terms during *in situ* growth.

Upregulation of genes within COG categories further reveals broad functional processes associated with growth of the eight candidates on *Pst*

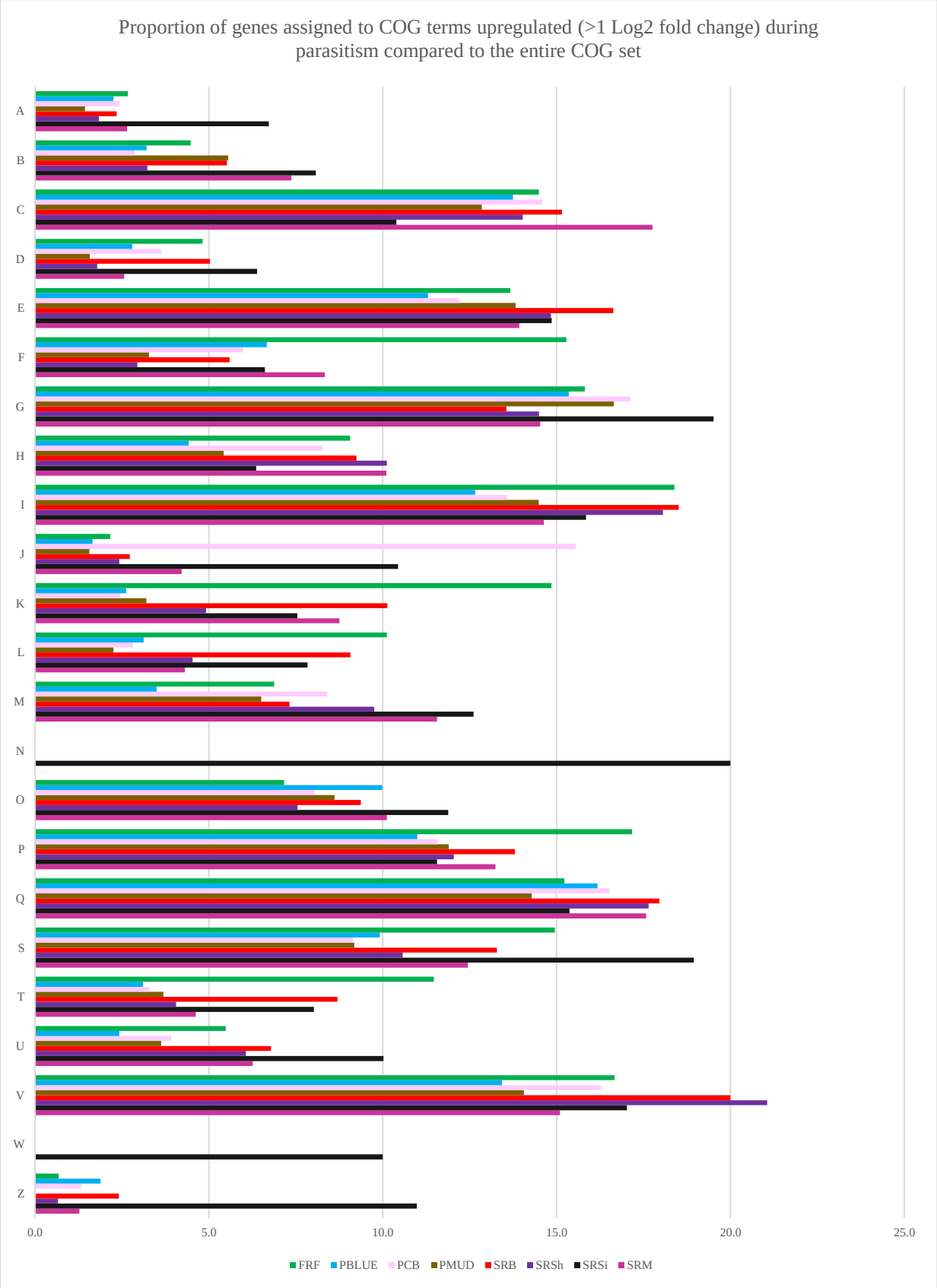

Figure 5.20. Bar graph showing the proportion (%) of genes within each Cluster of Orthologous Groups (COG) functional category that are upregulated (Log_2 fold change > 1) during growth on *Pst* spores in eight different hyperparasite candidates. Each COG category is represented on the X axis with individual bars representing each candidate hyperparasite. Bars are colour-coded by isolate to allow direct comparison across within categories. The Y axis indicates the proportion (%) of genes within each category that are upregulated. COG categories are abbreviated using the standard COG codes. Each COG family is identified as follows; A, RNA processing and modification, B, Chromatin structure and dynamics, C, Energy production and conversion, D, Cell cycle control, cell division, chromosome partitioning, E, Amino acid metabolism and transport, F, Nucleotide transport and metabolism, G, Carbohydrate transport and metabolism, H, Coenzyme transport and metabolism, I, Lipid transport and metabolism, J, Translation, ribosomal structure and biogenesis, K, Transcription, L, Replication, recombination and repair, M, Cell wall/membrane/envelope biogenesis, N, Cell motility, O, Post-translational modification, P, Inorganic ion transport and metabolism, Q, Secondary metabolites biosynthesis, S, Function unknown, T, Signal transduction mechanisms, U, Intracellular trafficking, secretion and vesicular transport, V, Defence mechanisms, W, Extracellular structures, Y, Nuclear structure and Z, Cytoskeleton.

COG analysis identified 9,507 genes (average 1,188 per genome) that were both differentially expressed during growth on *Pst* and assigned to at least one functional category. A summary of COG enrichment patterns across isolates is presented in Figure 5.20. Overall, growth on *Pst* was characterised by broad activation of genes associated with core metabolic activity, including energy production, transport, and macromolecule metabolism. However, the proportion of genes assigned to individual COG categories varied considerably between candidates, indicating substantial differences in transcriptional investment across functional processes during *in situ* growth.

Genes within COG categories related to metabolism were enriched across the candidates during growth on *Pst*

Candidates upregulated an average of 14.1% of their genes related to energy production and conversion. *F. fujikuroi* SRM upregulated the highest proportion (17.8%), whereas *E. italicum* SRSi upregulated the lowest (10.4%). The greater investment in genes associated with energy production and conversion suggests that *F. fujikuroi* SRM may possess a broader capacity to exploit the nutrients available within *Pst*. In contrast, *E. italicum* SRSi appeared to place greater emphasis on carbohydrate utilisation (see below), potentially reflecting a more specialised nutrient acquisition strategy.

Carbohydrate transport and metabolism was the most universally enriched category (average 15.9% of genes upregulated), consistent with the requirement to degrade the polysaccharide-rich *Pst* urediniospore wall prior to nutrient access. *E. italicum* SRSi showed the highest proportional

upregulation of carbohydrate-associated genes (19.5%), followed by *T. crotocingenum* PCB (17.1%), suggesting a strong reliance on carbohydrate degradation and utilisation in these isolates. In contrast, *P. copticola* SRB exhibited the lowest proportion (13.6%), potentially reflecting a greater relative emphasis on alternative nutrient sources. Lipid transport and metabolism was the second most consistently enriched nutrient-related category (average 15.8%). This signal was strongest in the two *Penicillium* isolates, *P. copticola* SRB (18.5%) and *P. brevicompactum* FRF (18.4%), suggesting a comparatively greater reliance on fatty acid utilisation. In contrast, *C. austrohaemisphericum* PBLUE showed the lowest lipid-associated expression (12.7%), despite fatty acid β-oxidation being a core GO term, indicating potential differences in the breadth versus specificity of lipid utilisation strategies. Amino acid transport and metabolism was also broadly enriched (average 13.9%), with the highest levels observed in *P. copticola* SRB (16.6%), followed by *E. italicum* SRSi and *S. terricola* SRSh (both 14.8%). This suggests that protein-derived nutrients represent an important but more variable component of the nutritional strategy across candidates. Collectively, these patterns indicate that all candidates exploit the major nutrient classes present in *Pst* urediniospores, but differ in the relative emphasis placed on carbohydrate, lipid, and amino acid metabolism, consistent with possible divergence in substrate utilisation strategies.

Secondary metabolism and defence mechanisms were enriched in candidates during growth on *Pst*

Candidates upregulated an average of 16.3% of their genes related to secondary metabolism. The highest proportions were observed in *P. copticola* SRB (18.0%) and *S. terricola* SRSh (17.6%), while the lowest occurred in *A. prunicola* PMUD (14.9%). Alongside secondary metabolism, genes related to defence mechanisms were also highly upregulated during in situ growth on *Pst*. On average, 16.7% of genes assigned to defence mechanisms were upregulated. Again, I observed the highest proportions in *S. terricola* SRSh (21.1%) and *P. copticola* SRB (20.0%), while the lowest occurred in *A. prunicola* PMUD (14.1%) and *C. austrohaemisphericum* PBLUE (13.4%). *Sarocladium terricola* SRSh also showed the strongest enrichment of secondary metabolism-related GO terms. In contrast, the relatively low proportion of upregulated COG genes related to secondary metabolism in *A. prunicola* PMUD was surprising, given that this candidate also exhibited substantial GO enrichment for secondary metabolite biosynthesis, as did *C. austrohaemisphericum* PBLUE. The relatively small number of genes upregulated by *A. prunicola* PMUD and *C. austrohaemisphericum* PBLUE may indicate a more streamlined and specialised set of genes involved in parasitism.

The widespread upregulation of genes related to defence mechanisms may reflect protection against either host-derived responses or the toxic effects of self-produced secondary metabolites. The observation that *S. terricola* SRSh and *P. copticola* SRB exhibited both the highest levels of secondary

metabolism-related gene upregulation and the strongest investment in defence mechanisms suggests that protection against self-produced secondary metabolites may be the more likely explanation.

An upregulation in genes related to transmembrane transport and enzymatic action suggests they are important to candidates during growth on *Pst*

Coenzyme transport and metabolism encompasses the synthesis, transport and utilisation of cofactors that support a wide range of cellular processes (Galperin *et al.*, 2021). This category was particularly enriched in *S. terricola* SRSh (10.1%), *F. fujikuroi* SRM (10.1%), *P. copticola* SRB (9.2%) and *P. brevicompactum* FRF (9.1%), compared with a global average of 7.9%. Upregulation of genes within this category may reflect increased demand for cofactors associated with amino acid and lipid metabolism, both of which were also highly represented in these four candidates. Inorganic ion transport and metabolism was enriched across all candidates during *in situ* growth, with an average of 12.8% of genes upregulated. This category was particularly enriched in *P. brevicompactum* FRF (17.2%) and *P. copticola* SRB (13.8%). The upregulation of these genes likely reflects increased acquisition of inorganic ions required as enzyme cofactors and signalling molecules during growth on *Pst* (McCord & Fridovich 1969). A small proportion of genes related to intracellular trafficking, secretion and vesicular transport were upregulated across candidates, with an average of 5.6% of genes assigned to this category. *Epicoccum italicum* SRSi showed the greatest investment (10.0%), whereas *C. austrohaemisphericum* PBLUE upregulated only 2.4% of genes within this category. These genes may contribute to the secretion of enzymes, effector proteins and secondary metabolites involved in host colonisation and nutrient acquisition.

Genes related to sensing, signalling and transcription were uniquely enriched in the two *Penicillium* candidates during *in situ* growth

As expected, *P. brevicompactum* FRF (11.5%) and *P. copticola* SRB (8.7%) were the candidates with the highest proportions of upregulated genes related to signal transduction mechanisms. Unexpectedly, *E. italicum* SRSi also upregulated a relatively high proportion of genes within this category (8.0%), compared with a collective average of 5.9%. Genes related to transcription reflected the results of the GO enrichment analysis, with the highest proportions observed in the two *Penicillium* isolates, *P. brevicompactum* FRF (14.9%) and *P. copticola* SRB (10.1%), as well as *F. fujikuroi* SRM (8.8%), compared with a global average of 6.8%. Similarly, genes related to replication, recombination and repair were most highly upregulated in the two *Penicillium* isolates (*P. brevicompactum* FRF, 10.1%; *P. copticola* SRB, 9.1%), compared with a global average of 5.5%. I hypothesise that increased investment in these regulatory and genomic maintenance processes may be characteristic of the *Penicillium* approach to parasitism. Such a strong emphasis on sensing, signalling and transcription was not observed during growth of *P. coffeae* ANU01 on *Pst* pustules (Chapter Two). However, this

difference may reflect the distinct experimental systems used, namely RNA extracted from *P. coffeae* ANU01 growing on *Pst* pustules on wheat leaves compared with growth of the candidates on isolated *Pst* spores *in vitro*. The concurrent upregulation of genes associated with repair, stress responses and signalling in the *Penicillium* isolates suggests that they may interact particularly intensively with *Pst* during parasitism.

Candidates showed an investment in protein synthesis and processing

Genes related to nucleotide transport and metabolism showed greater variation between candidates than most other COG categories. *P. brevicompactum* FRF upregulated 15.8% of genes assigned to this category, substantially higher than the next highest candidate, *F. fujikuroi* SRM (8.3%). This pattern may be related to the increased importance of signalling processes observed in *P. brevicompactum* FRF (Figure 5.11) and, to a lesser extent, *F. fujikuroi* SRM (Figure 5.16), although this relationship was not evident in *P. copticola* SRB, which upregulated only 5.6% of genes within this category. Nevertheless, the substantial investment observed in *P. brevicompactum* FRF suggests that nucleotide metabolism and associated regulatory processes may be characteristic of its approach to parasitising *Pst*. Genes involved in translation, ribosomal structure and biogenesis were particularly highly upregulated in *T. crotocingenum* PCB (15.6%) and *E. italicum* SRSi (10.4%), compared with a global average of 5.1%. My analysis showed these two candidates also shared an emphasis on carbohydrate degradation and the production of lytic enzymes throughout this chapter. Increased investment in translation and ribosome biogenesis may therefore support elevated synthesis of these enzymes, although it could also reflect increased cellular growth and proliferation. Genes related to RNA processing and modification were relatively evenly upregulated across the eight isolates, with the exception of *E. italicum* SRSi, which upregulated 6.7% of genes assigned to this category. In contrast, the remaining candidates ranged from 1.4% in *A. prunicola* PMUD to 2.7% in *P. brevicompactum* FRF, with a global average of 2.8%. *Epicoccum italicum* SRSi again exhibited the highest proportion of upregulated genes related to chromatin structure and dynamics (8.1%), followed closely by *F. fujikuroi* SRM (7.4%), compared with a global average of 5.0%. Genes related to post-translational modification, protein turnover and chaperones were more uniformly upregulated across candidates, with an average of 9.1% of genes assigned to this category showing increased expression.

***Epicoccum italicum* SRSi showed unique upregulation in genes related to growth, cell wall remodelling, the cytoskeleton and cell motility**

Epicoccum italicum SRSi again emphasised the importance of regulation of cell structure, upregulating the highest proportion of genes related to cell wall/membrane/envelope biogenesis (12.6%). It was closely followed by *F. fujikuroi* SRM (11.6%) and *S. terricola* SRSh (9.6%), compared with a global average of 8.3%. The upregulation of these genes, particularly in fungi that I isolated from *Pst*, suggests

that this trait may be associated with specialisation for growth on rust fungi. *Epicoccum italicum* SRSi also upregulated the highest proportion of genes related to the cytoskeleton (11%), compared with a global average of 2.4%. I hypothesise that these genes may contribute to reinforcement of the fungal cell wall and cytoskeleton, facilitating mechanical lysis of *Pst* spores by invading hyphae. *Epicoccum italicum* SRSi was also the only candidate to upregulate genes assigned to the cell motility (20%) and extracellular structures (10%) COG categories. Together, these categories suggest that *E. italicum* SRSi may uniquely mobilise and reinforce its hyphae to penetrate and grow through *Pst* spores via mechanical action, as I believe I observed *in vitro* (Supplementary Figure 5.1). Chromatin plays a central role in gene regulation and the formation of compact chromosomes during cell division (Brosch *et al.*, 2008). The increased investment in chromatin-related processes observed in *E. italicum* SRSi may be associated with its unique potential phenotype of aggressive growth and apparent physical lysis of *Pst* spores. This hypothesis is supported by *E. italicum* SRSi exhibiting the highest proportion of upregulated genes related to cell cycle control, cell division and chromosome partitioning (6.4%), compared with a global average of 3.6%. Together, these findings suggest that *E. italicum* SRSi may invest more heavily in cellular proliferation and growth than the other candidate hyperparasites. Finally, an average of 12.3% of genes with unknown functions were upregulated across the candidates. Based on its unique phenotype, I expected *E. italicum* SRSi to contain the highest proportion of such genes, which it did (18.9%), followed by the two *Penicillium* isolates, *P. brevicompactum* FRF (15.0%) and *P. copticola* SRB (13.3%).

Similarities in COG enrichment between candidates primarily centred on secondary metabolism, carbohydrate metabolism and, to a lesser extent, lipid and amino acid metabolism. In contrast, candidate-specific patterns were most apparent in categories related to gene regulation, signalling and cell wall remodelling. Consistent with my GO enrichment analysis, both *Penicillium* isolates were distinguished by increased enrichment of genes associated with signalling, transcription and replication. The prominence of sensing and signalling processes in these candidates suggests they may be particularly effective at coordinating complex responses during growth on *Pst* compared with the other candidates.

The GO enrichment analysis also suggested that *E. italicum* SRSi and *T. crotocingenum* PCB may rely more heavily on cell wall-degrading enzymes and mechanical invasion to antagonise and kill *Pst* spores, rather than primarily employing chemical antagonism through secondary metabolite production. The distinctive COG enrichment profiles of these candidates may be linked to this strategy. In particular, the COG results reinforce the GO enrichment evidence for the unique biology underlying the phenotype of *E. italicum* SRSi. This isolate was the only candidate to upregulate genes related to cell motility and extracellular structures during parasitism, and it exhibited by far the highest proportion of upregulated genes related to the cytoskeleton. Together, these categories suggest that enhanced hyphal movement

and reinforcement of cellular structures may contribute to the physical penetration of *Pst* spores observed in *E. italicum* SRSi. Based on these findings, I predict that more detailed phenotypic characterisation may reveal *T. crotocingenum* PCB to possess a phenotype more similar to that of *E. italicum* SRSi than was initially apparent.

Investigating the top 20 most upregulated genes during growth on *Pst* reveals commonly upregulated genes and further insight into potential hyperparasitic strategy

I went beyond broad functional groups to examine which genes were at the very pinnacle of upregulation during growth on *Pst* spores. I did this by investigating the functional annotation of the top 20 most upregulated genes in each candidate during *in situ* growth, to identify possible cornerstone genes in parasitism. Importantly, setting the cut-off for this investigation at the 20th gene will always be an arbitrary decision, and due to word constraints, I am unable to describe each of the 160 top genes individually. Instead, for each candidate I selected a few genes from amongst the top 20 that appeared to contribute the most strongly to more understanding of its possible mode of action, and discuss them below. Finally, as with the GO and COG analysis I present in this thesis, the results of this analysis are based purely on gene expression data and therefore remain speculative until validated with further experiments.

Investigating the top 20 most upregulated genes during growth of *P. brevicompactum* FRF on *Pst* urediniospores

The 20 most upregulated genes in *P. brevicompactum* FRF during growth on *Pst* reinforced the major patterns identified in the GO and COG enrichment analyses, highlighting roles for cell wall degradation, secondary metabolism, signalling, and exploitation of lipid-derived nutrients. Rather than being dominated by a single functional category, the most highly expressed genes suggest that *P. brevicompactum* FRF coordinates several complementary mechanisms during growth *in situ*. The entire list of *P. brevicompactum* FRF genes, their functional annotation and regulation during *in situ* growth is presented in Supplementary Table 5.1.

Genes associated with degradation of the *Pst* spore coat were strongly represented among the most highly upregulated transcripts. The most upregulated gene, *PenFRF_002044-T1* (10.23 Log_2 fold change), encoded a secreted M35 metallopeptidase, a fungalysin family protease that may contribute to either antagonism of *Pst* or degradation of host proteins for nutrient acquisition (Ökmen *et al.*, 2018). Carbohydrate degradation was represented by the secreted CE5 cutinase *PenFRF_001707-T1* (7.70 Log_2 fold change) and the GH5 endo-α-1,6-mannanase *PenFRF_006336-T1* (5.96 Log_2 fold change). The absence of cutin from *Pst* spores (Xiao *et al.*, 2023) suggests that the CE5 cutinase may have been

co-opted to assist in degradation of the polysaccharide-rich rust spore coat (Armendáriz-Ruiz *et al.*, 2018; Novy *et al.*, 2021).

As with the GO and COG enrichment, the top expressed genes also supported a major role for signalling and secondary metabolism during parasitism. Three of the top 20 genes were associated with biosynthetic gene clusters, including a CE5 enzyme within an NRPS cluster, a fatty acid hydroxylase belonging to a T1PKS-betalactone cluster, and a transporter encoded within a T3PKS cluster. None of these clusters showed similarity to characterised biosynthetic pathways, raising the possibility that they encode metabolites specific to rust parasitism. Signalling-related genes were also highly represented, including the phosphatidylinositol transfer protein CSR1 encoding gene *PenFRF_008038-T1* (6.79 Log_2 fold change) and the Ras GTPase encoding *PenFRF_011166-T2* (6.50 Log_2 fold change). The upregulation of *CSR1* in both *P. copticola* SRB and *P. coffeae* ANU01 (Chapter Two) suggests that lipid-mediated signalling may be a conserved feature of *Penicillium* rust hyperparasitism.

Several of the highly expressed genes were consistent with the lipid-focused nutritional strategy that I observed in the functional enrichment analyses. The *STL1* glycerol transporter gene *PenFRF_011195-T1* (6.27 Log_2 fold change) was strongly upregulated and may facilitate uptake of glycerol released during fatty acid degradation. As with *CSR1*, an *STL1* transporter gene was also in the top 20 most upregulated genes in *P. coffeae* ANU01, suggesting that utilisation of glycerol may be another characteristic feature of *Penicillium* growth on rust spores. In addition, two secreted thaumatin-like protein encoding genes *PenFRF_009526-T1* (7.60 Log_2 fold change) and *PenFRF_009217-T1* (5.46 Log_2 fold change), which produce proteins secreted as antifungal effectors and associated with managing environmental stress (de Jesus-Pires *et al.*, 2020), may contribute to antagonism of *Pst* or defence against host-derived proteins.

Notably, four of the top 20 genes lacked any functional annotation, while a further two encoded only predicted secreted proteins. The abundance of highly expressed but uncharacterised genes, particularly those predicted to be secreted, suggests that novel proteins involved in antagonism or nutrient acquisition remain to be identified.

Overall, the most highly upregulated genes in *P. brevicompactum* FRF support the broader transcriptomic patterns identified in GO and COG analysis. Secreted proteases and CAZymes may facilitate penetration of the *Pst* spore coat, signalling pathways may coordinate the parasitic process, biosynthetic gene clusters may mediate chemical antagonism, and glycerol transporters support exploitation of lipid-derived nutrients.

Investigating the top 20 most upregulated genes during growth of *P. copticola* SRB on *Pst* urediniospores

The 20 most upregulated genes in *P. copticola* SRB during *in situ* growth on *Pst* reinforced the major patterns I observed in the GO and COG enrichment analyses, highlighting roles for signalling, secondary metabolism, lipid utilisation, and strong similarities to the other *Penicillium* candidates investigated in this study. A notable feature of the transcriptomic profile was the abundance of highly expressed genes with little or no functional annotation, suggesting that important aspects of *P. copticola* SRB parasitism remain to be characterised. The entire list of *P. copticola* SRB genes, their functional annotation and regulation during *in situ* growth is presented in Supplementary Table 5.2.

The most upregulated gene, *PenSRB_008749-T1* (8.39 Log_2 fold change), lacked any annotation beyond belonging to an NRPS-like biosynthetic gene cluster with no similarity to known clusters. This pattern continued in the second (*PenSRB_004126-T1*; 7.70 Log_2 fold change), third (*PenSRB_005596-T1*; 7.36 Log_2 fold change), and fourth (*PenSRB_001514-T1*; 7.30 Log_2 fold change) most highly upregulated genes, all of which lacked functional annotation. In total, four of the top 20 genes belonged to unidentified biosynthetic gene clusters, including two genes predicted to encode a transporter and an anion channel within the same NRPS-like cluster. These findings further support the importance of secondary metabolism during growth on *Pst* and raise the possibility that *P. copticola* SRB produces metabolites unique to rust parasitism.

The top expressed genes also supported the lipid-focused nutritional strategy that I observed in the functional enrichment analyses. The STL1 glycerol transporter gene *PenSRB_009983-T1* (6.20 Log_2 fold change) was strongly upregulated and, importantly, *STL1* was also among the most highly expressed genes in the other two *Penicillium* isolates examined. In this study, I only identified *STL1* within *Penicillium* genomes, suggesting that glycerol uptake may represent a conserved mechanism that facilitates exploitation of lipid-derived nutrients during rust parasitism. Similarly, the CSR1 phosphatidylinositol transfer protein encoding gene *PenSRB_011778-T1* (6.47 Log_2 fold change also highly expressed in *P. brevicompactum* FRF and *P. coffeae* ANU01, may contribute to the lipid-mediated signalling processes that appear characteristic of *Penicillium* growth on *Pst*.

Genes potentially involved in antagonism were also represented among the most highly expressed transcripts. The secreted CE5 cutinase *PenSRB_009468-T1* (6.66 Log_2 fold change) was the only CAZyme present in the top 20 genes and may assist other carbohydrate degrading enzymes in weakening the *Pst* spore coat (Novy *et al.*, 2021). In addition, the secreted thaumatin-like protein, encode by *PenSRB_008229-T1* (7.22 Log_2 fold change), an aspect also shared with *P. brevicompactum* FRF, may contribute to antagonism of *Pst* or protection against host-derived defence molecules. Only four of the top 20 genes encoded predicted secreted proteins, while many lacked any functional

annotation, including one gene containing only a secretion signal peptide and another containing only a predicted transmembrane domain.

Overall, the most highly upregulated genes of *P. copticola* SRB provide the potential molecular mechanisms underlying the broader transcriptomic patterns identified in this study. The repeated upregulation of *STL1*, *CSR1*, and thaumatin-like genes, together with the abundance of genes associated with uncharacterised biosynthetic gene clusters, highlights strong similarities between *Penicillium* candidates and suggests that these fungi may possess a distinctive genetic toolkit for exploitation of rust spores. Alternatively, these genes may represent a broader *Penicillium* repertoire that is simply preferentially deployed when rust spores are encountered.

Investigating the top 20 most upregulated genes during growth of *C. austrohaemisphericum* PBLUE on *Pst* urediniospores

The 20 most upregulated genes in *C. austrohaemisphericum* PBLUE during growth on *Pst* reinforced the importance of cell wall degradation, nutrient acquisition, and active interaction with the host. The transcriptomic profile was dominated by secreted enzymes, particularly CAZymes and proteases. The entire list of *C. austrohaemisphericum* PBLUE genes, their functional annotation and regulation during *in situ* growth is presented in Supplementary Table 5.3.

The two most highly upregulated genes encoded secreted carbohydrate-active enzymes. The most upregulated gene, *CladBLUE_002287-T1* (8.89 Log_2 fold change), encoded a secreted CE5 cutinase, while the second most upregulated gene, *CladBLUE_010352-T1* (8.38 Log_2 fold change), encoded a secreted GH75 chitosanase. Together, these enzymes may act cooperatively to weaken the protective layers of the *Pst* spore coat. Although chitosan is absent from mature rust spores and is instead associated with the germ tube, the repeated upregulation of GH75 chitosanases in rust hyperparasites, including *P. coffeae* ANU01 (Chapter Two), suggests these enzymes may facilitate entry through the germ pore, as has been proposed for other rust hyperparasitic fungi (Srivastava *et al.*, 1985). Six of the top 20 genes encoded CAZymes, including a GH5 (*CladBLUE_000017-T1*, 7.12 Log_2 fold change) and a GH43 (*CladBLUE_004360-T1*, 5.56 Log_2 fold change) glycoside hydrolase and a CE-CBM (*CladBLUE_005137-T1*, 8.14 Log_2 fold change) hybrid enzyme, while the AA4 (*CladBLUE_012377-T1*, 5.4 Log_2 fold change) FAD-dependent oxidase may enhance the activity of these enzymes through redox reactions (Trisolini *et al.*, 2019).

Protein degradation also appeared to be an important aspect of parasitism. Two of the top 20 genes encoded secreted metalloproteases, including an M43B protease *CladBLUE_002298-T1* (5.97 Log_2 fold change) and an M36 fungalysin *CladBLUE_009677-T1* (5.65 Log_2 fold change), which may function both as antagonistic effectors and as enzymes to liberate amino acids from *Pst* tissues. Nine of the top

20 genes encoded predicted secreted proteins, the highest proportion observed among the candidates, suggesting that *C. austrohaemisphericum* PBLUE maintains extensive extracellular interaction with its host during parasitism.

Secondary metabolism was less dominant than in the *Penicillium* isolates, although two of the top 20 genes belonged to previously uncharacterised biosynthetic gene clusters. Namely *CladBLUE_010339-T1* (8.17 Log_2 fold change), a component of a T1PKS BGC and *CladBLUE_004360-T1* (5.56 Log_2 fold change) a component of a NRPS-like BGC. In addition, the iron-dependent dehydrogenase/isopenicillin N synthase gene *CladBLUE_003461-T1* (5.78 Log_2 fold change) may contribute to biosynthesis of secondary metabolites and could explain the increased emphasis on iron uptake I observed in the GO enrichment analysis (Figure 5.13). A secreted thaumatin-like protein was also highly upregulated through *CladBLUE_002615-T1* (5.75 Log_2 fold change), suggesting that antagonism remains an important component of the interaction with *Pst*.

Several highly expressed metabolic genes further supported the broad nutrient utilisation strategy that I observed in the GO and COG analyses. A short-chain dehydrogenase (*CladBLUE_004500-T1* (5.7 Log_2 fold change)) may contribute to metabolism of liberated *Pst*-derived nutrients (Kavanagh *et al.*, 2008) while strong upregulation of an acid/histidine phosphatase (*CladBLUE_002343-T1* (5.37 Log_2 fold change)), together with enrichment of phosphate transport (Figure 5.15), suggests phosphate may also represent an important nutrient target during parasitism (Bull *et al.*, 2002). Four of the top 20 genes lacked any functional annotation, although none encoded predicted secreted proteins, suggesting that these uncharacterised genes may contribute primarily to intracellular metabolic processes.

Overall, I predict that the most highly upregulated genes of *C. austrohaemisphericum* PBLUE support a strategy centred on enzymatic degradation of the rust spore coat, active extracellular interaction with the host, and efficient utilisation of multiple nutrient sources. Compared with the *Penicillium* candidates, fewer highly expressed genes were associated with biosynthetic gene clusters, while the abundance of secreted CAZymes and proteases suggests that physical degradation of host structures is a particularly important feature of *C. austrohaemisphericum* PBLUE parasitism.

Investigating the top 20 most upregulated genes during growth of *A. prunicola* PMUD on *Pst* urediniospores

The 20 most upregulated genes in *A. prunicola* PMUD during growth on *Pst* spores reinforced the multifaceted parasitic strategy identified in the GO enrichment analyses, highlighting the importance of cell wall degradation, protein catabolism, lipid utilisation, and secondary metabolism. This observation is particularly notable given that PMUD mobilised the smallest proportion of its genome during *in situ* growth, suggesting that it may utilise a relatively streamlined set of specialised genes. The entire list of

A. prunicola PMUD genes, their functional annotation and regulation during *in situ* growth is presented in Supplementary Table 5.4.

The most upregulated gene was the secreted S01E serine peptidase *AltPMUD_000352-T1* (8.05 Log_2 fold change), which is likely involved in the breakdown of proteins in *Pst* (Muszewska *et al.*, 2017). The second most upregulated gene was the secreted PL1 CAZyme gene *AltPMUD_012265-T1* (8.05 Log_2 fold change). Polysaccharide lyase 1 enzymes are known to catalyse the degradation of pectin in plant cell walls (Atanasova *et al.*, 2018); however, during growth on *Pst*, this enzyme may be repurposed to degrade polysaccharides present within the rust spore coat. This process could be aided by *AltPMUD_007285-T1* (6.58 Log_2 fold change), encoding a secreted CE5 cutinase. Carbohydrate esterase 5 enzymes consistently ranked among the top 20 upregulated genes in candidates isolated from rust species outside of *Pst* and here I again hypothesise that they assist more aggressive glycoside hydrolases in degrading the *Pst* spore coat. In *A. prunicola* PMUD, the CE5 enzyme may specifically facilitate the activity of the GH28 encoding gene *AltPMUD_000869-T1* (7.50 Log_2 fold change) during degradation of the host spore coat. The final two CAZymes in the top 20 genes were the secreted AA9 enzyme encoding genes *AltPMUD_002570-T1* (7.14 Log_2 fold change) and *AltPMUD_010675-T1* (6.21 Log_2 fold change). AA9 enzymes facilitate polysaccharide breakdown through oxidation rather than hydrolysis (Corrêa *et al.*, 2016). Like the CE5 enzyme, these AA9s may contribute to weakening the spore coat through oxidative attack on tough polysaccharides.

Protein degradation was also strongly represented among the most highly expressed genes. In addition to *AltPMUD_000352-T1*, *A. prunicola* PMUD upregulated the S08A peptidase gene *AltPMUD_003030-T1* (7.53 Log_2 fold change), likely to degrade proteins in *Pst* (Page & Cera 2008), and the M35 metallopeptidase deuterolysin gene *AltPMUD_013613-T1* (6.10 Log_2 fold change), which may similarly function in antagonism and nutrient acquisition. The simultaneous presence of multiple CAZymes and proteases among the top 20 genes supports the conclusion that *A. prunicola* PMUD actively targets both the carbohydrate-rich spore coat and the internal protein reserves of *Pst*.

Although GO enrichment suggested an important role for secondary metabolism, only a single biosynthetic gene cluster component appeared among the top 20 genes. *AltPMUD_003411-T1* (6.05 Log_2 fold change) encoded an nMRA-like domain protein associated with a terpene biosynthetic gene cluster of unknown function. nMRA proteins are regulatory proteins involved in nitrogen metabolism and frequently act as molecular switches in secondary metabolism (Zhao *et al.*, 2010). A second nMRA-like gene, *AltPMUD_008010-T1* (6.32 Log_2 fold change), was also strongly upregulated and may perform a similar regulatory role. The presence of only one biosynthetic gene cluster component among the most highly expressed genes is consistent with the broader pattern observed throughout the

transcriptome, where *A. prunicola* PMUD appeared to achieve effective growth on *Pst* while mobilising comparatively few genes.

Several additional genes highlighted adaptation to growth on lipid-rich substrates. Two TauD/TfdA-like genes, *AltPMUD_012019-T1* (7.68 Log_2 fold change) and *AltPMUD_005065-T1* (7.49 Log_2 fold change), were among the most highly upregulated. These enzymes, also present among the top 20 genes of both *T. crotocingenum* PCB and *S. terricola* SRSh, are involved in making complex molecules more accessible for metabolism (Sundar Rajan *et al.,* 2025). *Alternaria prunicola* PMUD also strongly upregulated both transcript variants of the isocitrate lyase gene *ICL1*, *AltPMUD_011349-T2* (7.12 Log_2 fold change) and *AltPMUD_011349-T1* (6.36 Log_2 fold change). Isocitrate lyases facilitate growth on substrates rich in acetate, lipids, and fatty acids (Dunn *et al.,* 2009), suggesting adaptation to utilise host-derived lipids during parasitism. Similarly, the *YAT1* carnitine O-acetyltransferase gene *AltPMUD_008286-T2* (5.92 Log_2 fold change), which converts acetyl-CoA into acetyl-carnitine, is involved in fatty acid β-oxidation and utilisation of acetate and fatty acids for growth (Strijbis *et al.,* 2010).

Overall, the most highly upregulated genes of *A. prunicola* PMUD support a strategy centred on aggressive degradation of the *Pst* spore coat through a combination of CAZymes, oxidative enzymes, and proteases. At the same time, multiple genes involved in lipid metabolism suggest adaptation to exploit fatty acids released from the host, while the presence of regulatory genes associated with secondary metabolism indicates that chemical antagonism may also contribute to parasitism. Despite mobilising relatively few genes compared to other candidates, *A. prunicola* PMUD consistently exhibited strong representation of genes associated with nutrient acquisition, antagonism, and metabolic flexibility. This further supports the hypothesis that *A. prunicola* PMUD possesses a streamlined but highly effective genetic toolkit for exploitation of rust spores.

Investigating the top 20 most upregulated genes during growth of *T. crotocingenum* PCB on *Pst* urediniospores

The 20 most upregulated genes of *T. crotocingenum* PCB during growth on *Pst* spores reinforced the importance of carbohydrate degradation and nutrient acquisition observed in the GO enrichment analysis. The transcriptomic profile was dominated by secreted CAZymes, suggesting that degradation of the *Pst* spore coat is a central component of its parasitism. The entire list of *T. crotocingenum* PCB genes, their functional annotation and regulation during *in situ* growth is presented in Supplementary Table 5.5.

The most upregulated gene, *TrichoPCB_005582-T1* (9.74 Log_2 fold change), encoded a secreted GH5 mannan endo-1,4-beta-mannosidase. Glycoside hydrolases were highly represented amongst the top 20

genes, including the GH5 enzyme encoding *TrichoPCB_010213-T1* (6.86 Log_2 fold change) and *TrichoPCB_005454-T1* (4.72 Log_2 fold change), the GH2 β-mannosidase encoding gene *TrichoPCB_005658-T1* (6.11 Log_2 fold change), and the GH76 encoding enzyme *TrichoPCB_005292-T1* (4.72 Log_2 fold change). Together with the secreted CE5 enzyme encoding gene *TrichoPCB_001883-T1* (4.73 Log_2 fold change), these proteins likely act cooperatively to degrade the polysaccharide-rich *Pst* spore coat. Six CAZymes were present amongst the top 20 most upregulated genes and eight encoded predicted secreted proteins, providing strong support for my hypothesis that *T. crotocingenum* PCB relies on extensive extracellular enzymatic activity to facilitate parasitism. The abundance of carbohydrate degrading enzymes also suggests that, beyond host penetration, carbohydrates represent a major nutrient source for the candidate.

Interestingly, despite the absence of significant enrichment for secondary metabolism-related GO terms, five of the top 20 genes were components of biosynthetic gene clusters. These included the GH5 enzyme gene *TrichoPCB_005582-T1* (9.74 Log_2 fold change) and the sugar transporter encoding gene *TrichoPCB_008964-T1* (8.11 Log_2 fold change), both associated with distinct NRPS clusters lacking similarity to known pathways. As a sugar transporter, *TrichoPCB_008964-T1* may also contribute directly to uptake of carbohydrates liberated from the spore coat. Choline is an essential membrane component in filamentous fungi (Markham *et al.*, 1993), and increased expression of this gene may support hyphal growth or reinforcement during penetration of *Pst* spores. Additional BGC-associated genes included those encoding a metallopeptidase *TrichoPCB_004283-T1* (4.86 Log_2 fold change) and a PdxA protein *TrichoPCB_004236-T1* (4.64 Log_2 fold change), both associated with uncharacterised clusters. The prevalence of highly expressed genes within unknown BGCs suggests that aspects of chemical antagonism in *T. crotocingenum* PCB remain unresolved and may represent mechanisms specific to rust parasitism.

Several highly expressed genes also suggested adaptation to stress and efficient exploitation of released nutrients. The second most upregulated gene, *TrichoPCB_005657-T1* (8.77 Log_2 fold change), encoded an FMN-dependent dehydrogenase/oxidoreductase that may facilitate metabolism of diverse substrates released during parasitism. The sulphate-phosphate transporter *TrichoPCB_007664-T1* (5.71 Log_2 fold change), together with the TauD/Tfd-like protein *TrichoPCB_001370-T1* (6.48 Log_2 fold change), suggests increased sulphur scavenging during growth on *Pst* spores. Additional metabolic enzymes included the flavin oxidoreductase gene *TrichoPCB_008077-T2* (4.77 Log_2 fold change), which may contribute to metabolism and detoxification (Qin *et al.*, 2025).

Overall, the most highly upregulated genes of *T. crotocingenum* PCB support a strategy centred on extensive enzymatic degradation of the *Pst* spore coat followed by efficient utilisation of released nutrients. While large-scale induction of secondary metabolism was not apparent from my GO or COG

enrichment analyses, the presence of multiple highly expressed genes within uncharacterised biosynthetic gene clusters suggests that chemical antagonism may still contribute to parasitism. Together, these results suggest that *T. crotocingenum* PCB relies primarily on extracellular enzymatic attack, supplemented by specialised metabolic and stress-response mechanisms that potentially facilitate growth on *Pst* spores.

Investigating the top 20 most upregulated genes during growth of *F. fujikuroi* SRM on *Pst* urediniospores

The 20 most upregulated genes of *F. fujikuroi* SRM during growth on *Pst* spores reinforced the major patterns identified in the GO and COG enrichment analyses, highlighting roles for secondary metabolism, protein degradation, lipid utilisation, and environmental sensing. Unlike most candidates, *F. fujikuroi* SRM showed little emphasis on carbohydrate-active enzymes amongst its most highly expressed genes. The entire list of *F. fujikuroi* SRM genes, their functional annotation and regulation during *in situ* growth is presented in Supplementary Table 5.6.

The most upregulated gene, *FusSRM_016914-T1* (12.76 Log_2 fold change), lacked any annotation beyond a predicted secretion signal peptide, suggesting it may encode a novel secreted effector involved in interaction with *Pst*. A notable feature of the transcriptomic profile was the prominence of proteases, with the second, third, and fourth most upregulated genes all encoding proteins involved in proteolysis. These included the G01 peptidase gene *FusSRM_014603-T1* (11.75 Log_2 fold change), which lacked a secretion signal peptide and may contribute to intracellular protein turnover, as well as the secreted A01A peptidase gene *FusSRM_006304-T1* (10.88 Log_2 fold change) and S53 serine peptidase gene *FusSRM_015845-T1* (10.12 Log_2 fold change), which may function in degradation of host proteins or liberation of amino acids for nutrition. In total, four proteases were present amongst the top 20 genes. Five genes encoded predicted secreted proteins, while no CAZymes were present. Together with the relatively low abundance of CAZymes within the genome of *F. fujikuroi* SRM, this suggests a reduced reliance on carbohydrate degradation compared to the other candidates.

Secondary metabolism was strongly represented amongst the most highly upregulated genes. Five of the top 20 genes were associated with biosynthetic gene clusters, several of which showed similarity to characterised pathways producing biologically active compounds. *FusSRM_002308-T1* (10.04 Log_2 fold change) encoded an unannotated secreted protein within an NRPS-like cluster lacking similarity to known pathways. Two highly expressed genes, *FusSRM_013410-T1* (10.03 Log_2 fold change) and *FusSRM_013415-T1* (8.28 Log_2 fold change), belonged to a T1PKS cluster with high similarity to the hydroxyl-fumonisin biosynthetic pathway. As fumonisins act by disrupting host metabolic processes (Stockmann-Juvala & Savolainen 2008), mobilisation of this cluster may contribute to antagonism of *Pst*. Similarly, the pyruvate kinase gene *FusSRM_010731-T1* (9.34 Log_2 fold change) was associated

with a T1PKS cluster showing similarity to fosfonochlorin phosphonate, an antibiotic secondary metabolite (Takeuchi *et al.,* 1989). Production of such compounds may allow *F. fujikuroi* SRM to suppress host metabolism and reduce consumption of self-derived nutrients by *Pst* prior to invasion. Additional evidence for chemical antagonism was provided by the methyltransferase gene *FusSRM_013089-T1* (8.54 Log_2 fold change), associated with an ACT-toxin II-like cluster, the UstYa-like mycotoxin biosynthesis gene *FusSRM_011954-T1* (9.31 Log_2 fold change), and the isopenicillin N synthase gene *FusSRM_010893-T1* (8.14 Log_2 fold change), which may contribute to antibiotic production (Huang *et al.,* 2022). Together, these genes suggest that deployment of toxic secondary metabolites is a major component of the *F. fujikuroi* SRM parasitic strategy.

The most highly expressed genes also supported the importance of lipid metabolism observed in the enrichment analyses. The FPS1 glycerol channel encoding gene *FusSRM_014773-T1* (9.02 Log_2 fold change) was strongly upregulated during growth on *Pst*. While FPS1 channels are typically associated with osmoregulation (Beese *et al.,* 2009), the abundance of lipid catabolic pathways observed in this study suggests that the protein may additionally facilitate uptake of glycerol liberated during fatty acid degradation (Klein *et al.,* 2017). The acyl-CoA dehydrogenase gene *FusSRM_009071*-T1 (8.63 Log_2 fold change), a key enzyme in the first step of fatty acid β-oxidation (Ghisla & Thorpe 2004), further supports utilisation of lipid reserves contained within *Pst* spores. These findings suggest that, alongside protein degradation, exploitation of lipid-derived nutrients is a major component of growth on *Pst*.

Unlike most candidates, carbohydrate degrading enzymes were largely absent from the top expressed genes, indicating that carbohydrates may represent a secondary nutrient target. Instead, *F. fujikuroi* SRM appears to invest heavily in production of toxic secondary metabolites, potentially to suppress host metabolism prior to invasion, while simultaneously mobilising proteases and lipid catabolic pathways to exploit nutrients released from *Pst* spores. Although cell wall degrading enzymes were not amongst the most highly expressed genes, GO and COG enrichment analyses indicate that carbohydrate metabolism and therefore host penetration is still likely an important component of the interaction, albeit one that appears less dominant than in many of the other candidate hyperparasites.

Investigating the top 20 most upregulated genes during growth of *S. terricola* SRSh on *Pst* urediniospores

The 20 most upregulated genes in *S. terricola* SRSh during growth on *Pst* spores reinforced the major patterns I identified in the GO enrichment analyses, highlighting an emphasis on secondary metabolism, lipid utilisation, nutrient scavenging, and transmembrane transport. Unlike most candidates, *S. terricola* SRSh showed little representation of carbohydrate-active enzymes among its most highly expressed genes, instead appearing to prioritise chemical antagonism and metabolic exploitation of host-derived

nutrients. The entire list of *S. terricola* SRSh genes, their functional annotation and regulation during *in situ* growth is presented in Supplementary Table 5.7.

The most upregulated gene during growth on *Pst* spores was the TauD/TfdA-like protein encoding gene *SaroSRSh_004477-T1* (11.88 Log_2 fold change), potentially acting to mobilise *Pst*-derived compounds. A second TauD/TfdA-like protein, *SaroSRSh_006654-T1* (8.38 Log_2 fold change), was also present among the top 20 genes, suggesting that the metabolism of complex host-derived compounds is an important aspect of growth on *Pst*. Five of the top 20 genes contained secretion signal peptides, indicating substantial interaction with the host during potential parasitic growth.

A striking feature of the transcriptomic profile was the absence of CAZymes among the top 20 most highly upregulated genes. Alongside *F. fujikuroi* SRM, *S. terricola* SRSh was the only candidate to show this pattern. Similarly, only a single protease appeared among the top genes, the S33 peptidase gene *SaroSRSh_001213-T1* (8.52 Log_2 fold change), which formed part of an NRPS biosynthetic gene cluster with low similarity to Apicidin. Apicidin is a histone deacetylase inhibitor that induces hyperacetylation of histones in protozoan and apicomplexan parasites (Darkin-Rattray *et al.,* 1996). Interestingly, I previously observed massive upregulation of a biosynthetic gene cluster with similarity to depudecin, another histone deacetylase inhibitor, during growth of *P. coffeae* ANU01 on *Pst* (Chapter Two). Taken together, these observations suggest that inhibition of histone deacetylases in *Pst* may represent a common strategy amongst hyperparasites that rely heavily on secondary metabolites. However, *P. copticola* SRB also contained the depudecin biosynthetic gene cluster but did not upregulate its genes during *in situ* growth, casting doubt on this hypothesis.

Secondary metabolism was further represented by three additional biosynthetic gene cluster-associated genes. The alcohol dehydrogenase gene *SaroSRSh_007827-T1* (10.37 Log_2 fold change) belonged to an unidentified NRPS biosynthetic gene cluster, while the secreted protein encoding gene *SaroSRSh_009147-T1* (7.84 Log_2 fold change) and iron-dependent dioxygenase gene *SaroSRSh_009151-T1* (7.39 Log_2 fold change) were both components of an NRPS-like cluster with no similarity to known biosynthetic pathways. As observed in several other candidates, the lack of annotation for highly upregulated biosynthetic genes suggests that these clusters may encode metabolites specifically involved in rust parasitism, a process that remains poorly understood.

The top expressed genes also supported the strong emphasis on lipid metabolism identified in the GO enrichment analyses. The acyl-CoA dehydrogenase gene *SaroSRSh_006593-T1* (11.06 Log_2 fold change) is likely upregulated to facilitate catabolism of the abundant fatty acids present within *Pst* spores (Ghisla & Thorpe 2004), potentially including acetate imported through the acetate transporter from *SaroSRSh_006592-T1* (9.34 Log_2 fold change). The alkanesulfonate monooxygenase gene *SaroSRSh_001736-T1* (9.48 Log_2 fold change) may similarly contribute to metabolism of fatty acids

and other assorted compounds (Ellis 2011). Together, these genes support the conclusion that lipids represent a major nutrient target for *S. terricola* SRSh during growth on *Pst*.

Nutrient scavenging and transport were also prominent features of the top 20 genes. The OPT6 oligopeptide transporter *SaroSRSh_011209-T1* (10.64 Log_2 fold change) was the fourth most upregulated gene and may facilitate uptake of peptides liberated through proteolysis (Pike *et al.*, 2009). Similarly, the sodium/solute urea symporter gene *SaroSRSh_001735-T1* (8.18 Log_2 fold change) may be involved in scavenging nitrogen from *Pst* spores (Henriquez *et al.*, 2021). Two major facilitator superfamily transporters, encoded by *SaroSRSh_008620-T1* (8.04 Log_2 fold change) and *SaroSRSh_004282-T1* (7.81 Log_2 fold change), further support the importance of transmembrane transport during parasitism and may function in either toxin export or nutrient uptake.

Overall, the most highly upregulated genes of *S. terricola* SRSh suggest a strategy centred on chemical antagonism and metabolic exploitation of host-derived nutrients. The candidate appears to deploy biosynthetic gene clusters that may interfere with host cellular regulation, while simultaneously upregulating genes involved in lipid metabolism, nutrient scavenging, and transmembrane transport. Unlike most other candidates, *S. terricola* SRSh lacked CAZymes among its most highly expressed genes, suggesting that direct enzymatic degradation of the spore wall is not the dominant feature of its highest-level transcriptional response. Importantly, both CAZymes and proteases were still significantly upregulated elsewhere in the transcriptome and therefore remain important components of parasitism. The choice of how many genes to consider among the "top" genes will always be somewhat arbitrary, yet examining these subsets remains valuable in identifying those genes most likely to play instrumental roles during growth on *Pst* spores.

The top 20 most upregulated genes during growth of *E. italicum* SRSi on *Pst* urediniospores

The 20 most upregulated genes in *E. italicum* SRSi during growth on *Pst* spores reinforced the distinctive transcriptomic profile identified in the GO enrichment analysis, highlighting an apparent emphasis on cell wall remodelling, extracellular antagonism, and physical invasion of host spores. Compared with most other candidates, relatively few highly upregulated CAZymes were observed, suggesting that *E. italicum* SRSi may rely on a smaller but highly effective set of enzymes combined with extensive host interaction and structural reinforcement. Notably, many of the most highly expressed genes lacked functional annotation, indicating that important components of the interaction remain poorly understood. The entire list of *E. italicum* SRSi genes, their functional annotation and regulation during *in situ* growth is presented in Supplementary Table 5.8.

The most upregulated gene, *EpicSRSi_009026-T1* (7.97 Log_2 fold change), lacked any annotation beyond the presence of a secretion signal peptide, potentially representing a novel effector or

extracellular protein involved in host interaction. Similarly, the second most upregulated gene, *EpicSRSi_006109-T1* (7.79 Log_2 fold change), contained no annotation beyond a predicted transmembrane localisation, suggesting a role in transport of an unknown metabolite or uptake of a specialised substrate. In total, eight of the top 20 genes were predicted to encode extracellularly secreted proteins, the highest proportion among the candidates and consistent with extensive interaction between putative parasite and host.

Unexpectedly, only two CAZymes were present within the top 20 genes, despite the strong enrichment of carbohydrate degradation terms observed in the GO analysis. The secreted GH71 glucan endo-1,3-alpha-glucosidase encoded by *EpicSRSi_011096-T1* (7.27 Log_2 fold change) is likely involved in degradation of the *Pst* spore coat and may facilitate the mechanical invasion phenotype observed *in vitro*. The GH47 MNS1 CAZyme encoded by *EpicSRSi_011725-T1* (6.94 Log_2 fold change) lacked a secretion signal peptide and is more likely involved in increased protein production and quality control during *in situ* growth (Hüttner *et al.*, 2014). Together, these genes may provide a streamlined but highly effective mechanism for weakening host structures while simultaneously reinforcing the parasite cell wall.

Proteolysis also appeared to contribute to the interaction. Two of the top 20 genes encoded secreted serine peptidases. *EpicSRSi_012516-T1* (6.48 Log_2 fold change) encodes an S01A serine endopeptidase likely involved in pathogenesis and extracellular protein degradation (Parente *et al.*, 2010). Similarly, *EpicSRSi_003796-T1* (6.48 Log_2 fold change) encodes a secreted S01E streptogrisin-type serine protease containing an alpha-lytic pro-domain. Such enzymes commonly function in aggressive extracellular proteolysis and may contribute to degradation of structural, defence, or cell-surface proteins associated with *Pst*.

Several highly expressed genes suggested that antagonism of *Pst* may also be important to the parasitic strategy of *E. italicum* SRSi. *EpicSRSi_006205-T1* (6.79 Log_2 fold change) lacked annotation beyond a secretion signal peptide and was the only top-ranked gene associated with a biosynthetic gene cluster. The gene belongs to a T1PKS-NRPS-like cluster with high similarity to the cluster responsible for production of 2,4-dihydroxy-5,6-dimethyl bezaldehyde, a metabolite with uncharacterised function (Wang *et al.*, 2014). Secreted Egh16-like virulence factors are commonly associated with the formation and penetration ability of appressorium by plant pathogens (Xue *et al.*, 2002). The Egh16-like gene possessed by *E. italicum* SRSi in *EpicSRSi_009405-T1* (7.72 Log_2 fold change) may act in a similar function in penetrating *Pst* spores, though this would require further phenotyping to determine.

In addition to genes associated with antagonism and host interaction, several highly upregulated genes pointed towards increased growth and metabolic activity. The phenylalanine-tRNA ligase encoded by *EpicSRSi_007612-T*1 (7.01 Log_2 fold change) likely supports elevated rates of translation required for

active growth (Xie *et al.,* 2025). The SUR7 transmembrane protein encoded by *EpicSRSi_001401-T1* (6.83 Log_2 fold change) is perhaps involved in maintaining cell wall integrity and plasma membrane organisation during invasion (Alvarez *et al.,* 2008), while the magnesium transporter encoded by *EpicSRSi_010422-T1* (6.66 Log_2 fold change) may facilitate uptake of magnesium required for numerous enzymatic reactions (Pasternak *et al.,* 2010).

Overall, the most highly upregulated genes of *E. italicum* SRSi support the hypothesis that this candidate employs a distinctive strategy compared with the other hyperparasites. Rather than strongly inducing large numbers of CAZymes or genes associated with secondary metabolism, *E. italicum* SRSi appears to rely on a limited but highly expressed set of carbohydrate degrading enzymes, extracellular proteases, and putative effector proteins, alongside extensive cell wall remodelling and reinforcement. These findings support the hypothesis generated from the GO enrichment analysis that *E. italicum* SRSi weakens the rust spore through targeted enzymatic action before physically penetrating and lysing the host, consistent with the aggressive invasion phenotype observed *in vitro*.

Across the eight candidates, growth on *Pst* urediniospores elicited a broadly shared strategy centred on antagonism of host spores, secretion of cell wall degrading enzymes, mobilisation of liberated nutrients through transmembrane transport, and rewiring of metabolic machinery to exploit host-derived resources. While these core processes were present in most candidates, clear lineage- and isolate-specific specialisations were evident in the identities of the most highly upregulated genes and the mechanisms used to achieve these functions.

Despite substantial variation between candidates, several genes or gene families were repeatedly among the most highly upregulated transcripts during *in situ* growth. The recurrent induction of these genes across phylogenetically distinct fungi suggests they may represent important components of rust hyperparasitism. I examine and discuss some of these potentially cornerstone genes below.

Identifying potential cornerstone genes in categories highly upregulated across all candidates during growth on *Pst*

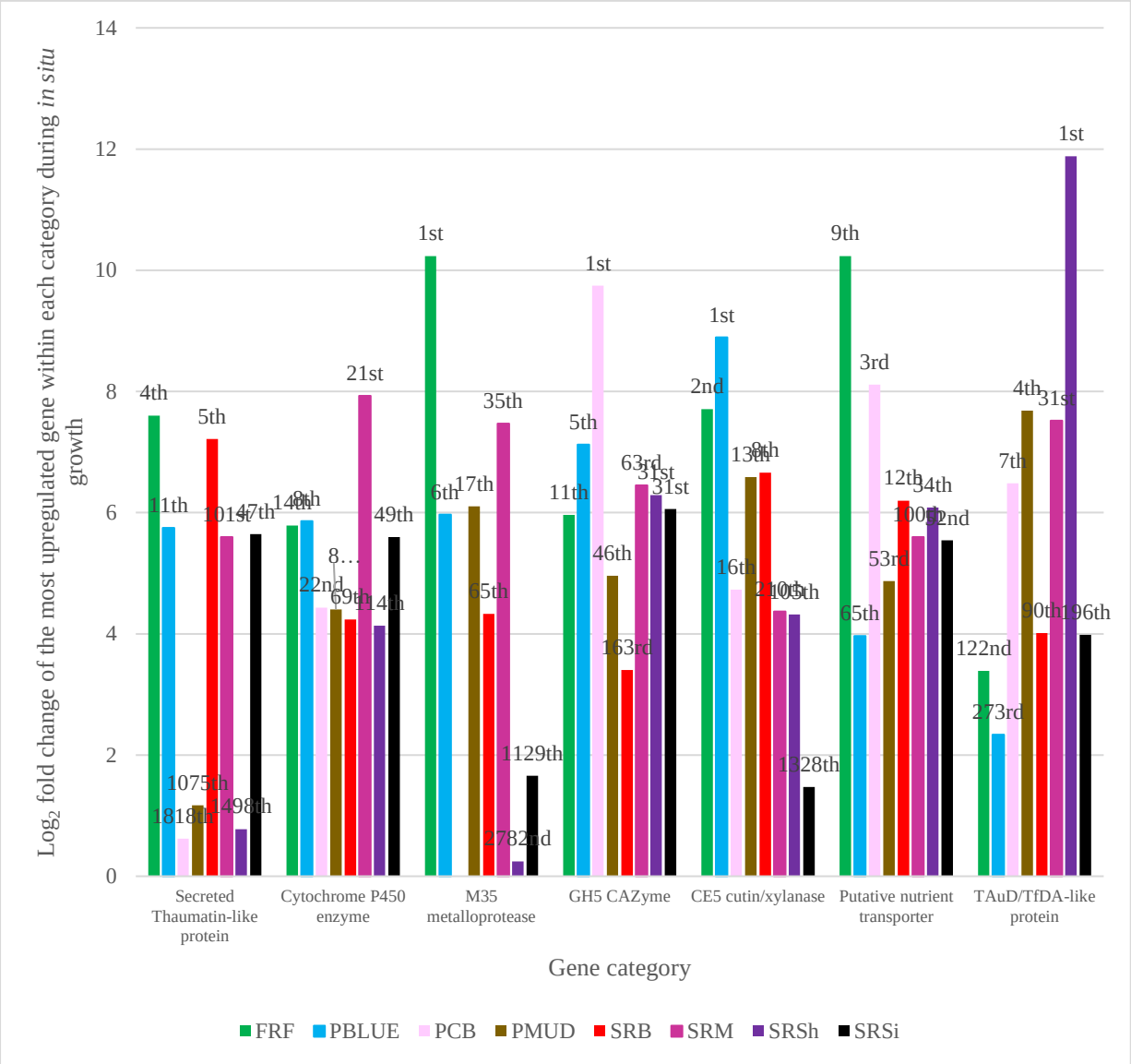

Figure 5.21. Bar graph showing the $\log_2$ fold change of the most upregulated gene within each designated functional gene type across the eight candidates. Numbers above the bars indicate the position within the list of genes, ranked by $\log_2$ fold change from highest to lowest.

Production of secondary metabolites was a major component of growth on *Pst*, reflected in GO and COG enrichment patterns as well as the most highly upregulated genes of individual candidates. Cytochrome P450 enzymes, which are essential for both secondary metabolite biosynthesis and xenobiotic detoxification (Črešnar & Petrič 2011), were highly upregulated across all eight candidates and were among the most strongly induced genes in several candidates (Figure 5.21). Cytochrome P450s appeared in the top 20 genes for *P. brevicompactum* FRF and *C. austrohaemisphericum* PBLUE, the top 50 genes for *E. italicum* SRSi, *F. fujikuroi* SRM and *T. crotocingenum* PCB and the top 150

genes for *A. prunicola* PMUD, *P. copticola* SRB and *S. terricola* SRSh. Based on the literature (Nasini *et al.*, 2004; Wilson *et al.*, 2020), and my observations of *P. coffeae* ANU01 growing on *Pst* in Chapter Two, I hypothesised that antagonistic secondary metabolites form a fundamental component of the parasitic process, potentially inhibiting *Pst* germination and suppressing host defences prior to invasion. The widespread upregulation of cytochrome P450s during *in situ* growth strongly supports this hypothesis. Interestingly, cytochrome P450s appeared less prominent in *S. terricola* SRSh despite this candidate showing the strongest overall evidence of secondary metabolite biosynthesis, suggesting that alternative biosynthetic pathways or regulatory mechanisms may contribute to metabolite production in this candidate. Together, the recurrent upregulation of cytochrome P450s, enrichment of secondary metabolism-related functional categories, and mobilisation of numerous biosynthetic gene clusters emphasise the importance of secondary metabolite production during parasitism of *Pst*. However, the lack of functional annotation for most induced biosynthetic gene clusters limits interpretation of the specific compounds involved. These uncharacterised clusters may encode metabolites specialised for rust parasitism and therefore represent promising targets for future investigation.

Thaumatin-like proteins are often secreted as antifungal effectors and can also play important roles in mediating responses to environmental stress (de Jesus-Pires *et al.*, 2020). I observed a thaumatin-like protein-encoding gene among the 20 most upregulated genes in three of the eight candidates: *P. brevicompactum* FRF, *P. copticola* SRB, and *C. austrohaemisphericum* PBLUE. Thaumatin-like genes were also highly upregulated in both *E. italicum* SRSi and *F. fujikuroi* SRM. In contrast, thaumatin-like proteins did not appear to be relevant to *T. crotocingenum* PCB, *S. terricola* SRSh, or *A. prunicola* PMUD, where they were absent from even the top 1000 upregulated genes. In *P. brevicompactum* FRF, *P. copticola* SRB, and *F. fujikuroi* SRM, thaumatin-like proteins may contribute to the extensive environmental sensing and signalling observed during parasitic growth. Importantly, *S. terricola* SRSh and *A. prunicola* PMUD were among the candidates in which I observed the greatest degree of SM production during *in situ* growth. The absence of thaumatin-like proteins from their transcriptomes suggests that these species may rely more heavily on SM-mediated antagonism of *Pst*. More broadly, thaumatin-like proteins may form part of a larger antagonistic strategy, acting in concert with antifungal SMs to suppress rust spores before they can germinate or mount defensive responses.

M35 metalloproteases primarily function as secreted fungal effectors, facilitating virulence on plant tissue as well as breaking down proteins into smaller amino acids for absorption (Ökmen *et al.*, 2018; Pan *et al.*, 2020). A M35 fungalysin enzyme was the most upregulated gene in *P. brevicompactum* FRF during *in situ* growth, and was within the top 20 most upregulated genes for *C. austrohaemisphericum* PBLUE and *A. prunicola* PMUD. I observed a fungalysin within the top 100 genes for *P. copticola* SRB and *F. fujikuroi* SRM. Fungalysins were not as important to *S. terricola* SRSh and *E. italicum* SRSi where they only appeared as the 1129th and 2782nd most upregulated genes respectively. A

fungalysin was not upregulated whatsoever in *T. crotocingenum* PCB during *in situ* growth. Fungalysins may form a component of the enriched proteolysis that I observed in *C. austrohaemisphericum* PBLUE, *A. prunicola* PMUD and *F. fujikuroi* SRM. I did not observe proteolysis as a core aspect of growth of *P. brevicompactum* FRF on *Pst* spores, making the upregulation of a M35 fungalysin in its dataset unexpected. In this candidate, the enzyme may function primarily as an antagonistic or virulence factor rather than as a protease used to break down substrates for nutrition. Conversely, *E. italicum* SRSi and *T. crotocingenum* PCB showed a much stronger emphasis on carbohydrate catabolism during *in situ* growth. Their lack of upregulated fungalysins suggest these candidates prioritise degradation of the carbohydrate-rich spore coat over protein acquisition. Together, these results indicate that while fungalysins are not universally required for rust parasitism, they might represent an important component of the parasitic toolkit in candidates that place greater emphasis on antagonism and protein utilisation.

Following antagonism of the host, a hyperparasite must still penetrate the tough *Pst* spore coat to access the abundant nutrients contained within. The spore coat is rich in protective polysaccharides, including chitin and β-glucans (Xiao *et al.*, 2023), and in Chapter Two I established the likely importance of cell wall degrading enzymes in overcoming this barrier. Consistent with this hypothesis, all candidates showed evidence of extensive cell wall degradation during *in situ* growth, primarily through the upregulation of secreted CAZymes and other extracellular enzymes. While the specific enzymes deployed varied between candidates, degradation of the carbohydrate-rich spore coat emerged as one of the most conserved features of parasitism, highlighting its importance as a prerequisite for nutrient acquisition from *Pst*.

GH5 CAZymes are secreted enzymes involved in the degradation of beta-glucans (Qi *et al.*, 2025). GH5 CAZymes were relevant and highly upregulated in all eight candidates, making them one of the most consistently upregulated gene families observed during growth on *Pst* (Figure 5.21). Their importance was particularly evident in *T. crotocingenum* PCB, where a GH5 was the most upregulated gene and two additional GH5 enzymes were present within the top 20 most upregulated genes. This observation is consistent with the GO and COG enrichment profile of *T. crotocingenum* PCB, which suggested a greater reliance on cell wall degradation than secondary metabolite production during parasitism. GH5 enzymes were also among the most highly upregulated genes in several other candidates, including *P. brevicompactum* FRF and *C. austrohaemisphericum* PBLUE, where they were in the top 20 most upregulated genes. A GH5 CAZyme was also in the top 50 for *A. prunicola* PMUD, *S. terricola* SRSh and *E. italicum* SRSi and was the 63rd and 163rd most upregulated gene for *F. fujikuroi* SRM and *P. copticola* SRB respectively. I hypothesise GH5 CAZymes are the predominant factor behind degradation of the rust spore coat during parasitism. More than any other aspect of parasitism, cleaving

polysaccharides in the rust spore coat appeared to be absolutely fundamental to growth on *Pst* across the candidates.

CE5 CAZymes primarily act as cutin/xylan targeting enzymes, helping break down polysaccharides in the plant cell wall (Novy *et al.,* 2021). As both cutin and xylan are absent in *Pst*, I hypothesise that within the context of *in situ* growth these enzymes are upregulated to assist other more aggressive cell wall degrading enzymes, such as GH5s, in breaking down polysaccharides in the rust spore coat. A secreted CE5 enzyme was present in the top 20 most upregulated genes for all of the candidates, except those that I originally isolated from *Pst*; *E. italicum* SRSi, *F. fujikuroi* SRM and *S. terricola* SRSh. CE5 enzymes appeared significantly less important to *Pst*-hyperparasites, especially *E. italicum* SRSi where a CE5 first appeared only as the 1328th most upregulated gene during *in situ* growth. The reduced significance in fungi isolated from *Pst* suggests that assistant CE5 enzymes may be required for candidates that are not accustomed to degrading polysaccharides in the spore coat of *Pst* specifically, to assist their less specialised GHs to action. I believe this is a small but perhaps significant piece of evidence regarding questions of hyperparasite host range and specialisation of the niche.

I hypothesised that the ultimate reason for rust parasitism was the uptake of nutrients from *Pst*, in part through the action of transmembrane transporters. As such, I observed highly upregulated nutrient transporters in all candidates. A sugar transporter was in the top 20 most upregulated genes for *P. brevicompactum* FRF, *T. crotocingenum* PCB and *P. copticola* SRB, and the top 100 genes for all other candidates. In *Penicillium* candidates, the nutrient transporter gene was the same STL1 glycerol transporter I observed in *P. coffeae* ANU01 (Chapter Two), suggesting specialisation in the niche or at the least an ability to use the same genetic tool kit to facilitate growth on *Pst*. The STL1 glycerol transporters were unique to *Penicillium*, absent from the genomes of all other candidates, potentially the difference because they were so adept at making use of glycerol. Sugar importers were the most common amongst the highest upregulated transmembrane transporters. However, carbohydrates are not the only substrate available within *Pst* and I expect that given more time I would identify key shared fatty acid and amino acid transporters between the candidates. The universal upregulation of nutrient transporters suggests that all candidates ultimately aim to exploit *Pst* spores as a nutritional resource, with the primary differences between them lying in the chemical and physical mechanisms they employ in doing so.

Pst urediniospores are a rich source of nutrients and metabolism of substrates requires mobilisation of key metabolic pathways. TauD/TfD-like proteins act to make more complex molecules more readily usable in metabolism (Sundar Rajan *et al.,* 2025). By far, TauD/TfD-like proteins were the most important to *S. terricola* SRSh, where one was the most upregulated gene. TauD/TfD-like proteins were also in the top 20 most upregulated genes for *T. crotocingenum* PCB and *A. prunicola* PMUD, the top 100 for *F. fujikuroi* SRM and *P. copticola* SRB and the top 300 for *P. brevicompactum* FRF, *C.*

austrohaemisphericum PBLUE and *E. italicum* SRSi. I did not observe any patterns regarding initial host or genus of the candidates regarding the importance of TauD/TfD-like proteins, rather they stand to show the importance of regulating metabolism, as a component of rust parasitism.

5.4 Conclusions

The results presented in this chapter suggest that the key genes and biological processes identified across candidate rust hyperparasites represent the core mechanisms underlying rust parasitism. Hyperparasitism appears to begin with antagonism of the host spore through the production of secondary metabolites and effector proteins, potentially inhibiting spore germination or host defence responses and thereby preserving nutrient resources within the rust spore. Following host recognition and antagonism, hyperparasites likely gain access to these nutrients through the secretion of CAZymes, particularly GHs and, to a lesser extent CEs, which may facilitate degradation of the rust spore wall. Subsequent breakdown and uptake of nutrients is likely mediated by secreted enzymes and transmembrane transporters, allowing the hyperparasite to exploit the nutritional resources contained within the *Pst* spore. Collectively, these findings support a model in which rust hyperparasites share a common objective, exploitation of *Pst* as a nutrient source, while differing in the substrates they preferentially target and the molecular mechanisms they employ. This suggests that rust hyperparasitism is underpinned by a conserved ecological strategy but can be achieved through multiple evolutionary solutions.

All of the candidates were capable of growth on *Pst* urediniospores, regardless of the rust species I originally isolated them from. Little is known regarding the host specificity of rust hyperparasites, often hyperparasites are simply discovered, isolated from and grown on a single rust species. Growth of fungi isolated from poplar, flax and stem rust on *Pst* suggests several possibilities. Firstly, *Pst* urediniospores are sufficiently similar to those of the other rusts that recognition, penetration of the spore coat and digestion and uptake of nutrients was possible. Secondly, that these candidates are generalists in their approach, meaning they are suited to attack and antagonise a wide variety of rusts, and I simply encountered them while growing on one specific species. Thirdly, these are not truly selective hyperparasites but instead opportunistic saprophytic fungi that exist in the environment and are equipped with a very generalist gene set for making use of a wide variety of nutrients when available. The *Pst* urediniospores that I grew isolates on were from frozen stock. It is possible that freezing and thawing the spores could lead to reduced viability or the presence of dead urediniospores, making invasion easier for fungi not well adapted to attacking *Pst*. Time permitting, using an *on planta* set-up identical to the one I used for *P. coffeae* ANU01 (Chapter Two) would provide a true assessment of the ability of the candidates to act as hyperparasites of *Pst*.

Several limitations were associated with this study. Firstly, the ability of each of the candidate hyperparasites to grow on *Pst* spores on glass microscope slides or 2 mL Eppendorf tubes does not indicate they are true rust hyperparasites. To allow better understanding of the transcriptomic results I observed in this report, the ability of these hyperparasites to grow and complete their lifecycles on rust pustules *on planta* must be addressed. Secondly, by comparing the transcriptomes of hyperparasites grown on a rust species to which they may not be naturally adapted, I may have detected expression patterns that do not accurately reflect their behaviour when interacting with their native rust hosts. Consequently, some of the genes and processes identified here may not represent universally conserved mechanisms of stripe rust hyperparasitism. Thirdly, by growing the fungi on *Pst* urediniospores in 2 mL microcentrifuge tubes, I excluded the third component of the interaction: the plant host. Fungi that function as opportunistic hyperparasites, exploiting rust urediniospores when they are available, may also utilise genes involved in colonisation of plant tissue disrupted during pustule formation. Such genes would not be induced under the experimental conditions used in this study and would therefore be absent from the resulting transcriptomes. As a result, the data presented here may provide only a partial representation of the processes involved in rust parasitism. If this experiment were to be repeated, I would first follow Koch's postulates to confirm the ability of each of the candidates to complete its lifecycle on *Pst* pustules on the leaves of wheat plants. After this, I would conduct comparative transcriptomic analyses of the candidate hyperparasites during interaction with *Pst on planta*. Comparing gene expression between *in vitro* and *on planta* conditions would grant a more comprehensive and better understanding of the genes and pathways behind true rust hyperparasitism.

5.5 Bibliography

Alexa, A., & Rahnenführer, J. (2009). Gene set enrichment analysis with topGO. Bioconductor improv, 27(1-26), 776.

Almagro Armenteros, J. J., Tsirigos, K. D., Sønderby, C. K., Petersen, T. N., Winther, O., Brunak, S., von Heijne, G., & Nielsen, H. (2019). SignalP 5.0 improves signal peptide predictions using deep neural networks. Nature Biotechnology, 37(4), 420-423. https://doi.org/10.1038/s41587-019-0036-z

Alvarez Francisco, J., Douglas Lois, M., Rosebrock, A., Konopka James, B., & Lew Daniel, J. (2008). The Sur7 protein regulates plasma membrane organization and prevents intracellular cell wall growth in *Candida albicans*. Molecular Biology of the Cell, 19(12), 5214-5225. https://doi.org/10.1091/mbc.e08-05-0479

Armendáriz-Ruiz, M., Rodríguez-González, J. A., Camacho-Ruíz, R. M., & Mateos-Díaz, J. C. (2018). Carbohydrate esterases: An overview. Lipases and Phospholipases: Methods and Protocols, 39-68.

Atanasova, L., Dubey, M., Grujić, M., Gudmundsson, M., Lorenz, C., Sandgren, M., Kubicek, C. P., Jensen, D. F., & Karlsson, M. (2018). Evolution and functional characterization of pectate lyase PEL12, a member of a highly expanded *Clonostachys rosea* polysaccharide lyase 1 family. BMC Microbiology, 18(1), 178. https://doi.org/10.1186/s12866-018-1310-9

Baramidze, V., Sella, L., Japaridze, T., Dzotsenidze, N., Lamazoshvili, D., Abashidze, N., Basilidze, M., & Tomashvili, G. (2025). A barcoded ITS primer-based nanopore sequencing protocol for detection of *Alternaria* species and other fungal pathogens in diverse plant hosts. Journal of Fungi, 11(4), 249.

Beese, S. E., Negishi, T., & Levin, D. E. (2009). Identification of positive regulators of the yeast Fps1 glycerol channel. PLOS Genetics, 5(11), e1000738. https://doi.org/10.1371/journal.pgen.1000738

Bensch, K., Groenewald, J. Z., Braun, U., Dijksterhuis, J., de Jesús Yáñez-Morales, M., & Crous, P. W. (2015). Common but different: The expanding realm of *Cladosporium*. Studies in Mycology, 82(1), 23-74.

Blighe, K. R., Sharmila; Lewis, Myles. (2020). EnhancedVolcano volcano plots with enhanced colouring and labeling. R package version 1.7.14. https://github.com/kevinblighe/EnhancedVolcano

Blin, K., Shaw, S., Kloosterman, A. M., Charlop-Powers, Z., van Wezel, G. P., Medema, Marnix H., & Weber, T. (2021). antiSMASH 6.0: improving cluster detection and comparison capabilities. Nucleic Acids Research, 49(W1), W29-W35. https://doi.org/10.1093/nar/gkab335

Brosch, G., Loidl, P., & Graessle, S. (2008). Histone modifications and chromatin dynamics: a focus on filamentous fungi. FEMS Microbiology Reviews, 32(3), 409-439. https://doi.org/10.1111/j.1574-6976.2007.00100.x

Bu, Y.-Y., Yamazaki, H., Ukai, K., & Namikoshi, M. (2015). Penicillimide, an open-chain hemisuccinimide from Okinawan marine-derived *Penicillium copticola*. The Journal of Antibiotics, 68(8), 537-539. https://doi.org/10.1038/ja.2015.21

Bull, H., Murray, P. G., Thomas, D., Fraser, A., & Nelson, P. N. (2002). Acid phosphatases. Molecular Pathology, 55(2), 65.

Cen, Y.-K., Lin, J.-G., Wang, Y.-L., Wang, J.-Y., Liu, Z.-Q., & Zheng, Y.-G. (2020). The gibberellin producer *Fusarium fujikuroi*: methods and technologies in the current toolkit. Frontiers in Bioengineering and Biotechnology, 8. https://doi.org/10.3389/fbioe.2020.00232

Chen, S., Zhou, Y., Chen, Y., & Gu, J. (2018). fastp: an ultra-fast all-in-one FASTQ preprocessor. Bioinformatics, 34(17), i884-i890.

Corrêa, T. L. R., dos Santos, L. V., & Pereira, G. A. G. (2016). AA9 and AA10: from enigmatic to essential enzymes. Applied Microbiology and Biotechnology, 100(1), 9-16. https://doi.org/10.1007/s00253-015-7040-0

Cortiello, M., Bellameche, F., Montorsi, A., Stefani, E., & Giovanardi, D. (2026). First report of *Epicoccum italicum* causing postharvest rot on pear fruits in Italy. New Disease Reports, 53(1). https://doi.org/10.1002/ndr2.70105

Črešnar, B., & Petrič, Š. (2011). Cytochrome P450 enzymes in the fungal kingdom. Biochimica et Biophysica Acta (BBA) - Proteins and Proteomics, 1814(1), 29-35. https://doi.org/https://doi.org/10.1016/j.bbapap.2010.06.020

Darkin-Rattray, S. J., Gurnett, A. M., Myers, R. W., Dulski, P. M., Crumley, T. M., Allocco, J. J., Cannova, C., Meinke, P. T., Colletti, S. L., & Bednarek, M. A. (1996). Apicidin: a novel antiprotozoal agent that inhibits parasite histone deacetylase. Proceedings of the National Academy of Sciences, 93(23), 13143-13147.

De Coster, W., D'Hert, S., Schultz, D. T., Cruts, M., & Van Broeckhoven, C. (2018). NanoPack: visualizing and processing long-read sequencing data. Bioinformatics, 34(15), 2666-2669. https://doi.org/10.1093/bioinformatics/bty149

de Jesús-Pires, C., Ferreira-Neto, J. R. C., Pacifico Bezerra-Neto, J., Kido, E. A., de Oliveira Silva, R. L., Pandolfi, V., Wanderley-Nogueira, A. C., Binneck, E., da Costa, A. F., Pio-Ribeiro, G., Pereira-Andrade, G., Sittolin, I. M., Freire-Filho, F., & Benko-Iseppon, A. M. (2020). Plant thaumatin-like proteins: function, evolution and biotechnological applications. Current Protein and Peptide Science, 21(1), 36-51. https://doi.org/https://doi.org/10.2174/1389203720666190318164905

Dhakal, R., Bajpai, V. K., & Baek, K.-H. (2012). Production of gaba - aminobutyric acid by microorganisms: a review. Brazilian Journal of Microbiology, 43(4), 1230-1241. https://doi.org/10.1590/s1517-83822012000400001

Dunn, M. F., Ramírez-Trujillo, J. A., & Hernández-Lucas, I. (2009). Major roles of isocitrate lyase and malate synthase in bacterial and fungal pathogenesis. Microbiology, 155(10), 3166-3175. https://doi.org/https://doi.org/10.1099/mic.0.030858-0

Ellis, H. R. (2011). Mechanism for sulfur acquisition by the alkanesulfonate monooxygenase system. Bioorganic Chemistry, 39(5), 178-184. https://doi.org/https://doi.org/10.1016/j.bioorg.2011.08.001

Falk De Avila, L. G., Rey, M. d. S., Júnior, A. W., Villa, T. C., Chierrito de Oliveira, G., Vaz de Oliveira Candido, L. H., Claudino, P. H., Gabiatti, N. C., Ortoncelli, A. R., Borin, R. C., & Lima, N. B. (2025). First report of *Epicoccum italicum* causing leaf spots on *Eugenia uniflora* in Brazil. Plant Disease, 109(12), 2600. https://doi.org/10.1094/PDIS-04-25-0788-PDN

Galperin, M. Y., Wolf, Y. I., Makarova, K. S., Vera Alvarez, R., Landsman, D., & Koonin, E. V. (2021). COG database update: focus on microbial diversity, model organisms, and widespread pathogens. Nucleic Acids Research, 49(D1), D274-D281.

Garnica, D. P., Nemri, A., Upadhyaya, N. M., Rathjen, J. P., & Dodds, P. N. (2014). The ins and outs of rust haustoria. PLOS Pathogens, 10(9), e1004329. https://doi.org/10.1371/journal.ppat.1004329

Ge, H., Peng, Z., Lu, D., Yang, Z., & Li, H. (2024). Biodegradation of high molecular weight polycyclic aromatic hydrocarbons by *Sarocladium terricola* strain PYR-233 isolated from petrochemical

contaminated sediment. Journal of Environmental Management, 363, 121419. https://doi.org/https://doi.org/10.1016/j.jenvman.2024.121419

George, M., Colombo, D. N., Ajayi-Banji, I., Clementson, C., Webster, R., & Mathew, F. M. (2025). First report of soybean seed disease caused by *Epicoccum italicum* in North Dakota. Plant Disease, 110(3), 1013. https://doi.org/10.1094/PDIS-09-25-1871-PDN

Ghisla, S., & Thorpe, C. (2004). Acyl-CoA dehydrogenases. European Journal of Biochemistry, 271(3), 494-508. https://doi.org/https://doi.org/10.1046/j.1432-1033.2003.03946.x

Gurevich, A., Saveliev, V., Vyahhi, N., & Tesler, G. (2013). QUAST: quality assessment tool for genome assemblies. Bioinformatics, 29(8), 1072-1075. https://doi.org/10.1093/bioinformatics/btt086

Hacquard, S., Petre, B., Frey, P., Hecker, A., Rouhier, N., & Duplessis, S. (2011). The poplar-poplar rust interaction: insights from genomics and transcriptomics. Journal of Pathogens, 2011(1), 716041. https://doi.org/https://doi.org/10.4061/2011/716041

Henriquez, T., Wirtz, L., Su, D., & Jung, H. (2021). Prokaryotic solute/sodium symporters: versatile functions and mechanisms of a transporter family. International Journal of Molecular Sciences, 22(4), 1880.

Huang, S., Jia, Z., Li, H., Zhang, S., Shen, J., Gai, Y., Jiao, C., Sun, X., Duan, S., Wang, M., & Ma, H. (2022). ACT-Toxin, the key effector for the virulence of *Alternaria alternata* tangerine pathotype to specific citrus species. Agronomy, 12(12), 3181.

Hüttner, S., Veit, C., Vavra, U., Schoberer, J., Liebminger, E., Maresch, D., Grass, J., Altmann, F., Mach, L., & Strasser, R. (2014). *Arabidopsis* class I α-Mannosidases MNS4 and MNS5 are involved in endoplasmic reticulum–associated degradation of misfolded glycoproteins The Plant Cell, 26(4), 1712-1728. https://doi.org/10.1105/tpc.114.123216

Jones, A., & Schwessinger, B. (2021). High-molecular weight DNA extraction from challenging fungi using CTAB for lysis and precipitation v3. https://doi.org/10.17504/protocols.io.bwr8pd9w

Jones, P., Binns, D., Chang, H.-Y., Fraser, M., Li, W., McAnulla, C., McWilliam, H., Maslen, J., Mitchell, A., Nuka, G., Pesseat, S., Quinn, A. F., Sangrador-Vegas, A., Scheremetjew, M., Yong, S.-Y., Lopez, R., & Hunter, S. (2014). InterProScan 5: genome-scale protein function classification. Bioinformatics, 30(9), 1236-1240. https://doi.org/10.1093/bioinformatics/btu031

Käll, L., Krogh, A., & Sonnhammer, E. L. (2004). A combined transmembrane topology and signal peptide prediction method. Journal of molecular biology, 338(5), 1027-1036.

Kavanagh, K. L., Jörnvall, H., Persson, B., & Oppermann, U. (2008). Medium- and short-chain dehydrogenase/reductase gene and protein families. Cellular and Molecular Life Sciences, 65(24), 3895. https://doi.org/10.1007/s00018-008-8588-y

Kim, D., Paggi, J. M., Park, C., Bennett, C., & Salzberg, S. L. (2019). Graph-based genome alignment and genotyping with HISAT2 and HISAT-genotype. Nature Biotechnology, 37(8), 907-915.

Klein, M., Swinnen, S., Thevelein, J. M., & Nevoigt, E. (2017). Glycerol metabolism and transport in yeast and fungi: established knowledge and ambiguities. Environmental Microbiology, 19(3), 878-893. https://doi.org/10.1111/1462-2920.13617

Kolmogorov, M., Yuan, J., Lin, Y., & Pevzner, P. A. (2019). Assembly of long, error-prone reads using repeat graphs. Nature Biotechnology, 37(5), 540-546. https://doi.org/10.1038/s41587-019-0072-8

Kusari, P., Kusari, S., Spiteller, M., & Kayser, O. (2013). Endophytic fungi harbored in Cannabis sativa L.: diversity and potential as biocontrol agents against host plant-specific phytopathogens. Fungal Diversity, 60(1), 137-151. https://doi.org/10.1007/s13225-012-0216-3

Li, J., Xiao, X., Zhou, M., & Zhang, Y. (2023). Strategy for the adaptation to stressful conditions of the novel isolated conditional piezophilic strain *Halomonas titanicae* ANRCS81. Applied and Environmental Microbiology, 89(3), e01304-01322. https://doi.org/10.1128/aem.01304-22

Liu, Q., & Dong, C. H. (2020). First report of white mold caused by *Trichothecium crotocinigenum* on *Cordyceps militaris* in China. Plant Disease, 104(12), 3253-3253. https://doi.org/10.1094/PDIS-05-20-1024-PDN

Lösel, D., & Sancholle, M. (2017). Fungal lipids. In Lipids of Pathogenic Fungi. 27-62. CRC Press.

Macara, I. G., Lounsbury, K. M., Richards, S. A., McKiernan, C., & Bar-Sagi, D. (1996). The Ras superfamily of GTPases. The FASEB Journal, 10(5), 625-630. https://doi.org/https://doi.org/10.1096/fasebj.10.5.8621061

Markham, P., Robson, G. D., Bainbridge, B. W., & Trinci, A. P. J. (1993). Choline: Its role in the growth of filamentous fungi and the regulation of mycelial morphology. FEMS Microbiology Reviews, 10(3-4), 287-300. https://doi.org/10.1111/j.1574-6968.1993.tb05872.x

McCord, J. M., & Fridovich, I. (1969). Superoxide dismutase. Journal of Biological Chemistry, 244(22), 6049-6055. https://doi.org/10.1016/s0021-9258(18)63504-5

McDonald, M., & Schwessinger, B. (2017). High quality DNA from fungi for long read sequencing e.g. PacBio, Nanopore MinION v2. https://doi.org/10.17504/protocols.io.hadb2a6

Mendgen, K. (1981). Growth of *Verticillium lecanii* in pustules of stripe rust (*Puccinia striiformis*). Phytopathologische Zeitschrift 102, 301-309.

Muszewska, A., Stepniewska-Dziubinska, M. M., Steczkiewicz, K., Pawlowska, J., Dziedzic, A., & Ginalski, K. (2017). Fungal lifestyle reflected in serine protease repertoire. Scientific Reports, 7(1), 9147. https://doi.org/10.1038/s41598-017-09644-w

Nasini, G., Arnone, A., Assante, G., Bava, A., Moricca, S., & Ragazzi, A. (2004). Secondary mould metabolites of *Cladosporium tenuissimum*, a hyperparasite of rust fungi. Phytochemistry, 65(14), 2107-2111. https://doi.org/10.1016/j.phytochem.2004.03.013

Novy, V., Carneiro, L. V., Shin, J. H., Larsbrink, J., & Olsson, L. (2021). Phylogenetic analysis and in-depth characterization of functionally and structurally diverse CE5 cutinases. Journal of Biological Chemistry, 297(5), 101302. https://doi.org/10.1016/j.jbc.2021.101302

Ökmen, B., Kemmerich, B., Hilbig, D., Wemhöner, R., Aschenbroich, J., Perrar, A., Huesgen, P. F., Schipper, K., & Doehlemann, G. (2018). Dual function of a secreted fungalysin metalloprotease in *Ustilago maydis*. New Phytologist, 220(1), 249-261. https://doi.org/https://doi.org/10.1111/nph.15265

Page, M. J., & Di Cera, E. (2008). Serine peptidases: classification, structure and function. Cellular and Molecular Life Sciences, 65(7), 1220-1236. https://doi.org/10.1007/s00018-008-7565-9

Palmer, J., Stajich, J. (2020). Funannotate v1.8.1: Eukaryotic genome annotation (v1.8). Zenodo. https://doi.org/https://doi.org/10.5281/zenodo.1134477

Pan, L., Wen, S., Yu, J., Lu, L., Zhu, X., & Zhang, Z. (2020). Genome-wide identification of M35 family metalloproteases in *Rhizoctonia cerealis* and functional analysis of RcMEP2 as a virulence factor during the fungal infection to wheat. International Journal of Molecular Sciences, 21(8), 2984.

Parente, J. A., Salem-Izacc, S. M., Santana, J. M., Pereira, M., Borges, C. L., Bailão, A. M., & Soares, C. M. A. (2010). A secreted serine protease of *Paracoccidioides brasiliensis* and its interactions with fungal proteins. BMC Microbiology, 10(1), 292. https://doi.org/10.1186/1471-2180-10-292

Pasternak, K., Kocot, J., & Horecka, A. (2010). Biochemistry of magnesium. Journal of Elementology, 15(3), 601-616.

Patro, R., Duggal, G., Love, M. I., Irizarry, R. A., & Kingsford, C. (2017). Salmon provides fast and bias-aware quantification of transcript expression. Nature Methods, 14(4), 417-419. https://doi.org/10.1038/nmeth.4197

Pike, S., Patel, A., Stacey, G., & Gassmann, W. (2009). *Arabidopsis* OPT6 is an oligopeptide transporter with exceptionally broad substrate specificity. Plant and Cell Physiology, 50(11), 1923-1932. https://doi.org/10.1093/pcp/pcp136

Qi, X., Wang, Y., Feng, N., Kong, Y., Zhang, K., Ouyang, X., & Liu, M. (2025). Competitive inhibition of family GH5 *Aspergillus niger* endo-glucanase A (AnglA5) by rice xylanase inhibitor (RIXI): Experimental and *in silico* insights. International Journal of Biological Macromolecules, 307, 142011. https://doi.org/https://doi.org/10.1016/j.ijbiomac.2025.142011

Qin, W., Lin, Y., Xu, L., Li, Q., Tang, A., Li, Q., Liang, H., & Liu, Y. (2025). NADH flavin oxidoreductase and catalase-induced reactive oxygen species and key enzymes synergistically drive oxidative degradation of xanthene dye Rose Bengal in *Aspergillus flavus* A5P1. International Journal of Biological Macromolecules, 314, 144136. https://doi.org/https://doi.org/10.1016/j.ijbiomac.2025.144136

Rashad, Y. M., El-Sharkawy, H. H. A., Abdalla, S. A., Ibrahim, O. M., & Elazab, N. T. (2025). Unraveling the regulating effect of the endophyte *Epicoccum italicum* HE20 on the biosynthesis genes of polyphenols in wheat in response to yellow rust. Physiological and Molecular Plant Pathology, 138, 102705. https://doi.org/https://doi.org/10.1016/j.pmpp.2025.102705

Ritchie, M. E., Phipson, B., Wu, D., Hu, Y., Law, C. W., Shi, W., & Smyth, G. K. (2015). limma powers differential expression analyses for RNA-sequencing and microarray studies. Nucleic Acids Research, 43(7), e47-e47.

Rodríguez-Navarro, A. (2000). Potassium transport in fungi and plants. Biochimica et Biophysica Acta (BBA) - Reviews on Biomembranes, 1469(1), 1-30. https://doi.org/https://doi.org/10.1016/S0304-4157(99)00013-1

Roy, A., Kumar, A., Baruah, D., & Tamuli, R. (2021). Calcium signaling is involved in diverse cellular processes in fungi. Mycology, 12(1), 10-24. https://doi.org/10.1080/21501203.2020.1785962

Rudall, K., & Kenchington, W. (1973). The chitin system. Biological Reviews, 48(4), 597-633.

Schoch, C. L., Seifert, K. A., Huhndorf, S., Robert, V., Spouge, J. L., Levesque, C. A., Chen, W., Fungal Barcoding, C., Fungal Barcoding Consortium Author, L., Bolchacova, E., Voigt, K., Crous, P. W., Miller, A. N., Wingfield, M. J., Aime, M. C., An, K.-D., Bai, F.-Y., Barreto, R. W., Begerow, D., . . . Schindel, D. (2012). Nuclear ribosomal internal transcribed spacer (ITS) region as a universal DNA barcode marker for Fungi. Proceedings of the National Academy of Sciences, 109(16), 6241-6246. https://doi.org/10.1073/pnas.1117018109

Schultz, J. A., & Coleman, H. D. (2021). Pectin and xylan biosynthesis in poplar: implications and opportunities for biofuels production. Frontiers in Plant Science, 12. https://doi.org/10.3389/fpls.2021.712083

Schulz, H. (1991). Beta oxidation of fatty acids. Biochimica et Biophysica Acta (BBA) - Lipids and Lipid Metabolism, 1081(2), 109-120. https://doi.org/https://doi.org/10.1016/0005-2760(91)90015-A

Schwessinger, B., Sperschneider, J., Cuddy, W. S., Garnica, D. P., Miller, M. E., Taylor, J. M., Dodds, P. N., Figueroa, M., Park, R. F., & Rathjen, J. P. (2018). A near-complete haplotype-phased genome of the dikaryotic wheat stripe rust fungus *Puccinia striiformis* f. sp. *tritici* reveals high interhaplotype diversity. mBio, 9(1), e02275-02217. https://doi.org/10.1128/mbio.02275-17

Shi, L., & Tu, B. P. (2015). Acetyl-CoA and the regulation of metabolism: mechanisms and consequences. Current Opinion in Cell Biology, 33, 125-131. https://doi.org/https://doi.org/10.1016/j.ceb.2015.02.003

Simão, F. A., Waterhouse, R. M., Ioannidis, P., Kriventseva, E. V., & Zdobnov, E. M. (2015). BUSCO: assessing genome assembly and annotation completeness with single-copy orthologs. Bioinformatics, 31(19), 3210-3212. https://doi.org/10.1093/bioinformatics/btv351

Şimşek, A., Dinler, H., & Uysal Morca, A. (2022). Identification and pathogenicity of *Alternaria alternata* causing leaf spot disease on sweet cherry in Province of Turkey. Journal of Plant Diseases and Protection, 129(6), 1355-1366. https://doi.org/10.1007/s41348-022-00648-x

Sperschneider, J. (2020). FindTelomeres. https://github.com/JanaSperschneider/FindTelomeres

Srivastava, A. K., Défago, G., & Kern, H. (1985). Hyperparasitism of *Puccinia horiana* and other microcyclic Rusts. Journal of Phytopathology, 114(1), 73-78. https://doi.org/10.1111/j.1439-0434.1985.tb04338.x

Staples, R. C., & Wynn, W. K. (1965). The physiology of uredospores of the rust fungi. The Botanical Review, 31(4), 537-564. https://doi.org/10.1007/BF02858608

Stockmann-Juvala, H., & Savolainen, K. (2008). A review of the toxic effects and mechanisms of action of fumonisin B1. Human & Experimental Toxicology, 27(11), 799-809. https://doi.org/10.1177/0960327108099525

Strijbis, K., van Roermund, C. W., van den Burg, J., van den Berg, M., Hardy, G. P. M., Wanders, R. J., & Distel, B. (2010). Contributions of carnitine acetyltransferases to intracellular acetyl unit transport in *Candida albicans*. Journal of Biological Chemistry, 285(32), 24335-24346. https://doi.org/https://doi.org/10.1074/jbc.M109.094250

Sundar Rajan, M., Jayavelu, T., & Pennathur, G. (2025). Phylogenetic studies on taurine dioxygenase (TauD). Current Microbiology, 82(11). https://doi.org/10.1007/s00284-025-04494-6

Takeuchi, M., Nakajima, M., Ogita, T., Inukai, M., Kodama, K., Furuya, K., Nagaki, H., & Haneishi, T. (1989). Fosfonochlorin, a new antibiotic with spheroplast forming activity. The Journal of Antibiotics, 42(2), 198-205. https://doi.org/10.7164/antibiotics.42.198

Tian, X., Sun, T., Lin, R., Liu, R., Yang, Y., Xie, B., & Mao, Z. (2022). Genome sequence resource of *Sarocladium terricola* TR, an endophytic fungus as a potential biocontrol agent against *Meloidogyne incognita*. Molecular Plant-Microbe Interactions®, 35(6), 505-508. https://doi.org/10.1094/MPMI-11-21-0284-A

Trisolini, L., Gambacorta, N., Gorgoglione, R., Montaruli, M., Laera, L., Colella, F., Volpicella, M., De Grassi, A., & Pierri, C. L. (2019). FAD/NADH dependent oxidoreductases: from different amino acid sequences to similar protein shapes for playing an ancient function. Journal of Clinical Medicine, 8(12), 2117.

Tulloch, A. P., Craig, B. M., & Ledingham, G. A. (1959). The oil of wheat stem rust uredospores: II. The isolation of *cis*-9,10-epoxyoctadecanoic acid, and the fatty acid composition of the oil. Canadian Journal of Microbiology, 5(5), 485-491. https://doi.org/10.1139/m59-060

Uma, N. U., & Taylor, G. S. (1987). Parasitism of leek rust urediniospores by four fungi. Transactions of the British Mycological Society, 88(3), 335-340. https://doi.org/https://doi.org/10.1016/S0007-1536(87)80007-4

Vaser, R., Sović, I., Nagarajan, N., & Šikić, M. (2017). Fast and accurate de novo genome assembly from long uncorrected reads. Genome Research, 27(5), 737-746. https://doi.org/10.1101/gr.214270.116

Wang, M., & Zhao, H. (2014). Characterization and engineering of the adenylation domain of a NRPS-Like protein: A Potential Biocatalyst for Aldehyde Generation. ACS Catalysis, 4(4), 1219-1225. https://doi.org/10.1021/cs500039v

Wang, N., Fan, X., Zhang, S., Liu, B., He, M., Chen, X., Tang, C., Kang, Z., & Wang, X. (2020). Identification of a hyperparasitic *Simplicillium obclavatum* strain affecting the infection dynamics of *Puccinia striiformis* f. sp. *tritici* on wheat. Frontiers in Microbiolgy, 11, 1277. https://doi.org/10.3389/fmicb.2020.01277

Wess, J., Hu, Y., Periyannan, S., Jones, A., & Rathjen, J. P. (2025). Global transcriptome changes during growth of a novel *Penicillium coffeae* isolate on the wheat stripe rust fungus, *Puccinia striiformis* f. sp. *tritici*. Fungal Genetics and Biology, 176, 103956. https://doi.org/https://doi.org/10.1016/j.fgb.2024.103956

Wick, R., & Menzel, P. (2019). Filtlong: quality filtering tool for long reads. Github.

Whipps, J. (1993). A review of white rust (*Puccinia horiana* Henn.) disease on chrysanthemum and the potential for its biological control with *Verticillium lecanii* (Zimm.) Viégas. Annals of Applied Biology, 122(1), 173-187.

Wiemann, P., Willmann, A., Straeten, M., Kleigrewe, K., Beyer, M., Humpf, H.-U., & Tudzynski, B. (2009). Biosynthesis of the red pigment bikaverin in *Fusarium fujikuroi*: genes, their function and regulation. Molecular Microbiology, 72(4), 931-946. https://doi.org/https://doi.org/10.1111/j.1365-2958.2009.06695.x

Wilson, A., Cuddy, W. S., Park, R. F., Harm, G. F. S., Priest, M. J., Bailey, J., & Moffitt, M. C. (2020). Investigating hyperparasites as potential biological control agents of rust pathogens on cereal crops. Australasian Plant Pathology, 49(3), 231-238. https://doi.org/10.1007/s13313-020-00695-8

Xia, Y., Chen, F., Du, Y., Liu, C., Bu, G., Xin, Y., & Liu, B. (2019). A modified SDS-based DNA extraction method from raw soybean. Bioscience Reports, 39(2), BSR20182271. https://doi.org/10.1042/BSR20182271

Xiao, M., Chen, D., Liu, S., Chen, A., Fang, A., Tian, B., Yu, Y., Bi, C., Kang, Z., & Yang, Y. (2023). A chitin deacetylase Ps CDA2 from *Puccinia striiformis* f. sp. *tritici* confers disease pathogenicity by suppressing chitin-triggered immunity in wheat. Molecular Plant Pathology, 24(12), 1467-1479.

Xie, W., Luo, D., Wu, M., Sun, Y., & Wang, Z. (2025). The evaluation of Phenylalanine-tRNA ligase beta unit (PheT), as a potential target in *Mycobacterium abscessus*. Tuberculosis, 152, 102626. https://doi.org/https://doi.org/10.1016/j.tube.2025.102626

Xue, C., Park, G., Choi, W., Zheng, L., Dean, R. A., & Xu, J.-R. (2002). Two novel fungal virulence genes specifically expressed in appressoria of the rice blast fungus. The Plant Cell, 14(9), 2107-2119.

Yang, H.-X., Ai, H.-L., Feng, T., Wang, W.-X., Wu, B., Zheng, Y.-S., Sun, H., He, J., Li, Z.-H., & Liu, J.-K. (2018). Trichothecrotocins A–C, Antiphytopathogenic agents from potato endophytic fungus *Trichothecium crotocinigenum*. Organic Letters, 20(24), 8069-8072. https://doi.org/10.1021/acs.orglett.8b03735

Zambettakis, C., Sankara, P., & Métivier, A. (1985). *Darluca filum*, *Tuberculina costaricana* and *Verticillium lecanii*, hyperparasites of *Puccinia arachidis* considered as elements of an integrated control [*Darluca filum*, *Tuberculina costaricana* et *Verticillium lecanii*, hyperparasites de Puccinia arachidis, considérés comme éléments d'une lutte integrée.]. Bulletin Trimestriel de la Société Mycologique de France, 101(2), 165–181.

Zhan, G., Tian, Y., Wang, F., Chen, X., Guo, J., Jiao, M., Huang, L., & Kang, Z. (2014). A novel fungal hyperparasite of *Puccinia striiformis* f. sp. *tritici*, the causal agent of wheat stripe rust. PLoS One, 9(11), e111484. https://doi.org/10.1371/journal.pone.0111484

Zhang, H., He, M., Fan, X., Dai, L., Zhang, S., Hu, Z., & Wang, N. (2022). Isolation, identification and hyperparasitism of a novel *Cladosporium cladosporioides* isolate hyperparasitic to *Puccinia striiformis* f. sp. *tritici*, the wheat stripe rust pathogen. Biology, 11(6), 892.

Zhang, M., Ou, X., Shi, H., Huang, W., Song, L., Zhu, J., & Yu, R. (2023). Isolation, structures and biological activities of medicinal glycoproteins from natural resources: A review. International Journal of Biological Macromolecules, 244, 125406. https://doi.org/https://doi.org/10.1016/j.ijbiomac.2023.125406

Zhao, X., Hume, S. L., Johnson, C., Thompson, P., Huang, J., Gray, J., Lamb, H. K., & Hawkins, A. R. (2010). The transcription repressor NmrA is subject to proteolysis by three *Aspergillus nidulans* proteases. Protein Science, 19(7), 1405-1419. https://doi.org/https://doi.org/10.1002/pro.421

Zheng, L., Zhao, J., Liang, X., Zhan, G., Jiang, S., & Kang, Z. (2017). Identification of a novel *Alternaria alternata* strain able to hyperparasitize *Puccinia striiformis* f. sp. *tritici*, the causal agent of wheat stripe rust. Frontiers in Microbiology, 8. https://doi.org/10.3389/fmicb.2017.00071

5.6 Supplementary Material

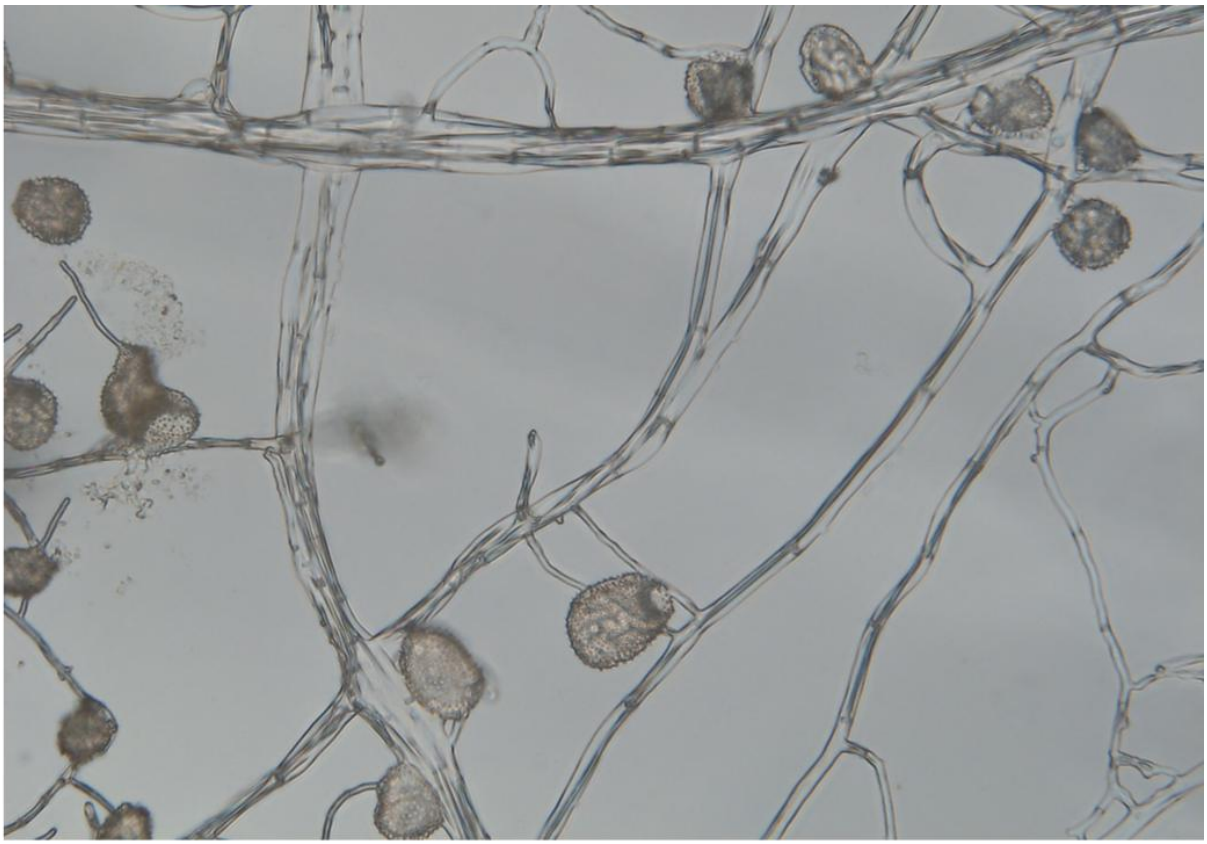

Supplementary Figure 5.1. Putative evidence of *Pst* urediniospore (large ovate spores) lysis by *E. italicum* SRSi hyphae (thick, root-like structures) during co-inoculation on glass slides.

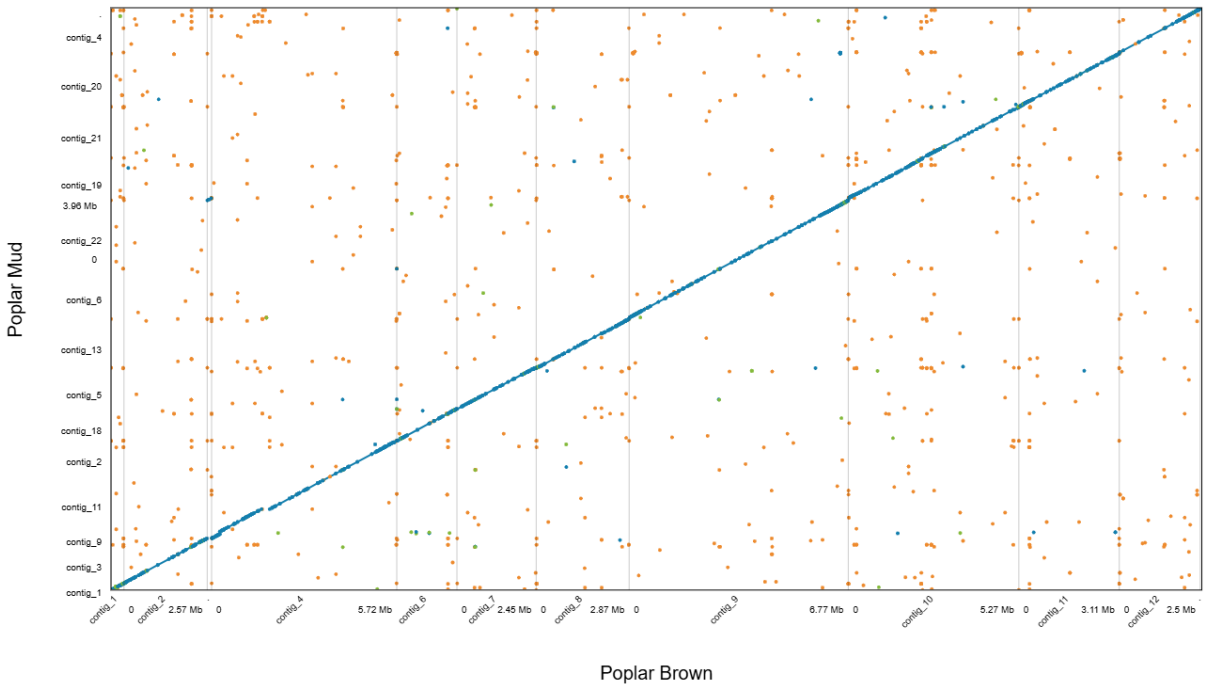

Supplementary Figure 5.2. Dotplot representing a whole genome comparison between *Alternaria* candidates Poplar Brown (X axis) and Poplar Mud (Y axis). Each blue dot represents forwards similarity at a given position between the two genomes. Vertical grid lines represent the beginning and end of contigs for Poplar Brown. Horizontal grid lines represent the beginning and end of contigs for Poplar Mud.

Chapter Six

General Discussion and Concluding Remarks

6.1 Preface

Everything in this thesis began with a speck of white fluff. The chance observation of *something* growing on *Pst* pustules ended up being the catalyst for both my PhD and a thousand awkward answers to questions in dentists' offices, barber chairs and house parties. *Yes, I'm sure it's a fungus, Yes, we might be able to use it to protect crops, No, it doesn't eat the brown stuff on your tools, that's a different sort of rust.* But these sorts of questions are exactly the sort I asked myself when I began working on the speck of white fluff. What is this thing? How does it eat rust spores? Did it evolve to do that? And is this superpower a result of genes that only it is lucky enough to possess? The only thing we knew about rust hyperparasites when we began this journey was that we knew we wanted to know more about them. It is my pleasure to say that this research is a direct result of that curiosity.

What started with a speck, evolved over time into a sprawling web of questions. I began by questioning the identity of this specific fungus, but later evolved to question the identity and therefore diversity of rust hyperparasites beyond that original discovery. My curiosity regarding the genes behind our *Penicillium* eating *Pst* led to me questioning whether all hyperparasites contained and mobilised similar genes in eating rust spores. As my understanding of the complexity and intensity of parasitic attack grew, I naturally began to wonder if *Pst* was simply a sitting duck or if it was also capable of putting up a fight. A question that has never been asked nor addressed in literature.

Put succinctly, the research that came as a result of this serendipitous discovery can be boiled down into two major aspects:

- Investigating the genes behind rust hyperparasitism
- Exploring the diversity of fungi that parasitise rusts

While working on these major aspects, I discovered a third avenue worthy of research:

- Uncovering if *Pst* urediniospores mount a defence response against parasitic attack

6.2 Chapter Summaries

The list of papers investigating the hyperparasites of stripe rust is short. Amongst the papers, few describe or discuss in detail the molecular mechanisms the fungi use in their parasitism. My review of the literature in Chapter One was succinct because it had to be. Within it, I focussed on wheat rust hyperparasites and their interactions with and their effects on rust urediniospores. The majority of investigations of wheat rust hyperparasites are descriptive reports, describing physical invasion of urediniospores and reduced rust viability after interaction with the hyperparasite. The sparsely populated literature regarding the mechanisms behind these observations left questions to be answered; what are these fungi consuming when they target rust fungi, how are they attacking and extracting nutrients, and which genes are they using to do it?

Chapter Two introduced *P. coffeae* ANU01, the cornerstone of my work and the fungus that started my investigation of rust hyperparasites. The first part of the chapter focussed on the serendipitous discovery of *P. coffeae* ANU01 growing on *Pst* pustules in wheat, and its identification and verification as a rust hyperparasite. Later, I investigated how the genome of *P. coffeae* ANU01 differed from *Penicillium* not known to parasitise *Pst*, and what an enrichment in genes related to lipid, amino acid and carbohydrate metabolism might mean regarding evolution of rust hyperparasites. Finally, I compared transcriptome profiles of *P. coffeae* ANU01 growing on *Pst* pustules on wheat, to growing axenically on nutrient agar. The genetic pathways upregulated during *in situ* growth suggested that the core of parasitism lay in carbohydrate metabolism, mobilisation of rust-derived lipids and the production of toxic secondary metabolites. Beyond broad terms, I also investigated individual genes at the highest level of upregulation during *in situ* growth. Here I observed genes with potential importance including two components of a BGC responsible for production of a depudecin-like SM, potentially important to reducing the ability of urediniospores to regulate their own DNA transcription (Kwon *et al.*, 2003) and a chitosanase potentially used by *P. coffeae* ANU01 to penetrate urediniospores. Based on my analysis I hypothesised a putative model of rust hyperparasitism. Recognition of the rust host leads to the production of toxic secondary metabolites by *P. coffeae* ANU01 to limit host response and germination. Secretion of cell wall degrading enzymes help facilitate break down of the host spore coat and physical invasion of urediniospores. Secretion of carbohydrate active enzymes, proteases and lipases liberate and break down nutrients *in situ*, before uptake by nutrient transporters. Without functional validation this model remains purely speculative. However, the upregulation of similar genes in subsequent candidate hyperparasites (Chapter Five) supports it as a hypothesis. It has also long been known that rust spores are nutrient-rich targets, containing abundant lipid (20%), carbohydrates (22%) and protein (25%) resources (Staples and Wynn 1965, Tulloch *et al.*, 1959). However, the hypothesis that a fungus capable of exploiting these nutrients might need to evolve a gene set enriched in tools to make use of them has not yet been advanced. Here I described a genome enriched in genes related to metabolism of

these substrates and significant changes in regulation of metabolic pathways likely associated with targeting of these substrates by *P. coffeae* ANU01 during growth on *Pst.* My assembly and investigation of *P. coffeae* ANU01 provides a fundamental stepping stone for the broader investigation of rust hyperparasites, and serves as the basis for understanding parasitism in the remainder of my thesis.

Chapter Three built directly on the findings of Chapter Two by testing my hypothesis regarding the genes underlying rust parasitism through the generation and characterisation of loss-of-function knockouts. I selected 18 highly upregulated *P. coffeae* ANU01 genes for validation by CRISPR-mediated knock out. I selected genes based primarily on the three functional groupings I proposed in Chapter Two; antagonism and defence, degradation of the host spore coat and nutrient mobilisation and acquisition. I attempted deletion in 15 of these target genes, successfully confirming insertion of the hyg^{+} cassette at the intended locus in nine. These nine mutant *P. coffeae* ANU01 strains were used for various downstream assays including the final tube experiment, in which all nine were tested together. Difficult to control experimental variables including humidity and spore density required me to change from an *on planta* assay on wheat to try several *in vitro* phenotyping approaches. Unfortunately, I was ultimately unable to develop a phenotyping method that reliably detected the impact of loss-of-function mutations in candidate genes on the ability of *P. coffeae* ANU01 to grow on *Pst* urediniospores. However, my phenotyping results did show that loss-of-function in none of the candidate genes completely eliminated the ability of *P. coffeae* ANU01 to grow on *Pst*. This was likely in part due to the presence of genetic redundancy, i.e., unrelated genes with similar function, or homologs for each gene reducing the impact of gene loss even in highly upregulated genes. Alternatively, upregulation is not as indicative as participation in the parasitic process as I had hoped when selecting genes. The ability of *P. coffeae* ANU01 to maintain parasitic ability after knockout suggests two possibilities for the specialisation of its gene set. Either *P. coffeae* ANU01 is a generalist that makes use of a generalist gene set to attack and consume *Pst* urediniospores when present, or that it contains a specialist gene set that contains redundant genes that mask loss of function. This was the first use of CRISPR-mediated knockouts in a fungal rust hyperparasite and highlighted the inherent difficulties in working in a system where one fungus grows on another fungus growing on a plant.

Chapter Four continued my exploration of the interaction between *P. coffeae* ANU01 and *Pst*. Here I presented the first investigation of rust parasitism from the perspective of the host transcriptome. My transcriptomic analysis in Chapter Four provided evidence that the implicit assumption that *Pst* urediniospores are inert or dormant up until hydration and germination (Wiese & Ravenscroft 1979) is unfounded. The results suggest that urediniospores are in fact capable of recognising parasitic attack and engaging a complex and coordinated defence response. I propose that this defence is divided into six major aspects; parasite recognition and downstream signalling, fortification of the urediniospore coat to protect against enzymatic and mechanical damage, maintenance of homeostasis to protect *Pst* in a rapidly changing environment, detoxification of SMs and harmful ROS induced by *P. coffeae*

ANU01, repair of potentially SM/ROS- induced damage to DNA, and finally a mobilisation of metabolites, primarily lipids, to fuel the process. However, differences between the conditions regarding sample age, humidity and tissue collection methods, may impact the certainty of these conclusions. This newly revealed defensive capability against parasites may be the driving factor behind the diverse antagonistic responses that I observed in Chapter Five. Additionally, the absence of a clear loss-of-function phenotype in the growth assays I described in Chapter Three may reflect the possibility that *P. coffeae* ANU01 genes involved in overcoming a possible coordinated rust defence response in fresh *Pst* urediniospores within pustules on wheat were less important for growth on *Pst* urediniospores isolated in tubes.

Chapter Five expanded my investigation of rust hyperparasitism beyond *P. coffeae* ANU01. In this chapter I isolated nine potential hyperparasites from a variety of wild and cultivated rust species in the Australian Capital Territory and sequenced their genomes and transcriptomes. This revealed genomes enriched in BGC, CAZyme and protease genes. During growth on *Pst,* fungi appeared to upregulate genes related to a series of "core" functions in transmembrane transport, and carbohydrate and fatty acid metabolism. This core elements of parasitism were complemented by elements unique to each isolate in terms of preference for core and secondary nutrients, production of toxic SMs, cell wall degrading enzymes and signalling. One isolate, *Epicoccum italicum* SRSi, possessed a unique phenotype in seemingly aggressively penetrating and lysing *Pst* urediniospores *in vitro.* This was reflected in a unique transcriptomic profile focussed on carbohydrate metabolism and remodelling of the parasite cell wall. Though different species, the two *Penicillium* isolates appear to share key aspects in sensing, signalling and glycerol utilisation, as derived from gene ontology analyses. Comparing the top upregulated genes across isolates, I uncovered a rudimentary understanding of a possible "genetic toolkit" consisting of genes that were highly upregulated in almost all isolates. The transcriptomic investigations in Chapter Five suggest that while there may be core elements to hyperparasitism, each hyperparasite deploys a slightly different method in growing on *Pst.*

6.3 What is a rust hyperparasite?

"What is a (fungal) rust hyperparasite?" is a fundamental question. A rust hyperparasite is defined in literature simply as an organism that parasitises rust fungi (Moricca & Ragazzi 2008). However, does this mean that any fungus that can grow on rust spores is considered a hyperparasite? Or is it a more nuanced phenomenon. The definition stated above also does not address the influence of evolution on the niche. Put simply, are these fungi highly evolved to antagonise and consume rust nutrients? Or are they simply opportunistic saprophytes that occasionally exploit rust spores amongst many other possible substrates? Rust fungi are obligate biotrophs, meaning they can only grow on specific living hosts

(Lorrain *et al.*, 2019), whereas all of the fungal rust hyperparasites identified in the literature and this thesis were also capable of growth on nutrient media, showing they are not obligate parasites. The absence of *Pst* urediniospores year-round also suggests that being an obligate parasite of rust spores is not a plausible lifestyle.

As a genomics-based analysis, my thesis was not able to directly address the question as to what specifically defines a rust hyperparasite. However, by investigating the genes encoded and deployed by these fungi, I can speculate as to why each might be a hyperparasite, and what genes are necessary to allow a fungus to be capable of rust parasitism.

The results of this thesis would suggest that exploitation of the rich nutrient stores within rust urediniospores are the driving reason why fungi act as rust hyperparasites. Rust spores are composed of 20% lipids, 22% carbohydrates and 25% protein (Staples & Wynn 1965; Tulloch *et al.*, 1959), attractive substrates for fungi on an infected leaf. As one would therefore expect, metabolism, particularly lipid and carbohydrate metabolism, were universally amongst the most significantly enriched pathways during growth on *Pst* (Chapter Two & Chapter Five). This would suggest that nutrient acquisition is perhaps the most fundamental aspect of rust hyperparasitism, as it allows the fungi to grow and ultimately reproduce. However, except in the case of *P. coffeae* ANU01, my analysis focussed solely on interaction between hyperparasite and rust fungi, in a scenario in which they were essentially forced to grow on *Pst* or remain quiescent. These assays exclude the host plant's potential role(s) as a provider of habitat or shelter for the fungi. As obligate plant pathogens (Lorrain *et al.*, 2019), rust fungi pose a direct threat to the plant, and therefore the potential "habitat" of epiphytic fungi which act as hyperparasites. I did not determine the relationship between the fungi I investigated in this thesis and the plants I isolated them from. However, it is possible that these fungi are epiphytic to those plants and make use of rust urediniospores when they are present. If this is the case, the litany of toxic SMs and cell wall degrading enzyme genes that I observed upregulated during growth on *Pst* might be used not only to inhibit rust defence for nutrient acquisition, but also to reduce disease severity and protect the plant. Plant endophytic fungi are capable of suppressing rust infection without direct interaction with urediniospores. *Epicoccum italicum* HE20 is capable of reducing the severity of *Pst* infection in wheat by producing secondary metabolites and promoting upregulation of wheat genes related to production of polyphenols (El-Sharkawy *et al.*, 2023; Rashad *et al.*, 2025). Therefore, a secondary driver promoting the evolution of rust hyperparasitism may be the protection of the fungal habitat. By suppressing rust pathogens, hyperparasites could reduce damage to the plant host on which they reside, thereby preserving a favourable environment for growth and reproduction. However, a more comprehensive understanding of the ecology and lifestyle of the eight candidate hyperparasites when not growing on *Pst* would be required before this can be considered a potential driver of their parasitism. Ultimately, despite the potential benefits described above, not all fungi are rust hyperparasites. If such a rich source of nutrients is available, why don't all epiphytic or endophytic fungi make use of them?

Put otherwise, what sets a hyperparasite apart from other foliar fungi and how is a fungus able to act as a hyperparasite?

To parasitise *Pst* spores, a fungus should be able to recognise rust spores as a food source, survive or potentially disable host defence, breach the spore coat, and mobilise its metabolic machinery to make use of rust-derived nutrients. In this thesis I believe I have identified potential genetic elements underpinning these functions. I observed highly upregulated genes encoding SM biosynthetic machinery, including cytochrome P450 genes, in each of the hyperparasite candidates during growth on *Pst*. The upregulation of toxin detoxification genes in *Pst* during parasitism (Chapter Four) also suggests that antagonism of the host using an SM is a fundamental aspect of being a hyperparasite. Taken together, my analysis suggests that possession of a BGC or at the very least genes with an ability to produce toxic metabolites, is important for a hyperparasite genome. The majority of *Pst* nutrients are protected by the urediniospore coat (Xiao *et al.,* 2023). I observed a litany of highly upregulated carbohydrate degrading enzyme genes in the isolates when growing on *Pst,* however I observed a specific enrichment of GH CAZyme genes. Interestingly, in all candidates except those isolated from *Pst* pustules, deployment of a GH enzyme was complemented with a CE5 CAZyme, which assists in the breaking down of polysaccharides (Novy *et al.,* 2021). This would suggest that while a GH CAZyme is important to hyperparasitism, it may be specific to the host rust species, and that a fungal hyperparasite genome likely must possess several carbohydrate degrading enzymes to break through spore coats.

As discussed above, nutrition is possibly the most fundamental reason as to why fungi act as rust hyperparasites. Concordantly, the most universally upregulated nutrition-related gene type between all candidates encoded a sugar transporter. Carbohydrates are the second-most abundant substrate in rust urediniospores (~22% by spore weight) and my analysis compliments the literature in suggesting that penetrating the spore coat is fundamental to growth on rusts (Srivastava *et al.,* 1985). It is therefore for fungi to maximise nutritional uptake from rust spores, they should possess at least one nutrient importer gene within their genome. I hypothesise that the secreted CAZymes described above act extracellularly on polysaccharides present within the *Pst* cell wall and spore contents, releasing smaller soluble sugars that can subsequently be transported into the hyperparasite and utilised as carbon and energy sources. Alongside carbohydrates, secreted lipases may act to break down the abundant lipids present within urediniospores, releasing further nutrients for uptake. In all three *Penicillium* species I examined; the most upregulated nutrient transporter was specifically the glycerol transporter *STL1*. The gene was uniquely present in the *Penicillium* genomes with respect to my set of hyperparasite candidates, and may therefore be a particular adaptation in *Penicillium* species that parasitise rusts in order to mobilise glycerol. More unique elements that I did not observe specifically in my datasets but that I expect are relevant for an organism to be a parasite may lie in genes that I was unable to identify in this thesis. Firstly, each of the above genes would be useless to parasitism if the fungus cannot recognise *Pst* as a

potential source of nutrients. Therefore, I hypothesise that rust hyperparasites express some form of receptor, perhaps a cell-surface GPCR protein, that allows them to recognise rust spores on the leaf (Lara-Martinez *et al.,* 2025). Secondly, I observed several highly upregulated but unannotated transcription factors (TF) across the isolates. I propose that some of these TFs may serve roles in upregulating parasitism-related genes after recognition of rust spores. Importantly however, each of these genes could be possessed by any fungus that lives on the wheat leaf but do not engage the rust hyperparasite lifestyle. Ultimately, the results of my CRISPR analysis in Chapter Three suggest that it is not necessarily a single gene that facilitates hyperparasitism. Instead, a genome enriched in genes adapted to metabolism of lipids and carbohydrates, production of secondary metabolites, cell wall degrading enzymes and nutrient transporters, provides an advantage in acting as a hyperparasite.

Briefly, one cannot address the question of evolution of a parasite without also addressing adaptation to a specific host. All of the fungi that I isolated growing on rust species beyond *Pst* were also capable of growing on and completing their lifecycles using *Pst* urediniospores as the sole source of nutrition. This ability would suggest that these potential hyperparasites were not limited to one species of rust. However, I expect that growth on *Pst* urediniospores in tubes where there was no alternative food source, and growth on *Pst*-infected wheat might yield different results. I propose that host range of a hyperparasite is primarily affected by the physical attributes of the host rust urediniospores, and similarities in host rust defence systems. For example, it may be easier for a hyperparasite isolated from *Pst* to grow on other species of wheat rusts, than on more distantly related rust species. Measuring the ability of all candidates in this thesis to grow on *Pst* pustules in wheat should be the first step in determining if they are truly capable of acting as *Pst* hyperparasites. I would then follow this up by examining the ability of the candidates to grow on a variety of different rust species on their respective plant hosts to truly understand their host range. This would however raise another question, if a fungus is capable of growth on multiple rust species, does that suggest it is a more or less evolved hyperparasite?

There is still much work to be done in understanding the evolutionary history of rust hyperparasitism. However, this thesis provides the groundwork in understanding which kind of genes might be required for a fungus to act as a hyperparasite. Genetic elements upregulated during growth of all of the fungi investigated in my thesis on *Pst* suggest there are elements that might be characteristic of or used by hyperparasites. However, more unique phenotypes and transcriptomic profiles such as *Epicoccum italicum* SRSi lysing *Pst* urediniospores through carbohydrate metabolism and cell wall remodelling (Chapter Five, Supplementary Figure 5.1) suggest it may have evolved a more specialised method of acting as a hyperparasite. The ability of *P. coffeae* ANU01 to grow on *Pst* despite loss-of-function mutations in specific highly upregulated genes suggests that parasitism does not lie in a singular gene, but in an expanded gene set. Beyond in-depth phylogenetic studies to investigate the lineages of hyperparasite genomes, experiments should focus on understanding elements such as host range, impact

of loss-of-function in multiple candidate genes, and the ability of known saprophytes to grow on *Pst* in wheat to assist in better understanding evolution of the niche.

6.4 Limitations and Future Directions

A fundamental limitation of this work was the prioritisation of genetic investigation over detailed physical phenotyping of the parasitic interaction. While this thesis focused heavily on identifying and characterising the genetic mechanisms underlying rust hyperparasitism, comparatively little attention was given to the physical progression of infection itself. Important aspects that remain unresolved include the precise points of spore penetration, mechanisms of rust spore recognition, the physical effects on rust spores, impacts on germination, and the structural changes that occur throughout colonisation. Future work incorporating scanning electron microscopy (SEM) would provide valuable insight into these processes by enabling detailed visualisation of the interaction at different stages of parasitism. Perhaps most fundamentally, the temporal progression of parasitism was insufficiently characterised. A detailed understanding of the daily, or even hourly, sequence of events leading from initial recognition, to interaction, colonisation, and ultimately fruiting body production, would have substantially strengthened the interpretation of this work. Establishing a clear infection timeline would have been particularly valuable for the CRISPR experiments, as improved temporal resolution could have enabled more accurate selection of biomass sampling time points. This would be especially important for interpreting the function of specific knockout lineages. For example, understanding the conformation and timing of physical penetration of urediniospores may have allowed more targeted investigation of genes such as cell wall degrading enzymes, while identifying the onset of rapid fungal growth may have better captured the activity of nutrient acquisition genes such as the *STL1* glycerol transporter. Additionally, I was ultimately unable to determine whether *P. coffeae* ANU01 was capable of directly inhibiting rust spore germination or viability. This represents an important unresolved aspect of the interaction and warrants further investigation in future studies.

The effectiveness of rust hyperparasites as biological control agents is influenced by a range of environmental, biological and ecological factors, which my research did not investigate. Primarily, rust hyperparasites rely on high relative humidity in order to grow on *Pst* (Zhan *et al.,* 2014). This would limit the areas they can be deployed as biocontrols to regions of the world with humid climates. I did not research the possibility of using exudate or a cocktail of isolated enzymes and metabolites from the hyperparasites in order to combat *Pst*. If high relative humidity is a limiting factor to growth of the living hyperparasite, rather than action of its enzymatic and chemical molecular mechanisms, this may be a method to increase its reach. Deploying metabolites rather than the living organism would however negate the effect of parallel evolution of the antagonist alongside the rust, a benefit which biological

controls supposedly hold over chemical approaches to targeting disease. My research also did not investigate the impact that hyperparasites have on the plant or its associated microbiome. As with *E. italicum* in wheat, several biological controls have been shown to not only limit disease but to provide benefits to the plant regarding increased growth (Rashad *et al.*, 2025; Sood *et al.*, 2020). Finally, as a living organism, hyperparasites have the possibility to persist in the environment between growing seasons, again leading back to the question of specialisation or what substrates the fungi access when rust spores are not present.

The findings of this thesis provide a foundation for future investigations into the molecular mechanism of rust parasitism. Literature in this field remains sparse and I am proud that our work on *P. coffeae* ANU01 has been published to provide new insight into the genome and transcriptome of a rust hyperparasite. As mentioned in Chapter Three, development of a reliable method for phenotyping impact of loss-of-function mutants is imperative in understanding if the conclusions drawn from my genetic and transcriptomic data hold. Once reliable methods are developed, I believe CRISPR using multiple-gene combination knockouts will be the most effective way to understand which processes are instrumental in parasitism. To complement my work in revealing the perspective of *Pst* during pathogenic attack, I propose an identical transcriptomic investigation of the gene expression of the host *Pst* spores under infection by the other eight isolates. Comparing and contrasting these datasets to each other and that of *P. coffeae* ANU01 would aid understanding of if *Pst* mounts a similar defence response to each, or if defence responses are characteristic to each hyperparasite. Finally, I suggest that fungi not known to parasitise wheat fungi be tested for their ability to grow on *Pst* spores. For example, I suggest isolating fungi from an environment devoid of rust or plants and attempting to grow them on *Pst* infected wheat. If these fungi were to prove capable of growth on *Pst* spores *on planta*, it would suggest that rust parasitism is not a trait that requires evolution and would go far in aiding understanding of just how specialised the niche is.

6.5 Conclusion

Collectively, the chapters in this thesis advance our understanding of rust hyperparasitism by identifying the potential genetic mechanisms that underpin the interaction between rust hyperparasites and their hosts. Through genomics and comparative transcriptomics this work provides new insight into the genes behind rust hyperparasitism and establishes a foundation for future studies. I present the first comparative transcriptomic investigation of a *Pst* hyperparasite, the first loss-of-function CRISPR study conducted in a rust hyperparasitic fungus, and the first transcriptomic investigation of hyperparasitism from the perspective of *Pst* itself. While many aspects of the interaction remain unresolved, particularly regarding the timeline of parasitism and recognition of the host, the pipeline described above, combined with deep phenotyping, can serve as a powerful example of how to investigate future rust hyperparasites. Ultimately, I hope my work contributes a strong first step in a walk that will lead to finally understanding these fascinating fungi, their history and their future.

6.6 Bibliography

El-Sharkawy, H. H., Rashad, Y. M., & Elazab, N. T. (2023). Biocontrol potential of the endophytic Epicoccum nigrum HE20 against stripe rust of wheat. Pesticide Biochemistry and Physiology, 194, 105517.

Kwon, H. J., Kim, J.-H., Kim, M., Lee, J.-K., Hwang, W.-S., & Kim, D.-Y. (2003). Anti-parasitic activity of depudecin on *Neospora caninum* via the inhibition of histone deacetylase. Veterinary Parasitology, 112(4), 269-276. https://doi.org/https://doi.org/10.1016/S0304-4017(03)00035-9

Lara-Martínez, D., Tristán-Flores, F. E., Cervantes-Montelongo, J. A., & Silva-Martínez, G. A. (2025). Fungal stress responses and the importance of GPCRs. Journal of Fungi, 11(3), 213. https://doi.org/10.3390/jof11030213

Lorrain, C., Gonçalves dos Santos, K. C., Germain, H., Hecker, A., & Duplessis, S. (2019). Advances in understanding obligate biotrophy in rust fungi. New Phytologist, 222(3), 1190-1206. https://doi.org/https://doi.org/10.1111/nph.15641

Moricca, S., & Ragazzi, A. (2008). Biological and integrated means to control rust diseases. In,303-329. https://doi.org/10.1007/978-1-4020-8571-0_15

Novy, V., Carneiro, L. V., Shin, J. H., Larsbrink, J., & Olsson, L. (2021). Phylogenetic analysis and in-depth characterization of functionally and structurally diverse CE5 cutinases. Journal of Biological Chemistry, 297(5), 101302. https://doi.org/10.1016/j.jbc.2021.101302

Rashad, Y. M., El-Sharkawy, H. H. A., Abdalla, S. A., Ibrahim, O. M., & Elazab, N. T. (2025). Unraveling the regulating effect of the endophyte *Epicoccum italicum* HE20 on the biosynthesis genes of polyphenols in wheat in response to yellow rust. Physiological and Molecular Plant Pathology, 138, 102705. https://doi.org/https://doi.org/10.1016/j.pmpp.2025.102705

Sood, M., Kapoor, D., Kumar, V., Sheteiwy, M. S., Ramakrishnan, M., Landi, M., Araniti, F., & Sharma, A. (2020). *Trichoderma*: the “secrets” of a multitalented biocontrol agent. Plants, 9(6), 762.

Srivastava, A. K., Défago, G., & Kern, H. (1985). Hyperparasitism of *Puccinia horiana* and other microcyclic Rusts. Journal of Phytopathology, 114(1), 73-78. https://doi.org/10.1111/j.1439-0434.1985.tb04338.x

Staples, R. C., & Wynn, W. K. (1965). The physiology of uredospores of the rust fungi. The Botanical Review, 31(4), 537-564. https://doi.org/10.1007/BF02858608

Tulloch, A. P., Craig, B. M., & Ledingham, G. A. (1959). The oil of wheat stem rust uredospores: II. The isolation of *cis*-9,10-epoxyoctadecanoic acid, and the fatty acid composition of the oil. Canadian Journal of Microbiology, 5(5), 485-491. https://doi.org/10.1139/m59-060

Wiese, M., & Ravenscroft, A. (1979). Environmental effects on inoculum quality of dormant rust uredospores. Phytopathology, 69(10), 1106.

Xiao, M., Chen, D., Liu, S., Chen, A., Fang, A., Tian, B., Yu, Y., Bi, C., Kang, Z., & Yang, Y. (2023). A chitin deacetylase Ps CDA2 from *Puccinia striiformis* f. sp. *tritici* confers disease pathogenicity by suppressing chitin-triggered immunity in wheat. Molecular Plant Pathology, 24(12), 1467-1479.

Zhan, G., Tian, Y., Wang, F., Chen, X., Guo, J., Jiao, M., Huang, L., & Kang, Z. (2014). A novel fungal hyperparasite of *Puccinia striiformis* f. sp. *tritici*, the causal agent of wheat stripe rust. PLoS One, 9(11), e111484. https://doi.org/10.1371/journal.pone.0111484